

5.15	SEM micrograph of nominal $\text{Ru}_{22}\text{Al}_{63}$ annealed at 1200°C for 312 hours (backscattered electron mode).	100
5.16	SEM micrograph of (contaminated) nominal $\text{Ru}_{22}\text{Al}_{63}$ annealed at 1200°C for 480 hours and 1050°C for 24 hours (backscattered electron mode).	104
5.17	SEM micrograph of (contaminated) nominal $\text{Ru}_{22}\text{Al}_{63}$ annealed at 1200°C for 480 hours and 1050°C for 24 hours (backscattered electron mode).	105
5.18	SEM micrograph of nominal $\text{Ru}_{35}\text{Al}_{65}\text{-a}$ (backscattered electron mode).	106
5.19	SEM micrograph of nominal $\text{Ru}_{35}\text{Al}_{65}\text{-a}$ (backscattered electron mode).	107
5.20	SEM micrograph of nominal $\text{Ru}_{35}\text{Al}_{65}\text{-a}$ (secondary electron mode).	107
5.21	SEM micrograph of (contaminated) nominal $\text{Ru}_{35}\text{Al}_{65}\text{-am}$ before heat treatment (backscattered electron mode).	111
5.22	SEM micrograph of (contaminated) nominal $\text{Ru}_{35}\text{Al}_{65}\text{-am}$ annealed at 1300°C for 6.5 hours and 1100°C for 65.5 hours (secondary electron mode).	113
5.23	SEM micrograph of (contaminated) nominal $\text{Ru}_{35}\text{Al}_{65}\text{-am}$ annealed at 1300°C for 6.5 hours and 1100°C for 65.5 hours (backscattered electron mode).	114
5.24	Macroscopic photograph of nominal $\text{Ru}_{35}\text{Al}_{65}\text{-b}$ . "Tree" structure formed by fused elements.	115
5.25	SEM micrograph of (contaminated) nominal $\text{Ru}_{35}\text{Al}_{65}\text{-b}$ (backscattered electron mode).	116
5.26	SEM micrograph of (contaminated) nominal $\text{Ru}_{35}\text{Al}_{65}\text{-b}$ (backscattered electron mode).	117
5.27	Optical micrograph of nominal $\text{Ru}_{37}\text{Al}_{63}$ annealed at 1200°C for 168 hours (Murakami's etch).	119
5.28	SEM micrograph of nominal $\text{Ru}_{37}\text{Al}_{63}$ annealed at 1200°C for 168 hours (backscattered electron mode).	119
5.29	SEM micrograph of nominal $\text{Ru}_{37}\text{Al}_{63}$ annealed at 1200°C for 168 hours (backscattered electron mode).	120
5.30	SEM micrograph of nominal $\text{Ru}_{37}\text{Al}_{63}$ annealed at 1200°C for 168 hours (backscattered electron mode).	121
5.31	SEM micrograph of (contaminated) nominal $\text{Ru}_{37}\text{Al}_{63}$ annealed at 1200°C for 840 hours (secondary electron mode).	124
5.32	SEM micrograph of (contaminated) nominal $\text{Ru}_{37}\text{Al}_{63}$ annealed at 1200°C for 840 hours (secondary electron mode).	124
5.33	Optical micrograph of nominal $\text{Ru}_{47}\text{Al}_{53}$ annealed at 1200°C for 2 hours.	126
5.34	SEM micrograph of nominal $\text{Ru}_{47}\text{Al}_{53}$ annealed at 1200°C for 2 hours (backscattered electron mode).	127
5.35	Optical micrograph of nominal $\text{Ru}_{50}\text{Al}_{50}$ annealed at 1200°C for 2 hours.	129
5.36	SEM micrograph of nominal $\text{Ru}_{50}\text{Al}_{50}$ annealed at 1200°C for 2 hours (backscattered electron mode).	129
6.1	Modified Ru-Al Phase Diagram.	168

4.20	SEM micrograph of nominal $\text{Ru}_{10}\text{Al}_{90}$ before heat treatment (secondary electron mode).	68
4.21	SEM micrograph of nominal $\text{Ru}_{10}\text{Al}_{90}$ before heat treatment (backscattered electron mode).	69
4.22	SEM micrograph of nominal $\text{Ru}_{10}\text{Al}_{90}$ before heat treatment (backscattered electron mode).	70
4.23	SEM micrograph of nominal $\text{Ru}_{10}\text{Al}_{90}$ before heat treatment (backscattered electron mode).	71
4.24	SEM micrograph of nominal $\text{Ru}_{10}\text{Al}_{90}$ annealed at 475°C for 168 hours (secondary electron mode).	74
4.25	SEM micrograph of nominal $\text{Ru}_{10}\text{Al}_{90}$ annealed at 475°C for 168 hours (secondary electron mode).	75
4.26	SEM micrograph of nominal $\text{Ru}_{10}\text{Al}_{90}$ annealed at 475°C for 168 hours (secondary electron mode).	76
4.27	SEM micrograph of nominal $\text{Ru}_{10}\text{Al}_{90}$ annealed at 475°C for 168 hours (secondary electron mode).	77
4.28	Optical micrograph of nominal $\text{Ru}_{18}\text{Al}_{82}\text{-b}$ (etched).	81
4.29	SEM micrograph of nominal $\text{Ru}_{18}\text{Al}_{82}\text{-b}$ (backscattered electron mode).	81
4.30	SEM micrograph of nominal $\text{Ru}_{18}\text{Al}_{82}\text{-b}$ (backscattered electron mode).	82
4.31	SEM micrograph of nominal $\text{Ru}_{20}\text{Al}_{80}$ (backscattered electron mode).	84
4.32	SEM micrograph of nominal $\text{Ru}_{20}\text{Al}_{80}$ (backscattered electron mode).	84
5.1	Optical micrograph of nominal $\text{Ru}_{23}\text{Al}_{77}$ before heat treatment (Murakami's etch).	88
5.2	Optical micrograph of nominal $\text{Ru}_{23}\text{Al}_{77}$ before heat treatment (Murakami's etch).	88
5.3	SEM micrograph of nominal $\text{Ru}_{23}\text{Al}_{77}$ before heat treatment (secondary electron mode).	89
5.4	SEM micrograph of nominal $\text{Ru}_{23}\text{Al}_{77}$ annealed at 1300°C for 6.5 hours (secondary electron mode).	91
5.5	SEM micrograph of nominal $\text{Ru}_{23}\text{Al}_{77}$ annealed at 1300°C for 6.5 hours (secondary electron mode).	91
5.6	SEM micrograph of nominal $\text{Ru}_{23}\text{Al}_{77}$ annealed at 1300°C for 6.5 hours (secondary electron mode).	92
5.7	First DTA trace for nominal $\text{Ru}_{23}\text{Al}_{77}$ .	94
5.8	Second DTA trace for nominal $\text{Ru}_{23}\text{Al}_{77}$ .	94
5.9	Third DTA trace for nominal $\text{Ru}_{23}\text{Al}_{77}$ .	95
5.10	SEM micrograph of (contaminated) nominal $\text{Ru}_{23.3}\text{Al}_{76.7}$ (backscattered electron mode).	96
5.11	SEM micrograph of (contaminated) nominal $\text{Ru}_{23.3}\text{Al}_{76.7}$ (secondary electron mode).	96
5.12	Optical micrograph of nominal $\text{Ru}_{32}\text{Al}_{68}$ annealed at 1200°C for 312 hours.	98
5.13	Optical micrograph of nominal $\text{Ru}_{32}\text{Al}_{68}$ annealed at 1200°C for 312 hours (etched with Murakami's reagent).	99
5.14	Optical micrograph of nominal $\text{Ru}_{32}\text{Al}_{68}$ annealed at 1200°C for 312 hours (etched with Murakami's reagent).	100

## LIST OF FIGURES

Figure		Page
2.1	The Ru-Al phase diagram as drawn by Obrowski <sup>[4]</sup> .	3
2.2	The Ru-Al phase diagram as interpreted by Shunk <sup>[6]</sup> .	4
2.3	Phase diagram proposed by Anlage <sup>[5]</sup> .	12
2.4	Variations of the Al-rich end of the Phase Diagram.	15
4.1	Optical micrograph of (contaminated) nominal Ru <sub>3</sub> :Al <sub>97</sub> -a (528 hours at 550°C).	43
4.2	SEM micrograph of (contaminated) nominal Ru <sub>3</sub> :Al <sub>97</sub> -b before heat treatment (secondary electron mode).	44
4.3	SEM micrograph of (contaminated) nominal Ru <sub>3</sub> :Al <sub>97</sub> -b before heat treatment (backscattered electron mode).	45
4.4	Optical micrograph of nominal Ru <sub>4</sub> :Al <sub>96</sub> -a before heat treatment.	47
4.5	SEM micrograph of nominal Ru <sub>4</sub> :Al <sub>96</sub> -a before heat treatment (secondary electron mode).	48
4.6	SEM micrograph of nominal Ru <sub>4</sub> :Al <sub>96</sub> -a before heat treatment (backscattered electron mode).	48
4.7	SEM micrograph of nominal Ru <sub>4</sub> :Al <sub>96</sub> -a before heat treatment (secondary electron mode).	49
4.8	SEM micrograph of nominal Ru <sub>4</sub> :Al <sub>96</sub> -a annealed at 475°C for 168 hours (secondary electron mode).	52
4.9	SEM micrograph of nominal Ru <sub>4</sub> :Al <sub>96</sub> -a annealed at 475°C for 168 hours (secondary electron mode).	53
4.10	SEM micrograph of nominal Ru <sub>4</sub> :Al <sub>96</sub> -a annealed at 475°C for 168 hours (secondary electron mode).	54
4.11	SEM micrograph of (contaminated) nominal Ru <sub>4</sub> :Al <sub>96</sub> -b (backscattered electron mode).	57
4.12	SEM micrograph of nominal Ru <sub>4</sub> :Al <sub>96</sub> -b (backscattered electron mode).	58
4.13	SEM micrograph of top region of nominal Ru:Al <sub>12</sub> (secondary electron mode).	60
4.14	SEM micrograph of bottom region of nominal Ru:Al <sub>12</sub> (secondary electron mode).	60
4.15	Optical micrograph of bottom region of nominal Ru:Al <sub>12</sub> (etched).	61
4.16	SEM micrograph of nominal Ru:Al <sub>12</sub> (secondary electron mode).	62
4.17	SEM micrograph of (contaminated) nominal Ru <sub>7</sub> :Al <sub>93</sub> after sintering (secondary electron mode).	65
4.18	SEM micrograph of nominal Ru <sub>10</sub> :Al <sub>90</sub> before heat treatment (backscattered electron mode).	67
4.19	SEM micrograph of nominal Ru <sub>10</sub> :Al <sub>90</sub> before heat treatment (secondary electron mode).	68

## CONTENTS

Page

APPENDIX XV	EXPERIMENTAL DATA FOR $\text{Ru}_{35}\text{:Al}_{65}\text{-am}$	229
APPENDIX XVI	EXPERIMENTAL DATA FOR $\text{Ru}_{35}\text{:Al}_{65}\text{-b}$	233
APPENDIX XVII	EXPERIMENTAL DATA FOR $\text{Ru}_{37}\text{:Al}_{63}$	236
APPENDIX XVIII	EXPERIMENTAL DATA FOR $\text{Ru}_{47}\text{:Al}_{53}$	245
APPENDIX XIX	EXPERIMENTAL DATA FOR $\text{Ru}_{50}\text{:Al}_{50}$	249
APPENDIX XX	JCPDS LATTICE DATA CARDS	253

## REFERENCES

261

<b>CONTENTS</b>		<b>Page</b>
<b>6.4</b>	<b>Modifications to the Phase diagram</b>	<b>157</b>
<b>6.5</b>	<b>X-Ray Diffraction</b>	<b>170</b>
<b>7</b>	<b>CONCLUSIONS AND RECOMMENDATIONS</b>	<b>173</b>
<b>7.1</b>	<b>Summary and Conclusions</b>	<b>173</b>
<b>7.2</b>	<b>Recommendations for Future Work</b>	<b>173</b>
<b>APPENDIX I</b>	<b>EMSSA CONFERENCE PAPER</b>	<b>174</b>
<b>APPENDIX II</b>	<b>EXPERIMENTAL DATA FOR <math>Ru_3:Al_{97}</math>-a</b>	<b>175</b>
<b>APPENDIX III</b>	<b>EXPERIMENTAL DATA FOR <math>Ru_3:Al_{97}</math>-b</b>	<b>176</b>
<b>APPENDIX IV</b>	<b>EXPERIMENTAL DATA FOR <math>Ru_4:Al_{96}</math>-a</b>	<b>179</b>
<b>APPENDIX V</b>	<b>EXPERIMENTAL DATA FOR <math>Ru_4:Al_{96}</math>-b</b>	<b>184</b>
<b>APPENDIX VI</b>	<b>EXPERIMENTAL DATA FOR <math>Ru:Al_{13}</math></b>	<b>187</b>
<b>APPENDIX VII</b>	<b>EXPERIMENTAL DATA FOR <math>Ru_7:Al_{93}</math></b>	<b>192</b>
<b>APPENDIX VIII</b>	<b>EXPERIMENTAL DATA FOR <math>Ru_{10}:Al_{90}</math></b>	<b>195</b>
<b>APPENDIX IX</b>	<b>EXPERIMENTAL DATA FOR <math>Ru_{18}:Al_{82}</math>-b</b>	<b>203</b>
<b>APPENDIX X</b>	<b>EXPERIMENTAL DATA FOR <math>Ru_{20}:Al_{80}</math></b>	<b>208</b>
<b>APPENDIX XI</b>	<b>EXPERIMENTAL DATA FOR <math>Ru_{28}:Al_{72}</math></b>	<b>210</b>
<b>APPENDIX XII</b>	<b>EXPERIMENTAL DATA FOR <math>Ru_{28.3}:Al_{71.7}</math></b>	<b>217</b>
<b>APPENDIX XIII</b>	<b>EXPERIMENTAL DATA FOR <math>Ru_{32}:Al_{68}</math></b>	<b>218</b>
<b>APPENDIX XIV</b>	<b>EXPERIMENTAL DATA FOR <math>Ru_{35}:Al_{65}</math>-a</b>	<b>226</b>

<b>CONTENTS</b>		<b>Page</b>
3.1.4	Graphite resistance furnace method	30
3.1.5	Muffle furnace technique	31
3.1.6	Sinter - hot isostatic pressing technique	32
3.1.7	Induction furnace method	32
3.1.8	Comparison of the production methods	33
3.2	Heat Treatment	36
3.3	Metallographic Preparation	38
3.4	SEM Studies	38
3.5	X-Ray Analysis	39
3.5.1	Debye-Scherrer powder diffraction	39
3.5.2	Bulk sample x-ray diffraction	40
3.6	Thermal Analysis	41
4	<b>RESULTS FROM LOW RUTHENIUM ALLOYS</b>	42
5	<b>RESULTS FROM HIGH RUTHENIUM ALLOYS</b>	87
6	<b>DISCUSSION AND PROPOSALS</b>	131
6.1	Critical Appraisal of Literature Survey	131
6.2	Discussion of the Individual Samples	140
6.3	Discussion of the Thermal Analysis	155

<b>CONTENTS</b>	<b>Page</b>
<b>DECLARATION</b>	<b>ii</b>
<b>ABSTRACT</b>	<b>iii</b>
<b>DEDICATION</b>	<b>iv</b>
<b>ACKNOWLEDGEMENTS</b>	<b>v</b>
<b>CONTENTS</b>	<b>vi</b>
<b>LIST OF FIGURES</b>	<b>x</b>
<b>LIST OF TABLES</b>	<b>xiii</b>
<b>1 INTRODUCTION</b>	<b>1</b>
<b>2 LITERATURE SURVEY</b>	<b>3</b>
<b>2.1 Phases and Phase Relationships</b>	<b>3</b>
<b>2.2 Lattice Parameters</b>	<b>15</b>
<b>2.3 Production Techniques</b>	<b>23</b>
<b>3 EXPERIMENTAL PROCEDURE</b>	<b>26</b>
<b>3.1 Production of the Alloys</b>	<b>26</b>
<b>3.1.1 Button-arc furnace method</b>	<b>28</b>
<b>3.1.2 Improved arc-melting procedure</b>	<b>29</b>
<b>3.1.3 Liquid-phase sintering method</b>	<b>30</b>

## ACKNOWLEDGEMENTS

The first thanks must go to Dr L.A. Cernish, supervisor of this project, for her tremendous support and encouragement. Secondly, many thanks to MINTEK for financing the MSc.

The following MINTEK personnel also made a great contribution to this project:

Dr M. Cortie, Dr I. Wolff, Mrs I. Klingbiel, Mrs A. Wedepohl, Mr H. Le Lagadec, Mr C. Fletcher, Mrs P. De Visser, Mrs L. Lombaard, Mrs S. Taylor, Mr G. Verney, Mr R. Visser, Mr R. Watt, Mr J. Maskrey, Mrs E. Jackson, Mr V. Pretorius, Mr L. Missio.

Thanks to Mr I. Northrop at Boart Research Centre for use of equipment; to Mr J. Askeland of Hulett Metals for his generous donation of high purity aluminium; and to Mr R. Stanton of Premier Technologies for conducting the thermal analysis investigations.



In memory of an extraordinary lady

and dearest grandmother

Dora Mynors Byrne

1914 - 1993

## **ABSTRACT**

Recent international investigations into new advanced materials have shown that the intermetallic compound, RuAl, possesses promising characteristics for high-temperature use in corrosive environments. In order to optimise production of this alloy, an understanding of the Ru-Al system is necessary.

This investigation assesses the validity of the existing phase diagrams for this system, using optical microscopy, scanning electron microscopy, X-ray diffraction, and exploratory thermal analysis. It is proposed that, below 50 at% Ru, the phase diagram consists of a cascade of peritectic reactions.

## DECLARATION

I declare that this dissertation is my own, unaided work. It is being submitted for the Degree of Master of Science in Engineering in the University of the Witwatersrand, Johannesburg. It has not been submitted before for any degree or examination in any other University.

H Bonifase

(Signature of candidate)

21<sup>st</sup> day of June 1994

# **THE RUTHENIUM-ALUMINIUM PHASE DIAGRAM**

**Tracy Diane Boniface**

**A dissertation submitted to the Faculty of Engineering, University of the Witwatersrand,  
in partial fulfilment of the requirements for the degree of Master of Science in Engineering**

**Johannesburg, 1994**

In 1963 Schwomma<sup>[7]</sup> stated that he obtained a mixture of  $\text{RuAl}_2$  and  $\text{RuAl}$  in samples containing 33.3 at% Ru by a slow cool from 1750°C to 1350°C over 3 hours, which he stated agreed with Obrowski's phase diagram. Further information regarding the heat treatment was not provided. The specimens were used for X-ray investigations. He also recorded the possibility of problems with contamination from silicon and oxygen.

In 1965 Edshammar<sup>[8]</sup>, without reference to Obrowski's work, investigated the crystal structure of  $\text{Ru}_4\text{Al}_{13}$ . He compared  $\text{Ru}_4\text{Al}_{13}$  with  $\text{Fe}_4\text{Al}_{13}$  and found the same prismatic twinned structure, and so deduced the ruthenium-aluminum intermetallic to have the same crystal structure. He found that  $\text{Ru}_4\text{Al}_{13}$  had similar atomic co-ordination numbers to  $\text{Fe}_4\text{Al}_{13}$ , but was more similar to  $\text{Os}_4\text{Al}_{13}$ . He also found that  $\text{Ru}$  atoms were absent from some of the sites in  $\text{Ru}_4\text{Al}_{13}$  which were partially (30-70%) occupied by Al in  $\text{Fe}_4\text{Al}_{13}$  and  $\text{Co}_4\text{Al}_{13}$ . He said that  $\text{Fe}_4\text{Al}_{13}$  is the ideal composition of  $\text{FeAl}_3$ , and hence it has been assumed that he considers  $\text{Ru}_4\text{Al}_{13}$  to be the ideal composition of Obrowski's  $\text{RuAl}_3$ .

A year later Edshammar published an X-ray investigation of this system<sup>[9]</sup>. He identified the phases  $\text{Ru}_4\text{Al}_{13}$ ,  $\text{RuAl}$ ,  $\text{Ru}_2\text{Al}_3$ ,  $\text{RuAl}_2$  and the extra phase  $\text{RuAl}_{2.5}$ , using X-ray powder methods. The phase  $\text{RuAl}_{2.5}$  was only observed in the arc-melted samples and not in the heat-treated ones<sup>[9]</sup>. Table 2.2 is a list of the phases found in Edshammar's samples<sup>[9]</sup>.

Table 2.1: Obrowski's Samples<sup>[4]</sup>.

Ru Content (at%)	Phases Present (According to Obrowski)	Etched Colour of Phase
96.3 FIG 19*	Ru-rich solid solution	white
83.5 FIG 12	Primary Ru-rich solid solution RuAl (eutectic with Ru-rich solid)	white black
67 FIG 13	Primary RuAl Ru-rich solid solution (eutectic with RuAl)	white black
50 FIG 20	RuAl	dark grey + white
33 FIG 14	Primary RuAl Ru <sub>2</sub> Al <sub>3</sub>	white dark grey
33 FIG 21	Primary RuAl Ru <sub>2</sub> Al <sub>3</sub>	white black
25 FIG 15	Primary Ru <sub>2</sub> Al <sub>3</sub> RuAl <sub>4</sub> (eutectic with Ru <sub>2</sub> Al <sub>3</sub> ) RuAl <sub>3</sub> (transformed from eutectic)	black white grey
19.3 FIG 16	Primary Ru <sub>2</sub> Al <sub>3</sub> RuAl <sub>4</sub> (eutectic with Ru <sub>2</sub> Al <sub>3</sub> ) RuAl <sub>2</sub> (transformed from Ru <sub>2</sub> Al <sub>3</sub> )	black white grey
19.3 FIG 22 (local area at high mag.)	Ru <sub>2</sub> Al <sub>3</sub> in eutectic RuAl <sub>4</sub> in eutectic RuAl <sub>2</sub> (transformed from Ru <sub>2</sub> Al <sub>3</sub> )	black white grey
13.75 FIG 17	RuAl <sub>4</sub> (needle-like) RuAl <sub>12</sub> (peritectic) Al (eutectic with RuAl <sub>12</sub> )	grey white black
0.5 FIG 18	RuAl <sub>12</sub> (eutectic with Al) Al	white black

\*Obrowski's figure numbers

$\text{RuAl}_2$ , as well as the Al-rich phase boundary of  $\text{Ru}_2\text{Al}_3$ .

Table 2.1 contains a list of the samples which Obrowski depicted in his publication<sup>[4]</sup>, together with his figure numbers, the phases identified, and their etched colour. Most of the samples were etched with Murakami's reagent, except for the sample containing 96.3 at% Ru, which was electrolytically etched with a 10% KCN solution using an alternating current.

Obrowski stated that the samples were "subjected to various heat treatments"<sup>[4]</sup>, but did not give specific details, which makes his work very difficult to follow and verify. The only depicted microstructure for which he did specify the heat treatment is the sample containing 96.3 at% Ru. This alloy was annealed for two hours at 1800°C. The caption for the other figures stated "solidified in crucible"<sup>[4]</sup>, except for that of the sample containing 33 at% Ru, which stated "slowly solidified in crucible".

It can be seen (in Table 2.1) that the colours of the phases are inconsistent, even though they were supposed to have been etched with the same solution. For example, the phase  $\text{RuAl}_3$  is grey in one sample and white in another;  $\text{RuAl}$  is black or white in different samples, as is the Ru-rich solid solution;  $\text{Ru}_2\text{Al}_3$  is black or dark grey. The latter result could be due to different etching times.

phase. He stated that the Al-rich phases are line compounds i.e. they do not exist over discernable ranges in composition. He could not find any detectable solubility of Ru in Al, but determined the solubility of Al in Ru to be a maximum of about 4 at%\* at the eutectic temperature of  $1920^{\circ}\text{C} \pm 20^{\circ}\text{C}$ . The eutectic composition, corresponding to the reaction  $\text{L} \rightarrow \text{RuAl} + \text{Ru-rich solid solution}$ , was found to be 70 at% Ru. RuAl was found to melt congruently at  $2060^{\circ}\text{C}$  and 50 at% Ru, and there is a peritectic reaction at about  $1600^{\circ}\text{C}$  and 40 at% Ru to form  $\text{Ru}_2\text{Al}_3$  ( $\text{L} + \text{RuAl} \rightarrow \text{Ru}_2\text{Al}_3$ ). Both RuAl and  $\text{Ru}_2\text{Al}_3$  were found to have wide composition ranges (up to 9 at%). However the latter compound was found to be unstable at lower temperatures and decomposed eutectoidally at about  $1000^{\circ}\text{C}$  to form RuAl and  $\text{RuAl}_2$ . Obrowski also proposed that the compound  $\text{RuAl}_2$  melted congruently and formed a eutectic with  $\text{Ru}_2\text{Al}_3$  at about  $1300^{\circ}\text{C}$  on its Ru-rich side. Below this temperature he observed the formation of  $\text{RuAl}_2$  via a peritectoid reaction between  $\text{RuAl}_3$  and  $\text{Ru}_2\text{Al}_3$  (depicted as occurring at  $1200^{\circ}\text{C}$  in Figure 2.2). To accommodate his observations and above-mentioned proposals, Obrowski suggested that  $\text{RuAl}_2$  formed via a peritectoid reaction between  $\text{RuAl}_3$  and  $\text{Ru}_2\text{Al}_3$  at about  $1100^{\circ}\text{C}$  (Figure 2.2).

Obrowski proposed that the phase  $\text{RuAl}_{12}$  is formed via a peritectic reaction involving  $\text{RuAl}_6$  ( $\text{L} + \text{RuAl}_6 \rightarrow \text{RuAl}_{12}$ ). The reported coarse needle-like structure of  $\text{RuAl}_6$  was taken to indicate that the phase is a primary one. The final reaction was said to be the formation of a eutectic mixture of Al and  $\text{RuAl}_{12}$  with the eutectic point at 0.5 at% Ru, near the melting point of pure aluminium. Obrowski stated that he was unsure of the solid state relationships in the region 20 to 40 at% Ru; this includes the formation of  $\text{RuAl}_3$  and

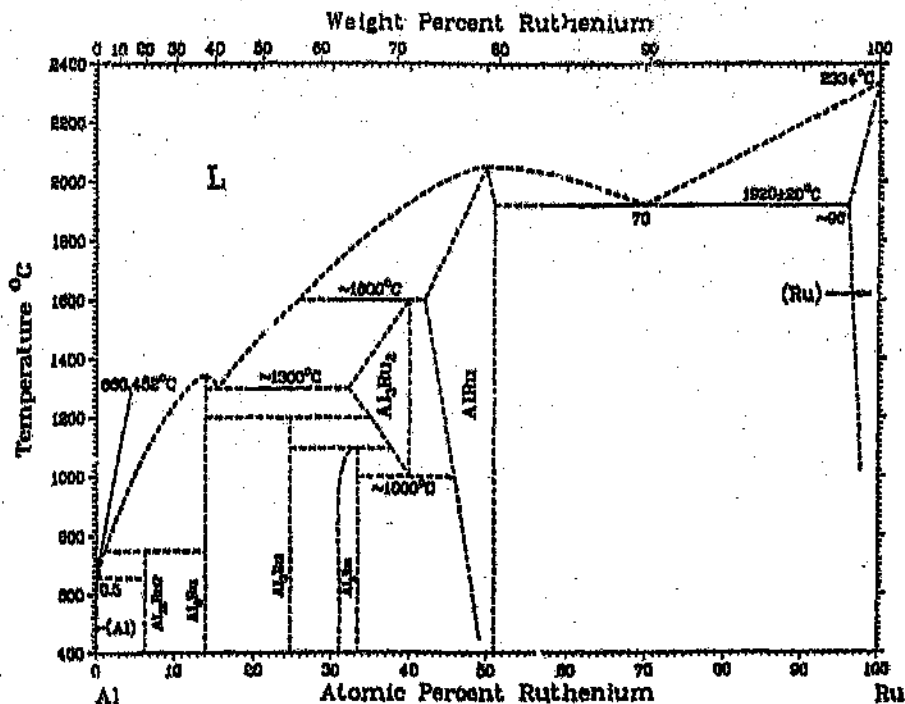
---

\*All compositions are expressed in atomic percentages



Figure 2.2 depicts Shunk's<sup>[6]</sup> interpretation of the information provided by Obrowski, and is much clearer than Obrowski's original diagram, although the information is the same.

Figure 2.2: The Ru-Al phase diagram as interpreted by Shunk<sup>[6]</sup>.



Obrowski's<sup>[4]</sup> published phase diagram comprised two congruently melting intermetallics, three eutectic reactions, two peritectic reactions, two peritectoid reactions, and a eutectoid reaction. The phase diagram is described below in his terms, working from the ruthenium-rich end.

Obrowski<sup>[4]</sup> proposed the existence of six intermetallic compounds in this system:  $\text{RuAl}$ ,  $\text{Ru}_2\text{Al}_3$ ,  $\text{RuAl}_2$ ,  $\text{RuAl}_3$ ,  $\text{RuAl}_5$ , and  $\text{RuAl}_{12}$ , but was unsure of the composition of the latter

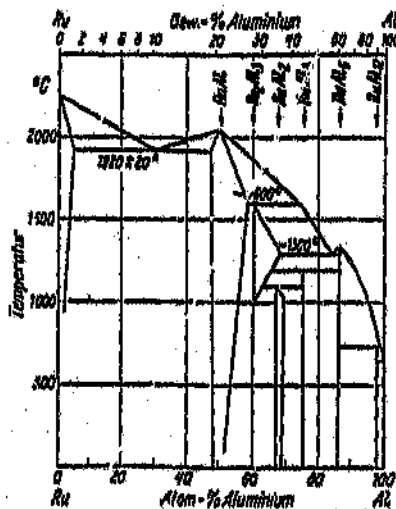
## 2 LITERATURE SURVEY

Various workers have studied the ruthenium-aluminium system and the results have been dissimilar. This review has been divided into sections pertaining to the different areas of the research, to aid comparison, and the widely differing manufacturing techniques employed by the investigators.

### 2.1 Phases and Phase Relationships

The first ruthenium-aluminium phase diagram was published in 1963 by Obrowski<sup>[4]</sup> (Figure 2.1), and was based upon experimental observations. Microscopic, X-ray, and thermoanalytical techniques were employed to determine the compositions of the phases and their phase relationships.

Figure 2.1: The Ru-Al phase diagram as drawn by Obrowski<sup>[4]</sup>.



methods of manufacture, and the available techniques resulted in inhomogeneous samples. Attempts at homogenisation treatments were largely unsuccessful due to the very slow diffusion rates encountered in this system. High temperature investigations were limited by lack of suitable equipment.

The available literature has been reported and reviewed. The alloys used for this investigation were manufactured in various ways, but most were melted in a button arc furnace. Characterisation of the alloys was undertaken using optical microscopy, scanning electron microscopy, energy dispersive analysis of X-rays, and X-ray diffraction experiments. The results are presented in two chapters; the first covers the higher aluminium content alloys, and the second covers alloys with 28 at% to 50 at% ruthenium. (Investigations beyond these compositions were not necessary, since there is only one reaction in the high ruthenium region of the phase diagram.) Finally, a phase diagram is proposed with the modification of a cascade of peritectic reactions on the Al-rich side of RuAl.

At an intermediate stage, the work was presented at the Electron Microscopy Society of South Africa Conference 1993 (Berg-en-dal). The paper is contained in Appendix I.

## 1 INTRODUCTION

Intermetallics are solid-state chemical compounds which are formed between two (or more) metals. They often have small ranges of composition and the most useful have very high melting points. These compounds are generally brittle at room temperature, and much research has been conducted since the 1950s into improving their mechanical properties and investigation of possible high-temperature applications.

Interest in the Ru-Al binary system was provoked by Fleischer<sup>[1]</sup>, who claimed that the intermetallic compound RuAl, already known to have a high melting point, also had relatively good room-temperature toughness. Raub and Woppersnow<sup>[2]</sup> had also shown that it has high corrosion resistance over a range of temperatures. Difficulties with production of these alloys<sup>[3]</sup> necessitated a better understanding of this system. Uncertainty of the original phase diagram<sup>[4]</sup> was instigated by a later publication<sup>[5]</sup> which stated that it is incorrect.

The purpose of this investigation was to determine the applicability of the published phase diagrams<sup>[4,5]</sup> to the ruthenium - aluminium system and to modify these diagrams, if necessary. A small part of the investigation involved a brief look at the crystal structures and lattice parameters of the various intermetallic compounds formed by these two elements.

The investigation was made difficult by the inhomogeneity of the samples, which resulted from a number of causes. The large difference in melting points of the elements limited the

Errata:

- p.118 The last sentence should be part of the penultimate one.
- p.156 6th line: This should read: "The reaction at 656°C .... was attributed to the Al-rich + RuAl<sub>3</sub> eutectic".
- p.157 Section 6.4, 3rd sentence: "chapter" should read "section".
- p.158 Insert a penultimate sentence: "These agreed well with the temperatures in the current investigation of 656°C and 730°C respectively."
- p. 158 and 159  
The phrase in the tables "melts peritectically" is clearer if changed to "forms peritectically".
- p.159 Near the top of the page: Replace "Anlage's reaction temperatures.." to the end of the paragraph with "Anlage's reaction temperature of 1403°C is comparable with the value of 1417°C found in this investigation, given the error in calibration."
- p.160 1st paragraph: Replace the last sentence with "The formation temperature of RuAl<sub>3</sub> as reported by Anlage, was roughly confirmed in this investigation."
- p.160 Table: Add "at 1460°C" to "RuAl<sub>3</sub> forms via a peritectic reaction".

6.4	Proposals for the phase $Ru_2Al_3$ .	161
6.5	Proposals for the phase $RuAl$ .	162
6.6	Deduction of limits of peritectic reaction lines, and peritectic reaction points, using Edshamar's data.	165
6.7	Deduction of limits of peritectic reaction lines, and peritectic points, using the samples from this work.	165
6.8	Phase Composition Boundaries.	166
6.9	Deduction of limits of peritectic reaction lines, and peritectic reaction points, using all available data.	167

4.13	Quantitative chemical analyses for nominal $\text{Ru}_{10}\text{:Al}_{90}$ (No heat treatment).	72
4.14	Debye-Scherrer Diffraction Data For $\text{Ru}_{10}\text{:Al}_{90}$ (No Heat Treatment) ( $\text{CuK}\alpha$ ).	73
4.15	Quantitative chemical analyses for nominal $\text{Ru}_{10}\text{:Al}_{90}$ ( $475^\circ\text{C}$ for 168 hours).	78
4.16	Debye-Scherrer Diffraction Data For $\text{Ru}_{10}\text{:Al}_{90}$ ( $475^\circ\text{C}$ for 168 hours) ( $\text{CuK}\alpha$ ).	79
4.17	Chemical analyses for nominal $\text{Ru}_{13}\text{:Al}_{87}\text{-b}$ (No heat treatment).	83
4.18	Quantitative chemical analyses for nominal $\text{Ru}_{20}\text{:Al}_{80}$ (No heat treatment).	85
5.1	Quantitative chemical analyses for nominal $\text{Ru}_{23}\text{:Al}_{77}$ (No heat treatment).	89
5.2	Quantitative chemical analyses for nominal $\text{Ru}_{23}\text{:Al}_{77}$ ( $1300^\circ\text{C}$ for 6.5 hours).	92
5.3	Semi-quantitative chemical analyses for nominal $\text{Ru}_{23.3}\text{:Al}_{76.7}$ ( $1200^\circ\text{C}$ for 312 hours).	97
5.4	Chemical analyses of nominal $\text{Ru}_{32}\text{:Al}_{68}$ annealed at $1200^\circ\text{C}$ for 312 hours.	101
5.5	Debye-Scherrer Diffraction Data For $\text{Ru}_{32}\text{:Al}_{68}$ ( $1200^\circ\text{C}$ for 312 hours) ( $\text{CuK}\alpha$ ).	102
5.6	Quantitative chemical analyses for nominal $\text{Ru}_{32}\text{:Al}_{68}$ ( $1200^\circ\text{C}$ for 480 hours, $1050^\circ\text{C}$ for 48 hours).	104
5.7	Chemical analyses for nominal $\text{Ru}_{35}\text{:Al}_{65}\text{-a}$ (No heat treatment).	108
5.8	Debye-Scherrer Diffraction Data For $\text{Ru}_{35}\text{:Al}_{65}\text{-a}$ (No heat treatment) ( $\text{CuK}\alpha$ ).	109
5.9	Quantitative chemical analyses for nominal $\text{Ru}_{35}\text{:Al}_{65}\text{-am}$ (No heat treatment).	112
5.10	Quantitative chemical analyses for nominal $\text{Ru}_{35}\text{:Al}_{65}\text{-am}$ ( $1300^\circ\text{C}$ for 6.5 hours, $1100^\circ\text{C}$ for 65.5 hours).	115
5.11	Quantitative chemical analyses for nominal $\text{Ru}_{35}\text{:Al}_{65}\text{-b}$ (No heat treatment).	118
5.12	Quantitative chemical analyses for nominal $\text{Ru}_{37}\text{:Al}_{63}$ ( $1200^\circ\text{C}$ for 168 hours).	121
5.13	Debye-Scherrer Diffraction Data For $\text{Ru}_{37}\text{:Al}_{63}$ ( $1200^\circ\text{C}$ for 168 hours) ( $\text{CuK}\alpha$ ).	122
5.14	Semi-quantitative chemical analyses for nominal $\text{Ru}_{37}\text{:Al}_{63}$ ( $1200^\circ\text{C}$ for 840 hours).	125
5.15	Quantitative chemical analyses for nominal $\text{Ru}_{47}\text{:Al}_{53}$ ( $1200^\circ\text{C}$ for 2 hours).	127
5.16	Quantitative chemical analyses for nominal $\text{Ru}_{50}\text{:Al}_{50}$ ( $1200^\circ\text{C}$ for 2 hours).	130
6.1	Proposals for the phase $\text{RuAl}_6$ .	158
6.2	Proposals for the phase $\text{Ru}_4\text{Al}_{13}$ .	159
6.3	Proposals for the phase $\text{RuAl}_2$ .	160

## LIST OF TABLES

Table		Page
2.1	Obrowski's Samples <sup>[4]</sup> .	7
2.2	Edshammar's Samples <sup>[9]</sup> .	9
2.3	Crystallographic data of the elements <sup>[12]</sup> .	15
2.4	Edshammar's Ru <sub>4</sub> Al <sub>13</sub> Guinier powder pattern (CuK $\alpha$ ) <sup>[8]</sup> .	17
2.5	Edshammar's RuAl <sub>1.5</sub> Guinier powder pattern (CuK $\alpha$ ) - annealed at 1100°C <sup>[9]</sup> .	18
2.6	Comparison of Edshammar's RuAl <sub>2</sub> Guinier powder pattern (CuK $\alpha$ ) <sup>[9]</sup> and Schwomma's RuAl <sub>2</sub> rotating crystal data (CrK $\alpha$ ) <sup>[7]</sup> .	19
2.7	RuAl <sub>2</sub> interatomic distances ( $\text{\AA}$ ), as calculated by Edshammar <sup>[9]</sup> .	20
2.8	RuAl <sub>2.5</sub> reflections obtained by Edshammar (CuK $\alpha$ ) <sup>[9]</sup> .	20
2.9	Lattice parameters as reported by Obrowski, Edshammar, and Schwomma.	21
2.10	Lattice parameters as reported by Obrowski and Edshammar.	22
3.1	Sample list and form of aluminium.	27
3.2	Heat treatment details of the alloys.	37
4.1	Average chemical analyses of nominal Ru <sub>3</sub> Al <sub>97</sub> -a (528 hours at 550°C).	43
4.2	Semi-quantitative chemical analyses for nominal Ru <sub>3</sub> Al <sub>97</sub> -b (No heat treatment).	46
4.3	Semi-quantitative chemical analyses for nominal Ru <sub>3</sub> Al <sub>97</sub> -b (550°C for 1176 hours).	46
4.4	Quantitative chemical analyses for nominal Ru <sub>4</sub> Al <sub>96</sub> -a (No heat treatment).	50
4.5	Debye-Scherrer Diffraction Data For Ru <sub>4</sub> Al <sub>96</sub> -a (No Heat Treatment) (CuK $\alpha$ ).	51
4.6	Quantitative chemical analyses for nominal Ru <sub>4</sub> Al <sub>96</sub> -a (475°C for 168 hours).	55
4.7	Debye-Scherrer Diffraction Data for Ru <sub>4</sub> Al <sub>96</sub> -a (475°C for 168 hours) (CuK $\alpha$ ).	56
4.8	Phase analyses for nominal Ru <sub>4</sub> Al <sub>96</sub> -b (All quantitative except for the overall composition).	59
4.9	EDAX analyses for nominal Ru:Al <sub>12</sub> .	62
4.10	Debye-Scherrer Diffraction Data For Ru:Al <sub>12</sub> (CuK $\alpha$ ).	63
4.11	Semi-quantitative chemical analyses for nominal Ru <sub>7</sub> Al <sub>93</sub> (No heat treatment).	65
4.12	Semi-quantitative chemical analyses for nominal Ru <sub>7</sub> Al <sub>93</sub> (550°C for 1176 hours).	66



Edshammar's observed values were reported to agree with calculated data<sup>[9]</sup>. He also predicted the interatomic distances (Table 2.7) in the  $\text{RuAl}_2$  lattice.

Table 2.7:  $\text{RuAl}_2$  interatomic distances ( $\text{\AA}$ ), as calculated by Edshammar<sup>[9]</sup>.

Atomic Relationship	Distance ( $\text{\AA}$ )	Atomic Relationship	Distance ( $\text{\AA}$ )
Ru - 4 Al	2.57	Al - 2 Al	2.60
2 Al	2.64	2 Al	2.68
4 Al	2.73	1 Al	2.73
4 Ru	3.20	2 Ru	2.57
		1 Ru	2.64
		2 Ru	2.73
		4 Al	3.20

Edshammar could not obtain single crystals of  $\text{RuAl}_{2.5}$ . The structure of this phase was not determined, but the corresponding reflections were listed (Table 2.8).

Table 2.8:  $\text{RuAl}_{2.5}$  reflections obtained by Edshammar ( $\text{CuK}\alpha_1$ )<sup>[9]</sup>.

$I_{\text{obs}}$	$\sin^2\theta_{\text{obs}}$
medium	0.0237
medium	0.0390
weak	0.0557
strong	0.0564
medium	0.0570

It should be noted that the lattice structures and parameters determined by Edshammar<sup>[8,9]</sup> contradict those reported by Obrowski<sup>[4]</sup>. The conflicting published results are summarised

Table 2.6: Comparison of Edshammur's  $\text{RuAl}_2$  Guinier powder pattern ( $\text{CuK}\alpha$ )<sup>[6]</sup> and Schwomma's  $\text{RuAl}_2$  rotating crystal data ( $\text{CrK}\alpha$ )<sup>[7]</sup>.

hkl	Edshammur			Schwomma		
	$\sin^2\theta_{\text{obs}}$	$d_{\text{obs}}$ (nm)	$I_{\text{obs}}$	$\sin^2\theta_{\text{calc}}$	$d_{\text{calc}}$ (nm)	$I_{\text{calc}}$
111	0.04238	0.368962	st	0.0976	0.366466	st
202	0.06772	0.293999	mt	0.1514	0.294396	m
1-13	0.18508	0.237823	m	0.2336	0.237006	w
311	0.11731	0.254703	st	0.2622	0.223707	vw
004	0.12289	0.219731	mt	0.2746	0.218297	m
0-2	0.19737	0.207825	st	0.3070	0.206741	m
220	0.14350	0.203340	m	0.3192	0.202731	w
400	0.14783	0.200340	w	0.3274	0.200196	vw
313	Not observed			0.3987	0.181414	st
413	0.17660	0.182063	m	Not observed		
115	0.22806	0.161296	vw	0.5070	0.160876	vw
131	0.25686	0.151945	vw	0.5730	0.151327	vw
511	0.26544	0.149509	vw	0.5920	0.148879	m
224	0.26660	0.149183	m			
404	0.27082	0.148016	w	0.6005	0.147822	w
422	0.28729	0.144213	m	0.6328	0.144000	w
315	0.30199	0.140169	m	0.6694	0.140008	m
206	0.31366	0.137537	vw	0.6954	0.137366	vw
133	0.31638	0.136514	vw	0.7050	0.136427	vw
513	0.32698	0.134707	vw	0.7239	0.134634	vw
331	0.33078	0.133931	m	0.7316	0.133924	m
602	Not observed			0.8037	0.121776	m
026	Not observed			0.8486	0.121349	m
333	Not observed			0.8680	0.122952	m
117	Not observed			0.9126	0.119910	w
040	Not observed			0.9431	0.117938	m
620	Not observed			0.9704	0.116284	st

\*KEY: vw = very very weak; w = very weak; m = medium; st = strong; st = very strong

**Table 2.5: Edshammar's RuAl<sub>1.5</sub> Guinier powder pattern (CuK $\alpha$ ) - annealed at 1100°C<sup>[9]</sup>.**

$I_{\text{obs}}$	$\sin^2\theta_{\text{obs}}$	$h\ k\ l$
weak	0.01160	0 0 2
medium	0.04630	0 0 4
strong	0.06547	1 0 1
medium	0.08856	1 0 3
strong	0.12517	1 1 0
very strong	0.13483	1 0 5
medium	0.17140	1 1 4

Both Edshammar<sup>[9]</sup> and Schwomma<sup>[7]</sup> published diffraction data for the compound RuAl<sub>1.5</sub> (Table 2.6). These two workers reported that the phase has a TiSi<sub>2</sub> structure type with  $R\bar{3}m$  symmetry. Schwomma's data is similar to that obtained by Edshammar, the only noticeable exception being the (8 1 3) plane in Edshammar's data which occurs in the same position in the table as the (3 1 3) plane in Schwomma's results. It appears that the reported (8 1 3) plane is a misprint of (3 1 3) for two reasons. Firstly, the former is a very high index line and should thus be reported much later in the table. (The lines usually appear in approximate ascending order of  $(h^2 + k^2 + l^2)$ ). Secondly, the plane spacing ( $d$ ) was calculated for both sets of indices, and only that of (3 1 3) matched with the observed value. The rest of the  $(h\ k\ l)$  values are in agreement, but the  $\sin^2\theta$  values do not match, because different radiations were used. The plane spacings were calculated from the observed  $\sin^2\theta$  values, and these were a very close match for the two sets of data (Table 2.6). Most of the reported intensity estimations are the same or similar. The lack of higher order peaks in Edshammar's data is possibly due to the technique which was employed.

Table 2.4: Edshammar's  $\text{Ru}_4\text{Al}_{13}$  Guinier powder pattern ( $\text{CuK}\alpha_1$ )<sup>[8]</sup>.

$hkl$	$\sin^2\theta_{\text{obs}}$	$I_{\text{obs}}$
110	0.01144	very weak
111	0.01348	weak
111	0.01747	weak
201	0.01839	very very weak
202	0.01859	very weak
202	0.03442	strong
203	0.03452	strong
020	0.03438	medium
003	0.03626	strong
401	0.03773	medium
021	0.03946	very weak
400	0.04164	strong
402	0.04194	strong
220/221	~0.04582*	very strong
022	0.05154	strong
401/113/221/224/03	~0.05380	very strong
203	0.05854	very weak
204	0.05912	very weak
004	0.06458	very weak
222	0.06982	very weak
223	0.07026	very weak
023	0.01775	very weak

Edshammar again calculated  $\sin^2\theta$  values for the  $\text{RuAl}_{13}$  compound, and found good agreement with those observed<sup>[8]</sup>.

---

\*Edshammar displayed some values as approximates since they were an average reflection from a number of planes

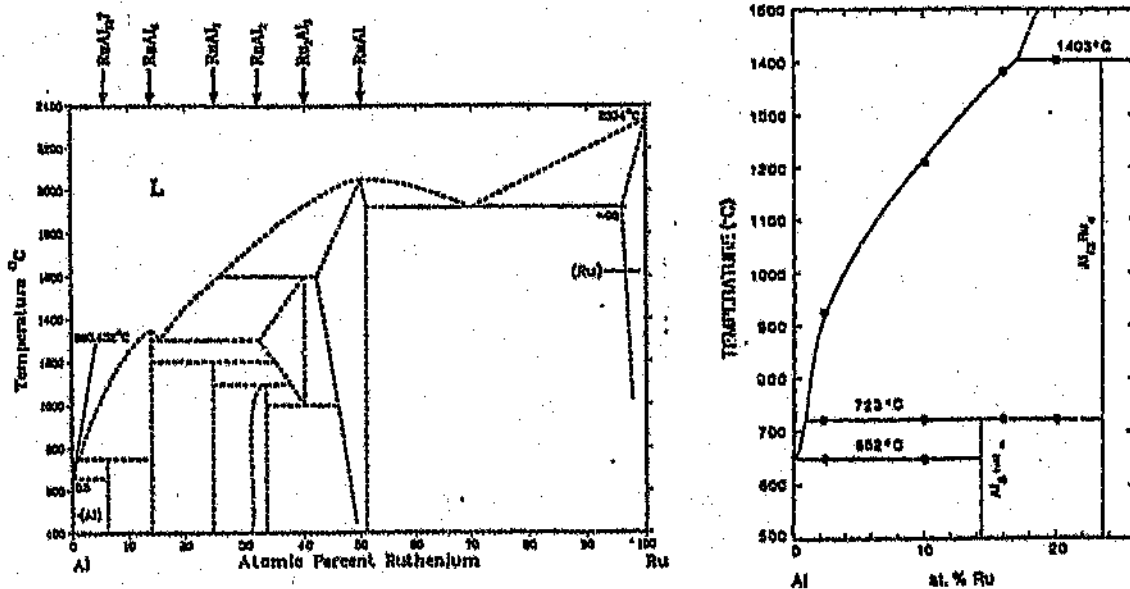
Obrowski<sup>[6]</sup>, Edshammar<sup>[8,9]</sup>, and Schwomma<sup>[7]</sup> undertook structural studies of the compounds formed in the ruthenium-aluminum system. Edshammar used a Guinier focusing camera with  $\text{CuK}\alpha_1$  radiation to determine the cell dimensions of the compounds, and employed the rotating crystal method in a Weissenberg camera with molybdenum  $\text{K}$  radiation to investigate the symmetry in the lattice structures<sup>[8,9]</sup>. Schwomma<sup>[7]</sup> also used a rotating crystal method for his study of  $\text{RuAl}_2$ , but made use of chromium  $\text{K}\alpha$  radiation.

The powder diffraction pattern of  $\text{Ru}_4\text{Al}_{13}$ , as observed by Edshammar<sup>[8]</sup>, is given in Table 2.4. Only those reflections which he actually observed have been reported here. Edshammar calculated  $\sin^2\theta$  and intensity values for this pattern, and there was very good agreement between the observed and calculated values. He predicted the space group of this compound to be  $\text{C2/m}$  and also predicted the interatomic distances in the lattice.

The last  $\sin^2\theta$  value does not fit the trend of the other values in Table 2.4. The calculated value (from the Miller indices) is 0.07170, thus the former is thought to be a misprint of 0.07175.

Edshammar attempted to obtain a single-phase sample of  $\text{Ru}_2\text{Al}_3$  ( $\text{RuAl}_{1.5}$ ) by annealing an alloy containing 40 at% Ru at 800-1200°C<sup>[9]</sup>. According to Obrowski's phase diagram, heat treatment of this alloy above 1000°C should have resulted in the desired microstructure. However, Edshammar's attempts were unsuccessful, and the diffraction pattern of  $\text{Ru}_2\text{Al}_3$  (Table 2.5) was obtained after subtracting the spectrum of the still-present  $\text{RuAl}_2$ .

Figure 2.4: Variations of the Al-rich end of the Phase Diagram.



## 2.2 Lattice Parameters

The structures and parameters of the elemental components are shown in Table 2.3. The d-spacings can be found in Appendix XX.

Table 2.3: Crystallographic data of the elements<sup>[12]</sup>.

ELEMENT		Ru	Al
STRUCTURE		Close packed hexagonal	Face centred cubic
LATTICE PARAMETER (nm)	a	0.27058	0.40494
	c	0.42819	

phases are beyond the scope of this investigation, and will not be discussed any further.

Anlage undertook Differential Scanning Calorimeter (DSC) measurements on four alloys to obtain the reaction temperatures. At various compositions he identified peaks corresponding to the stable ( $L \rightarrow \text{RuAl}_6 + \text{Al-rich}$ ) eutectic at  $652^\circ\text{C}$ , the peritectic reaction  $L + \text{Ru}_4\text{Al}_{15} \rightarrow \text{RuAl}_6$  ( $723^\circ\text{C}$ ), and for the liquidus. At faster cooling rates of  $20 \text{ K min}^{-1}$  (as opposed to  $10 \text{ K min}^{-1}$ ),  $\text{RuAl}_6$  could not form peritectically, and instead formed by a eutectic reaction at  $652^\circ\text{C}$ . He differentiated between peritectic reactions and crossing of the liquidus by the shape of the peaks, and their presence or absence on heating and cooling. He assumed that on heating an alloy, the liquidus line would be missed because the amount of the melting species would decrease steadily to zero, and so no discernable final reaction could occur. On cooling there would be a continuous deflection starting at the liquidus and ending when solidification was complete. Conversely, a peritectic reaction would always be present, on both heating and cooling, and would have a distinct sharp peak. From these deductions he was able to identify the peak at  $1403^\circ\text{C}$  as being a peritectic peak (after his alloy was pre-annealed at this temperature).

Anlage's diagram and the aluminium rich end of Obrowski's diagram are shown together in Figure 2.4 for ease of comparison.

Anlage employed scanning electron microscopy, X-ray diffraction, and thermal analysis to determine his phase diagram. The phase diagram depicts the formation of  $\text{Ru}_4\text{Al}_{13}$  at  $1403^\circ\text{C}$  via a peritectic reaction; the peritectic formation of  $\text{RuAl}_6$  at  $723^\circ\text{C}$  from  $\text{Ru}_4\text{Al}_{13}$ ; and a eutectic reaction between  $\text{RuAl}_6$  and Al at  $652^\circ\text{C}$ . Accordingly, all of his alloys below 20 at% Ru contained the phases  $\text{Ru}_4\text{Al}_{13}$ ,  $\text{RuAl}_6$ , and Al. The phase analyses were obtained using standardless energy dispersive X-ray (EDX) analysis. He found that  $\text{Ru}_4\text{Al}_{13}$  contained 24.1 at% Ru and  $\text{RuAl}_6$  contained 15.9 at% Ru, and assumed the stoichiometric compositions of 23.6 and 14.3 at% Ru for  $\text{Ru}_4\text{Al}_{13}$  and  $\text{RuAl}_6$  respectively (Figure 2.3). The sample containing 10 at% Ru contained needles of  $\text{Ru}_4\text{Al}_{13}$  with a peritectic layer of  $\text{RuAl}_6$  around them, when cooled at 1 K per minute<sup>[3]</sup>. However, when cooled at 20 K per minute, the  $\text{RuAl}_6$  had not formed around the needles. Anlage concluded that the "formation of  $\text{RuAl}_6$  is a very sluggish reaction which is bypassed at the cooling rate of  $20\text{ K min}^{-1}$ "<sup>[5]</sup>. He stated that the peritectic growth of the  $\text{RuAl}_6$  phase was continuous, and that of  $\text{Ru}_4\text{Al}_{13}$  is along atomic ledges. The different growth mechanisms provide different morphologies to the phases; hence  $\text{Ru}_4\text{Al}_{13}$  is faceted and  $\text{RuAl}_6$  is non-faceted (allotriomorphic). The phase  $\text{RuAl}_{12}$  was not observed in this investigation, even at very slow cooling rates of 1 K per min.

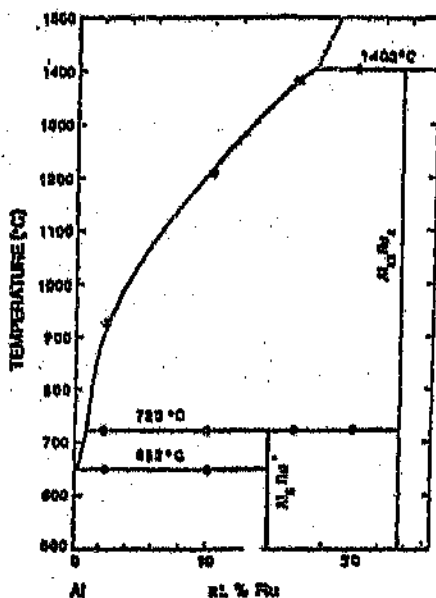
It is interesting to note that Anlage admitted the difficulty in obtaining homogeneity in his alloys. The Al-rich solid solution was present in some higher Ru content alloys (20 at% Ru), and  $\text{Ru}_4\text{Al}_{13}$  was also found where it should have been decomposed peritectically ( $\text{L} + \text{Ru}_4\text{Al}_{13} \rightarrow \text{RuAl}_6$ ). Anlage states that in his mechanical alloyed powders he detected the presence of an amorphous metastable phase<sup>[5]</sup>. He also reports the formation of icosahedral phases in the region 2.4 to 23.5 at% Ru by rapid solidification<sup>[5]</sup>. However, these metastable



hours and quenched in water. In his conclusions he stated that "the metastable  $\text{Al}_3\text{Ru}$  phase was observed in the alloys"<sup>[11]</sup>. He presumed that  $\text{RuAl}_3$  was metastable on the basis of Obrowski's work. Varich found that, when cooling from  $1400^\circ\text{C}$  at  $10^6 \text{ deg.s}^{-1}$ , the solubility of Ru in the Al-rich solid solution increases linearly with composition to a maximum of 3.23 at% Ru. Maximum solubility as a result of superheat was obtained at  $1360^\circ\text{C}$ . Varich also reported that the metastable solid solutions have high bond forces, and thus have "considerable thermal stability"<sup>[11]</sup>.

In 1988 Anlage<sup>[5]</sup> stated that the Al-rich end of Obrowski's phase diagram is incorrect, and proposed modifications for the region below 26 at% Ru (Figure 2.3).

Figure 2.3: Phase diagram proposed by Anlage<sup>[5]</sup>.



Additionally, the formation of  $\text{Ru}_2\text{Al}_3$  during heat treatment also indicates a greater stability than Obrowski's reported lower limit of  $\sim 1000^\circ\text{C}^{[4]}$ . The samples containing 14 at% and 20 at% Ru consisted only of  $\text{Ru}_4\text{Al}_{13}$  and Al after arc-melting. According to Obrowski's phase diagram one would expect to observe  $\text{RuAl}_6$  and possibly  $\text{RuAl}_{12}$  in these samples as well. Edshammar's results may reflect lower temperatures of formation for  $\text{RuAl}_6$  and  $\text{RuAl}_{12}$  than was suspected by Obrowski, which renders them more difficult to form with the given heat treatment. Edshammar also claims to have observed "one or more additional CaCl-like phases around the composition  $\text{RuAl}^{[19]}$  in samples heat treated between  $800^\circ\text{C}$  and  $1200^\circ\text{C}$ , but no comprehensive X-ray data was reported. He suggested that further work at about  $1000^\circ\text{C}$  was necessary to deduce the phase relationships in the central part of the phase diagram. He thought that part of the problem with interpretation could be due to slow reactions and possible contamination of the samples.

In 1968 Edshammar extended his investigation of the Ru-Al system to incorporate the phase  $\text{RuAl}_6^{[10]}$ . His samples contained less than 23 at% Ru and were arc-melted, annealed at  $660^\circ\text{C}$ , and then water-quenched. The phases  $\text{Ru}_4\text{Al}_{13}$ ,  $\text{RuAl}_6$ , and the Al-rich solid solution were observed, but the samples did not contain  $\text{RuAl}_{12}$ . This may be because the temperature of formation of  $\text{RuAl}_{12}$  is actually lower than Obrowski proposed, or because the phase does not exist.

In 1973 Varich<sup>[11]</sup> conducted an investigation into the effects of rapid solidification on the solubility in Ru-Al alloys. He used alloys containing less than 4.16 at% Ru and cooled them at  $10^4 \text{ deg.s}^{-1}$ . Varich determined the equilibrium solubility of Ru in Al to be less than 0.03 at%. This value was obtained from samples which had been annealed at  $650^\circ\text{C}$  for 50

It can be seen that  $\text{Ru}_2\text{Al}_3$  is not present in any of the arc-melted samples, but formed after the anneal at  $950^\circ\text{C}$  in samples between 36.36 - 44.44 at% Ru. In his text<sup>[9]</sup>, Edshammar ambiguously states that  $\text{Ru}_2\text{Al}_3$  (initially described as  $\text{RuAl}_{1.5}$ ) was formed in heat treated alloys that had previously contained  $\text{RuAl}_{2.5}$  upon quenching, which suggests a direct transformation between these two intermetallic phases. His table of samples, however, does not reflect such a transformation.

The  $\text{RuAl}_2$  phase was found to form (where it had not existed before) in alloys in the range 27 - 30.77 at% Ru. It appeared to be stable over a wide range of temperatures (i.e. found before and after heat treatment) between 33.33 and 44.44 at% Ru. The phase  $\text{RuAl}_{2.5}$  was found in the arc-melted samples in the composition range 27 - 33.33 at% Ru. Some phases found in the arc-melted samples disappeared with the heat treatment. These included:  $\text{RuAl}$  (sometimes),  $\text{RuAl}_{2.5}$ , and  $\text{Ru}_4\text{Al}_{13}$ . The last phase,  $\text{Ru}_4\text{Al}_{13}$ , is formed over a wide composition range of 14 - 33.33 at% Ru, whereas  $\text{RuAl}_{2.5}$  is formed only between 27 and 33.33 at% Ru, according to this investigation. It is important to realise that the composition ranges quoted above are not the absolute limits of the phase fields, but only the compositions of the alloys in this particular work.

The changes in structure are due to reactions and transformations, and these should be consistent with the Ru-Al phase diagram. The phases observed in the samples containing 36.36 at% to 66.67 at% Ru, prior to heat treatment, agree with Obrowski's phase diagram (Figure 2.2). However, the phase  $\text{Ru}_2\text{Al}_3$  was not observed in the arc-melted samples, whereas Obrowski's phase diagram shows its peritectic formation at about  $1600^\circ\text{C}$ . Thus one would expect to observe this phase in as-cast samples of the appropriate compositions.

Table 2.2: Edshammar's Samples<sup>[9]</sup>.

Atomic % Ru	Phases identified after arc-melting	Phases identified after 1 week at 950°C
66.67	Ru RuAl	No heat treatment
57.14	Ru RuAl	No heat treatment
50	RuAl	No heat treatment
44.44	RuAl RuAl <sub>2</sub>	RuAl? <sup>*</sup> Ru <sub>2</sub> Al <sub>3</sub> RuAl <sub>2</sub>
40	RuAl RuAl <sub>2</sub>	Ru <sub>2</sub> Al <sub>3</sub> RuAl <sub>2</sub> RuAl?
36.36	RuAl <sub>2</sub> RuAl	RuAl <sub>2</sub> Ru <sub>2</sub> Al <sub>3</sub>
33.33	RuAl <sub>2</sub> Trace RuAl <sub>2.5</sub> Trace Ru <sub>4</sub> Al <sub>13</sub>	RuAl <sub>2</sub>
30.77	RuAl <sub>2.5</sub> Ru <sub>4</sub> Al <sub>13</sub> Trace RuAl <sub>2</sub>	RuAl <sub>2</sub>
28.57	RuAl <sub>2.5</sub> Ru <sub>4</sub> Al <sub>13</sub>	RuAl <sub>2</sub> Trace Ru <sub>4</sub> Al <sub>13</sub>
27	RuAl <sub>2.5</sub> Ru <sub>4</sub> Al <sub>13</sub>	RuAl <sub>2</sub> Ru <sub>4</sub> Al <sub>13</sub>
25	Ru <sub>4</sub> Al <sub>13</sub>	Ru <sub>4</sub> Al <sub>13</sub>
20	Ru <sub>4</sub> Al <sub>13</sub> Al	No heat treatment
14	Ru <sub>4</sub> Al <sub>13</sub> Al	No heat treatment

<sup>\*</sup>RuAl? refers to "CsCl-like phases"<sup>[9]</sup> which Edshammar identified from the sample powder diffraction patterns.

containing equal quantities of potassium chloride and sodium chloride (which had previously been tested on pure aluminium) was poured over the alumina pellets and ruthenium powder. The furnace was preheated to 1200°C and the crucible was inserted for about 10 minutes. The crucible was then transferred to another furnace which had been preheated to 1000°C and was furnace cooled to approximately 750°C before water-quenching.

### 3.1.6 Sinter - Hot Isostatic Pressing (HIP) technique

Another sample,  $Ru_{12}Al_{12}$ -b, was produced by melting aluminium pellets and compacted Ru powder in a zirconia crucible with an argon overpressure. The reason for applying a high pressure was to attempt to reduce the loss of aluminium by vaporisation. The charge was heated to 1520°C with an argon overpressure of 1 bar (750 torr). After 30 minutes at temperature, the overpressure was increased to 45 bar (33753 torr) and the temperature was held for another 30 minutes. The temperature was then reduced to 1100°C, which, according to Obrowski's phase diagram (Figure 2.2), is in the solid state region for this composition. This temperature was also held for an hour and the sample was furnace cooled. The applied pressure was only diminished once cooling was complete.

### 3.1.7 Induction furnace method

The alloy  $Ru_{12}Al_{12}$ -a was produced in an induction furnace in an argon atmosphere. The aluminium pellets were rolled into discs and placed in a zirconia crucible and the ruthenium powder was sprinkled between the discs. The crucible was inserted into a graphite susceptor

exothermic reaction, into a structure which was stable at the high temperatures reached (about 1400°C). Just after the reaction had occurred, argon was released into the chamber. The pressure was 400 mbar (300 torr) when the maximum temperature was reached. After furnace-cooling, the product was found to be fragile and dissociated, and was thus unsuitable as a sample in this investigation.

Since this procedure did not yield satisfactory results, the product of this method was subsequently remelted in an electric arc furnace. The furnace chamber was pumped out to  $1 \times 10^{-2}$  torr and flushed with argon twice. It was then filled with argon to just below atmospheric pressure (760 torr). Titanium was again used as an oxygen and nitrogen getter. The compact was then heated on the copper hearth and the current was slowly increased until it melted. The compact was then inverted and remelted. This sample was again arc-melted at a later stage to heal a crack, which was produced while attempting to introduce strain into the sample for an upset-annealing procedure.

### 3.1.5 Muffle furnace technique

A sample of approximate nominal composition  $\text{Ru:Al}_{12}$  was produced in a muffle furnace without a protective atmosphere. The charge consisted of an unusable Ru-Al alloy and the appropriate amount of aluminum powder. These were placed in an alumina crucible and heated to 1200°C. The crucible was held at temperature for 10 minutes, furnace cooled to 800°C, and then air cooled to room temperature.

The sample  $\text{Ru}_{41}\text{Al}_{98}\text{-b}$  was melted in an alumina crucible in a muffle furnace. A flux

exhibited low surface tension by flattening and cracking upon cooling.

### 3.1.3 Liquid-phase sintering method

The samples of nominal atomic compositions  $\text{Ru}_3\text{Al}_7$  (alloy b) and  $\text{Ru}_7\text{Al}_{23}$  were consolidated by liquid-phase sintering in a vacuum furnace. The aluminium and ruthenium powders were mixed together and this mixture was compressed in a 20 mm diameter die. A force of 50 kN was applied to the samples. The powders in the die were compacted for a period of 5 minutes. In each case titanium turnings were placed in the tube of the furnace with the sample (to act as a nitrogen and oxygen getter), and the tube was evacuated to  $3 \times 10^{-2}$  torr and flushed with argon thrice, prior to the final evacuation. The sample containing 3 at% Ru was held at 700°C for an hour and then furnace cooled. The other sample was held at 800°C for an hour and then cooled at 1°C per min to 720°C before furnace-cooling. This treatment was applied to the second sample in order to facilitate the formation of  $\text{RuAl}_{12}$  as predicted by Obrowski's phase diagram (Figure 2.2).

### 3.1.4 Graphite resistance furnace method

One sample (nominal  $\text{Ru}_{18}\text{Al}_{22}$ -a) was initially melted in a graphite resistance furnace. The ruthenium powder was compressed in 20 mm diameter die at 100 kN for 1 minute and then placed on top of aluminium pellets in an alumina crucible. The crucible was then placed in a graphite resistance furnace. The furnace was evacuated, flushed twice with argon, and then evacuated to  $1 \times 10^{-4}$  mbar ( $7.5 \times 10^{-3}$  torr). The temperature was estimated using an optical pyrometer. At a fairly low temperature (about 900°C), the two metals fused, via an

### 3.1.2 Improved arc-melting procedure

The arc-melting procedure was improved by altering the technique employed. Instead of mixing the elements before melting, the elements were melted separately using the procedure described above. This allowed the use of aluminium pellets rather than oxidised powder particles. The ruthenium button was then placed on top of the aluminium button and the Ru was remelted. The higher melting point of ruthenium meant that by the time it was molten, so was the aluminium. The heavier ruthenium then dropped into, and mixed with, the aluminium. The button was then inverted and remelted. Some aluminium vaporisation still occurred, but the extent of this phenomenon was greatly reduced.

The samples of nominal compositions  $\text{Ru}_{32}:\text{Al}_{68}$ ,  $\text{Ru}_{23.3}:\text{Al}_{71.7}$ ,  $\text{Ru}_{37}:\text{Al}_{63}$  and  $\text{Ru}:\text{Al}_3$  were made in a batch using the improved arc-melting procedure. For this purpose the ruthenium powder was first compacted in a 20 mm diameter die for 1 minute at 100 kN.  $\text{Ru}:\text{Al}_3$  and  $\text{Ru}_{37}:\text{Al}_{63}$  were inverted and remelted once, but the other samples had to be remelted twice since they had lower surface tension and thus flattened and cracked extensively upon cooling. Of the remelted samples,  $\text{Ru}_{32}:\text{Al}_{68}$  appeared to have the better surface tension.  $\text{Ru}_{23.3}:\text{Al}_{71.7}$  was the first sample of the batch.

Chunks of aluminium were used in the next batch of samples. The ruthenium powder was compacted and then placed on top of the aluminium in the button-arc furnace. The samples were melted once to initiate fusion, and then melted again to ensure complete reaction of the elements. An argon atmosphere of the same pressure was used. The samples made using this technique were nominally  $\text{Ru}_4:\text{Al}_{96-\alpha}$ ,  $\text{Ru}_{15}:\text{Al}_{90}$ ,  $\text{Ru}_{20}:\text{Al}_{80}$ , and  $\text{Ru}_{23}:\text{Al}_{72}$ ,  $\text{Ru}_{28}:\text{Al}_{72}$ .



### 3.1.1 Button-arc furnace method

The aluminium and ruthenium powders were mixed together for 5 minutes, and this mixture was compressed in a 20 mm diameter die. A force of 180 kN was applied and the powders in the die were compacted for a period of 5 minutes.

The first two samples (of nominal atomic compositions\*  $\text{Ru}_{20}\text{Al}_{30}$  and  $\text{Ru}_{47}\text{Al}_{53}$ ) were produced using a button arc furnace. The furnace chamber was pumped out to  $1 \times 10^{-2}$  torr and flushed with argon twice. It was then filled with argon to just below atmospheric pressure. A low current was initially supplied to melt a piece of titanium and keep it molten for 1 minute to remove any remaining oxygen and nitrogen. The compact was then heated on the copper hearth and the current was slowly increased until it melted. The maximum current was high, because much heat was required to melt the oxide surrounding the aluminium particles. A slow exothermic reaction occurred. The compact was then inverted and remelted.

The next sample,  $\text{Ru}_{31}\text{Al}_{69}\text{-a}$ \* was also produced by arc-melting mixed elemental powders. It must be noted here that the aluminium powder was only 95% pure. The aluminium and ruthenium powders were mixed together for 5 minutes, and this mixture was compressed in a 20 mm diameter die for 5 minutes at 50 kN. The compact was then melted three times in an electric arc furnace using the same procedure described previously.

---

\* All compositions are expressed in atomic percentages.

pure. Table 3.1 gives a list of the samples and the form of aluminium used in their production.

**Table 3.1: Sample list and form of aluminium.**

ALLOY	$Ru_3:Al_{97}-a^*$	$Ru_3:Al_{97}-b$	$Ru_4:Al_{96}-a$	$Ru_4:Al_{96}-b$	$Ru:Al_{12}$
FORM OF Al	Powder	Powder	Chunks	Pellets	Unknown**

ALLOY	$Ru_7:Al_{93}$	$Ru_{10}:Al_{90}$	$Ru_{18}:Al_{82}-a$	$Ru_{18}:Al_{82}-b$	$Ru_{20}:Al_{80}$
FORM OF Al	Powder	Chunks	Pellets	Pellets	Chunks

ALLOY	$Ru:Al_3$	$Ru_{25}:Al_{75}$	$Ru_{25.2}:Al_{74.7}$	$Ru_{32}:Al_{68}$	$Ru_{33}:Al_{67}-a$
FORM OF Al	Pellets	Chunks	Pellets	Pellets	Pellets

ALLOY	$Ru_{35}:Al_{65}-b$	$Ru_{37}:Al_{63}$	$Ru_{47}:Al_{53}$	$Ru_{50}:Al_{50}$
FORM OF Al	Chunks	Pellets	Unknown**	Unknown

The production methods which were investigated are discussed separately in the sections which follow.

---

\*This convention is employed to distinguish between different samples of the same nominal composition

\*\*This sample was produced independently at MINTEK

### **3 EXPERIMENTAL PROCEDURE**

#### **3.1 Production of the Alloys**

Many different production methods were used in an attempt to optimise the quality of the samples. The aims were to minimise chemical segregation and maximise the purity of the samples. The large difference in the melting points of ruthenium and aluminium provides the basis of the production problems - aluminium melts at 660°C and ruthenium at 2334°C. High temperatures are required to produce most of the alloys of this system due to the high melting point of ruthenium. However, aluminium oxidises readily at elevated temperatures, and so an inert atmosphere or vacuum must be used. Aluminium also has a high partial pressure and thus vaporises readily; hence the alloys should not be melted under vacuum. The extent of vaporisation can be reduced by employing an inert atmosphere. Even with a backfill pressure, the aluminium still tends to vaporise at the temperatures used, altering the composition of the alloys. Ruthenium's high melting point means that diffusion of this species will only occur readily at high temperatures. An additional problem is that RuAl appears to form readily and be very stable, which also spoils the homogeneity of these alloys.

The samples were mainly produced from the elements. The ruthenium was in powder form, whereas the aluminium was used in three forms. The purity of the aluminium powder initially available was unfortunately 95%, which is not ideal for phase diagram investigation, but that of the chunks was 99.99%, and the purity of the pellets was unknown, but estimated to be 99% pure. The ruthenium powder was never less than 99.5%

problems with silicon and oxygen. Edshammar<sup>[5]</sup> also had some samples, even after heat treatment, with more than the two phases required for an equilibrated binary alloy. Even Anlage<sup>[5]</sup> commented on the presence of the aluminium-rich solid solution, and the retention of the Al-rich solid and  $\text{Ru}_4\text{Al}_{13}$  phases where they were not energetically favourable according to the phase diagram.

Obrowski<sup>[4]</sup> melted his materials in a high frequency induction furnace with an argon atmosphere. A frequency of 1MHz was applied for a period of 2 minutes to limit loss of material by evaporation. Zirconia crucibles were used for the alloys with high melting points, and the others were melted in alumina crucibles. Various unspecified heat treatments were employed after production.

Schwomma<sup>[7]</sup> did not disclose the technique used to produce his samples.

Edshammar<sup>[8,9,10]</sup> melted Ru powder and Al ribbon together in an electric arc furnace under an argon atmosphere. The samples were cooled rapidly<sup>[9]</sup> because a furnace with a water-cooled copper base was used. The samples were then sealed in evacuated silica tubes and heat treated. Tantalum foils were used to prevent the samples from reacting with the silica. Some of the samples were annealed at 950°C for 1 week<sup>[9]</sup> and others at 660°C for 1 day<sup>[10]</sup> prior to quenching in water.

Anlage<sup>[5]</sup> went to great lengths to deoxidise his Ru powder and Al rods. The ruthenium powder was compacted, melted, and then crushed to obtain a coarse powder. The aluminium rods were etched to remove the oxide layer. Both metals were then heated in an alumina crucible which had been placed in a glove box containing argon. The samples were furnace-cooled and then powdered, either by mechanical alloying or in a ceramic mortar and pestle.

It is noteworthy that several authors had difficulty in producing equilibrated structures. Obrowski<sup>[4]</sup> had three phases in at least three of his alloys. Schwomma<sup>[7]</sup> reported possible

of the latter (which it should be if  $\text{RuAl}_{12}$  is derived from the aluminium lattice).

The  $\text{Ru}_4\text{Al}_{13}$  and  $\text{RuAl}_5$  phases appear to be the same phase (only one or the other is reported in each phase diagram, and the compositions are similar). These phases not only have different structures attributed to them, but apart from one parameter (value roughly 1.60 nm) are seen to have different parameters too. It is also to be noted that both structures have two normal axes, and one axis angle which is greater than  $90^\circ$ .

Only Edshammar<sup>9,10</sup> determined a structure and parameters for  $\text{RuAl}_6$  (Table 2.10), whereas for  $\text{Ru}_2\text{Al}_3$  two different structures and two disagreeing sets of parameters were reported. There is a discrepancy with the angles between the axes; tetragonal structures have axes which are all normal to each other, and in hexagonal structures there are two angles of  $90^\circ$  and one of  $120^\circ$ .

Varich<sup>11</sup> found that rapid solidification of Al-Ru alloys decreased the f.c.c. (Al-rich solid solution) lattice parameter from 0.4049 nm to 0.4020 nm as the solubility of Ru in Al increased. He conducted the X-ray diffraction experiments using copper  $K\alpha$  radiation.

### 2.3 Production Techniques

A wide variety of production techniques were employed by the different workers. The distinct possibility exists that the production affects the homogeneity of the phases produced, and thus the particular worker's perception of the phase diagram.

the same structure for  $\text{RuAl}_2$  and their parameter values are in good agreement. Obrowski found this phase to have a different structure, and only one of his reported lattice parameters is near those found by the other investigators.

Table 2.10: Lattice parameters as reported by Obrowski and Edshammar.

PHASE	LATTICE PARAMETER (nm)	
	Obrowski <sup>[4]</sup> (1963)	Edshammar <sup>[9,10]</sup> (1965-68)
$\text{RuAl}_6$ Space Group a b c	Could not determine	Orthorhombic $\text{MnAl}_6$ type Cnrm $0.74882 \pm 0.4$ $0.65559 \pm 0.3$ $0.89605 \pm 0.5$
$\text{RuAl}_3$ ( $\text{Ru}_4\text{Al}_{12}$ ) Space Group a b c c/a $\beta$	Hexagonal $\text{TiNi}_3$ type $\text{P6}_3/\text{mmc}$ 0.481 (= a) 0.784* 1.63	c. monoclinic $\text{Fe}_4\text{Al}_{13}$ type $\text{C2/m}$ $1.5862 \pm 0.0006$ $0.8188 \pm 0.0003$ $1.2736 \pm 0.0004$ $107.77^\circ \pm 0.08$
$\text{RuAl}_{12}$ a	P. cubic with substructure 0.812	Not detected

Obrowski found the phase  $\text{RuAl}_{12}$  to have "a complex structure"<sup>[4]</sup>. He stated that it "seems to be primitive cubic with a substructure with a  $\sim 8.12 \text{ \AA}$ "<sup>[4]</sup>. This value does not appear to be particularly related to the size of the unit cell of Al, since it is not related to a multiple

\*Calculated from the other values

in Tables 2.9 and 2.10. It can be seen that there is only agreement for the cubic RuAl structure. Although Edshammar<sup>[9]</sup> reported possible variations in this structure between 800 and 1200°C, he only reported a single set of parameters. The disagreements for the other structures could be due to differing interpretations due to orientation effects. However, there appear to be major inconsistencies in the angles between the major axes, which are not due to the relative orientation, and does perhaps suggest that different structures may exist.

Table 2.9: Lattice parameters as reported by Obrowski, Edshammar, and Schwomma.

PHASE	LATTICE PARAMETER (nm)		
	Obrowski <sup>[4]</sup> (1963)	Edshammar <sup>[8,9]</sup> (1965-68)	Schwomma <sup>[7]</sup> (1963)
RuAl Space group a	Cubic CsCl type Pm3m 0.303	Cubic CsCl type Pm3m 0.295	Cubic CsCl type Pm3m
RuAl <sub>2</sub> Space group a b c c/a	b.c. tetragonal CaC <sub>2</sub> type I4/mmm 0.440 → 0.446 (= a) 0.638 → 0.656* 1.45 → 1.47	f.c. orthorhombic TiSi <sub>2</sub> type Fddd 0.8012 ± 0.0002 0.4717 ± 0.0001 0.8785 ± 0.0002	f.c. orthorhombic TiSi <sub>2</sub> type Fddd 0.8015 0.4715 0.8780
Ru <sub>2</sub> Al <sub>3</sub> Space group a c c/a	Hexagonal Ni <sub>2</sub> Al <sub>3</sub> type P3m1 0.405 → 0.407 0.494 → 0.537* 1.22 → 1.32	Tetragonal Os <sub>2</sub> Al <sub>3</sub> type I4/mmm 0.3079 ± 0.0002 1.433 ± 0.001 4.65	

The reported parameters of RuAl are similar. Edshammar<sup>[8,9]</sup> and Schwomma<sup>[7]</sup> interpreted

\*Calculated from the other values



### Nominal Ru<sub>3</sub>:Al<sub>7</sub>-b

Prior to heat treatment this sample appeared to consist of two phases. Much porosity was observed in the sample as a result of the production method. Initially the alloy appeared to be homogeneous (Figure 4.2), even though the discrete RuAl<sub>6</sub> phase was irregular and disseminated. Unfortunately, silicon and iron were present, which limited the use of this alloy in this investigation. The matrix consisted of the Al-rich solid solution (Table 4.2).

Figure 4.2: SEM micrograph of (contaminated) nominal Ru<sub>3</sub>:Al<sub>7</sub>-b before heat treatment (secondary electron mode). RuAl<sub>6</sub> in an Al-rich matrix. Micron marker: 50μm.



Figure 4.1: Optical micrograph of (contaminated) nominal  $\text{Ru}_3\text{Al}_{17}$ -a (528 hours at  $550^\circ\text{C}$ ).  
 $\text{RuAl}_6$  "needles" in an Al-rich matrix.



Table 4.1: Average chemical analyses of nominal  $\text{Ru}_3\text{Al}_{17}$ -a (528 hours at  $550^\circ\text{C}$ ).

PHASE	Al-rich solid	$\text{RuAl}_6$
PHASE DESCRIPTION	Matrix	Discrete phase
Ru (atomic %)	$0.05 \pm 0.05$	$15.4 \pm 0.5$
Al	$99.6 \pm 0.2$	$77.50 \pm 0.08$
Si	$0.3 \pm 0.1$	$5.1 \pm 0.2$
Cr	$0.005 \pm 0.005$	$0.03 \pm 0.02$
Mn	0.0	$0.18 \pm 0.08$
Fe	$0.015 \pm 0.005$	$1.7 \pm 0.2$
Ni	0.0	$0.07 \pm 0.07$
Cu	$0.04 \pm 0.02$	$0.05 \pm 0.05$

#### 4 RESULTS FROM LOW RUTHENIUM ALLOYS

The alloys discussed in this chapter are those comprising (nominally) up to 25 at% ruthenium. According to the published phase diagrams (Figure 2.4), the phases which one would expect to observe in these samples are  $\text{Ru}_4\text{Al}_{13}$  (or  $\text{RuAl}_3$ ),  $\text{RuAl}_6$ , the Al-rich solid solution, and possibly  $\text{RuAl}_{12}$ . The results reported below were obtained from optical and SEM examination, EDAX analyses, and X-ray diffraction experiments. The latter were used to distinguish between  $\text{Ru}_4\text{Al}_{13}$  and  $\text{RuAl}_3$ .

##### Nominal $\text{Ru}_{10}\text{Al}_{70}$ -a

This sample was heat treated at 550°C for 528 hours before examining. It appeared to be two-phase, with the second phase having very different morphologies in various regions of the sample. These morphologies are depicted in Figure 4.1.

This sample was found to be of limited use in the current investigation, due to the presence of relatively large quantities of iron and silicon in the discrete phase. Smaller amounts of chromium, nickel, manganese and copper were also present in the sample. The standardless analyses are given in Table 4.1. Examples of the analyses can be found in Appendix II. It was not possible to obtain standards by which to accurately measure the compositions of the contaminated samples.

technique. After several attempts it became obvious that the samples were too porous and inhomogeneous to obtain accurate results, and very little information could be obtained from the scans, thus the use of this method was abandoned.

### 3.6 Thermal Analysis

Premier Technologies conducted an exploratory investigation of the reaction temperatures, using a TA INSTRUMENTS SDT 2960 Simultaneous TGA-DTA. Differential Thermal Analysis (DTA) experiments were conducted on nominal  $\text{Ru}_4\text{:Al}_{36}\text{-a}$  and  $\text{Ru}_{22}\text{:Al}_{72}$ . The TGA-DTA was calibrated using indium and aluminum; but the melting point of the latter was given as  $661.73^\circ\text{C}$  rather than  $660.1^\circ\text{C}$ . The alloy  $\text{Ru}_4\text{:Al}_{36}\text{-a}$  was subjected to one heating cycle, while  $\text{Ru}_{22}\text{:Al}_{72}$  was heated three times. Most of the scans employed a protective nitrogen environment, which was maintained by passing the gas through the furnace at 100ml per minute. The only exception was the third heating cycle for  $\text{Ru}_{22}\text{:Al}_{72}$ , which did not have an inert atmosphere. The maximum temperature, in most cases, was  $1480^\circ\text{C}$ , except for the first cycle for  $\text{Ru}_{22}\text{:Al}_{72}$ , which was only heated to  $850^\circ\text{C}$ . The scans were taken during heating only, and the heating and cooling rates were not recorded, but were not rapid. The results for  $\text{Ru}_4\text{:Al}_{36}\text{-a}$  were inconclusive, especially considering that it had only one heating cycle; and those for  $\text{Ru}_{22}\text{:Al}_{72}$  are given in Chapter 5.

and placed on the tip of a short bristle. The bristle was inserted into the centre of a 57.3 mm diameter Debye-Scherrer camera and aligned to be in the exact centre of the camera. X-ray film was cut and placed inside the camera, which was then attached to a PHILIPS PW X-ray generator, which had a copper anode and a nickel filter. The film was exposed for 24 hours, after which it was removed and developed. The films were compared against each other and the published data. The latter was facilitated by drawing out the published lines. The data was acquired for all of the phases from JCPDS<sup>[12]</sup> - CD ROM, except that for  $\text{RuAl}_3$ . The latter was calculated using the "CC Miller" program\* and inputting the atomic positions for its structure type ( $\text{Ni}_3\text{Ti}$ )<sup>[13]</sup>. This was undertaken to confirm the phases identified with EDAX, especially  $\text{Ru}_2\text{Al}_3$  and  $\text{RuAl}_2$  which have overlapping composition ranges (albeit at different temperatures).

### 3.5.2 Bulk sample X-ray diffraction

The resin mounts of the polished samples were melted and the samples were removed and attached to the X-ray sample-holder using plasticine. X-ray diffraction experiments were then conducted on these samples at MINTEK using a SIEMENS D500 diffractometer which had a molybdenum anode. The step size ranged from 0.02 to 0.05 degrees. The maximum angle did not exceed  $2\theta \approx 65^\circ$ . An in-run peak scan was initially employed to search for the peaks in the patterns; at a later stage a peak search was done after the scan, using updated computer software. The sample peaks were compared with the available phase data cards<sup>[12]</sup> in an attempt to confirm the results obtained using the Debye-Scherrer

---

\*A SHAREWARE package written by C.L. Churms, Somerset West, South Africa.

backscattered and secondary electron modes, and standardless semi-quantitative chemical analyses of the various distinguishable phases were carried out using Energy Dispersive Analysis of X-rays (EDAX). During the course of this work microprobe analysis became available\*, and the standardless analyses were evaluated using the  $Ru_{32}Al_{68}$  sample (being the most homogeneous, un-contaminated sample available at the time). The microprobe analyses were checked using an updated EDAX system on a JEOL JSM-840A SEM at MINTEK. These results were used to calibrate the HITACHI SEM. Hence it was then possible to obtain quantitative EDAX analyses with standards, which were more accurate than the standardless analyses. It was not possible to obtain accurate area analyses using the standards since they were only set for spot analysis conditions. In most cases the overall chemical compositions were therefore only estimated with standardless analyses.

### 3.5 X-Ray Analysis

X-ray experiments were conducted on the samples which contained only aluminium and ruthenium i.e. had no contaminants. The EDAX analyses were used to determine the appropriate alloys.

#### 3.5.1 Debye-Scherrer powder diffraction

Small quantities of powder were filed from each sample using a diamond file. Acetone was poured on to the powder and the finer particles were collected from the surface of the liquid and then dried. The fine powder was rolled into a small ball, with rubber cement,

---

\*JEOL SUPERPROBE 733 at MINTEK

### 3.3 Metallographic Preparation

Once the alloys were deemed fit for inspection, sections for metallographic study were cut from the samples using a thin circular wafering blade. These sections were then mounted in transparent resin (lucite) and ground on silicon carbide papers 220, 400, 800, and 1000. The samples were then polished to a 1 micron finish, using 1 micron diamond paste on a velvet polishing wheel.

It was initially considered unnecessary to etch the samples since the structures were revealed already. At a later stage some of the samples were etched with Murakami's reagent (10g  $K_2Fe(CN)_6$ , 10g KOH, 100ml  $H_2O$ ) to facilitate comparison with Obrowski's samples<sup>[4]</sup>. The low Ru alloys were etched for about 10 seconds, and the samples with a higher Ru content (near 50 at%) were etched for up to 30 seconds.

All polished samples were examined with the aid of an optical microscope, and micrographs were obtained using bright field illumination. The etched samples were viewed using dark field illumination in order to observe the colour changes of the phases under these conditions. The lighting was not sufficient to obtain photographs for a permanent record.

### 3.4 Scanning Electron Microscope (SEM) Studies

After observing the samples under an optical microscope, they were subjected to SEM studies using a HITACHI S-450 SEM at MINTEK. Photographs were taken in

Table 3.2: Heat treatment details of the alloys.

NOMINAL SAMPLE	TEMPERATURE (°C)	TIME (HOURS)	TYPE OF COOLING	COMMENT
Ru <sub>3</sub> Al <sub>97</sub> -a	550	528	Quench	
Ru <sub>3</sub> Al <sub>97</sub> -b	550	1176	Quench	Upset in a vice before anneal
Ru <sub>6</sub> Al <sub>94</sub> -a	475	168	Quench	To test for low-temperature reactions
Ru <sub>4</sub> Al <sub>96</sub> -b	No heat treatment			
RuAl <sub>12</sub>	No heat treatment			
Ru <sub>7</sub> Al <sub>93</sub>	550	1176	Quench	Upset in a vice before anneal
Ru <sub>10</sub> Al <sub>90</sub>	475	168	Quench	To test for low-temperature reactions
Ru <sub>18</sub> Al <sub>82</sub> -a	1200	312	Quench	Sealed in the same tube as RuAl <sub>3</sub>
Ru <sub>18</sub> Al <sub>82</sub> -b	No heat treatment			
Ru <sub>20</sub> Al <sub>80</sub>	1300 1100	6.5 65.5	Quench	The temperature was changed during treatment
RuAl <sub>3</sub>	1200	312	Quench	Sealed in the same tube as Ru <sub>18</sub> Al <sub>82</sub> -a
Ru <sub>25</sub> Al <sub>75</sub>	1300	6.5	Quench	Quartz tube expanded
Ru <sub>25</sub> Al <sub>75</sub>	1200	312	Quench	Sealed in the same tube as Ru <sub>25</sub> Al <sub>75</sub>
Ru <sub>32</sub> Al <sub>68</sub>	1200	312	Quench	Sealed in the same tube as Ru <sub>25</sub> Al <sub>75</sub>
Ru <sub>35</sub> Al <sub>65</sub> -a	No heat treatment			
Ru <sub>35</sub> Al <sub>65</sub> -am	1300 1100	6.5 65.5	Quench	The temperature was changed during treatment
Ru <sub>35</sub> Al <sub>65</sub> -b	No heat treatment			
Ru <sub>37</sub> Al <sub>63</sub>	1200 1200	168 672	Quench Quench	Two separate treatments
Ru <sub>47</sub> Al <sub>53</sub>	1200	2	Furnace	One of the first samples
Ru <sub>50</sub> Al <sub>50</sub>	1200	2	Furnace	One of the first samples



### 3.2 Heat Treatment

Homogenisation is the reduction of chemical segregation. It occurs by diffusion, and is enhanced by holding the alloy at high temperatures. Most of the samples were heat treated at various temperatures, in an attempt to homogenise the alloys, as well as to investigate the phases in equilibrium at these temperatures. To prevent any possible loss (of segregated aluminium) by oxidation, the arc-melted samples were placed in quartz ampoules which were flushed twice with argon and evacuated to a pressure of at least  $10^{-5}$  torr before sealing. The annealing treatments are listed in Table 3.2.

The annealing temperatures (Table 3.2) were chosen to lie in the particular reported solid state regions for all the samples and to facilitate batch processing. The treatment temperature did not exceed  $1300^{\circ}\text{C}$  to avoid the quartz tube being affected (quartz is annealed at about  $1400^{\circ}\text{C}$ ). Most of the samples were quenched in water after their respective heat treatments, in an attempt to preserve the structure at the annealing temperature. To this end, the tubes were removed from the furnace and broken above a water tank so that the samples were quenched as they fell in to the water.

The alloys  $\text{Ru}_{11}\text{Al}_{12}\text{-a}$  and  $\text{RuAl}_3$  had oxidised during the heat treatment, so the tube must have been improperly sealed. These samples had become friable and were coated in alumina powder.

resistance furnace and in the induction furnace, is thought to take place in samples which have a ruthenium content above a certain critical value. Fusion was not observed in the high-Al sintered samples of this investigation, but has been observed by other workers<sup>[3]</sup>. The problem encountered with the induction furnace and the graphite resistance furnace was merely that they were not capable of reaching the temperatures required to melt the fusion product.

The obvious problem with melting in a muffle furnace, without a protective atmosphere, is that of oxidation. Although the flux eradicated this problem, it introduced impurities such as chlorine into the alloy, rendering the sample less useful to the investigation.

The sinter-HIP procedure appeared to be successful in regard to macroscopic homogeneity of the sample. However the sample was rather porous and hence was mechanically weak and difficult to work with. Porosity would also have slowed down diffusion in subsequent heat treatments.

It was suggested that using laser techniques to produce these samples would be the least problematic production route. However, the necessary equipment was unavailable for the duration of this investigation.

that the result quoted for  $Ru_{47}Al_{53}$  cannot be statistically accurate since only six frames could be analysed.

The loss of aluminium by vaporisation was due to the repeated inverting and remelting of the sample during production and aluminium's high partial pressure. The remelting procedure was employed in order to ensure complete alloying of the elements. The button arc furnace has a water-cooled copper hearth, and heating the sample on this hearth led to the heat being concentrated at the top surface of the sample. Hence vaporisation of aluminium from the upper surface took place before the entire sample could reach a molten state.

The samples which were produced using the improved arc-melting procedure appeared to have a more homogeneous microstructure. This implies that the loss of aluminium from the surface of the samples was less severe due to the change in technique.

The liquid-phase sintering procedure also proved to be inadequate. The original powder particles could still be discerned in the microstructure after sintering. The liquid-phase sintering technique is not suitable for this alloy system since the procedures require more time and energy than arc-melting; and, despite repeated heat treatments, the required microstructures have not yet been attained by this method. The drawbacks of this method are mostly due to the high melting point of ruthenium, which causes it to have slow diffusion rates at the annealing temperatures employed.

The exothermic fusion of the elements, as observed during production in the graphite

in the furnace chamber. The chamber was evacuated to a pressure of 0.5 mbar (0.375 torr) and then backfilled with argon to 200 mbar (150 torr). The temperature was estimated using an optical pyrometer. Near 950°C the temperature of the sample escalated rapidly, exceeding the temperature of the crucible, and then reached an equilibrium again. It was obvious from these observations that an exothermic reaction had occurred. The maximum temperature obtained in the furnace was about 1300°C. The sample was furnace-cooled. The sample appeared to have fused to form a "tree" structure, as in previous experiments using a graphite resistance furnace. This sample was re-melted in the button-arc furnace (and then named Ru<sub>33</sub>:Al<sub>65</sub>-am) to investigate whether heating the sample to a temperature higher than 1300°C would have an effect on the microstructure of the alloy.

Another sample of the same nominal composition, Ru<sub>33</sub>:Al<sub>65</sub>-b, was made in the induction furnace using the same technique. This time, the sample was furnace-cooled as soon as the exothermic reaction had occurred, so that the products of the reaction could be investigated. Thus the alloy was not provided with ample time or heat to facilitate homogenisation, as the previous one was. The "tree" structure was formed once again.

### 3.1.8 Comparison of the production methods

The first melting technique in the button arc furnace led to macroscopic inhomogeneity. Chemical analyses of the outer two-phase regions of nominal Ru<sub>30</sub>:Al<sub>70</sub> and Ru<sub>17</sub>:Al<sub>83</sub> indicated that aluminium had been lost from the surface of these samples by vaporisation. Subsequent image analysis showed that approximately 4 at% aluminium was lost from the outer regions of each sample produced employing this method. However, it must be noted

Table 4.7: Debye-Scherrer Diffraction Data For  $\text{Ru}_4\text{Al}_9$ -a (475°C for 168 hours) (CuK $\alpha$ ).

d (OBS) (nm)	I (EST.)	PHASE	h k l	d (CALC)* (nm)
0.49159	medium	$\text{RuAl}_6$	1 1 0	0.49295
0.44892	weak	$\text{RuAl}_6$	0 0 2	0.44803
0.41031	weak	unidentified		
0.37244	weak	$\text{RuAl}_6$	2 0 0	0.37418
0.33079	medium	$\text{RuAl}_6$	1 1 2	0.33166
0.29966	strong	unidentified		
0.23443	very strong	Al	1 1 1	0.2338
0.22606	weak	$\text{RuAl}_6$	3 1 1	0.22576
0.21252	very strong	$\text{RuAl}_6$	2 2 2	0.21603
0.20750	weak	$\text{RuAl}_6$	3 1 2	0.20688
0.20296	strong	Al $\text{RuAl}_6$	2 0 0 1 1 4	0.2024 0.20396
0.17329	very very weak	unidentified		
0.15075	very weak	unidentified		
0.14407	medium	Al	2 2 0	0.1431
0.12296	strong	Al	3 1 1	0.1221
0.11770	weak	Al	2 2 2	0.1169
0.09297	very weak	Al	3 3 1	0.09289
0.09061	very weak	Al	4 2 0	0.09055
0.08273	very very weak	Al	4 2 2	0.08266
0.07850	weak	unidentified		

\*These values were taken from the JCPDS data cards<sup>[12]</sup>.

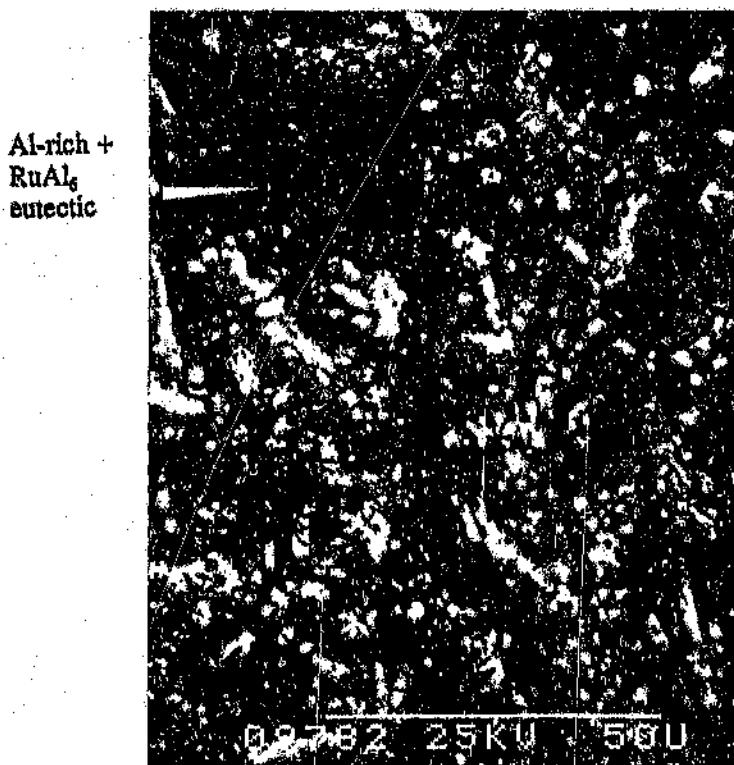
Table 4.6: Quantitative chemical analyses for nominal  $\text{Ru}_{41}\text{Al}_{59}$ -a (475°C for 168 hours).

PHASE	PHASE DESCRIPTION	ATOMIC % Ru
$\text{RuAl}$	Matrix of crystals	$48 \pm 1$
$\text{Ru}_2\text{Al}_3$	First layer	$35.5 \pm 0.4$
$\text{Ru}_4\text{Al}_{13}$	Second layer & centre of needles	$25.9 \pm 0.4$
$\text{RuAl}_6$	Third layer & needles	$16.0 \pm 0.4$
Al-rich solid	Matrix	$0.7 \pm 0.1$

Debye-Scherrer powder diffraction data (Table 4.7) confirmed the presence of  $\text{RuAl}_6$  and the Al-rich solid. The reasons for not detecting the other compounds are given in Chapter 6. The Straumanis factor was 2.5097 degrees per cm.

The inhomogeneous condition of the sample, caused by rapid cooling, precluded it from phase boundary determination. However, the phase layers were useful, since they indicate the order of formation.  $\text{RuAl}$  solidified first, followed by  $\text{Ru}_2\text{Al}_3$ ,  $\text{Ru}_4\text{Al}_{13}$ ,  $\text{RuAl}_6$ , and lastly the Al-rich solid solution. This also suggests that  $\text{Ru}_2\text{Al}_3$ ,  $\text{Ru}_4\text{Al}_{13}$ , and  $\text{RuAl}_6$  are formed via a series of peritectic reactions (in that order). There was no  $\text{RuAl}_2$  detected in this sample.

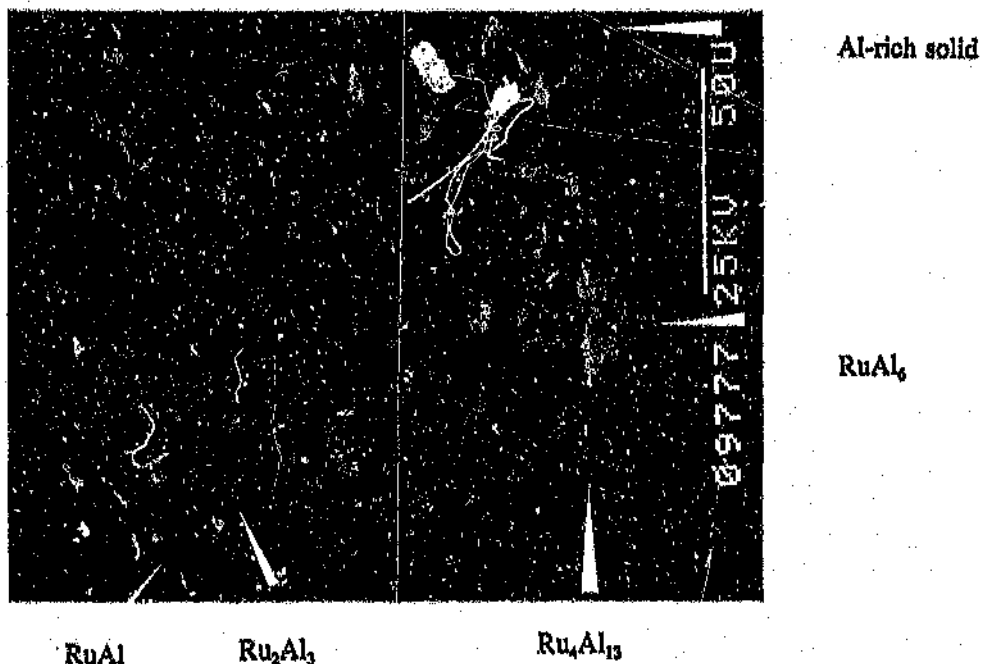
Figure 4.10: SEM micrograph of nominal  $\text{Ru}_4\text{Al}_{96}$ -a annealed at  $475^\circ\text{C}$  for 163 hours (secondary electron mode). Needles of  $\text{Ru}_4\text{Al}_{13}$  (white) surrounded by  $\text{RuAl}_6$ , eutectic of  $\text{RuAl}_6$  and Al-rich solid (black).



There were too many different phase regions to attempt an overall composition analysis. The average quantitative analyses are given in Table 4.6. The wt% totals for the matrix analyses (Appendix IV) were low due to the presence of oxide.

appeared to have a dendritic nature, suggesting that they can form directly from the melt. In the  $\text{Ru}_4\text{Al}_{13}$  layer there were small particles of  $\text{Ru}_2\text{Al}_3$ , adjacent to dendrites of this phase. The rest of the sample contained  $\text{RuAl}_6$  needles in an Al-rich matrix. A eutectic between these two phases was also visible (Figure 4.10). Again, the centres of some of the needles consisted of  $\text{Ru}_4\text{Al}_{13}$ . The phases  $\text{RuAl}_6$  and  $\text{Ru}_4\text{Al}_{13}$  appear cracked in Figure 4.9. The  $\text{Ru}_2\text{Al}_3$  dendrites and the  $\text{Ru}_4\text{Al}_{13}$  grains had a "chewed" appearance, indicating that the  $\text{Ru}_4\text{Al}_{13}$  and  $\text{RuAl}_6$  may have formed via peritectic reactions. This layered structure is discussed further in Chapter 6 in relation to the proposed modifications to the phase diagram.

Figure 4.9: SEM micrograph of nominal  $\text{Ru}_4\text{Al}_{13}$ -a annealed at  $475^\circ\text{C}$  for 168 hours (secondary electron mode).  $\text{RuAl}$  (lightest dendrites),  $\text{Ru}_2\text{Al}_3$  (darker dendrites of first layer),  $\text{Ru}_4\text{Al}_{13}$  (second layer),  $\text{RuAl}_6$  (third layer), Al-rich matrix.





After heat treatment at 475°C for 168 hours, this sample was sectioned and examined once more. The purpose of this treatment was to investigate the possible existence of the phase  $\text{RuAl}_{12}$ . The optical examination of a cross-section of this sample revealed a very different microstructure than the one previously encountered, and, again, not a homogeneous one. There were several different phases observed (Figure 4.8). The lightest phase was the Ru-rich solid solution (Table 4.6), and it formed a eutectic with RuAl (Appendix IV). The first layer surrounding this core was  $\text{Ru}_2\text{Al}_3$ , the second layer (and the lighter core of some of the needles) was  $\text{Ru}_4\text{Al}_{13}$ , the thin third layer was  $\text{RuAl}_6$ , and the dark matrix was found to consist of the Al-rich solid solution (Table 4.6).

Figure 4.8: SEM micrograph of nominal  $\text{Ru}_4\text{Al}_{20}$ -a annealed at 475°C for 168 hours (secondary electron mode). Ru-rich solid (lightest in core), RuAl (matrix of core),  $\text{Ru}_2\text{Al}_3$  (first layer),  $\text{Ru}_4\text{Al}_{13}$  (second layer),  $\text{RuAl}_6$  (third layer), Al-rich matrix.

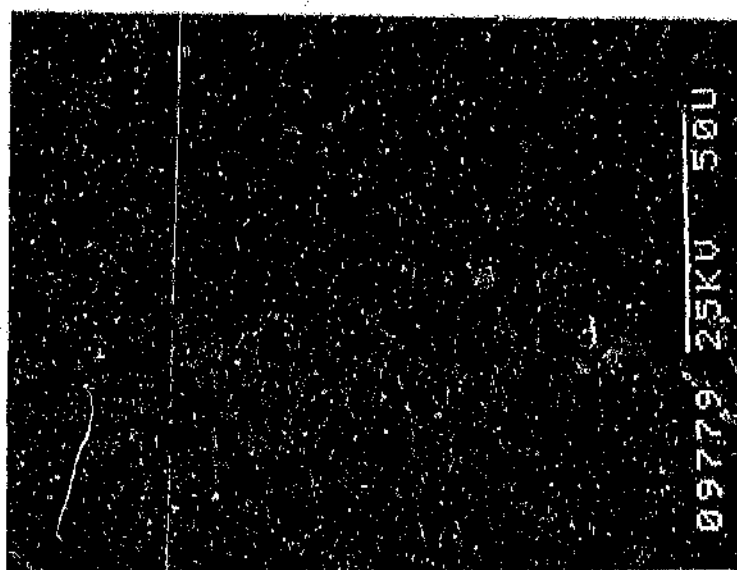


Figure 4.9 shows the phase layers more clearly. In this figure, the RuAl and  $\text{Ru}_2\text{Al}_3$  phases

Table 4.5: Debye-Scherrer Diffraction Data For Ru<sub>4</sub>Al<sub>96</sub>-a (No Heat Treatment) (CuK $\alpha$ ).

d (OBS) (nm)	I (EST.)	PHASE	h k l	d (CALC)* (nm)
0.49139	medium	RuAl <sub>6</sub>	1 1 0	0.49295
0.45230	very weak	RuAl <sub>6</sub>	0 0 2	0.44803
0.37382	very weak	Ru <sub>4</sub> Al <sub>13</sub> RuAl <sub>6</sub>	2 2 0 2 0 0	0.36 0.37418
0.33201	medium	RuAl <sub>6</sub> Ru <sub>4</sub> Al <sub>13</sub>	1 1 2 2 2 1	0.33166 0.332
0.30276	weak	unidentified		
0.26421	very very weak	unidentified		
0.23322	very strong	Al	1 1 1	0.2338
0.22457	very weak	RuAl <sub>6</sub>	3 1 1	0.22576
0.21632	very weak	RuAl <sub>6</sub>	2 2 2	0.21603
0.20689	very weak	RuAl <sub>6</sub>	3 1 2	0.20688
0.20207	strong	Al RuAl <sub>6</sub>	2 0 0 1 1 4	0.2024 0.20396
0.19954	very very weak	unidentified		
0.17608	very very weak	unidentified		
0.14312	strong	Al	2 2 0	0.1431
0.12209	strong	Al	3 1 1	0.1221
0.11691	weak	Al	2 2 2	0.1169
0.09299	weak	Al	3 3 1	0.09289
0.09065	weak	Al	4 2 0	0.09055
0.08273	weak	Al	4 2 2	0.08266
0.07800	medium	unidentified		

\*These values were taken from the JCPDS data cards<sup>(12)</sup>.

Table 4.4: Quantitative chemical analyses for nominal  $\text{Ru}_4\text{Al}_{96}\text{-a}$  (No heat treatment).

PHASE	PHASE DESCRIPTION	ATOMIC % Ru
	Overall	$3.31 \pm 0.03$
Al-rich solid	Matrix	$0.47 \pm 0.07$
$\text{RuAl}_6$	Fine needles	$15.7 \pm 0.1$
$\text{Ru}_4\text{Al}_{13}$	Coarse needles	$25.91 \pm 0.04$

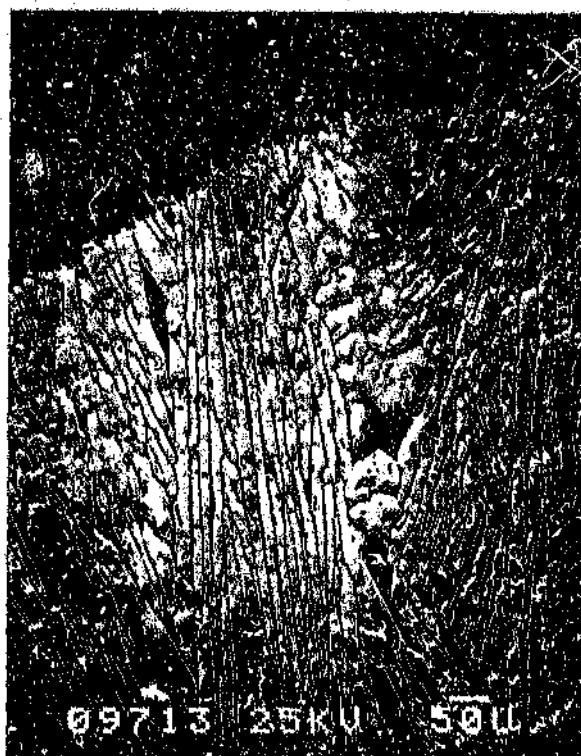
The low wt% totals of the matrix analyses (Appendix IV) indicated the presence of aluminium oxide. The overall analysis is not expected to be accurate, since the quantitative standards were compiled for spot analyses rather than area analyses.

Debye-Scherrer experiments (Table 4.5) confirmed the presence of  $\text{Ru}_4\text{Al}_{13}$ ,  $\text{RuAl}_6$ , and Al in this sample. The Straumanis factor was 2.5003 degrees per cm. It should be noted that the phase containing approximately 25 at% Ru was definitely  $\text{Ru}_4\text{Al}_{13}$ , and not  $\text{RuAl}_6$  (see Chapter 6). Some of the observed peaks were not identified as belonging to any of the known compounds of this system (Table 4.5); these may belong to oxides of the elements.

The value of the  $\text{RuAl}_6$  analysis (Table 4.4) was used as an indication of the phase boundary (Chapter 6). One Differential Thermal Analysis (DTA) scan was recorded for this sample, but was inconclusive, probably due to inhomogeneities in the alloy, and the fact that only one scan was done.

In one very small region at the edge of this sample was a cluster of  $\text{Ru}_4\text{Al}_{13}$  needles (Figure 4.7), which were much larger than the  $\text{RuAl}_6$  needles, surrounded by a single-phase Al-rich matrix. The geometric shape of these needles give an indication of the type of symmetry present in the  $\text{Ru}_4\text{Al}_{13}$  lattice.

Figure 4.7: SEM micrograph of nominal  $\text{Ru}_4\text{Al}_{9.6}$  before heat treatment (secondary electron mode). Fine  $\text{RuAl}_6$  needles, coarse  $\text{Ru}_4\text{Al}_{13}$  needles, Al-rich matrix.

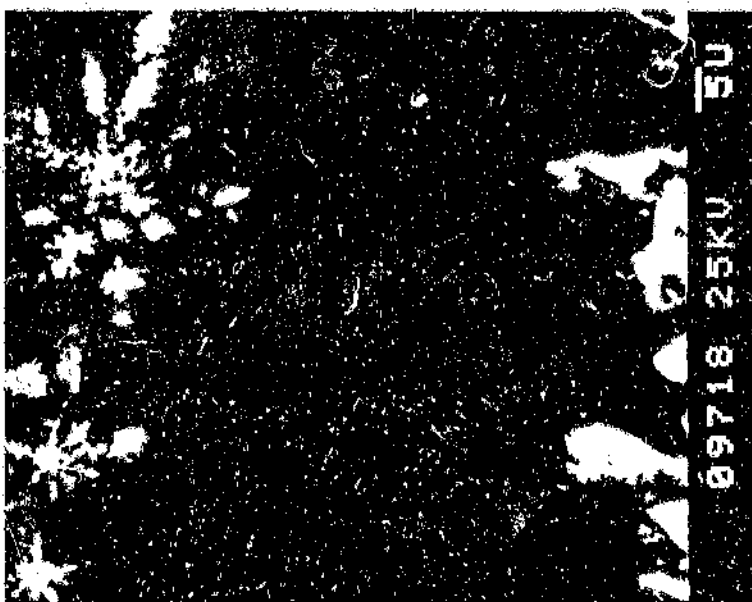


The sample was thus deduced to be inhomogeneous. The edges of the needles were fragmented, and there was no indication of a eutectic in this region. The average quantitative EDAX analyses (Appendix IV) are given in Table 4.4.

Figure 4.5: SEM micrograph of nominal  $\text{Ru}_4\text{Al}_{96}$ -a before heat treatment (secondary electron mode). Primary  $\text{RuAl}_6$  needles and fine eutectic in an Al-rich matrix.



Figure 4.6: SEM micrograph of nominal  $\text{Ru}_4\text{Al}_{96}$ -a before heat treatment (backscattered electron mode). Eutectic of  $\text{RuAl}_6$  and the Al-rich solid solution,  $\text{RuAl}_6$  dendrites.

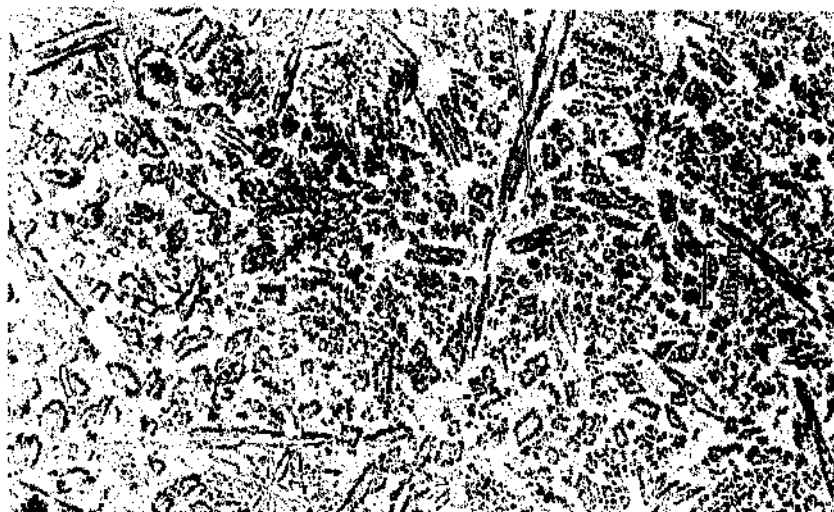


The average semi-quantitative analyses are given in Table 4.3. These results hardly differ from those obtained before the heat treatment.

#### Nominal Ru<sub>4</sub>:Al<sub>96</sub>-a

This alloy was initially examined in the as-cast condition. The particular cross-section which was examined, consisted mostly of RuAl<sub>6</sub> needles of various size and morphology, surrounded by a eutectic (Figure 4.4) of the same phase in an Al-rich matrix.

Figure 4.4: Optical micrograph of nominal Ru<sub>4</sub>:Al<sub>96</sub>-a before heat treatment. RuAl<sub>6</sub> needles and small particles in an Al-rich matrix.



The different RuAl<sub>6</sub> needle morphologies can be more clearly discerned in Figure 4.5, and the fine eutectic is also apparent. At higher magnifications the eutectic (Figure 4.6) between RuAl<sub>6</sub> and the Al-rich solid solution was more clearly visible.

The average semi-quantitative phase analyses are given in Table 4.2, together with an estimation of the overall aluminium and ruthenium content of the sample (the contamination was ignored for comparison with the phase diagram).

Table 4.2: Semi-quantitative chemical analyses for nominal  $\text{Ru}_3\text{Al}_{97}\text{-b}$  (No heat treatment).

PHASE		Al-rich solid	$\text{RuAl}_6$
PHASE DESCRIPTION	Overall	Matrix	Discrete phase
Ru (atomic %)	$2.2 \pm 0.1$	0.03	$12.9 \pm 0.3$
Al	$97.8 \pm 0.1$	99.64	$78.2 \pm 0.3$
Si	Omitted	0.27	$5.93 \pm 0.08$
Fe	Omitted	0.07	$2.9 \pm 0.5$

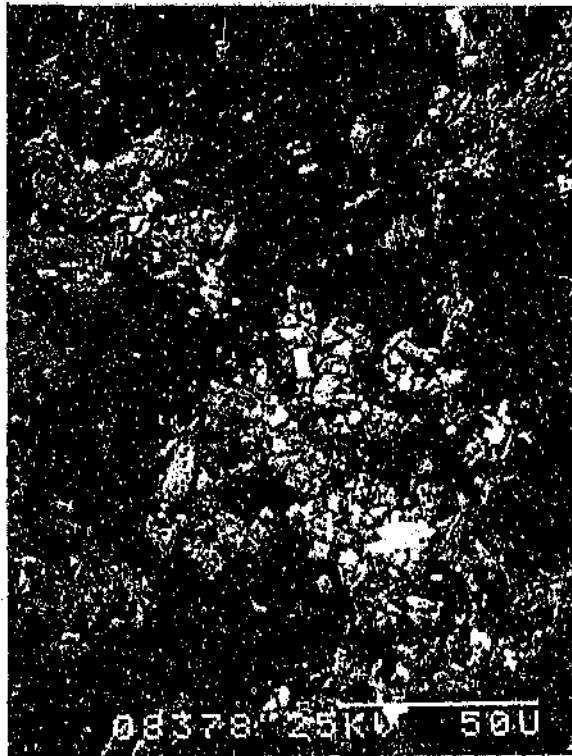
Table 4.3: Semi-quantitative chemical analyses for nominal  $\text{Ru}_3\text{Al}_{97}\text{-b}$  (550°C for 1176 hours).

PHASE	Al-rich solid	$\text{RuAl}_6$
PHASE DESCRIPTION	Matrix	Discrete phase
Ru (atomic %)	$0.05 \pm 0.05$	$14.5 \pm 0.6$
Al	$99.7 \pm 0.2$	$78 \pm 1$
Si	$0.2 \pm 0.1$	$4.6 \pm 0.6$
Fe	$0.03 \pm 0.02$	$2.8 \pm 0.4$

Since some of the original ruthenium was still present, the sample was squashed slightly in a vice, and subjected to homogenisation treatment at 550°C for 1176 hours. Semi-quantitative chemical analyses were again undertaken after the heat treatment (Appendix II). The microstructure of the sample had not changed much; it had only slightly coarsened.

At higher magnifications, light inclusions could be observed in backscattered electron mode (Fig 4.3). These consisted of pure ruthenium which had not been affected by sintering.

**Figure 4.3:** SEM micrograph of (contaminated) nominal  $\text{Ru}_3\text{Al}_7$ -b before heat treatment (backscattered electron mode).  $\text{RuAl}_6$  (discrete phase), Al-rich matrix, Unaltered Ru (small bright regions).



At increased magnification in secondary electron mode, dark, angular crystals were observed, which could not be discerned in backscatter mode. These were found, using semi-quantitative EDAX, to be aluminium-silicon crystals (Appendix III).



Figure 4.19: SEM micrograph of nominal  $\text{Ru}_{10}\text{Al}_{90}$  before heat treatment (secondary electron mode). Eutectic of  $\text{RuAl}$  (grey) and the Ru-rich solid solution (white).

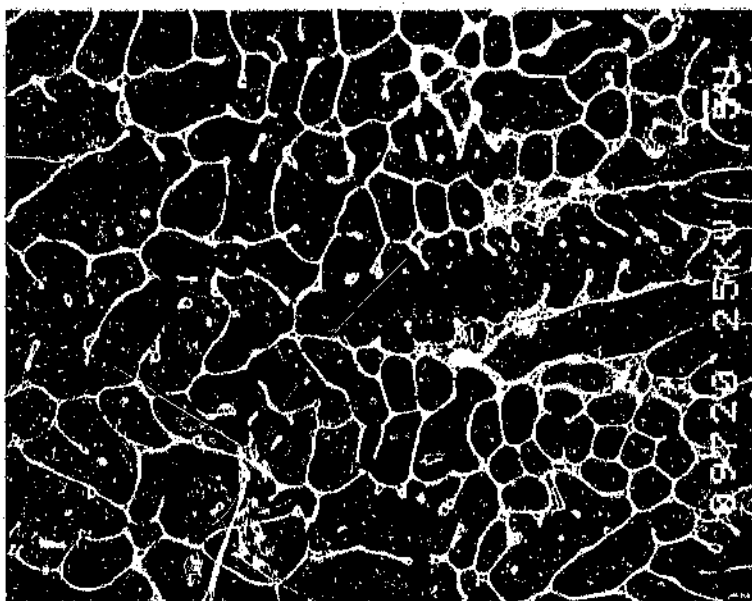


Figure 4.20: SEM micrograph of nominal  $\text{Ru}_{10}\text{Al}_{90}$  before heat treatment (secondary electron mode).  $\text{RuAl}$  (light grey) dendrites,  $\text{Ru}_2\text{Al}_3$  (dark grey) dendrites,  $\text{Ru}_4\text{Al}_{13}$  (black).

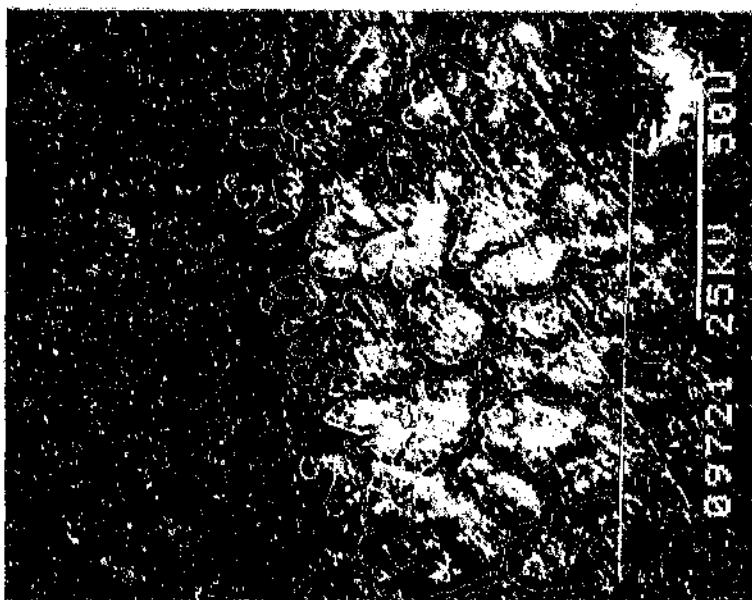
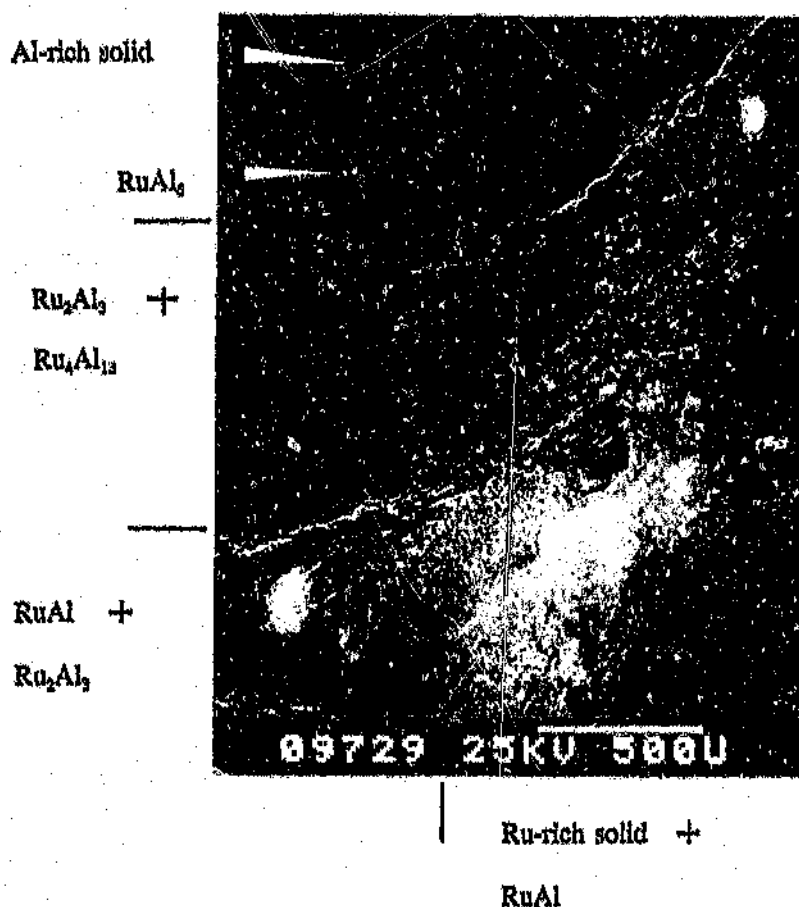


Figure 4.18: SEM micrograph of nominal  $\text{Ru}_{10}\text{Al}_{90}$  before heat treatment (backscattered electron mode). Core region of  $\text{RuAl}$  (light grey) and  $\text{Ru}$ -rich solid (white). Layers of  $\text{Ru}_2\text{Al}_3$  (dark grey),  $\text{Ru}_4\text{Al}_{13}$  (darkest grey), and  $\text{Al}$ -rich solid (black).



The sample was extensively cracked, but there was an un-cracked region containing dendrites of  $\text{RuAl}$  (Table 4.13) and a thin network of  $\text{Ru}$ -rich solid solution, which had formed a eutectic with the former, in the interdendritic regions (Figure 4.19).

After this sample had been upset-annealed at 550°C for 1176 hours, the microstructure had coarsened, but no other visible changes had occurred. The matrix was still mostly aluminium and the light phase was  $\text{RuAl}_4$  (Appendix VII). The only noticeable change was the introduction of silicon contamination in the sample (Table 4.12). This may have been due to silicon pick-up from the tube over the extensive treatment period.

Table 4.12: Semi-quantitative chemical analyses for nominal  $\text{Ru}_{10}\text{Al}_{90}$  (550°C for 1176 hours).

PHASE	Al-rich solid	$\text{RuAl}_4$
PHASE DESCRIPTION	Matrix	Discrete phase
Ru (atomic %)	$0.07 \pm 0.03$	$15 \pm 1$
Al	$99.61 \pm 0.08$	$81 \pm 3$
Si	$0.29 \pm 0.06$	$3 \pm 2$
Fe	$0.03 \pm 0.02$	$0.8 \pm 0.1$

#### Nominal $\text{Ru}_{10}\text{Al}_{90}$

This sample was examined prior to heat treatment. It became obvious that the alloy was inhomogeneous, since many different phase layers could be observed (Figure 4.18). The area consisting of  $\text{Ru}_2\text{Al}_3$  and  $\text{Ru}_4\text{Al}_{13}$ , in places, appears in Figure 4.18 to contain a third phase. This effect at low magnification was due to the intimate mixture of the two phases in various regions (Figure 4.21).

Figure 4.17: SEM micrograph of (contaminated) nominal  $\text{Ru}_7\text{Al}_{93}$  after sintering (secondary electron mode).  $\text{RuAl}_6$  (dark grey) in an Al-rich matrix (black).



The average semi-quantitative EDAX analyses are provided in Table 4.11, and the data can be viewed in Appendix VII. The sample was found to be contaminated with small amounts of iron, but there was no detectable silicon contamination.

Table 4.11: Semi-quantitative chemical analyses for nominal  $\text{Ru}_7\text{Al}_{93}$  (No heat treatment).

PHASE		Al-rich solid	$\text{RuAl}_6$
PHASE DESCRIPTION	Overall	Matrix	Discrete phase
Ru (atomic %)	$5.705 \pm 0.005$	$\sim 0.1$	$14.5 \pm 0.9$
Al	$93.985 \pm 0.005$	$\sim 99.89$	$84 \pm 1$
Fe	$0.31 \pm 0.02$	$\sim 0.0$	$0.8 \pm 0.2$

The average semi-quantitative EDAX analyses can be found in Appendix VI. The average quantitative analyses and the semi-quantitative overall composition are reported in Table 4.9. The overall composition analysis (Table 4.9) is very different to the nominal composition. However, in such an inhomogeneous sample, it is very difficult to accurately measure this parameter since the specimen is too large, and the wrong shape, to attempt a true overall measurement.

The Debye-Scherrer results (Table 4.10) confirmed the presence of  $\text{Ru}_4\text{Al}_{13}$  (not  $\text{RuAl}_3$  - see Chapter 6),  $\text{RuAl}_6$ , and Al-rich solid in this sample. The Straumanis factor was 2.5036 degrees per cm. The phases  $\text{RuAl}_6$  and Al could also be identified from bulk X-ray experiments (Appendix VI), but the scan was not representative, because the sample was too inhomogeneous and the scanned surface contained porosity. The quantitative  $\text{RuAl}_6$  analyses were used as an indication of the position of the phase boundary (Chapter 6).

#### Nominal $\text{Ru}_3\text{Al}_7$

Prior to heat treatment, this sample appeared to be very similar to the sintered  $\text{Ru}_3\text{Al}_{77}\text{-b}$ . It contained the same characteristic porosity, and was also two-phase. However, the  $\text{RuAl}_6$  particles were coarser and more geometrical (Figure 4.17) than those of  $\text{Ru}_3\text{Al}_{77}\text{-b}$ . This sample appeared to be completely sintered, and had an Al-rich matrix (Table 4.11). The darker regions at the edges of the light phase in Figure 4.17 were a polishing artifact, and were not observed in backscattered mode.

Table 4.10: Debye-Scherrer Diffraction Data For Ru:Al<sub>12</sub> (CuK $\alpha$ ).

d (OBS) (nm)	I (EST.)	PHASE	h k l	d (CALC)* (nm)
0.50593	medium	RuAl <sub>6</sub>	1 1 0	0.49295
0.41272	medium	Ru <sub>4</sub> Al <sub>13</sub>	$\bar{2}$ 0 3	0.413
0.38042	weak	RuAl <sub>6</sub> Ru <sub>4</sub> Al <sub>13</sub>	2 0 0 4 0 0	0.37418 0.378
0.36355	weak	Ru <sub>4</sub> Al <sub>13</sub>	$\bar{2}$ 2 0	0.36
0.33464	medium	RuAl <sub>6</sub> Ru <sub>4</sub> Al <sub>13</sub>	1 1 2 2 2 1	0.33166 0.332
0.30489	weak	unidentified		
0.26463	very weak	unidentified		
0.23483	very strong	Al	1 1 1	0.2338
0.21507	medium	RuAl <sub>6</sub>	2 2 2	0.21603
0.20890	medium	RuAl <sub>6</sub>	3 1 2	0.20688
0.20310	strong	Al RuAl <sub>6</sub>	2 0 0 1 1 4	0.2024 0.20396
0.17705	very very weak	unidentified		
0.16096	very very weak	unidentified		
0.14751	very very weak	unidentified		
0.14354	strong	Al	2 2 0	0.1431
0.12229	strong	Al	3 1 1	0.1221
0.11708	weak	Al	2 2 2	0.1169
0.09308	weak	Al	3 3 1	0.09289
0.09069	weak	Al	4 2 0	0.09055
0.08278	weak	Al	4 2 2	0.08266
0.07799	weak	unidentified		

\*These values were taken from the JCPDS data cards<sup>(12)</sup>.

$\text{RuAl}_6$  was formed via a peritectic reaction.

Figure 4.16: SEM micrograph of nominal  $\text{Ru:Al}_{12}$  (secondary electron mode).  $\text{Ru}_4\text{Al}_{13}$  (light grey),  $\text{RuAl}_6$  (dark grey), Al-rich solid (black matrix).



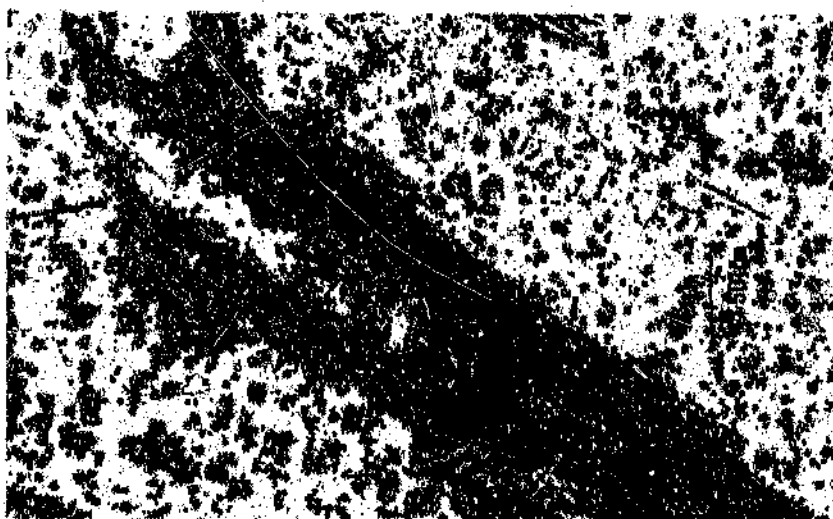
Table 4.9: EDAX analyses for nominal  $\text{Ru:Al}_{12}$ .

PHASE	PHASE DESCRIPTION	ATOMIC % Ru
	Overall	$1.1 \pm 0.7$
$\text{Ru}_4\text{Al}_{13}$	Needles	$23.9 \pm 0.4$
$\text{RuAl}_6$	Surrounding needles	$15.10 \pm 0.01$
	Dendrites	$15.20 \pm 0.02$
Al-rich solid	Matrix	$0.82 \pm 0.02$

The bottom region of this sample contained three phases (Figure 4.14). There were large needles of  $\text{Ru}_4\text{Al}_{13}$  (Table 4.9), surrounded by a thin layer  $\text{RuAl}_6$ . The  $\text{RuAl}_6$  phase was also present as small particles in the Al-rich matrix, suggesting a eutectic structure.

Figure 4.15 depicts the  $\text{Ru}_4\text{Al}_{13}$  needles as they appeared after etching with Murakami's reagent. The very dark areas in this figure are shadows and pores.

Figure 4.15: Optical micrograph of bottom region of nominal  $\text{Ru:Al}_{12}$  (etched).  $\text{Ru}_4\text{Al}_{13}$  (needle),  $\text{RuAl}_6$  (light grey), Al-rich solid (white matrix). The black regions are shadows and pores.



There were cracks in this region, which originated in the needles. This suggests a brittle nature; or an inability to withstand contraction during cooling, due to differing coefficients of expansion of the phases. The layered structure (Figure 4.16) indicates that the  $\text{RuAl}_6$  solidified later than the  $\text{Ru}_4\text{Al}_{13}$ , and the morphology of the needle edges suggests that the



**Figure 4.13:** SEM micrograph of top region of nominal  $\text{Ru:Al}_{12}$  (secondary electron mode).

$\text{RuAl}_6$  dendrites in Al-rich matrix, and eutectic.

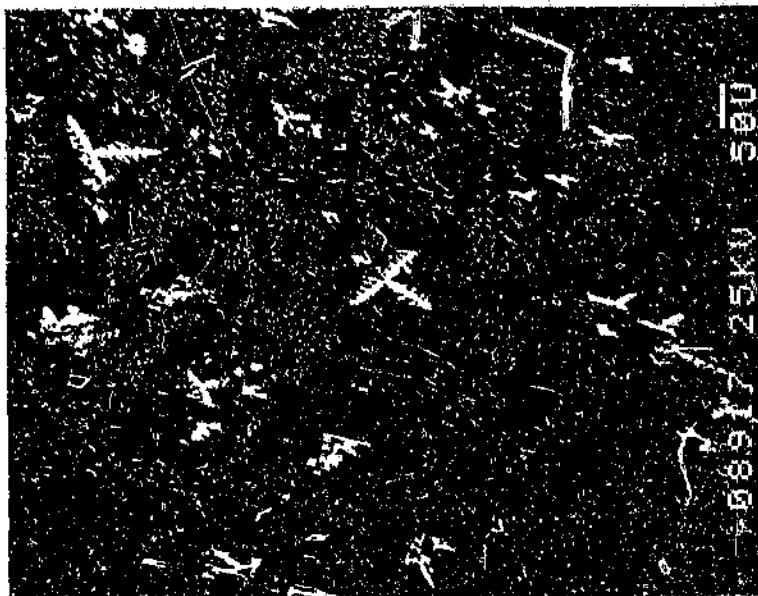
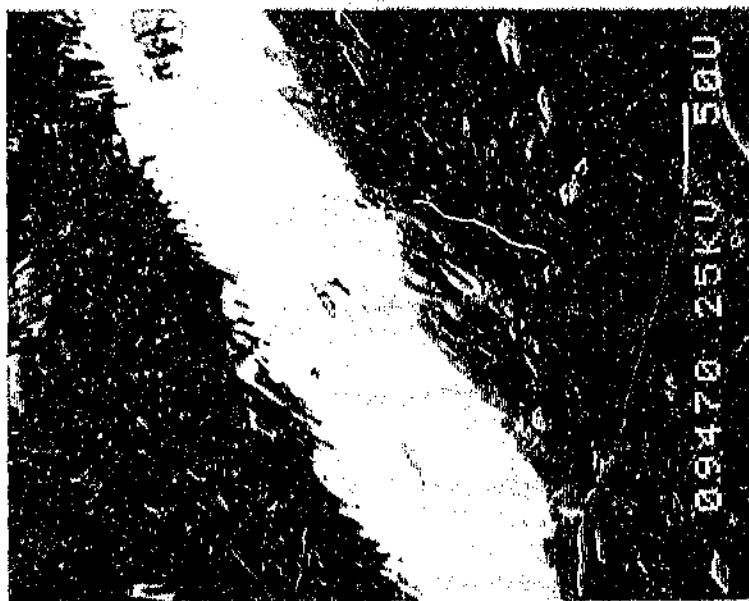


**Figure 4.14:** SEM micrograph of bottom region of nominal  $\text{Ru:Al}_{12}$  (secondary electron mode).  $\text{Ru}_4\text{Al}_{13}$  (needle),  $\text{RuAl}_6$  (layer and small particles), and Al-rich solid (matrix).



The average semi-quantitative phase analyses can be found in Appendix V, together with the individual overall analyses. For the sake of comparison with the phase diagram, the small amounts of chlorine, iron, silicon, and manganese, present in the phases have not been included in these analyses. The impurities could not be included in the quantitative analyses (Table 4.8), but a scan of the latter phase was plotted to show the presence of impurities (Appendix V).

Table 4.8: Phase analyses for nominal  $\text{Ru}_4\text{Al}_{13}$ -b (All quantitative except for the overall composition).

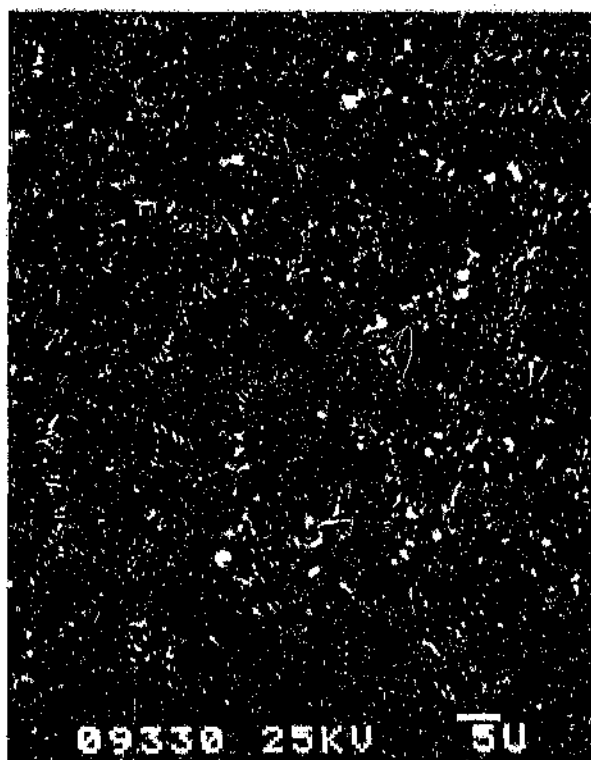
PHASE	PHASE DESCRIPTION	ATOMIC % Ru
	Overall	$3.10 \pm 0.09$
$\text{Ru}_4\text{Al}_{13}$	Needles	$24.73 \pm 0.05$
$\text{RuAl}_6$	At edge of needles	$17.8 \pm 0.7$
Al-rich solid	Matrix	approx. 0.6

#### Nominal $\text{Ru:Al}_{12}$

The top region of this sample appeared to consist of two phases. Figure 4.13 shows the nature of the discrete  $\text{RuAl}_6$  phase in that region. The dendritic morphology of the larger particles suggests that they solidified directly from the melt. There were zones around the larger particles which are depleted of the second phase. The fine dispersion of second phase in the balance of this figure appears to be a sparse eutectic mixture of  $\text{RuAl}_6$  in the Al-rich matrix (Table 4.9).

A fine eutectic was present between the needles (Figure 4.12). This mixture was not continuous in the region, but appeared to form between patches of Al-rich solid, as in the previous sample (Figure 4.6), and dissimilar to the particles in the contaminated specimen  $\text{Ru}_3\text{Al}_{77-\text{a}}$  (Figure 4.1). The light component of the eutectic could not be analysed because it was too small, but appeared to have the same colour as the  $\text{RuAl}_6$  in backscattered electron mode. Small aluminium particles (Appendix V) were also observed in the matrix (dark particles near the bottom of Figure 4.12).

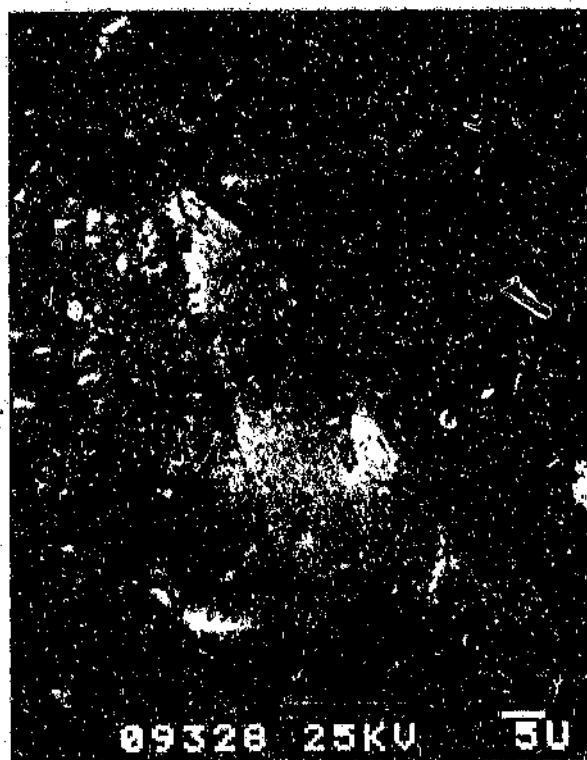
Figure 4.12: SEM micrograph of nominal  $\text{Ru}_4\text{Al}_{96-\text{b}}$  (backscattered electron mode). Eutectic of  $\text{RuAl}_6$  (white) and Al-rich solid (black).



### Nominal Ru<sub>4</sub>:Al<sub>96</sub>-b

Examination of this furnace-cooled sample revealed large Ru<sub>4</sub>Al<sub>13</sub> needles (Figure 4.11). The phase RuAl<sub>6</sub> (Table 4.8) had formed on some of these needles. Both these phases appeared to be extensively cracked. The matrix comprised Al-rich solid solution. This alloy was found to be contaminated, possibly from the flux which was used to prevent oxidation during melting of the elements.

Figure 4.11: SEM micrograph of (contaminated) nominal Ru<sub>4</sub>:Al<sub>96</sub>-b (backscattered electron mode). Ru<sub>4</sub>Al<sub>13</sub> needle, RuAl<sub>6</sub> on edge of needle and in eutectic with Al-rich solid (black).



#### Nominal Ru<sub>18.5</sub>Al<sub>82</sub>-a

This sample had the unusual history of being produced in a graphite resistance furnace, and subsequently being arc-melted when the initial treatment failed. In the graphite resistance furnace an exothermic reaction occurred in the vicinity of 900°C, and the elements had fused to form a friable mass. This product appeared to be stable to about 1400°C, since no further reactions were observed. In an attempt at high-temperature annealing, the sample oxidized and became friable. This made sectioning and examination impossible.

#### Nominal Ru<sub>18.5</sub>Al<sub>82</sub>-b

The sample exhibited extensive porosity (black regions in Figure 4.28), and consisted of four phases (see area near 'iron marker'). In Figure 4.28 there are very small quantities of the RuAl<sub>3</sub> and RuAl<sub>5</sub>\* phases, both are light grey (RuAl<sub>3</sub> is slightly darker), but only RuAl<sub>3</sub> is cracked. This microstructure was consistent throughout most of the sample. The majority of the sample consisted of Ru<sub>4</sub>Al<sub>13</sub> (Table 4.17), and the Al-rich solid solution was present in smaller amounts.

The nature of the phases can be clearly discerned in Figure 4.29, which suggests that the RuAl<sub>5</sub> formed between the Ru<sub>4</sub>Al<sub>13</sub> and RuAl<sub>3</sub> phases. However, this was not always the case, as can be observed in Figure 4.30, where RuAl<sub>5</sub> was found between RuAl<sub>3</sub> and Ru<sub>4</sub>Al<sub>13</sub>. Study of the whole sample rendered no particular trend in the location of RuAl<sub>5</sub>.

---

\*The phase containing approx. 18.5 at% Ru was named RuAl<sub>5</sub> for the purpose of this discussion

Table 4.16: Debye-Scherrer Diffraction Data For  $\text{Ru}_{10}\text{Al}_{90}$  (475°C for 168 hours) ( $\text{CuK}\alpha$ ).

d (OBS) (nm)	I (EST.)	PHASE	h k l	d (CALC) <sup>a</sup> (nm)
0.49309	medium	$\text{RuAl}_3$	1 1 0	0.49295
0.44804	weak	$\text{RuAl}_3$	0 0 2	0.44803
0.41537	medium	$\text{Ru}_2\text{Al}_{13}$	2 0 2	0.415
0.40280	weak	$\text{Ru}_2\text{Al}_{13}$	0 0 3	0.404
0.37630	weak	$\text{Ru}_2\text{Al}_{13}$ $\text{RuAl}_3$	4 0 2 2 0 0	0.376 0.37418
0.35980	weak	$\text{Ru}_2\text{Al}_{13}$	2 2 0	0.36
0.33955	weak	$\text{Ru}_2\text{Al}_{13}$	0 2 2	0.339
0.33148	medium	$\text{RuAl}_3$ $\text{Ru}_2\text{Al}_{13}$	1 1 2 2 2 1	0.33166 0.332
0.31675	very very weak	unidentified		
0.29763	very weak	unidentified		
0.28712	very very weak	$\text{RuAl}_3$	2 0 2	0.28734
0.27757	very very weak	unidentified		
0.23351	very strong	Al	1 1 1	0.2338
0.22469	weak	$\text{RuAl}_3$	3 1 1	0.22576
0.21984	very weak	$\text{RuAl}_3$	2 2 2	0.21603
0.21338	medium	$\text{RuAl}_3$	1 3 0	0.2098
0.20766	medium	$\text{RuAl}_3$	3 1 2	0.20688
0.20475	very weak	$\text{RuAl}_3$	1 1 4	0.20396
0.20215	strong	Al	2 0 0	0.2024
0.18211	very very weak	unidentified		
0.17265	very very weak	unidentified		
0.14770	very weak	unidentified		
0.14313	strong	Al	2 2 0	0.1431
0.12209	strong	Al	3 1 1	0.1221
0.11693	weak	Al	2 2 2	0.1169
0.09298	weak	Al	3 3 1	0.09289
0.09063	weak	Al	4 2 0	0.09055
0.08273	weak	Al	4 2 2	0.08266
0.07800	weak	unidentified		

<sup>a</sup>These values were taken from the JCPDS data cards<sup>[13]</sup>.

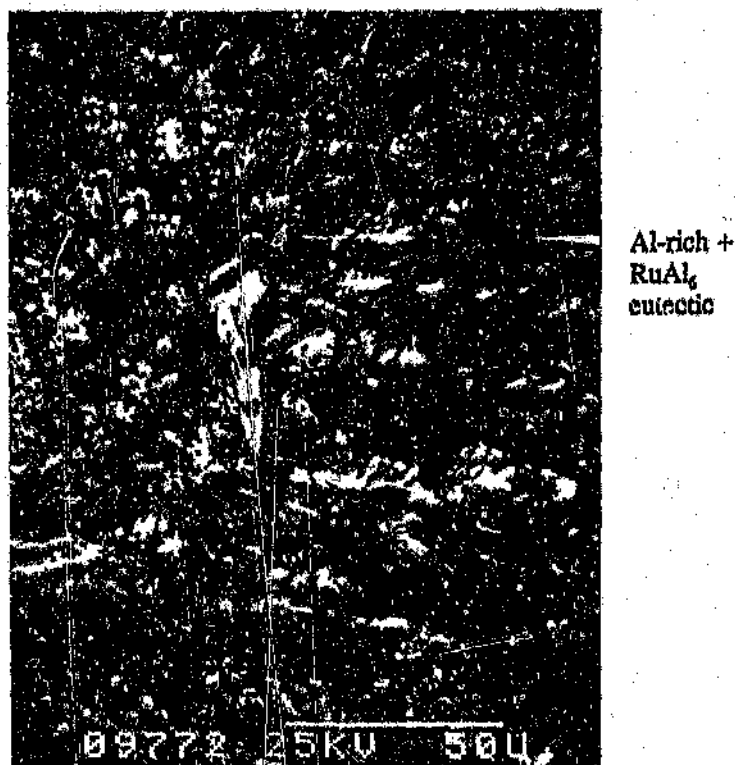
Table 4.15: Quantitative chemical analyses for nominal  $\text{Ru}_{10}\text{Al}_{90}$  (475°C for 168 hours).

PHASE	PHASE DESCRIPTION	ATOMIC % Ru
$\text{RuAl}$	Core dendrites	$49.4 \pm 0.7$
$\text{Ru}_2\text{Al}_3$	First layer	$36.0 \pm 0.5$
$\text{Ru}_4\text{Al}_{13}$	Second layer & needles	$26.0 \pm 0.1$
$\text{RuAl}_6$	Third layer, needles & edge of $\text{Ru}_4\text{Al}_{13}$	$15.80 \pm 0.02$
Al-rich solid	Matrix	$0.49 \pm 0.06$

The low weight percent totals of the matrix analyses indicated the presence of oxide (Appendix VIII). The phase analyses were not used for determining the phase boundaries since the sample was too inhomogeneous. The formation of the layered structure is discussed further in Chapter 6 in relation to the proposed modifications to the phase diagram.

Debye-Scherrer experiments (Table 4.16) confirmed the presence of the Al-rich solid,  $\text{RuAl}_6$ , and  $\text{Ru}_4\text{Al}_{13}$  (not  $\text{RuAl}_3$  - Chapter 6). The Straumanis factor was 2.502 degrees per cm. No other phases were detected because the powder was obtained only from the surface of the sample.

Figure 4.27: SEM micrograph of nominal  $\text{Ru}_{10}\text{:Al}_{90}$  annealed at  $475^\circ\text{C}$  for 168 hours (secondary electron mode).  $\text{Ru}_4\text{Al}_{13}$  (light grey) and  $\text{RuAl}_6$  (dark grey) needles in an Al-rich matrix (black).

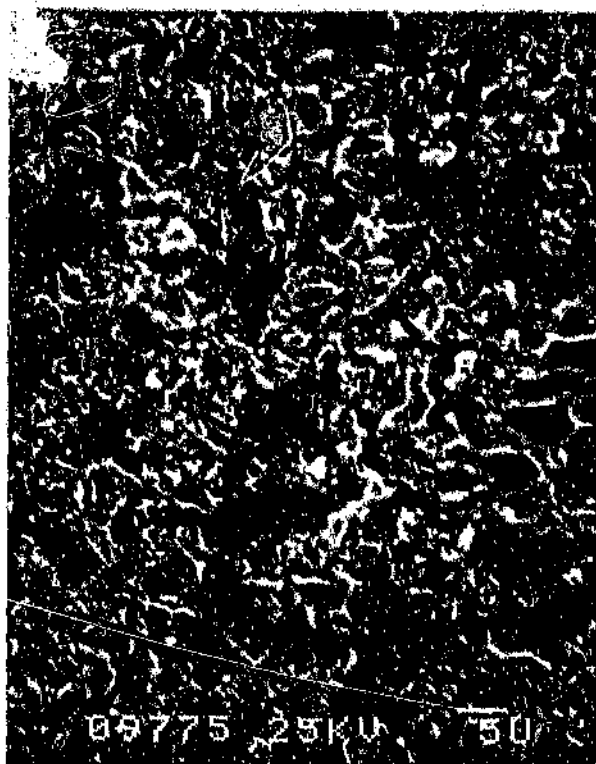


The average quantitative EDAX analyses are given in Table 4.15. Again, no overall composition measurement was attempted, because the sample was extremely inhomogeneous.



The heat treatment did not appear to have any effect on the localised "eutectic"-like mixture of  $\text{Ru}_2\text{Al}_3$  and  $\text{Ru}_4\text{Al}_{13}$ , since it was still observed during this examination (Figure 4.26).

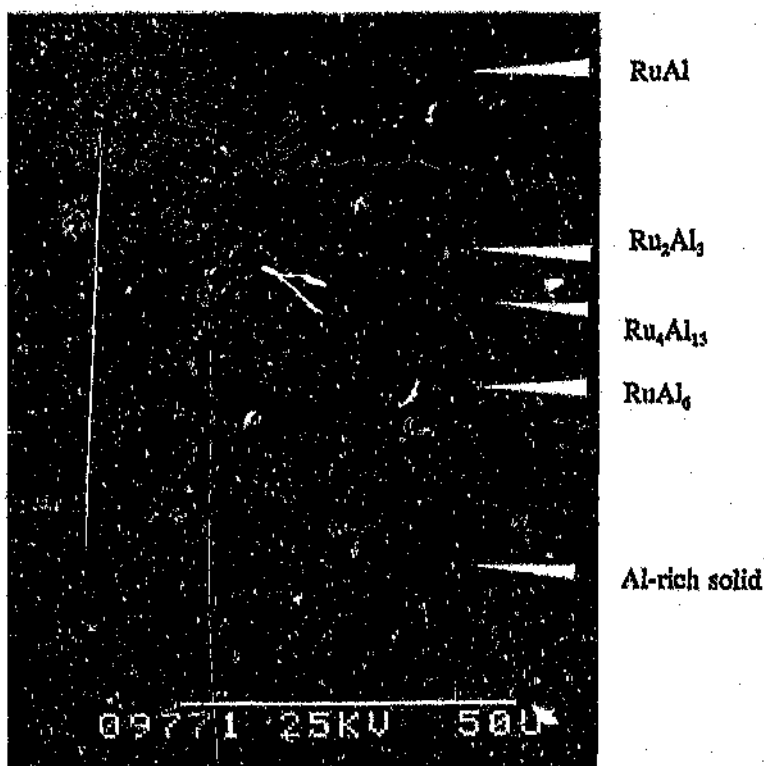
Figure 4.25: SEM micrograph of nominal  $\text{Ru}_{10}\text{Al}_{90}$  annealed at  $475^\circ\text{C}$  for 168 hours (secondary electron mode). "Eutectic"-like mixture of  $\text{Ru}_2\text{Al}_3$  (light grey) and  $\text{Ru}_4\text{Al}_{13}$  (dark grey matrix).



Again, the rest of the microstructure consisted of  $\text{Ru}_4\text{Al}_{13}$  needles surrounded by  $\text{RuAl}_6$ , or merely  $\text{RuAl}_6$  needles (Figure 4.27), all in an Al-rich matrix containing a fine, dispersed eutectic.

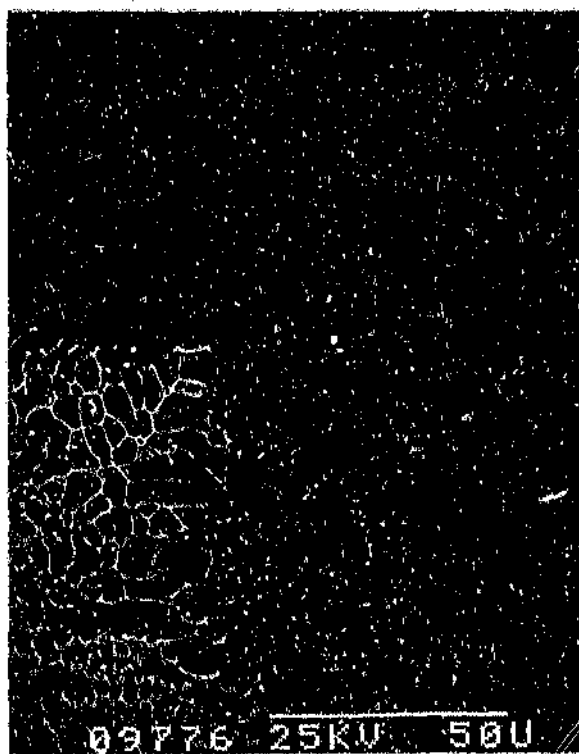
difference was that there was a layer of  $\text{RuAl}_6$  adjacent to the  $\text{Ru}_4\text{Al}_{13}$  layer (Figure 4.25). Also, the amount of  $\text{RuAl}_6$  in the Al-rich matrix appeared to have increased. The few reported changes may have been induced by the heat treatment, or may be a result of viewing a different cross-section of the sample (since the sample was very inhomogeneous).

Figure 4.25: SEM micrograph of nominal  $\text{Ru}_{10}\text{Al}_{90}$  annealed at  $475^\circ\text{C}$  for 168 hours (secondary electron mode).  $\text{RuAl}$  (light grey),  $\text{Ru}_2\text{Al}_3$  (first layer),  $\text{Ru}_4\text{Al}_{13}$  (second layer),  $\text{RuAl}_6$  (third layer), Al-rich solid (black matrix).



This sample was heat treated at 475°C for 168 hours in order to investigate the existence of  $\text{RuAl}_{12}$ . It was not expected that this anneal would have any effect on the high temperature phases, and indeed it did not. The eutectic between the Ru-rich solid solution and  $\text{RuAl}$  was still present (Figure 4.24), adjacent to an area of  $\text{RuAl}$  dendrites surrounded by  $\text{Ru}_2\text{Al}_3$  (Table 4.15).

Figure 4.24: SEM micrograph of nominal  $\text{Ru}_{18}\text{Al}_{90}$  annealed at 475°C for 168 hours (secondary electron mode). Ru-rich solid (light grey) in eutectic with  $\text{RuAl}$  (dark grey),  $\text{Ru}_2\text{Al}_3$  (black).



The  $\text{Ru}_2\text{Al}_3$  layer was again succeeded by a  $\text{Ru}_4\text{Al}_{13}$  layer (Table 4.15). The only noticeable

Table 4.14: Debye-Scherrer Diffraction Data For  $\text{Ru}_{10}\text{Al}_{90}$  (No Heat Treatment) ( $\text{CuK}\alpha$ ).

d (OBS) (nm)	I (EST.)	PHASE	h k l	d (CALC)* (nm)
0.41310	medium	$\text{Ru}_4\text{Al}_{13}$	$\bar{2} 0 3$	0.413
0.40247	weak	$\text{Ru}_4\text{Al}_{13}$	0 0 3	0.404
0.37640	medium	$\text{Ru}_4\text{Al}_{13}$	$\bar{4} 0 2$	0.376
0.35883	medium	$\text{Ru}_4\text{Al}_{13}$	$\bar{2} 2 0$	0.36
0.33774	very weak	$\text{Ru}_4\text{Al}_{13}$	0 2 2	0.339
0.33097	medium	$\text{Ru}_4\text{Al}_{13}$	2 2 1	0.332
0.30264	medium	$\text{Ru}_2\text{Al}_3$	1 0 1	0.3010
0.26392	very weak	unidentified		
0.23357	very strong	Al Ru	1 1 1 1 0 0	0.2338 0.2343
0.21380	strong	$\text{Ru}_2\text{Al}_3$ Ru	1 1 0 0 0 2	0.2117 0.2142
0.20760	medium	$\text{Ru}_2\text{Al}_3$	1 0 5	0.2098
0.20514	very strong	Ru	1 0 1	0.2056
0.20188	medium	Al	2 0 0	0.2024
0.17617	very very weak	unidentified		
0.15788	weak	Ru	1 0 2	0.15808
0.14763	very very weak	unidentified		
0.14317	medium	Al	2 2 0	0.1431
0.13536	weak	Ru	1 1 0	0.1353
0.12212	strong	Al Ru	3 1 1 1 0 3	0.1221 0.12189
0.11455	weak	Ru	1 1 2	0.11434
0.11326	weak	Ru	2 0 1	0.11299
0.09297	very weak	Al	3 3 1	0.09289
0.09063	weak	Al Ru	4 2 0 2 0 3	0.09055 0.09056
0.08681	weak	Ru	2 1 1	0.08673
0.08403	weak	Ru	1 1 4	0.08395
0.08274	very very weak	Al	4 2 2	0.08266
0.08192	very weak	Ru	2 1 2	0.08185
0.08051	very weak	Ru	1 0 5	0.08043
0.07818	very weak	unidentified		

\*These values were taken from the JCPDS data cards<sup>[12]</sup>.

**Table 4.13:** Quantitative chemical analyses for nominal  $\text{Ru}_{10}:\text{Al}_{90}$  (No heat treatment).

PHASE	PHASE DESCRIPTION	ATOMIC % Ru
Ru-rich solid	Eutectic network	$77 \pm 2$
$\text{RuAl}$	Core dendrites	$53.9 \pm 0.4$
$\text{Ru}_2\text{Al}_3$	First layer	$36.5 \pm 0.2$
"Eutectic"-like mixture	Second layer	$30.6 \pm 0.3$
$\text{RuAl}_2$	Small particles	$29.79 \pm 0.09$
$\text{Ru}_4\text{Al}_{13}$	Third layer & needles	$26.0 \pm 0.1$
$\text{RuAl}_6$	Needles & edge of $\text{Ru}_4\text{Al}_{13}$	$15.3 \pm 0.2$
Al-rich solid	Matrix	$0.7 \pm 0.2$

The analyses of the matrix (Appendix VIII) had low weight percent totals, indicating the presence of Al-oxide.

The presence of the Al-rich solid, Ru-rich solid,  $\text{Ru}_4\text{Al}_{13}$  (not  $\text{RuAl}_3$  - Chapter 6), and  $\text{Ru}_2\text{Al}_3$  were confirmed by Debye-Scherrer diffraction data (Table 4.14). The Straumanis factor was 2.5013 degrees per cm. The  $\text{Ru}_2\text{Al}_3$  values were masked by other phases in most cases, and it was possible to discern a small number of peaks which could have matched  $\text{RuAl}$ .

**Figure 4.23:** SEM micrograph of nominal  $\text{Ru}_{10}\text{Al}_{90}$  before heat treatment (backscattered electron mode).  $\text{Ru}_4\text{Al}_{13}$  (needles), eutectic of  $\text{RuAl}_6$  (dark grey) and Al-rich solid (black matrix).



The balance of the sample contained  $\text{RuAl}_6$  needles which were finer and more dendritic in morphology than the  $\text{Ru}_4\text{Al}_{13}$  needles. These were embedded in an Al-rich matrix containing the same eutectic mixture as depicted in Figure 4.23. All the chemical analyses were quantitative (Appendix VIII). There were too many different phase regions to attempt a meaningful overall composition analysis.

**Figure 4.22:** SEM micrograph of nominal  $\text{Ru}_{10}\text{Al}_{90}$  before heat treatment (backscattered electron mode).  $\text{Ru}_2\text{Al}_3$  (white),  $\text{RuAl}_2$  (light grey),  $\text{Ru}_4\text{Al}_{13}$  (dark grey) matrix, Al-rich (black) matrix.

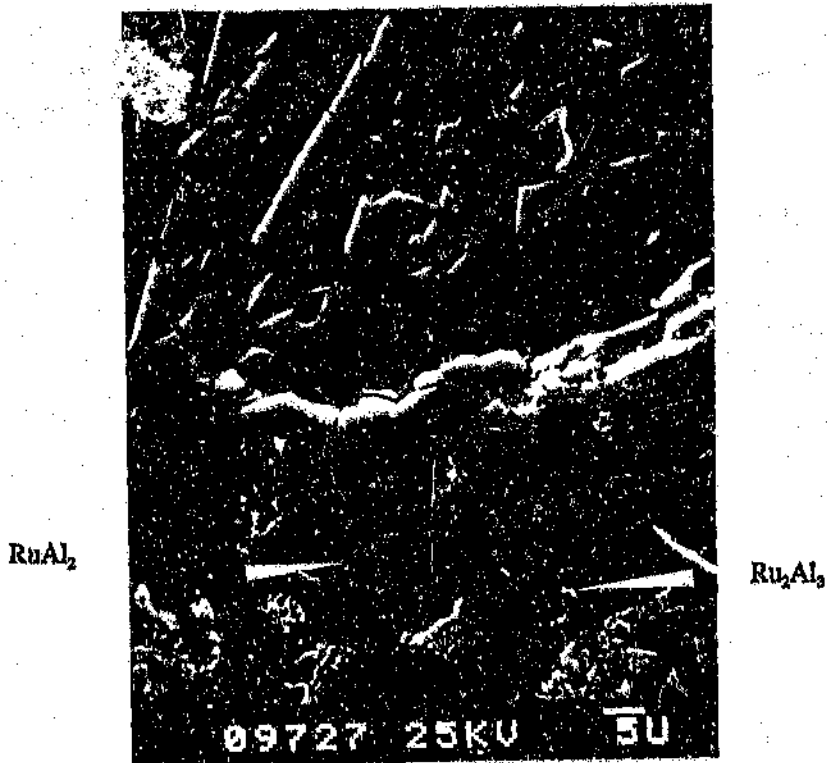


Figure 4.23 shows the  $\text{Ru}_4\text{Al}_{13}$  needles (Table 4.13) once again, with the phase  $\text{RuAl}_6$  at some of the edges of these needles. The fine eutectic particles of  $\text{RuAl}_6$  in the Al-rich matrix are also visible in this figure.

At the edge of this area was a single-phase  $\text{RuAl}$  region, followed by a two-phase layer containing  $\text{RuAl}$  dendrites surrounded by  $\text{Ru}_2\text{Al}_3$  (Table 4.13). The next layer was that of single-phase  $\text{Ru}_2\text{Al}_3$ , followed by a region containing dendrites of the latter surrounded by  $\text{Ru}_4\text{Al}_{13}$  (Figure 4.20).

It was found that  $\text{Ru}_2\text{Al}_3$  formed a eutectic-like mixture with the  $\text{Ru}_4\text{Al}_{13}$  matrix (Figure 4.21) in local patches between the  $\text{Ru}_2\text{Al}_3$  dendrites. This unusual mixture also existed as a separate layer (i.e. with no  $\text{Ru}_2\text{Al}_3$  dendrites), and eventually gave way to extensively cracked  $\text{Ru}_4\text{Al}_{13}$  needles in an Al-rich matrix (Figure 4.22). There were also small areas of  $\text{RuAl}_2$  (slightly lighter than the  $\text{Ru}_4\text{Al}_{13}$  matrix in Figure 4.22) observed in this sample.

**Figure 4.21:** SEM micrograph of nominal  $\text{Ru}_{10}\text{:Al}_{90}$  before heat treatment (backscattered electron mode). "Eutectic"-like mixture of  $\text{Ru}_2\text{Al}_3$  (light) and  $\text{Ru}_4\text{Al}_{13}$  (dark matrix).

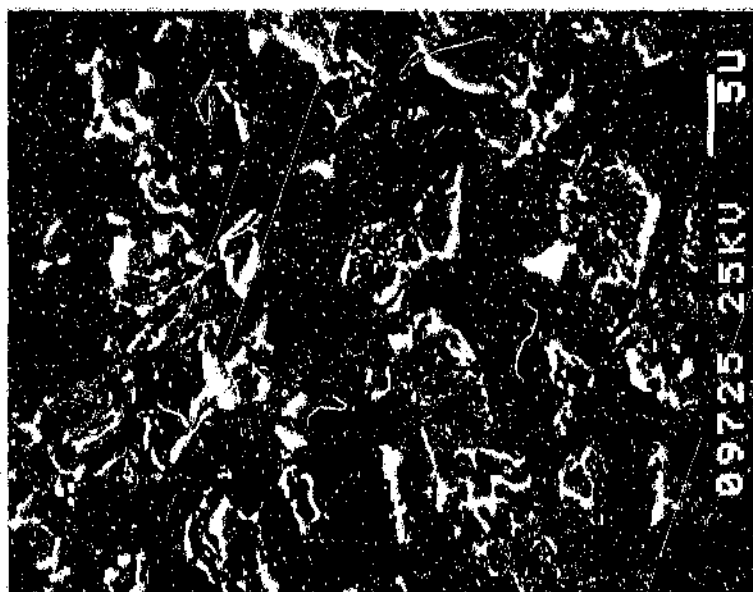
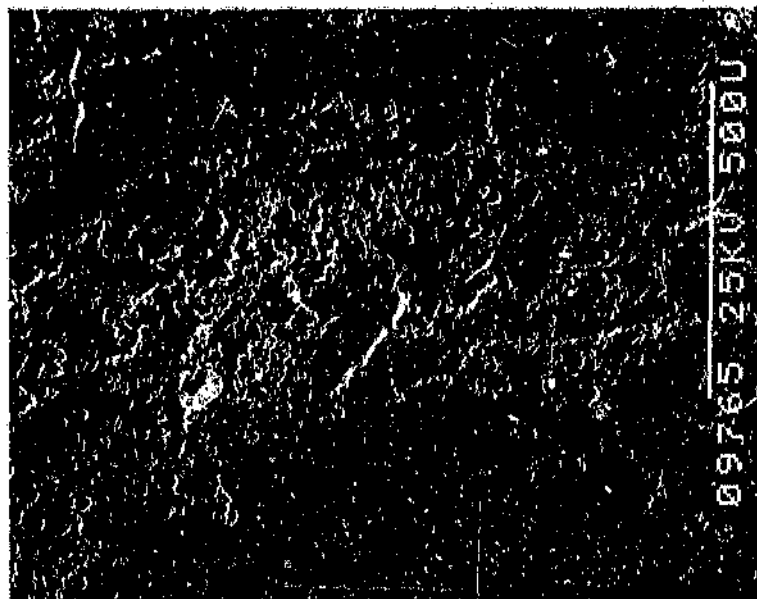




Figure 5.6: SEM micrograph of nominal  $\text{Ru}_{23}\text{Al}_{72}$  annealed at  $1300^\circ\text{C}$  for 6.5 hours (secondary electron mode).  $\text{RuAl}$ ,  $\text{Ru}_2\text{Al}_3$ ,  $\text{RuAl}_2$ ,  $\text{Ru}_4\text{Al}_{13}$ .



An overall composition analysis of this sample was not attempted, because the sample was too inhomogeneous. The average quantitative EDAX analyses are summarised in Table 5.2.

Table 5.2: Quantitative chemical analyses for nominal  $\text{Ru}_{23}\text{Al}_{72}$  ( $1300^\circ\text{C}$  for 6.5 hours).

PHASE	PHASE DESCRIPTION	ATOMIC % Ru
Ru-rich solid	Eutectic with RuAl	$88.005 \pm 0.005$
$\text{RuAl}$	Core phase	$54.1 \pm 0.8$
$\text{Ru}_2\text{Al}_3$	First layer	$43.3 \pm 0.8$
$\text{RuAl}_2$	Second layer	$36.05 \pm 0.03$
$\text{Ru}_4\text{Al}_{13}$	Matrix of third layer	$26.10 \pm 0.08$

Traces of silicon were observed in the scans, but could not be included in the analyses

Figure 5.4: SEM micrograph of nominal  $\text{Ru}_{28}\text{Al}_{72}$  annealed at  $1300^\circ\text{C}$  for 6.5 hours (secondary electron mode). Eutectic of  $\text{RuAl}$  (dark grey) and the Ru-rich solid solution (light grey).

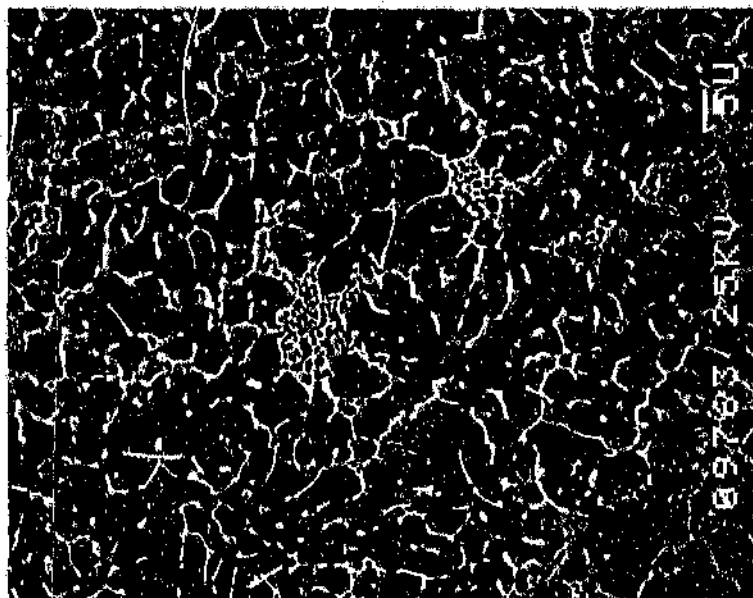
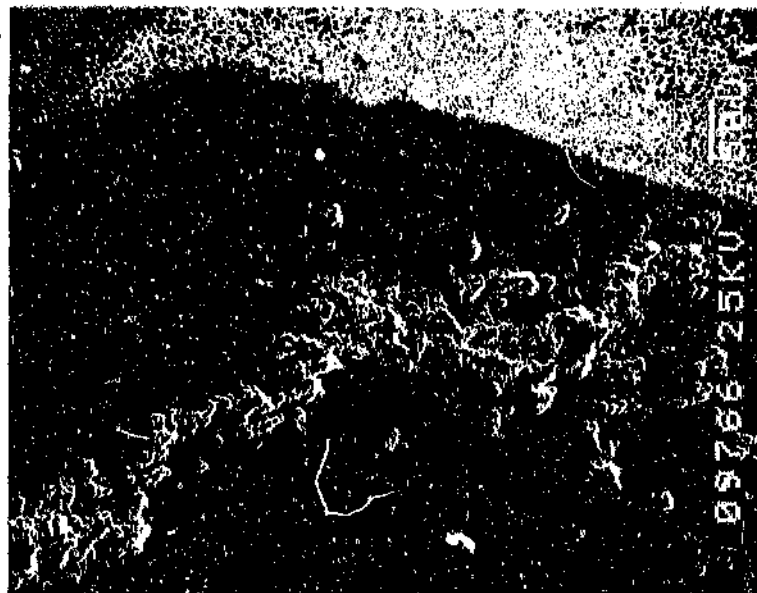


Figure 5.5: SEM micrograph of nominal  $\text{Ru}_{28}\text{Al}_{72}$  annealed at  $1300^\circ\text{C}$  for 6.5 hours (secondary electron mode). Ru-rich solid (white),  $\text{RuAl}$  (light grey),  $\text{Ru}_2\text{Al}_3$  (dark grey layer),  $\text{RuAl}_2$  (black).



There was a larger variation in the  $\text{Ru}_2\text{Al}_3$  analyses (Appendix XI), because the phase regions were very small, and thus the analyses can be affected by the underlying material. The overall composition analysis is not expected to be accurate, because it was an analysis of an area (the standards were obtained with spot analyses). The analyses for  $\text{RuAl}_2$  and  $\text{Ru}_2\text{Al}_3$  were used as an indication of the phase boundary position (Chapter 6).

Debye-Scherrer experiments confirmed the presence of  $\text{Ru}_4\text{Al}_{13}$  (not  $\text{RuAl}_3$  - Chapter 6) and  $\text{Ru}_2\text{Al}_3$ , although the lines pertaining to the latter phase were very light. This is an indication that the  $\text{Ru}_2\text{Al}_3$  phase was less abundant than  $\text{Ru}_4\text{Al}_{13}$ . Unfortunately, the presence of  $\text{RuAl}_2$  was not confirmed, possibly due to the region of the sample from which the powder was obtained.

Following heat treatment at  $1300^\circ\text{C}$  for 6.5 hours, a different cross-section was examined, which was vastly different from the first. The sample was very porous, and a wide range of phases were present (Figures 5.4, 5.5 & 5.6), which had formed in layers around a core of  $\text{RuAl}$  (as in the samples of nominal  $\text{Ru}_4:\text{Al}_{36}$  and  $\text{Ru}_{10}:\text{Al}_{30}$ ). The latter contained Ru-rich solid solution (Table 5.2) which formed a eutectic mixture at the  $\text{RuAl}$  grain boundaries (Figure 5.4).

The first phase layer (Figure 5.5) comprised  $\text{Ru}_2\text{Al}_3$ , and this led into a region containing a  $\text{RuAl}_2$  matrix with discrete grains of  $\text{Ru}_2\text{Al}_3$ . The latter region was very porous. The second single-phase layer consisted of  $\text{RuAl}_2$  (porous area in Figure 5.6), and the next region consisted of a  $\text{Ru}_4\text{Al}_{13}$  matrix, with  $\text{RuAl}_2$  as the included phase (left side of Figure 5.6).

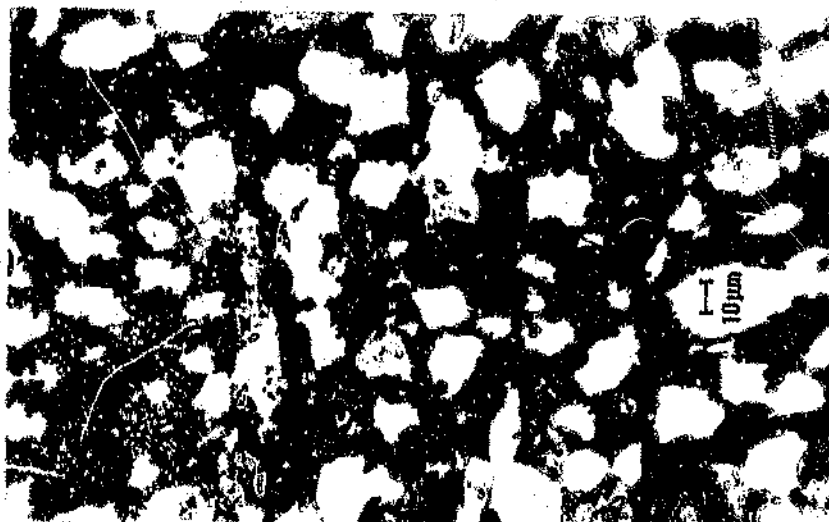
Figure 5.3: SEM micrograph of nominal  $\text{Ru}_{28}\text{Al}_{72}$  before heat treatment (secondary electron mode).  $\text{Ru}_2\text{Al}_3$  (white),  $\text{RuAl}_2$  (light grey grains),  $\text{Ru}_4\text{Al}_{13}$  (dark grey matrix).



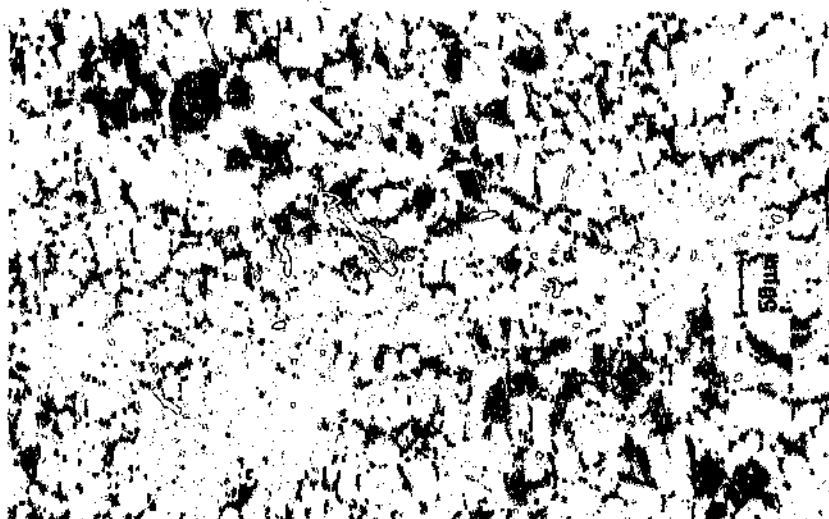
Table 5.1: Quantitative chemical analyses for nominal  $\text{Ru}_{28}\text{Al}_{72}$  (No heat treatment).

PHASE	PHASE DESCRIPTION	ATOMIC % Ru
	Overall	$27.64 \pm 0.06$
$\text{Ru}_2\text{Al}_3$	Sparse dispersion	$35.7 \pm 0.8$
$\text{RuAl}_2$	Discrete grains	$30.35 \pm 0.08$
$\text{Ru}_4\text{Al}_{13}$	Matrix	$25.43 \pm 0.07$

**Figure 5.1:** Optical micrograph of nominal  $\text{Ru}_{28}\text{Al}_{72}$  before heat treatment (Murakami's etch).  $\text{Ru}_4\text{Al}_{13}$  (matrix),  $\text{RuAl}_2$  ("bulky" light phase),  $\text{Ru}_2\text{Al}_7$  ("fine" light phase), dark pores.



**Figure 5.2:** Optical micrograph of nominal  $\text{Ru}_{28}\text{Al}_{72}$  before heat treatment (Murakami's etch). Region containing mostly  $\text{Ru}_4\text{Al}_{13}$  and dark pores.



## 5 RESULTS FROM HIGH RUTHENIUM ALLOYS

The alloys discussed in this chapter are those comprising (nominally) from 28 to 50 at% ruthenium. There is only one published phase diagram for this range of compositions (Figure 2.2), according to which, the phases encompassed by this range are  $\text{RuAl}_2$ ,  $\text{Ru}_2\text{Al}_3$ , and  $\text{RuAl}$ . The results reported below were obtained from optical and SEM examination, EDAX analyses, and X-ray diffraction experiments. The latter were used to distinguish between  $\text{RuAl}_2$  and  $\text{Ru}_2\text{Al}_3$ , which have similar composition ranges.

### Nominal $\text{Ru}_{25}\text{Al}_{75}$

During production of this sample, it appeared to have little surface tension as it flattened and cracked during cooling, thus loosing its button shape. Examination was initially conducted before annealing the alloy. Optical microscopy showed that most of the sample consisted of three phases (Figure 5.1).

There was an area, near one edge of the sample, which appeared to contain very little else but the  $\text{Ru}_4\text{Al}_{13}$  matrix (Figure 5.2), and a high degree of porosity.

The sample mainly consisted of discrete  $\text{RuAl}_2$  grains in a matrix of  $\text{Ru}_4\text{Al}_{13}$  (Table 5.1), with small amounts of  $\text{Ru}_2\text{Al}_3$  dispersed throughout the alloy (Figure 5.3). Most of the latter phase was adjacent to the  $\text{RuAl}_2$  grains.

### Assessment of the Samples

Many of the above samples contained undesirable elements originating from various sources. The most abundant contaminants were silicon and iron, which have a high affinity for aluminium. The most common source of these impurities was the aluminium powder, which was only 95% pure.

The average quantitative EDAX analyses (Appendix X) are given in Table 4.18. The overall analysis is not expected to be accurate (since the EDAX was calibrated only for spot analysis).

Table 4.18: Quantitative chemical analyses for nominal  $\text{Ru}_{20}\text{:Al}_{80}$  (No heat treatment).

PHASE	PHASE DESCRIPTION	ATOMIC % Ru
	Overall	~19.84
$\text{Ru}_4\text{Al}_{13}$	Needles	$26.6 \pm 0.1$
Al-rich solid	Matrix	$0.6 \pm 0.1$

The presence of  $\text{Ru}_4\text{Al}_{13}$  (not  $\text{RuAl}_3$  - Chapter 6) and the Al-rich solid were confirmed by Debye-Scherrer experiments. The  $\text{Ru}_4\text{Al}_{13}$  analyses were used to indicate the position of the phase boundary (Chapter 6).

Further heat treatment of this sample resulted in a friable mass, which could not be examined.

#### Nominal $\text{Ru:Al}_3$

This sample was arc-melted, and then heat treated in the same ampoule as the  $\text{Ru}_{18}\text{:Al}_{82}$ -a. The result of the treatment was a friable sample which was not examined.



**Figure 4.31:** SEM micrograph of nominal  $\text{Ru}_{20}\text{Al}_{80}$  (backscattered electron mode).  $\text{Ru}_4\text{Al}_{13}$  (needles), Al-rich solid (matrix).



**Figure 4.32:** SEM micrograph of nominal  $\text{Ru}_{20}\text{Al}_{80}$  (backscattered electron mode).  $\text{Ru}_4\text{Al}_{13}$  needles in an Al-rich matrix.



Table 4.17: Chemical analyses for nominal  $\text{Ru}_{18}:\text{Al}_{82}$ -b (No heat treatment).

PHASE	PHASE DESCRIPTION	ATOMIC % Ru
	Overall	$13.7 \pm 0.6$
$\text{Ru}_4\text{Al}_{13}$	Majority phase	$25.0 \pm 0.3$
" $\text{RuAl}_5$ "	Un-cracked minor phase	$18.54 \pm 0.03$
$\text{RuAl}_6$	Cracked minor phase	$15.1 \pm 0.2$
Al-rich solid	Dark regions in (SEM) backscatter mode	$0.87 \pm 0.02$

The Debye-Scherrer work confirmed the presence of  $\text{Ru}_4\text{Al}_{13}$  (not  $\text{RuAl}_2$  - Chapter 6),  $\text{RuAl}_6$ , and Al in this sample. There were no unique lines which could be attributed to  $\text{RuAl}_5$ . The bulk X-ray results (Appendix IX) also appeared to confirm these phases, but the results were not conclusive due to the large amount of porosity in the sample.

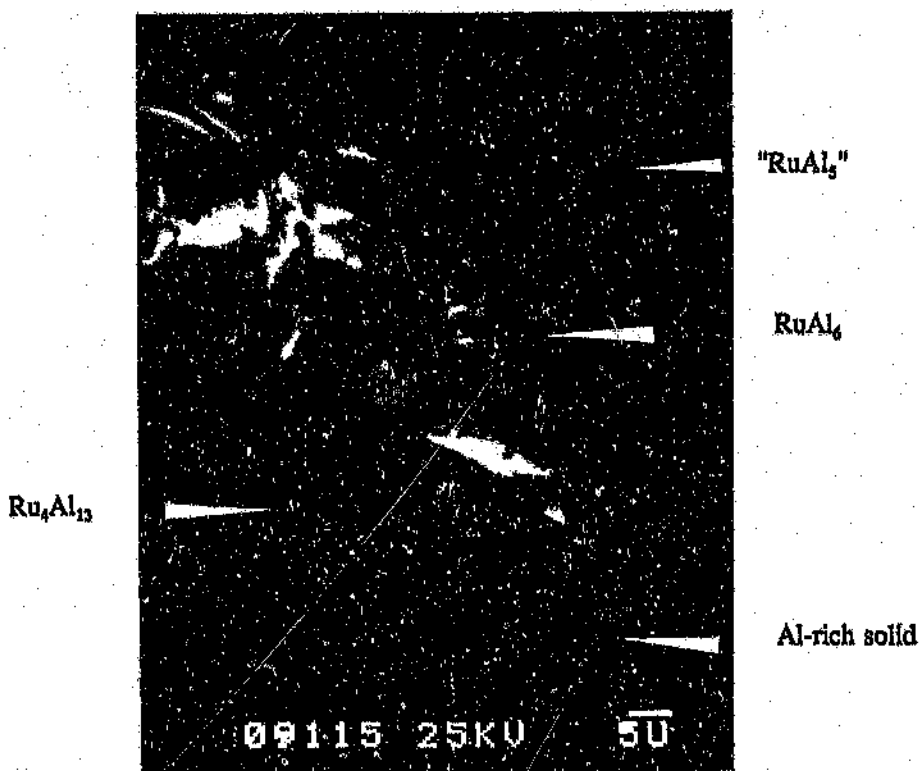
This sample was not heat treated because the porosity would have been too great a barrier to diffusion.

#### Nominal $\text{Ru}_{20}:\text{Al}_{80}$

This sample was first examined prior to heat treatment and appeared to be homogeneous. Coarse  $\text{Ru}_4\text{Al}_{13}$  needles (Figure 4.31) were observed in an Al-rich matrix which appeared to be single-phase. The needles (Figure 4.32) had fractured tips, probably acquired during grinding, due to the difference in phase hardness. The morphology of the  $\text{Ru}_4\text{Al}_{13}$  indicated that it solidified as a primary phase.

Figure 4.30: SEM micrograph of nominal  $\text{Ru}_{18}\text{Al}_{82}$ -b (backscattered electron mode).

$\text{Ru}_4\text{Al}_{13}$  (light grey), " $\text{RuAl}_5$ " (darker grey),  $\text{RuAl}_6$  (darkest grey), Al-rich solid (black).



The material surrounding the pores on one edge of this sample was found to contain zirconium, silicon, and some of the other materials from the crucible, mixed with the alloy elements. Thus the alloy had reacted with the crucible to a small extent.

The average standardless EDAX analyses can be viewed in Appendix IX. The average quantitative analyses are given in Table 4.17, together with a semi-quantitative overall composition analysis.

Figure 4.28: Optical micrograph of nominal  $\text{Ru}_{18}\text{Al}_{82}\text{-b}$  (etched). Al-rich solid (white),  $\text{RuAl}_6$  (light grey, cracked), " $\text{RuAl}_5$ " (light grey, un-cracked),  $\text{Ru}_4\text{Al}_{13}$  (dark grey).

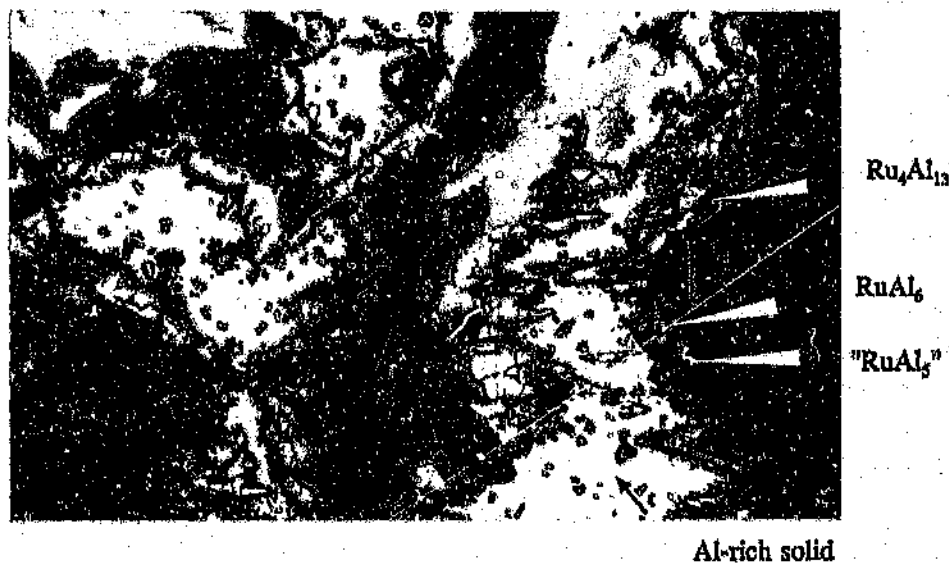


Figure 4.29: SEM micrograph of nominal  $\text{Ru}_{18}\text{Al}_{82}\text{-b}$  (backscattered electron mode).  $\text{Ru}_4\text{Al}_{13}$  (white), " $\text{RuAl}_5$ " (light grey),  $\text{RuAl}_6$  (dark grey), Al-rich solid (black).



Figure 5.16: SEM micrograph of (un-terminated) nominal  $\text{Ru}_{52}\text{Al}_{48}$  annealed at  $1200^\circ\text{C}$  for 480 hours and  $1050^\circ\text{C}$  for 24 hours (backscattered electron mode).  $\text{RuAl}_2$  (dark grey),  $\text{Ru}_2\text{Al}_3$  (light grey), Al-rich solid (lining the pores).

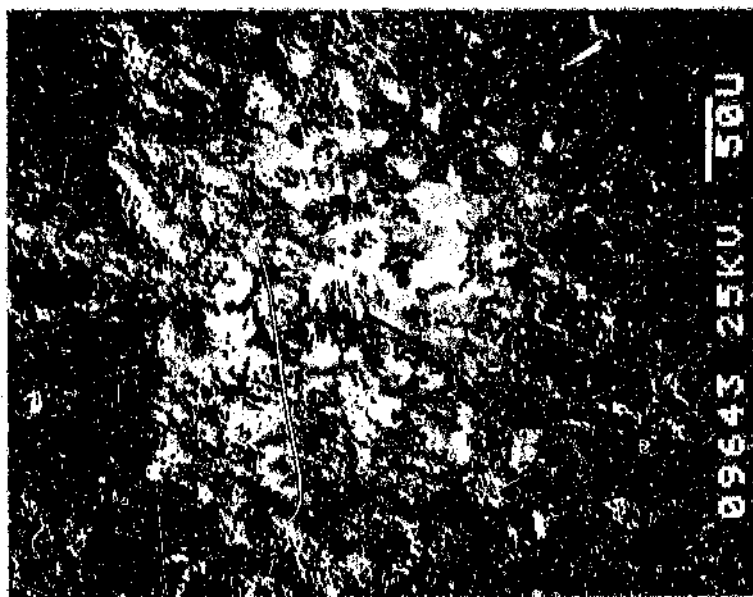


Table 5.6: Quantitative chemical analyses for nominal  $\text{Ru}_{52}\text{Al}_{48}$  ( $1200^\circ\text{C}$  for 480 hours,  $1050^\circ\text{C}$  for 48 hours).

PHASE	PHASE DESCRIPTION	ATOMIC % Ru
$\text{Ru}_2\text{Al}_3$	Discrete in 2-phase region	$44.13 \pm 0.08$
$\text{RuAl}_2$	Matrix in 2-phase region	$37.06 \pm 0.02$
	Single-phase regions	$36.61 \pm 0.02$
Al-rich solid	Lining pores	$99.74 \pm 0.06$
	Inclusions	$50 \pm 1$

Detailed microprobe analyses can be found in Appendix XIII, together with the semi-quantitative overall analyses. The former were used to determine the  $\text{RuAl}_2$  phase boundary position (Chapter 6).

Debye-Scherrer experiments (Table 5.5) confirmed the presence of  $\text{Ru}_4\text{Al}_{13}$  (not  $\text{RuAl}_3$  - Chapter 6) and  $\text{RuAl}_2$  in this sample. It is possible that faint Al-rich peaks were also present. The Straumanis factor was 2.5093 degrees per cm. The phase  $\text{RuAl}_2$  could also be discerned in the results from bulk X-ray experiments. The latter results, however, were unrepresentative because the sample was inhomogeneous.

This sample was heat treated at 1200°C for 168 hours and 1050°C for 24 hours, in order to investigate the high-temperature reactions. Most of the sample appeared to consist of single-phase  $\text{RuAl}_2$  (Table 5.6), allowing for the possibility of composition boundaries being distorted by the presence of silicon and iron contamination. There were some regions which contained grains of  $\text{Ru}_2\text{Al}_3$  (Figure 5.16). The sample was porous, and the Al-rich phase was observed to line these pores.

At higher magnification small inclusions (Figure 5.17) were discerned. Small amounts of manganese were detected in addition to iron and silicon. The impurities could not be included in the quantitative analyses, but a scan was plotted (Appendix XIII) to show the impurities present in the inclusions. A scan of the  $\text{Ru}_2\text{Al}_3$  phase is also given in Appendix XIII to depict the impurities present in this phase. The only possible source of contamination in this case was the tube in which the sample was annealed.

Table 5.5: Debye-Scherrer Diffraction Data For  $\text{Ru}_{12}\text{Al}_{48}$  (1200°C for 312 hours) (CuK $\alpha$ ).

d (OBS) (nm)	I (EST.)	PHASE	h k l	d (CALC) <sup>a</sup> (nm)
0.49716	very weak	unidentified		
0.42499	weak	unidentified		
0.36755	very strong	$\text{Ru}_2\text{Al}_3$ $\text{RuAl}_2$	$\bar{2}20$ 220	0.36 0.369
0.33297	very strong	$\text{Ru}_2\text{Al}_3$	221	0.332
0.30270	very very weak	unidentified		
0.29486	strong	$\text{RuAl}_2$	202	0.296
0.26348	very weak	unidentified		
0.25404	very very weak	unidentified		
0.24448	very very weak	unidentified		
0.23715	medium	$\text{RuAl}_2$	113	0.2376
0.22433	very strong	$\text{RuAl}_2$	311	0.2247
0.21948	strong	$\text{RuAl}_2$	004	0.2197
0.21315	weak	unidentified		
0.20754	very strong	$\text{RuAl}_2$	022	0.2078
0.20288	very weak	$\text{RuAl}_2$	220	0.2033
0.19980	very weak	$\text{RuAl}_2$	400	0.2003
0.18178	strong	$\text{RuAl}_2$	313	0.18206
0.17652	very very weak	unidentified		
0.16050	very weak	$\text{RuAl}_2$	115	0.16130
0.15425	very weak	unidentified		
0.15178	very weak	$\text{RuAl}_2$	131	0.15198
0.14951	weak	$\text{RuAl}_2$	511	0.14951
0.14404	weak	$\text{RuAl}_2$	422	0.14421
0.14033	weak	$\text{RuAl}_2$	315	0.14017
0.13759	weak	$\text{RuAl}_2$	206	0.13753
0.13397	weak	$\text{RuAl}_2$	331	0.13392
0.12784	weak	unidentified		
0.12627	weak	unidentified		
0.12455	weak	unidentified		
0.12318	ak	unidentified		
0.12003	very weak	unidentified		
0.11819	very weak	unidentified		
0.11642	very weak	unidentified		
0.10258	very very weak	unidentified		
0.09204	very very weak	unidentified		

<sup>a</sup>These values were taken from the JCPDS data cards<sup>[21]</sup>.

The standardless chemical analyses (Table 5.4) were deemed too inaccurate to distinguish between phases of similar compositions, so microprobe analyses were undertaken on the  $\text{RuAl}_2$  and  $\text{Ru}_4\text{Al}_{13}$  phases (Figure 5.15), and the sample was also subjected to further EDAX analyses using a different SEM and updated software. Both analyses used pure ruthenium and aluminium as standards.

Table 5.4: Chemical analyses of nominal  $\text{Ru}_{32}\text{Al}_{68}$  annealed at  $1200^\circ\text{C}$  for 312 hours.

Phase Description	Phase Name	Semi-quant. EDAX (at% Ru)	Microprobe (at% Ru)	Quant. EDAX - Jeol (at% Ru)	Quant. EDAX - Hitachi (at% Ru)
Light phase	$\text{RuAl}_2$	$30.5 \pm 0.4$	$35.8 \pm 0.2$	$36.94 \pm 0.09$	$35.7 \pm 0.2$
Dark phase	$\text{Ru}_4\text{Al}_{13}$	$21.2 \pm 0.16$	$25.08 \pm 0.05$	$26.2 \pm 0.1$	$24.8 \pm 0.1$
Dark phase lining cavities	Al-rich solid soln	$0.40 \pm 0.07$	-	-	-
Overall composition	-	$27.3 \pm 0.5$	-	-	-

The EDAX results obtained using the JEOL SEM (Table 5.4) appeared to reinforce the microprobe analyses, and the latter was used to calibrate the more readily available HITACHI SEM\*. The quantitative analyses obtained after calibration were in good agreement with the microprobe results (Table 5.4).

---

\*Provided by MINTEK



Figure 5.14: Optical micrograph of nominal  $\text{Ru}_{32}\text{Al}_{68}$  annealed at  $1200^\circ\text{C}$  for 312 hours (etched with Murakami's reagent).  $\text{RuAl}_2$  (white dendrites),  $\text{Ru}_4\text{Al}_{13}$  (dark grey), cracks and pores (black).

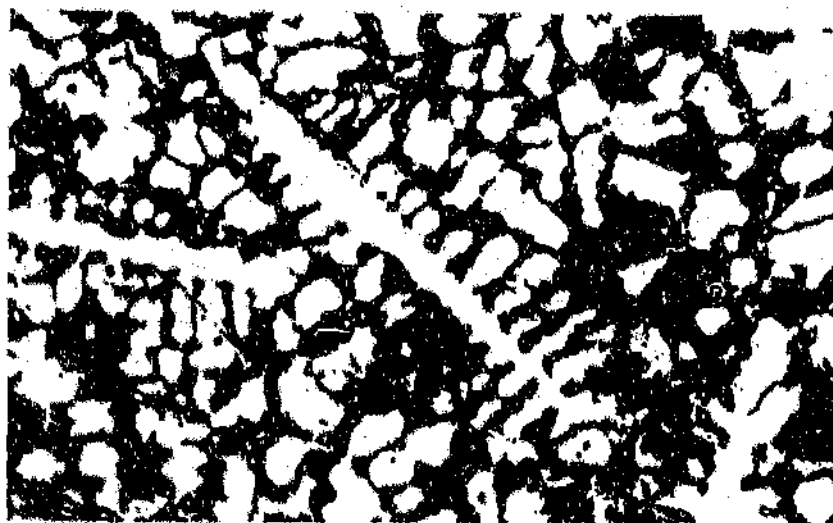
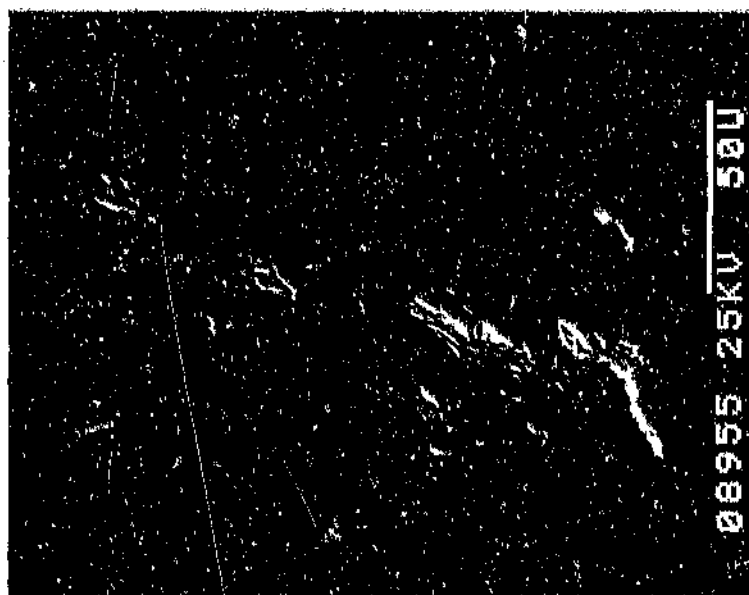
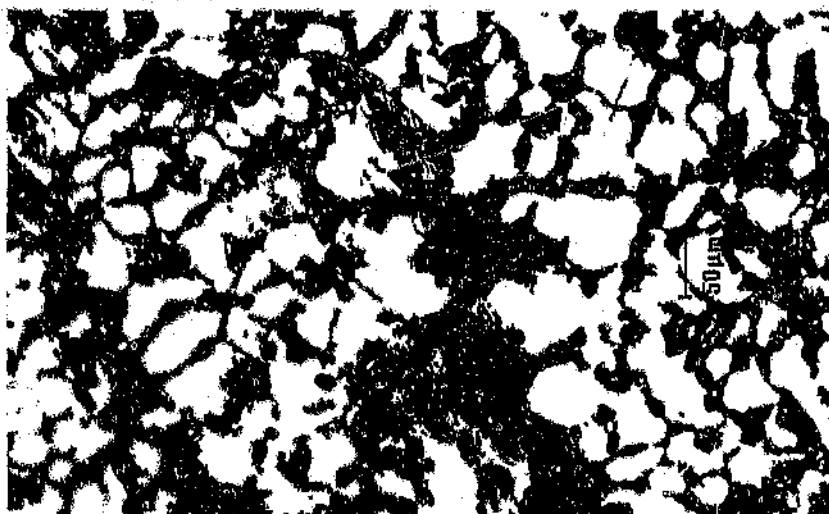


Figure 5.15: SEM micrograph of nominal  $\text{Ru}_{32}\text{Al}_{68}$  annealed at  $1200^\circ\text{C}$  for 312 hours (backscattered electron mode). Central region,  $\text{Ru}_4\text{Al}_{13}$  (dark grey),  $\text{RuAl}_2$  (light grey).



cases, the sparse aluminium-rich phase was not present in the matrix. An example of this can be viewed in Figure 5.13, where the dendrites have a "chewed" appearance. The latter observation may indicate the occurrence of a peritectic reaction subsequent to the formation of the dendrites.

Figure 5.13: Optical micrograph of nominal  $\text{Ru}_{22}\text{Al}_{68}$  annealed at  $1200^\circ\text{C}$  for 312 hours (etched with Murakami's reagent). Al-rich solid (lighter grey, lining cracks),  $\text{RuAl}_2$  (white dendrites),  $\text{Ru}_4\text{Al}_{13}$  (dark grey), cracks and pores (black).



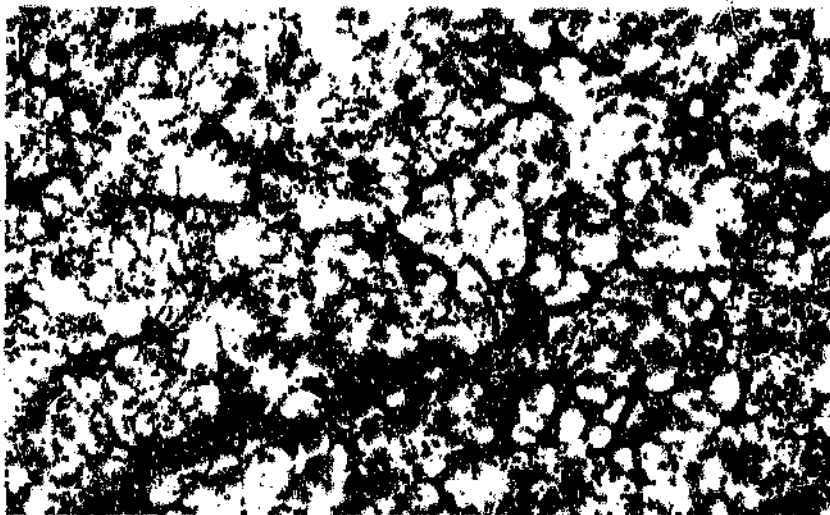
The balance of the sample consisted of  $\text{RuAl}_2$  dendrites with  $\text{Ru}_4\text{Al}_{13}$  in the interdendritic regions (Figure 5.14). Again, some of the dendrites had a "chewed" appearance (Figure 5.15). There were smaller cracks observed in this central region which were not lined with the Al-rich phase.

### Nominal Ru<sub>32</sub>:Al<sub>68</sub>

This sample exhibited a fairly low surface tension during production, by flattening upon cooling (as did the previous two samples). It was annealed at 1200°C for 312 hours before examining. The alloy appeared to have various different regions.

Near the upper and lower surfaces of the button-shaped sample many pores or cracks were present. They were lined with an Al-rich phase, and small irregular dispersions of the latter were present between the RuAl<sub>2</sub> dendrite arms in the vicinity of the cavities (Figure 5.12).

Figure 5.12: Optical micrograph of nominal Ru<sub>32</sub>:Al<sub>68</sub> annealed at 1200°C for 312 hours. Al-rich solid (dark grey), RuAl<sub>2</sub> (white dendrites), cracks and pores (black).



There were also regions in the sample which contained Al-lined cavities, with the adjacent microstructure consisting of dendrites of RuAl<sub>2</sub> in a Ru<sub>4</sub>Al<sub>13</sub> matrix (Table 5.4). In such

There were some regions which contained irregularly shaped Al-rich solid in the  $\text{RuAl}_2$  matrix, and the former was also found to line the cavities in these regions (Figure 5.11; the shiny areas are cavities).

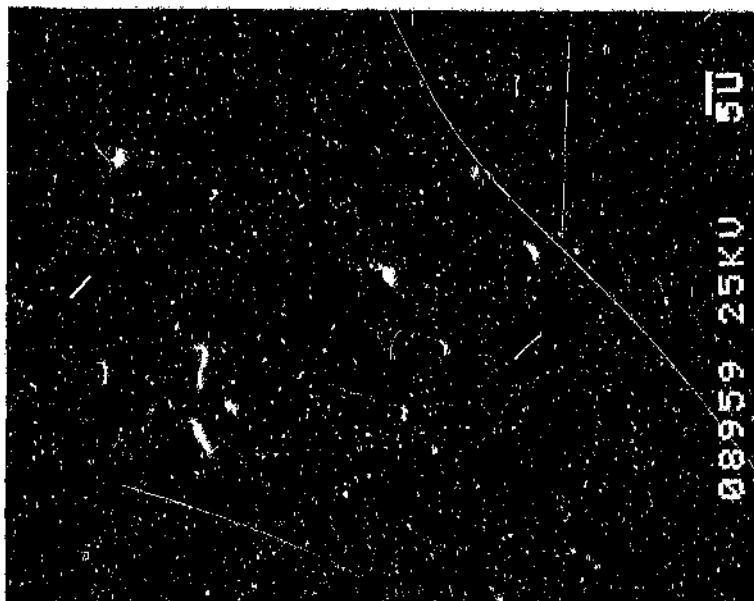
The average standardless chemical analyses are provided in Table 5.3, and examples of the individual results are contained in Appendix XII.

Table 5.3: Semi-quantitative chemical analyses for nominal  $\text{Ru}_{28.5}\text{Al}_{71.7}$  (1200°C for 312 hours),

PHASE	$\text{RuAl}_2$	Inclusions	Al-rich solid
PHASE DESCRIPTION	Matrix	Regular phase	Irregular phase
Ru (atomic %)	$30.7 \pm 0.2$	$39.8 \pm 0.3$	$0.39 \pm 0.05$
Al	$69.0 \pm 0.3$	$54.8 \pm 0.5$	$99.58 \pm 0.07$
Mn	$0.05 \pm 0.03$	$0.8 \pm 0.1$	$0.01 \pm 0$
Fe	$0.18 \pm 0.05$	$4.6 \pm 0.1$	$0.03 \pm 0.02$

Other scans (Appendix XII) also revealed silicon contamination in this sample. The source of the contamination did not lie in the elemental materials used. This sample was the first in the batch to be arc-melted, and since the electrode was not ground before commencing the melting, it is possible that the residue from prior use contaminated this sample. The silicon contamination may have stemmed from annealing the sample in a quartz tube. However, since the impurities are mostly confined to small inclusions in the matrix, this sample can bear some relevance to the current study.

**Figure 5.10:** SEM micrograph of (contaminated) nominal  $\text{Ru}_{22.3}\text{Al}_{71.7}$  (backscattered electron mode).  $\text{RuAl}_2$  (dark grey matrix), inclusions (light grey), pores (black).



**Figure 5.11:** SEM micrograph of (contaminated) nominal  $\text{Ru}_{22.3}\text{Al}_{71.7}$  (secondary electron mode).  $\text{RuAl}_2$  (dark grey matrix), Al-rich solid (black, discrete & lining cavities).

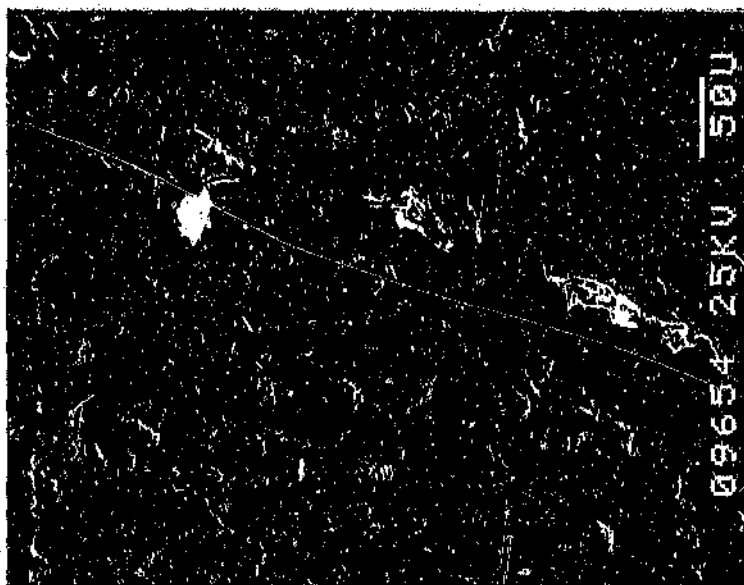
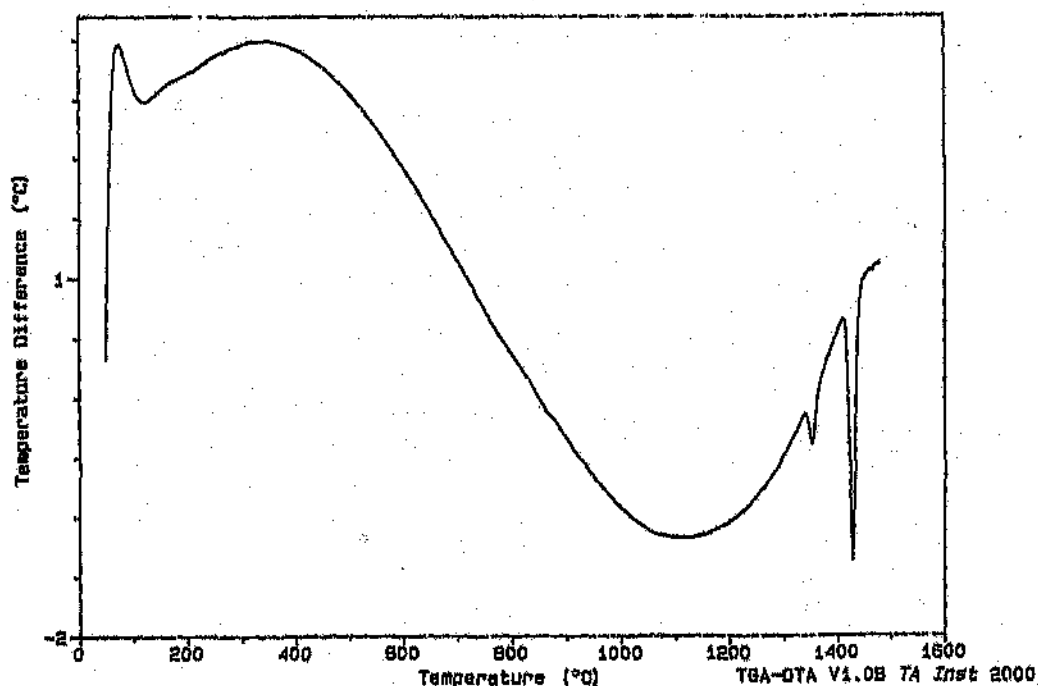


Figure 5.9: Third DTA trace for nominal  $\text{Ru}_{28.3}\text{Al}_{71.7}$ . Static air atmosphere.



#### Nominal $\text{Ru}_{28.3}\text{Al}_{71.7}$

This alloy displayed low surface tension in the same fashion as the previous one (by flattening and cracking upon cooling). Before examination, the sample was annealed at 1200° for 312 hours. It appeared to consist of two different regions and had many pores and cavities throughout (Figures 5.10 & 5.11). Most of this sample consisted of  $\text{RuAl}_2$  with small, regular, inclusions dispersed throughout (Figure 5.10; the dark areas are pores). It was contaminated with small amounts of manganese and iron, most of which was concentrated in the inclusions (Table 5.3).

Figure 5.7: First DTA trace for nominal  $\text{Ru}_{28}\text{Al}_{72}$ . Nitrogen flow of 100ml/min.

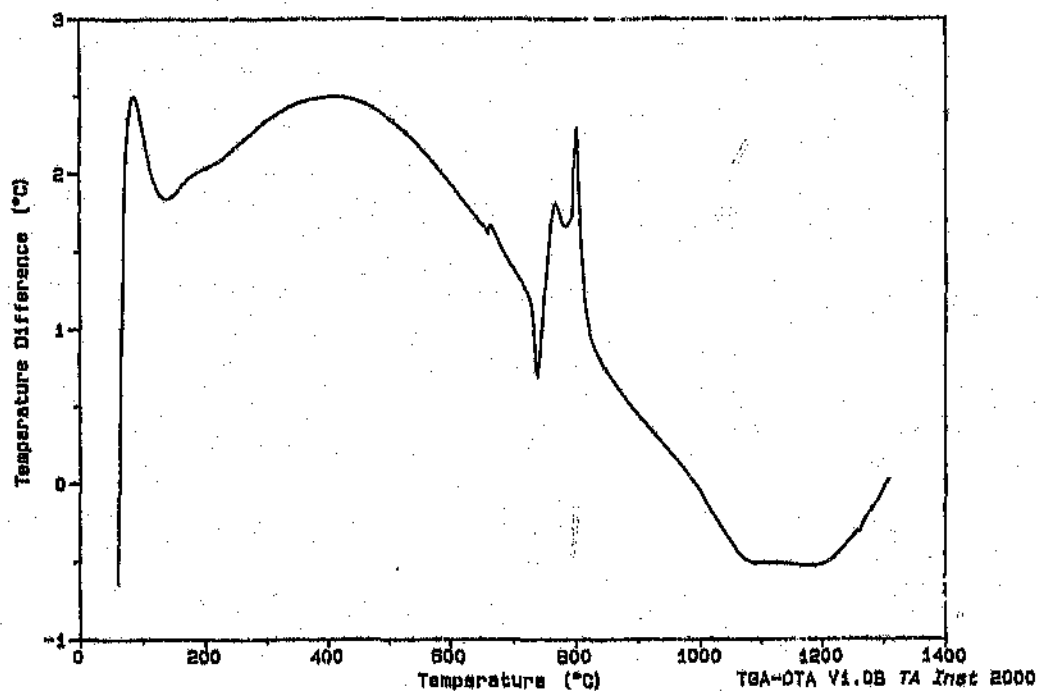
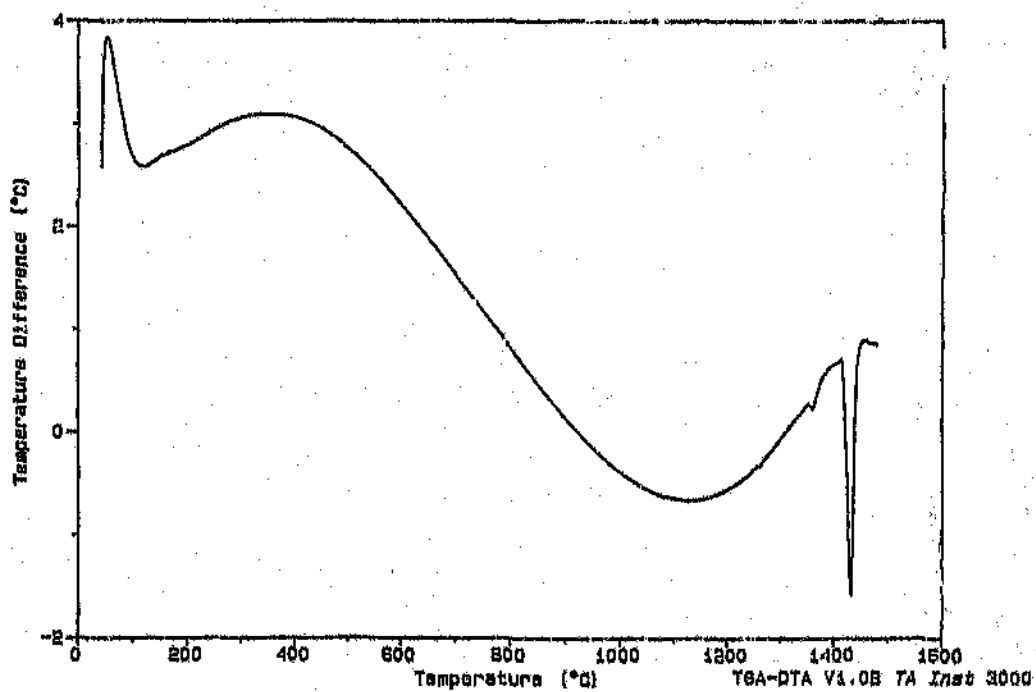


Figure 5.8: Second DTA trace for nominal  $\text{Ru}_{28}\text{Al}_{72}$ . Nitrogen flow of 100ml/min.



(Appendix XI). The silicon was possibly introduced during the heat treatment in a quartz tube.

Debye-Scherrer diffraction films confirmed the presence of  $\text{RuAl}_2$  and  $\text{Ru}_4\text{Al}_{13}$  (not  $\text{RuAl}_3$  - Chapter 6). There is a small possibility that faint Al-rich and  $\text{Ru}_2\text{Al}_3$  lines were also present on the film. The plane spacings could not be calculated because there were no high angle lines.

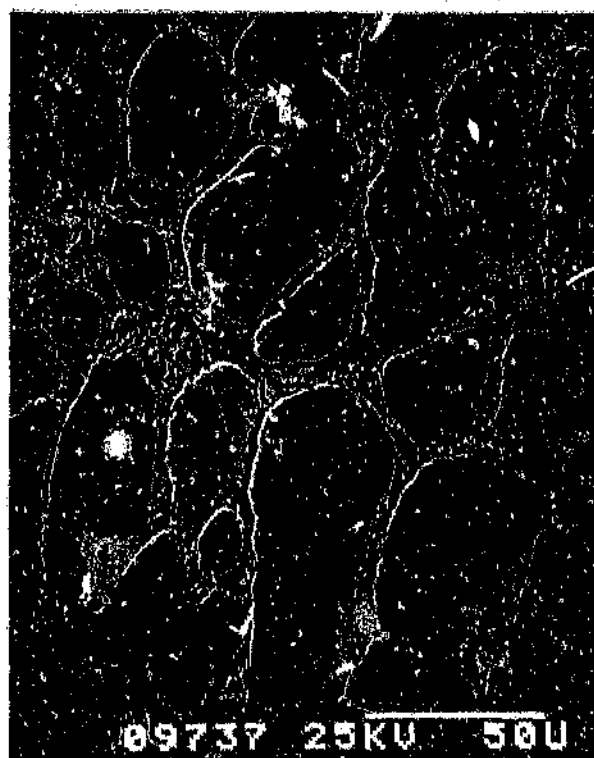
Three thermal analysis scans were run on this sample (Figures 5.7, 5.8 & 5.9). Magnified sections of these scans are given in Appendix XI, and show the reaction peaks in detail. The last two scans were similar, but very different to the first. The first reaction of the latter scan (Figure 5.7) was endothermic, with an onset temperature of  $656^\circ\text{C}$ , and peaked at  $660^\circ\text{C}$ . The second endothermic reaction had an onset temperature of  $730^\circ\text{C}$ , and peaked at  $741^\circ\text{C}$ . The third reaction was exothermic, and started at  $795^\circ\text{C}$  and peaked at  $803^\circ\text{C}$ .

The first two heating cycles employed an inert nitrogen atmosphere, while the third had no protection against oxidation. All of the reactions in the second and third scans (Figures 5.8 & 5.9) were endothermic. The first obvious reaction of the former (Figure 5.8) had an onset temperature of  $1353^\circ\text{C}$  and peaked at  $1363^\circ\text{C}$ . The second reaction started at  $1418^\circ\text{C}$  and peaked at  $1432^\circ\text{C}$ . The first reaction of the last scan (Figure 5.9) started at  $1343^\circ\text{C}$  and peaked at  $1355^\circ\text{C}$ . The second reaction started at  $1416^\circ\text{C}$  and peaked at  $1428^\circ\text{C}$ . In both of these scans there was a small dip in the plotted curve at about  $1460^\circ\text{C}$ . Since it was present in both curves, it is probably inherent to the system. The implications of these results are discussed in Chapter 6.



The sample appeared to have a two-phase dendritic microstructure (Figure 5.25) comprising  $\text{Ru}_2\text{Al}_3$  dendrites in a  $\text{Ru}_4\text{Al}_{13}$  matrix (Table 5.11). There were fine, intimate mixtures of the phases between the dendrites, which appeared as an additional phase when unresolved at low magnification (Figure 5.25).

**Figure 5.25:** SEM micrograph of (contaminated) nominal  $\text{Ru}_{33}\text{Al}_{33}\text{-b}$  (backscattered electron mode).  $\text{Ru}_2\text{Al}_3$  (dendrites),  $\text{Ru}_4\text{Al}_{13}$  (matrix).



At higher magnification, small amounts of a light, discrete phase were observed in the interdendritic regions (Figure 5.26), as well as two fine "eutectic"-like mixtures, having distinct morphologies. They had a different appearance to the small  $\text{RuAl}_2$  particles of the

**Table 5.10:** Quantitative chemical analyses for nominal  $\text{Ru}_{35}\text{Al}_{65}$ -am (1300°C for 6.5 hours, 1100°C for 65.5 hours).

PHASE	PHASE DESCRIPTION	ATOMIC % Ru
$\text{RuAl}$	Small single-phase region	$53.4 \pm 0.9$
$\text{Ru}_2\text{Al}_3$	Discrete phase	$42.8 \pm 0.3$
$\text{RuAl}_2$	Matrix	$35.91 \pm 0.08$

### Nominal $\text{Ru}_{35}\text{Al}_{65}$ -b

This sample was produced in an induction furnace in a zirconia crucible. An exothermic reaction occurred at about 950°C, and the sample was furnace-cooled and then air-cooled. The alloy had fused to form of a "tree" structure (Figure 5.24) on the side of the crucible.

**Figure 5.24:** Macroscopic photograph of nominal  $\text{Ru}_{35}\text{Al}_{65}$ -b. "Tree" structure formed by fused elements.

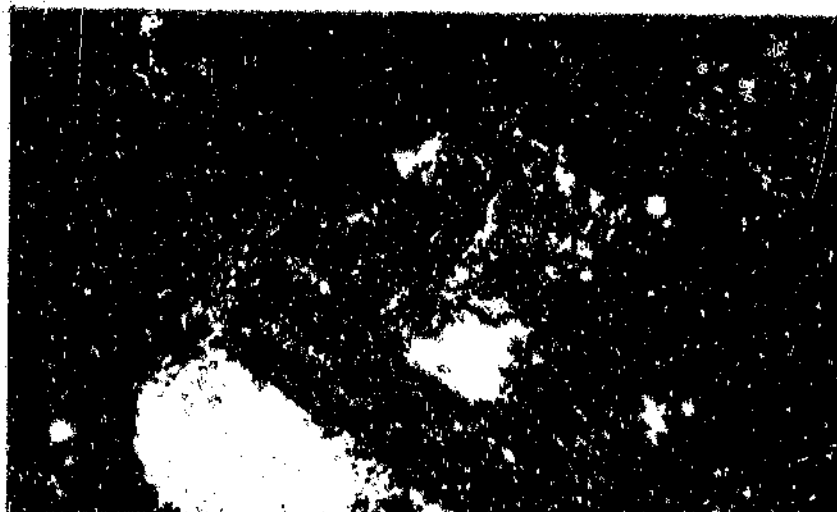
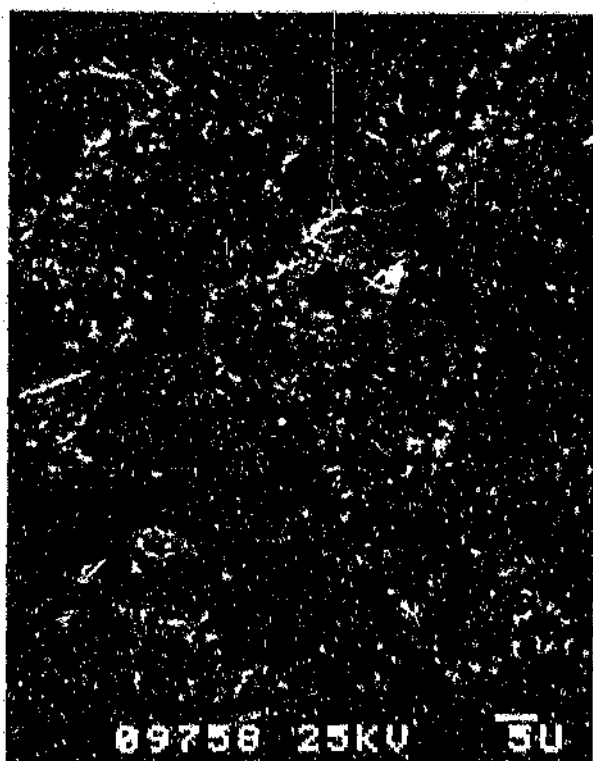


**Figure 5.23:** SEM micrograph of (contaminated) nominal  $\text{Ru}_{45}\text{Al}_{55}$  am annealed at  $1300^{\circ}\text{C}$  for 6.5 hours and  $1100^{\circ}\text{C}$  for 65.5 hours (backscattered electron mode). Majority of sample:  $\text{Ru}_2\text{Al}_3$  (dark grey),  $\text{RuAl}_2$  (black).



The average quantitative analyses are given in Table 5.10, and a standardless analysis of the RuAl phase is given in Appendix XV to show the low levels of silicon, iron, and zirconium contamination in the sample. The analyses could not be used to determine the positions of the phase boundaries. The microstructure of this sample was obviously not substantially affected by the anneal, because a region of RuAl was present.

and 5.23 did not differ significantly in composition from the phases in which they were observed, and were thus deduced to be polishing marks. The presence of  $\text{RuAl}_2$  as the matrix phase is an indication that this compound is formed directly from the melt, and not via a peritectoid reaction (Figure 2.2).

**Figure 5.22:** SEM micrograph of (contaminated) nominal  $\text{Ru}_{25}\text{Al}_{75}$  am annealed at  $1300^\circ\text{C}$  for 6.5 hours and  $1100^\circ\text{C}$  for 65.5 hours (secondary electron mode).  $\text{RuAl}$  (light grey),  $\text{Ru}_2\text{Al}_3$  (dark grey),  $\text{RuAl}_2$  (black).



silicon, and iron. A semi-quantitative analysis was obtained and scan was plotted to show the contamination (Appendix XV). The average quantitative analyses are given in Table 5.9. Nominal  $\text{Ru}_{35}\text{Al}_{65}$  had been melted in a zirconia crucible, and the edges of this sample must have reacted with the crucible and thus contaminated the subsequent re-melted sample.

Table 5.9: Quantitative chemical analyses for nominal  $\text{Ru}_{35}\text{Al}_{65}$ -am (No heat treatment).

PHASE	PHASE DESCRIPTION	ATOMIC % Ru
	Overall	~38.7
$\text{Ru}_2\text{Al}_3$	Dendrites	$46.6 \pm 0.2$
$\text{RuAl}_2$	Matrix	$36.7 \pm 0.2$

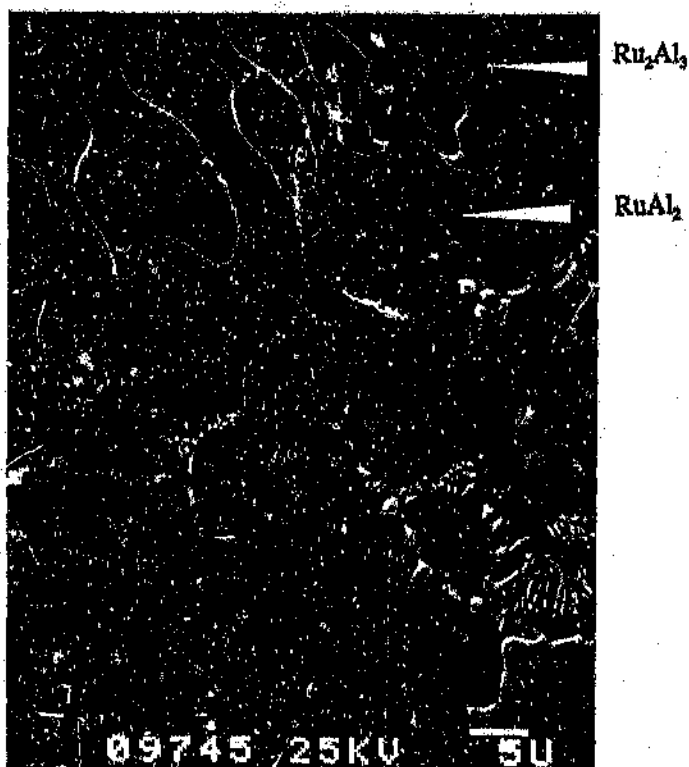
Debye-Scherrer experiments could not be used to facilitate phase identification, because the impurity elements would have altered the diffraction pattern, and rendered line identification near impossible.

The sample was heat treated at  $1300^\circ\text{C}$  for 6.5 hours, and then the temperature was reduced to  $1100^\circ\text{C}$  for 65.5 hours, because the quartz tube had expanded at the higher temperature. A different cross-section of the sample was examined.

A small single-phase region of  $\text{RuAl}$  was observed in the sample (Figure 5.22), which was surrounded by a layer of  $\text{Ru}_2\text{Al}_3$ . The rest of the microstructure (Figure 5.23) consisted of  $\text{Ru}_2\text{Al}_3$  in a matrix of  $\text{RuAl}_2$  (Table 5.10). The light spots which are present in Figures 5.22

cracked. The dendrites (Figure 5.21) appeared to contain a fine dispersion of particles, which were too small to analyse.

Figure 5.21: SEM micrograph of (contaminated) nominal  $\text{Ru}_{45}\text{Al}_{55}$ -am before heat treatment (backscattered electron mode).  $\text{Ru}_2\text{Al}_3$  (lighter coloured dendrites),  $\text{RuAl}_2$  (dark matrix), contaminated eutectic-like network.



The interdendritic region comprised three phases (Figure 5.21). The major phase,  $\text{RuAl}_2$  (black in Figure 5.21), appeared as large rounded particles. The other two phases formed a eutectic between these particles, and were found to contain large amounts of zirconium,

d (OBS) (nm)	I (EST.)	PHASE	h k l	d (CALC) (nm)
0.13389	very weak	$\text{RuAl}_2$	3 3 1	0.13392
0.12775	very weak	unidentified		
0.12608	very weak	unidentified		
0.12440	very weak	unidentified		
0.12298	very weak	unidentified		
0.11991	very weak	$\text{RuAl}$	2 1 1	0.1204
0.11802	very weak	unidentified		
0.11627	very weak	unidentified		
0.09214	very very weak	$\text{RuAl}$	3 1 0	0.0933
0.09005	very very weak	unidentified		
0.08853	very very weak	$\text{RuAl}$	3 1 1	0.08895
0.08710	very very weak	unidentified		
0.08674	very very weak	unidentified		
0.08518	very very weak	$\text{RuAl}$	2 2 2	0.08516
0.08190	very weak	$\text{RuAl}$	3 2 0	0.08182
0.08045	very very weak	unidentified		
0.07942	very very weak	$\text{RuAl}$	3 2 1	0.07884
0.07837	very very weak	unidentified		

#### Nominal $\text{Ru}_{45}\text{Al}_{55}$ am

This sample was produced by arc-melting  $\text{Ru}_{45}\text{Al}_{55}$ -a. It was first observed in the as-cast condition. There was difficulty identifying the phases from the quantitative analyses (Table 5.9), because they were contaminated with iron and zirconium, but it is thought that the dendrites were  $\text{Ru}_2\text{Al}_3$ , and the matrix was mainly  $\text{RuAl}_2$ . The latter phase was extensively

Table 5.8: Debye-Scherrer Diffraction Data For  $\text{Ru}_{35}\text{Al}_{65}$ -a (No heat treatment) (CuK $\alpha$ ).

d (OBS) (nm)	I (EST.)	PHASE	h k l	d (CALC)* (nm)
0.42684	medium	unidentified		
0.36833	strong	$\text{Ru}_4\text{Al}_{13}$ $\text{RuAl}_2$	2 2 0 1 1 1	0.36 0.369
0.33401	very strong	$\text{Ru}_4\text{Al}_{13}$	2 2 1	0.332
0.29530	medium	$\text{RuAl}_2$ $\text{RuAl}$	2 0 2 1 0 0	0.296 0.295
0.24508	very weak	unidentified		
0.23712	weak	$\text{RuAl}_2$	1 1 3	0.2376
0.22421	strong	$\text{RuAl}_2$	3 1 1	0.2247
0.21926	medium	$\text{RuAl}_2$	0 0 4	0.2197
0.21320	weak	unidentified		
0.20749	strong	$\text{RuAl}_2$ $\text{RuAl}$	0 2 2 1 1 0	0.2078 0.2086
0.20274	very very weak	$\text{RuAl}_2$	2 2 0	0.2033
0.18182	strong	$\text{RuAl}_2$	3 1 3	0.18206
0.16688	very weak	unidentified		
0.16110	very weak	$\text{RuAl}_2$	1 1 5	0.16130
0.15417	very weak	unidentified		
0.15182	very very weak	$\text{RuAl}_2$	1 3 1	0.15196
0.14923	very weak	$\text{RuAl}_2$	2 2 4	0.14917
0.14758	very very weak	$\text{RuAl}_2$ $\text{RuAl}$	4 0 4 2 0 0	0.14801 0.1475
0.14406	very weak	$\text{RuAl}_2$	4 2 2	0.14421
0.14021	very weak	$\text{RuAl}_2$	3 1 5	0.14017
0.13753	weak	$\text{RuAl}_2$	2 0 6	0.13753

\*These values were taken from the JCPDS data cards<sup>[12]</sup>.



Globular patches of  $\text{Ru}_4\text{Al}_{13}$ , containing small particles of  $\text{RuAl}_2$ , were observed near the  $\text{RuAl}_2$  dendrite arms (Figure 5.20). This feature is probably due to the high cooling rates experienced by the sample.

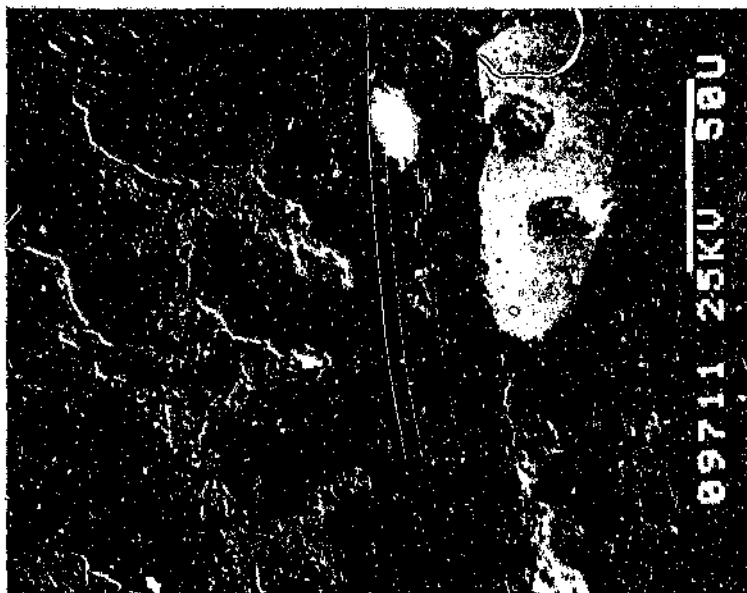
The average standardless EDAX analyses can be found in Appendix XIV. The average quantitative results are reported in Table 5.7, together with a semi-quantitative overall composition estimation.

Table 5.7: Chemical analyses for nominal  $\text{Ru}_{13}\text{Al}_{85}$ -a (No heat treatment).

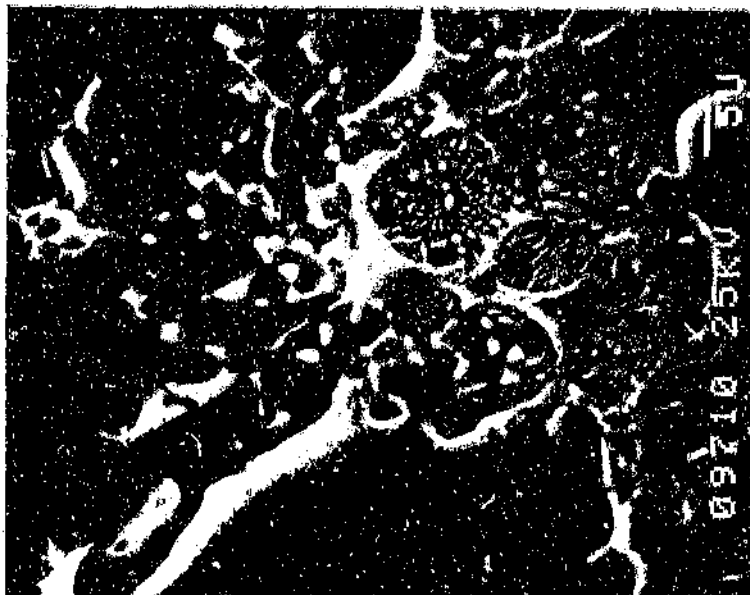
PHASE	PHASE DESCRIPTION	ATOMIC % Ru
	Overall	$28.2 \pm 0.2$
$\text{RuAl}$	Small area in dendrite	$53.6 \pm 0.2$
$\text{RuAl}_2$	Dendrites	$35.81 \pm 0.07$
$\text{Ru}_4\text{Al}_{13}$	Matrix	$25.00 \pm 0.05$

The quantitative results led to some uncertainty regarding phase identification. According to these analyses, the major phases could have been  $\text{Ru}_2\text{Al}_3$  and  $\text{RuAl}_3$ . However, the Debye-Scherrer results (Table 5.8) indicated the presence of  $\text{RuAl}_2$ ,  $\text{Ru}_4\text{Al}_{13}$  (not  $\text{RuAl}_3$  - Chapter 6), and  $\text{RuAl}$ . The Straumanis factor was 2.5013 degrees per cm. The  $\text{Ru}_4\text{Al}_{13}$  analyses gave an indication of the phase boundary position (Chapter 6).

**Figure 5.19:** SEM micrograph of nominal  $\text{Ru}_{35}\text{Al}_{65}$ -a (backscattered electron mode).  $\text{RuAl}$  (small light region),  $\text{RuAl}_2$  (darker grey),  $\text{Ru}_4\text{Al}_{13}$  (darkest grey).

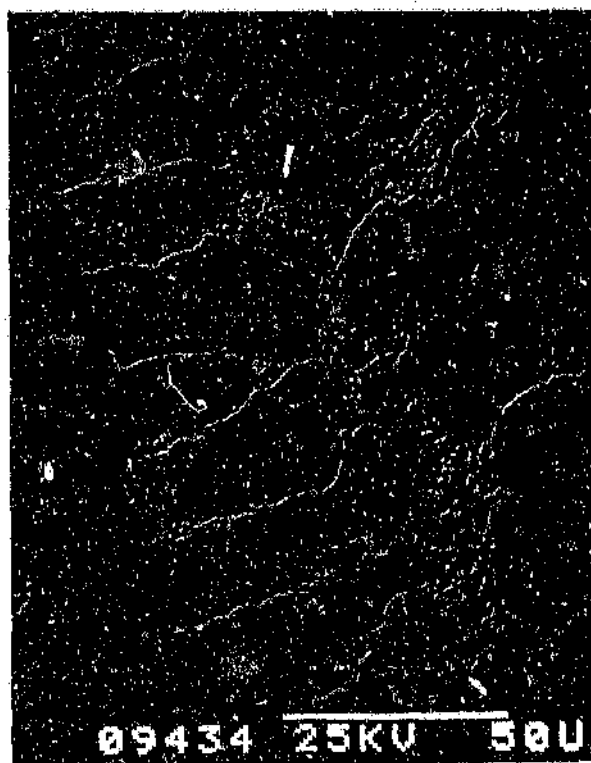


**Figure 5.20:** SEM micrograph of nominal  $\text{Ru}_{35}\text{Al}_{65}$ -a (secondary electron mode).  $\text{RuAl}$  (light grey),  $\text{Ru}_4\text{Al}_{13}$  (dark grey).



occurred, and the elements fused to form a "tree" structure, as did nominal  $\text{Ru}_{35}\text{Al}_{65}$ -b (see Figure 5.24). No further reactions were observed when this sample was heated to about  $1300^\circ\text{C}$ . Examination revealed a microstructure consisting of  $\text{RuAl}_2$  dendrites in a  $\text{Ru}_4\text{Al}_{13}$  matrix (Figure 5.18). The small particles of  $\text{RuAl}_2$  in the matrix possibly originated from decomposition of local inhomogeneities into  $\text{Ru}_4\text{Al}_{13}$  and  $\text{RuAl}_2$ , during fast cooling.

Figure 5.18: SEM micrograph of nominal  $\text{Ru}_{35}\text{Al}_{65}$ -a (backscattered electron mode).  $\text{RuAl}_2$  (light grey),  $\text{Ru}_4\text{Al}_{13}$  (dark grey).



A very small region of  $\text{RuAl}$  was observed in this sample (Figure 5.19). The edges of this region were irregular, possibly due the involvement of  $\text{RuAl}$  in a peritectic reaction.

The weight percent totals of the analyses for the Al-rich solid are low, due to the presence of oxide, and an oxide analysis is given in Appendix XIII, showing that it is  $\text{Al}_2\text{O}_3$ .

**Figure 5.17:** SEM micrograph of (contaminated) nominal  $\text{Ru}_{32}\text{Al}_{68}$  annealed at  $1200^\circ\text{C}$  for 480 hours and  $1050^\circ\text{C}$  for 24 hours (backscattered electron mode).  $\text{RuAl}_2$  (dark grey),  $\text{Ru}_2\text{Al}_3$  (light grey), Al-rich solid (black), inclusions (lightest).



#### Nominal $\text{Ru}_{32}\text{Al}_{68}$

This sample was produced in an induction furnace. Near  $950^\circ\text{C}$  an exothermic reaction

The analyses for RuAl in the two-phase region were used to modify the phase boundary (Chapter 6). The presence of RuAl and the Ru-rich solid solution were confirmed by the Debye-Scherrer experiments. Accurate plane spacings could not be reported, since there were no high angle peaks available for calculation of the shrinkage factor. Bulk X-ray results only confirmed the phase RuAl, because the sample was inhomogeneous and porous, and there was very little eutectic present.

Image analysis (Appendix XVIII) of this sample showed that approximately 4 at% Al was lost from the surface of this sample by vaporisation. It must be noted however, that the result quoted for  $\text{Ru}_{47}\text{Al}_{53}$  cannot be statistically accurate, since only six frames could be analysed.

#### Nominal $\text{Ru}_{50}\text{Al}_{50}$

This sample was seen to display a slow exothermic reaction during arc-melting. It was annealed at  $1200^{\circ}\text{C}$  for 2 hours before the first examination. As in the case of the previous sample, this alloy was found to have a central region which was mostly single-phase RuAl, and an outer region which was two-phase. Figure 5.35 shows the boundary between the two regions and gas porosity in the centre of the sample.

A fine eutectic between the Ru-rich solid solution and RuAl was observed at the grain boundaries of the latter phase (Figure 5.36). It had a different morphology compared to that observed in the previous sample (Figure 5.34).

**Figure 5.34:** SEM micrograph of nominal  $\text{Ru}_{47}\text{Al}_{53}$  annealed at  $1200^{\circ}\text{C}$  for 2 hours (backscattered electron mode). Eutectic mixture of Ru-rich solid (light grey) and  $\text{RuAl}$  (dark grey).

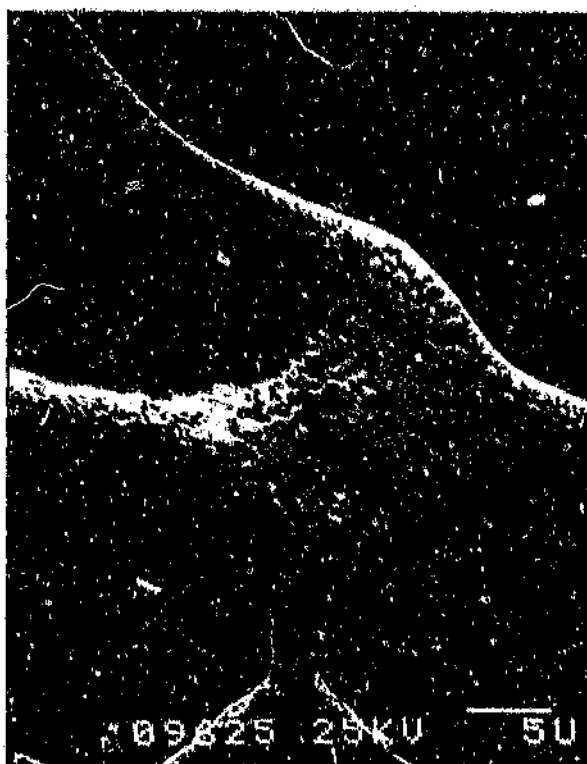
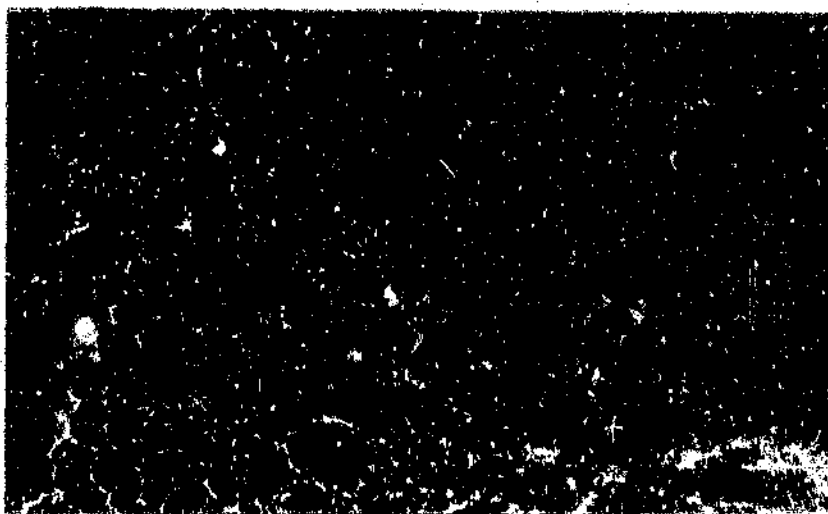


**Table 5.15:** Quantitative chemical analyses for nominal  $\text{Ru}_{47}\text{Al}_{53}$  ( $1200^{\circ}\text{C}$  for 2 hours).

PHASE	PHASE LOCATION	ATOMIC % Ru
Ru-rich solid	Eutectic with $\text{RuAl}$	$75.8 \pm 0.8$
$\text{RuAl}$	Two-phase region	$54.3 \pm 0.4$
	Single-phase centre	$51.77 \pm 0.06$

annealed at 1200°C for 2 hours before examining. It was found to have a central region which was mostly single-phase RuAl, with gas porosity resulting from the production method. The outer region near the surface of the sample contained the Ru-rich solid solution (Table 5.15) at the RuAl grain boundaries (Figure 5.33).

Figure 5.33: Optical micrograph of nominal Ru<sub>47</sub>:Al<sub>53</sub> annealed at 1200°C for 2 hours. RuAl (gray), Ru-rich solid (white).



The Ru-rich solid was found to form a fine eutectic with the RuAl (Figure 5.34).

The average semi-quantitative EDAX analyses are reported in Appendix XVIII, and the average quantitative results are given in Table 5.15.

The heat treatment had little effect on the homogeneity of this sample. Standardless EDAX analyses (Table 5.14 & Appendix XVII) showed that this sample was contaminated with silicon and small amounts of iron. The contamination must have been due to extensive heat treatment in a silica tube, since it was either not present before heat treatment, or not as obvious then. It could be a contributing factor to the difference in microstructures before and after heat treatment.

Table 5.14: Semi-quantitative chemical analyses for nominal  $\text{Ru}_{37}\text{Al}_{63}$  (1200°C for 840 hours).

PHASE	Ru-rich solid	RuAl		$\text{Ru}_2\text{Al}_3$
PHASE DESCRIPTION	Eutectic with RuAl	Un-cracked bands	Discrete phase	Majority of matrix
Ru (atomic %)	$91 \pm 1$	$48.8 \pm 0.4$	$44.56 \pm 0.02$	$38.0 \pm 0.1$
Al	$8 \pm 1$	$49.9 \pm 0.4$	$53.68 \pm 0.06$	$61.0 \pm 0.2$
Si	$1.0 \pm 0.2$	$1.1 \pm 0.2$	$1.1 \pm 0.1$	$1.0 \pm 0.1$
Fe	$0.13 \pm 0.06$	$0.138 \pm 0.008$	$0.65 \pm 0.06$	$0.08 \pm 0.02$

Since the sample was contaminated, and the observed phases (Ru-rich solid, RuAl, and  $\text{Ru}_2\text{Al}_3$ ) could easily be explained in terms of Obrowski's phase diagram (Figure 2.2), quantitative analyses of the phases were not undertaken.

#### Nominal $\text{Ru}_{47}\text{Al}_{53}$

During arc-melting of this sample, a slow exothermic reaction was observed. The alloy was



**Figure 5.31:** SEM micrograph of (contaminated) nominal  $\text{Ru}_{37}\text{Al}_{63}$  annealed at  $1200^\circ\text{C}$  for 841 hours (secondary electron mode).  $\text{RuAl}$  (light grey),  $\text{Ru}_2\text{Al}_3$  (dark grey).

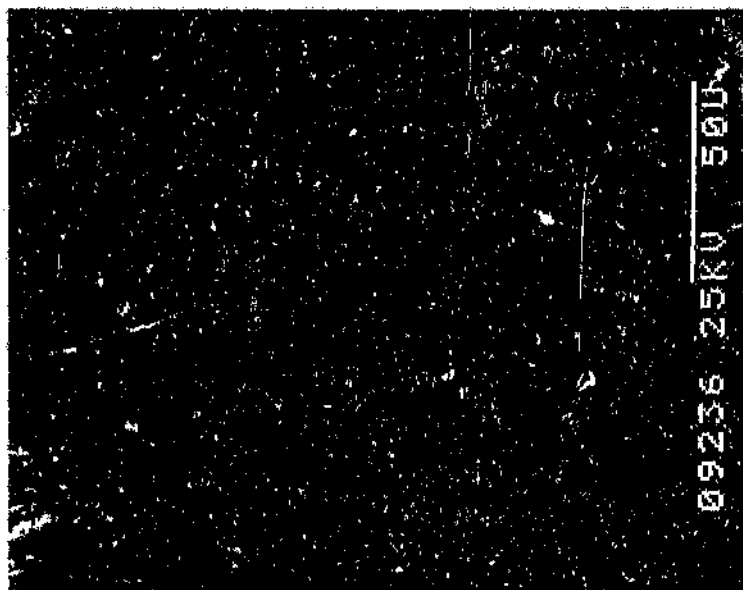
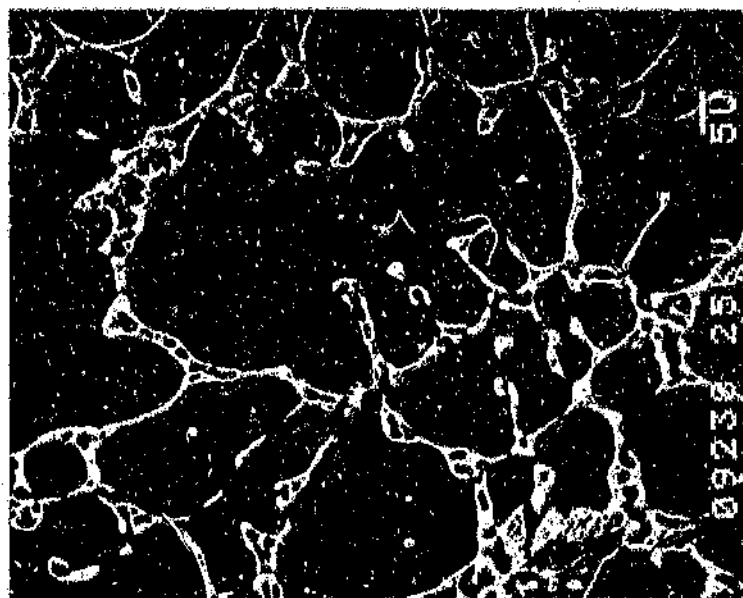


**Figure 5.32:** SEM micrograph of (contaminated) nominal  $\text{Ru}_{37}\text{Al}_{63}$  annealed at  $1200^\circ\text{C}$  for 840 hours (secondary electron mode). Ru-rich solid (light grey),  $\text{RuAl}$  (dark grey).



The average standardless chemical analyses are given in Appendix XVII, and include an analysis of the area depicted in Figure 5.29. The average quantitative analyses are reported in Table 5.12. The Ru-rich solid solution was not analysed with standards because the regions were too small, however the semi-quantitative result reported a ruthenium content of  $88 \pm 3$  at%.

The quantitative  $\text{Ru}_2\text{Al}_3$  and  $\text{RuAl}$  analyses were used to determine the position of their respective phase boundaries (Chapter 6). Bulk X-ray experiments only confirmed the presence of  $\text{RuAl}_2$ , probably because the sample was too inhomogeneous to obtain representative results. Debye-Scherrer results (Table 5.13) confirmed the presence of  $\text{RuAl}_2$  and  $\text{RuAl}$ . Some peaks were present which matched  $\text{Ru}_2\text{Al}_3$ , but the Ru-rich peaks were not present. The Straumanis factor was 2.5028 degrees per cm.

This sample was inhomogeneous, and was thus heat treated at  $1200^\circ\text{C}$  for a further 672 hours and water-quenched from this temperature. A different cross-section was examined, but the sample was still porous.

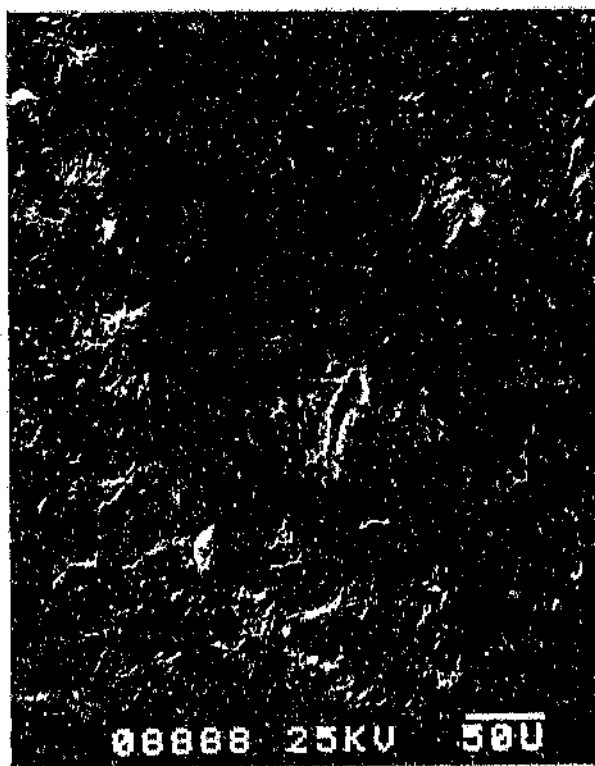
Most of the microstructure comprised discrete  $\text{RuAl}$  in a porous and cracked  $\text{Ru}_2\text{Al}_3$  matrix (Figure 5.31), but there were un-cracked bands in the microstructure consisting of  $\text{RuAl}$  grains. The Ru-rich solid solution had formed a eutectic with  $\text{RuAl}$  (Table 5.14) at the grain boundaries of the latter phase (Figure 5.32). There were also small areas in the un-cracked  $\text{RuAl}$ , which contained particles of  $\text{Ru}_2\text{Al}_3$ .

Table 5.13: Debye-Scherrer Diffraction Data For  $\text{Ru}_{77}\text{Al}_{23}$  (1200°C for 168 hours) (CuK $\alpha$ ).

d (OBS) (nm)	I (EST.)	PHASE	h k l	d (CALC) <sup>*</sup> (nm)
0.36849	very strong	$\text{RuAl}_2$	1 1 1	0.369
0.35720	very weak	$\text{Ru}_2\text{Al}_3$	0 0 4	0.358
0.29466	strong	$\text{RuAl}_2$ $\text{Ru}_2\text{Al}_3$ $\text{RuAl}$	2 0 2 1 0 1 1 0 0	0.296 0.301 0.295
0.23684	medium	$\text{RuAl}_2$	1 1 3	0.2376
0.22369	very strong	$\text{RuAl}_2$	3 1 1	0.2247
0.21900	strong	$\text{RuAl}_2$ $\text{Ru}_2\text{Al}_3$	0 0 4 1 1 0	0.2197 0.2177
0.20737	very strong	$\text{RuAl}_2$ $\text{Ru}_2\text{Al}_3$ $\text{RuAl}$	0 2 2 1 0 5 1 1 0	0.2078 0.2098 0.2086
0.20263	very weak	$\text{RuAl}_2$	2 2 0	0.2033
0.19966	very weak	$\text{RuAl}_2$	4 0 0	0.2003
0.18491	very weak	$\text{Ru}_2\text{Al}_3$	1 1 4	0.1861
0.18129	strong	$\text{RuAl}_2$	3 1 3	0.18206
0.16075	very weak	$\text{RuAl}_2$	1 1 5	0.16130
0.15351	very very weak	unidentified		
0.15135	very very weak	$\text{RuAl}_2$	1 3 1	0.15198
0.14899	weak	$\text{RuAl}_2$ $\text{RuAl}$	2 2 4 2 0 0	0.14917 0.1475
0.14388	very weak	$\text{RuAl}_2$	4 2 2	0.14421
0.13991	weak	$\text{RuAl}_2$	3 1 5	0.14017
0.13357	weak	$\text{RuAl}_2$	3 3 1	0.13392
0.12761	weak	unidentified		
0.12417	medium	unidentified		
0.12292	weak	unidentified		
0.11604	weak	unidentified		
0.10383	very weak	$\text{RuAl}$	2 2 0	0.1043
0.10259	very weak	unidentified		
0.09874	very very weak	$\text{RuAl}$	3 0 0	0.09833
0.09209	very very weak	unidentified		
0.07990	very very weak	$\text{RuAl}$	3 2 1	0.07884

<sup>\*</sup>These values were taken from the JCPDS data cards<sup>[12]</sup>.

**Figure 5.30:** SEM micrograph of nominal  $\text{Ru}_{37}\text{Al}_{63}$  annealed at  $1200^\circ\text{C}$  for 168 hours (backscattered electron mode). Small un-cracked area, working outwards:  $\text{RuAl}$  (light core) with Ru-rich solid (white),  $\text{Ru}_2\text{Al}_3$  (light grey layer),  $\text{RuAl}_2$  (dark grey matrix).



**Table 5.12:** Quantitative chemical analyses for nominal  $\text{Ru}_{37}\text{Al}_{63}$  ( $1200^\circ\text{C}$  for 168 hours).

PHASE	PHASE DESCRIPTION	ATOMIC % Ru
$\text{RuAl}$	Matrix of un-cracked region	$50.2 \pm 0.6$
$\text{Ru}_2\text{Al}_3$	Layer surrounding $\text{RuAl}$	$41.6 \pm 0.5$
$\text{RuAl}_2$	Matrix of cracked region	$34.7 \pm 0.5$

The matrix of the un-cracked region consisted of RuAl. In some parts of this region, the Ru-rich solid solution formed a eutectic with the RuAl at the grain boundaries (Figure 5.28). In the central areas of the un-cracked region,  $\text{Ru}_2\text{Al}_3$  had formed at the grain boundaries, with fine precipitates of this phase in the RuAl grains (Figure 5.29). There was also a layer of  $\text{Ru}_2\text{Al}_3$  surrounding the RuAl region.

Figure 5.29: SEM micrograph of nominal  $\text{Ru}_{37}\text{Al}_{63}$  annealed at  $1200^\circ\text{C}$  for 168 hours (backscattered electron mode). Un-cracked region: RuAl (light grey),  $\text{Ru}_2\text{Al}_3$  (dark grey).

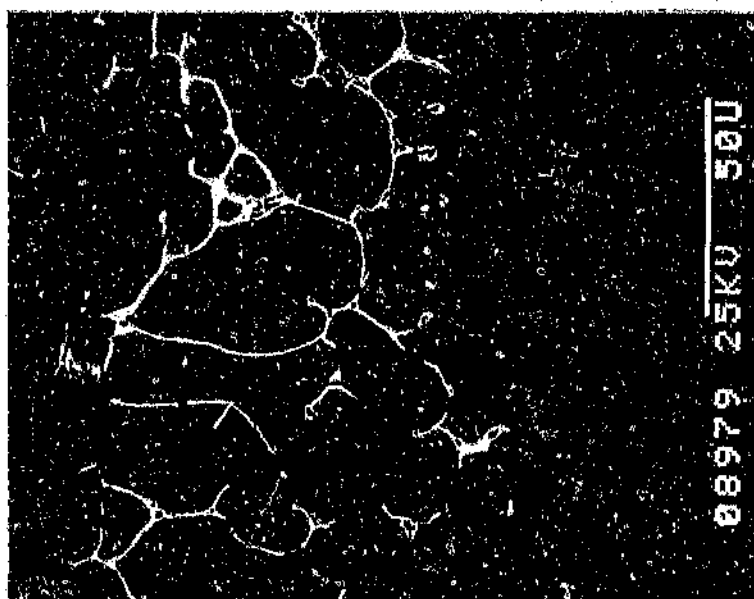


A small area in the cracked region appeared to be a miniature version of the entire sample (Figure 5.30). The balance of the cracked region consisted of discrete  $\text{Ru}_2\text{Al}_3$  grains in a RuAl<sub>2</sub> matrix.

**Figure 5.27:** Optical micrograph of nominal  $\text{Ru}_{37}\text{Al}_{63}$  annealed at  $1200^\circ\text{C}$  for 168 hours (Murakami's etch). Ru-rich solid (white),  $\text{RuAl}$  (un-cracked, light matrix),  $\text{Ru}_2\text{Al}_3$  (thin layer),  $\text{RuAl}_2$  (cracked, dark matrix) containing  $\text{Ru}_2\text{Al}_3$  grains.



**Figure 5.28:** SEM micrograph of nominal  $\text{Ru}_{37}\text{Al}_{63}$  annealed at  $1200^\circ\text{C}$  for 168 hours (backscattered electron mode). Un-cracked region: Ru-rich solid (white),  $\text{RuAl}$  (grey).



contamination). It was assumed that this phase was  $\text{Ru}_2\text{Al}_3$  because it formed a "eutectic"-like mixture with the  $\text{Ru}_4\text{Al}_{13}$  matrix, as in the case of the nominal  $\text{Ru}_{10}\text{Al}_{90}$  sample (Chapter 4).

Table 5.11: Quantitative chemical analyses for nominal  $\text{Ru}_{45}\text{Al}_{55}$ -b (No heat treatment).

PHASE	PHASE DESCRIPTION	ATOMIC % Ru
$\text{Ru}_2\text{Al}_3$	Dendrites	$36.53 \pm 0.02$
	"Eutectic"-like	$30.07 \pm 0.04$
$\text{Ru}_4\text{Al}_{13}$	Matrix	$26.7 \pm 0.1$
	Larger discrete phase	$\sim 28.8$

The semi-quantitative analysis of the overall composition showed that the sample contained about 29 at% Ru and 0.8 at% Zr (Appendix XVI).

#### Nominal $\text{Ru}_{37}\text{Al}_{63}$

Although the ampoule containing the  $\text{Ru}_{37}\text{Al}_{63}$  sample cracked during heat treatment ( $1200^\circ\text{C}$  for 168 hours), there seemed to be no obvious damage to this sample. This sample was definitely inhomogeneous, and comprised various phases. Macroscopically, it had a cracked region and an un-cracked region. Figure 5.27 shows the difference between the two regions, as well as the relative etch colours of the various phases. The variety in etch colour of a phase can be attributed to a variation in grain orientation. Especially in the thin  $\text{Ru}_2\text{Al}_3$  layer.

previous sample (Figure 5.20). The composition of the larger discrete particles appeared, in backscattered electron mode, to be similar to that of the dendrites.

Figure 5.26: SEM micrograph of (contaminated) nominal  $\text{Ru}_{25}\text{Al}_{75}$ -b (backscattered electron mode).  $\text{Ru}_2\text{Al}_3$  (light grey bulk),  $\text{Ru}_4\text{Al}_{13}$  (matrix), two contaminated eutectic-like mixtures.



The interdendritic mixtures contained a high proportion of zirconium. A scan was plotted in order to depict this observation (Appendix XVI). The larger discrete phase also contained zirconium, and hence an accurate quantitative analysis could not be obtained. It was not clear, from the chemical analyses (Table 5.11), whether the dendritic phase was  $\text{Ru}_2\text{Al}_3$  or  $\text{RuAl}_2$ , and Debye-Scherrer experiments could not be used to identify the phase (due to the



The absence of the phase  $\text{RuAl}_{12}$  from Edshammar's samples<sup>[10]</sup> (quenched from 660°C) agrees with the observations made by Anlage<sup>[5]</sup> which cast doubt over the existence of the phase, proposed by Obrowski to form at about 720°C.

During Varich's investigation of rapid solidification in this system<sup>[11]</sup> he did not observe  $\text{RuAl}_{12}$  in his alloys, which contained less than 4.16 at% Ru. All of his alloys contained more than 0.5 at% Ru, and those used for determining the equilibrium solubility of Ru in Al were annealed at 650°C for 50 hours. These alloys, according to Obrowski, should have contained  $\text{RuAl}_{12}$ , but  $\text{RuAl}_6$  was observed instead. This once again lends support to the idea that  $\text{RuAl}_{12}$  does not exist.

## 6.2 Discussion of Individual Samples

### Nominal $\text{Ru}_{31}\text{Al}_{67.8}$

Although this sample appeared to be promising in terms of homogeneity, it was rendered of limited use to the current investigation by the large quantities of impurities present (Table 4.1). These elements were probably introduced via the aluminium powder, which was only 95% pure. According to Obrowski's phase diagram<sup>[4]</sup>, the phase  $\text{RuAl}_{12}$  should be present in the sample. Its absence could be due to the contamination. In some regions the  $\text{RuAl}_6$  particles are very fine, and this could be interpreted as being the eutectic between  $\text{RuAl}_6$  and the Al-rich solid solution which Anlage proposed<sup>[5]</sup>. Since the "star" morphology of the fine  $\text{RuAl}_6$  particles (Figure 4.1) was not observed in other samples, it is likely that the contamination effected this.

was transformed, or  $\text{RuAl}_2$  forms directly from the melt. Therefore, there may be a peritectic reaction point (forming  $\text{RuAl}_2$ ) at 33.33 at% Ru or at a slightly higher composition. In the heat treated condition this alloy fits Obrowski's phase diagram.

In Edshammar's arc-melted samples containing 30.77, 28.57, and 27 at% Ru, little, if any,  $\text{RuAl}_2$  was detected (the remainder was  $\text{Ru}_4\text{Al}_{13}$ ). It is possible that the proposed peritectic point for  $\text{RuAl}_2$  lies at a higher Ru composition than these samples, and thus a metastable phase ( $\text{RuAl}_{2.5}$ ) forms instead. It was noted that there is no eutectic of  $\text{Ru}_4\text{Al}_{13}$  and  $\text{RuAl}_2$  in these samples. In the heat treated condition these samples conform to Obrowski's phase diagram.

Edshammar's sample containing 25 at% Ru was reported to consist only of  $\text{Ru}_4\text{Al}_{13}$  in the arc-melted condition. This would not be likely to occur if Obrowski's work is correct, since, according to his phase diagram, the  $\text{L} \rightarrow \text{RuAl}_2 + \text{Ru}_4\text{Al}_{13}$  eutectic reaction occurs before the solid state formation of  $\text{RuAl}_2$  (Figure 2.2). However, if Anlage's diagram is correct, then it is quite possible to form  $\text{Ru}_4\text{Al}_{13}$ , either peritectically or directly from the liquid, in an arc-melted sample.

The lack of the phase  $\text{RuAl}_2$  in Edshammar's samples (containing 14 at% Ru and 20 at% Ru) quenched from 950°C can be easily explained by Anlage's formation temperature of 723°C for  $\text{RuAl}_2$  (Figure 2.3). In Anlage's samples containing 10 at% Ru, the phase  $\text{RuAl}_2$  was found to form via a peritectic reaction when the sample was cooled slowly<sup>[5]</sup>. The fact that  $\text{RuAl}_2$  forms with slower rather than faster cooling perhaps indicates that  $\text{RuAl}_2$  is more likely to be a stable phase rather than a metastable one.

stable temperature range is incorrect, or that the phase is very difficult to decompose.

In the arc-melted condition, his samples containing 36.36 to 44.44 at% Ru consisted of the phases  $\text{RuAl}$  and  $\text{RuAl}_2$ . According to Obrowski's phase diagram, one would have expected to find  $\text{Ru}_2\text{Al}_3$  instead of  $\text{RuAl}_2$ . This suggests that  $\text{RuAl}_2$  forms at higher temperatures than Obrowski predicted<sup>(4)</sup>, possibly higher than the formation of  $\text{Ru}_2\text{Al}_3$ , or, if below, very close to it. (The current investigation has shown the possibility of a series of peritectic reactions forming  $\text{Ru}_2\text{Al}_3$ ,  $\text{RuAl}_2$ , and  $\text{Ru}_4\text{Al}_{13}$ , in that order.) If this is the case, then the reaction to form  $\text{Ru}_2\text{Al}_3$  could easily be missed by undercooling of the alloy, due to the fast cooling conditions (as in the metastable and stable Fe-C system when forming cementite or graphite respectively), especially if the two reaction temperatures are close together. The heat treatment at 950°C resulted in the formation of  $\text{Ru}_2\text{Al}_3$ , where it did not exist before. This suggests that  $\text{Ru}_2\text{Al}_3$  is stable to temperatures lower than 950°C. It also suggests that, in the composition range 36.36 to above 44.44 at% Ru and at the temperature of 950°C, there are two two-phase regions in the phase diagram:  $\text{RuAl}_2 + \text{Ru}_2\text{Al}_3$ , and  $\text{Ru}_2\text{Al}_3 + \text{RuAl}$ . If this is the case, the continued presence in the heat treated samples of  $\text{RuAl}$  (in the less Ru-rich samples) and  $\text{RuAl}_2$  (in the more Ru-rich samples) can be explained in terms of their high stability.

According to Obrowski's phase diagram (Figure 2.2), in an arc-melted alloy containing 33.33 at% Ru, one would expect to find at least the phases  $\text{RuAl}$  and  $\text{Ru}_2\text{Al}_3$ . The fact that  $\text{RuAl}_2$  was identified in Edshammar's arc-melted sample of this composition again suggests that  $\text{RuAl}_2$  forms at much higher temperatures than Obrowski predicted. In addition, the apparent absence of  $\text{RuAl}$  suggests that, either only a small amount of  $\text{RuAl}$  solidified and

of the phase, if he quenched the sample. Schwomma's work was difficult to assess due to lack of information regarding heat treatments, so it was difficult to ascertain the exact implications of his investigation; but there is an implication that  $\text{RuAl}_2$  is stable at higher temperatures than postulated by Obrowski.

Edshammar's<sup>[9]</sup> arc-melted and heat treated ( $950^\circ\text{C}$ ) samples (Tables 2.2) can be used to deduce the likely whereabouts of some of the liquidus and solidus lines, as well as the relative temperatures of formation of the phases.

During Edshammar's investigation of the Ru-Al system<sup>[9]</sup> the phase  $\text{RuAl}_{2.5}$  was observed, but only in the arc-melted samples. Hence this may simply be an inhomogeneity promoted by non-equilibrium cooling encountered during the arc-melting process, or it may be a high temperature metastable phase. The latter is the more probable suggestion, since the phase had its own X-ray powder pattern (Table 2.8), which suggests a distinct structure. This phase was found in four samples, but has not been reported in other publications concerning this system. There was a lack of clarity in his publication: in the table of sample phases (arc-melted and heat treated) he reported the phases as shown in Table 2.2, whereas in the text, he appears to be stating that the  $\text{RuAl}_{2.5}$  phase transforms directly to " $\text{RuAl}_{1.5}$ ", or  $\text{Ru}_2\text{Al}_3$ . If the textual description represents the case, then Obrowski's phase diagram is not necessarily contradicted; but if the results as presented in his table represent the situation, then Obrowski's phase diagram is compromised, as is discussed below.

The fact that Edshammar observed the phase  $\text{Ru}_2\text{Al}_3$  in samples quenched from  $950^\circ\text{C}$  (e.g. his sample containing 44.44 at% Ru<sup>[9]</sup>), suggests that either Obrowski's estimate<sup>[4]</sup> of its

phase  $\text{RuAl}_{12}$  has not been detected in any other independent studies of the system. Thirdly, the  $\text{Ru}_4\text{Al}_{13}$  and  $\text{RuAl}_6$  phases were found in a similar sample (nominal  $\text{Ru:Al}_{12}$ ), and looked similar to Obrowski's proposed phases. Fourthly, the proposal removes one of the inconsistencies in the etching colours of the phases (Table 2.1), which is that the relative etch colours differ in Obrowski's the samples. In the 19.3% and 25% Ru samples,  $\text{RuAl}_6$  is white, and  $\text{RuAl}_{12}$  as grey. However, in the 13.75% Ru sample,  $\text{RuAl}_6$  is grey, and the white phase is described as  $\text{RuAl}_{12}$  (as it is in the 0.5% Ru sample). If the  $\text{RuAl}_{12}$  was a misidentification of  $\text{RuAl}_6$  (which is the phase containing the least amount of Ru in all other investigations, including this one), then  $\text{RuAl}_6$  always appears white, and  $\text{RuAl}_3$  (or  $\text{Ru}_4\text{Al}_{13}$ ) is consistently grey. Lastly, Obrowski<sup>[4]</sup> reported the temperature of formation of  $\text{RuAl}_{12}$  and the eutectic temperature to be approximately 630°C and 750°C respectively, while Anlago<sup>[3]</sup> observed  $\text{RuAl}_6$  to form at 723°C and stated that the eutectic temperature is 652°C. These reaction temperatures are remarkably similar, and suggest that Obrowski may have made an error in deducing the reactions corresponding to these temperatures. It appears that he identified the phases using X-ray data. Since he incorrectly identified the crystal structures, it is feasible that he may have identified the phases incorrectly.

Schwomma's investigation<sup>[7]</sup> also shows inconsistencies with the published phase diagram. According to Obrowski's diagram, the slow cooling of Schwomma's samples containing 33.3 at% Ru from 1750°C to 1350°C should not form  $\text{RuAl}_2$  if it was subsequently quenched from 1350°C. However, the specified treatment would result in  $\text{RuAl}_2$  if this phase was stable at temperatures higher than 1350°C. Thus Schwomma found  $\text{RuAl}_2$  at much higher temperatures than is indicated by Obrowski's proposed solid state formation

according to his diagram, if the sample was quenched just below 1300°C, but above the lower temperature reactions. The heat treatment was not stated, other than "solidified in crucible"<sup>(4)</sup>. It is proposed, once again, that his phase identification was incorrect, and the "eutectic" mixture consisted of  $\text{Ru}_2\text{Al}_3$  and  $\text{Ru}_4\text{Al}_{13}$  instead.

Obrowski then stated that the  $\text{Ru}_2\text{Al}_3$  in the eutectic transformed directly to  $\text{RuAl}_2$ . It is more likely that  $\text{Ru}_2\text{Al}_3$  would undergo a peritectoid reaction with some of the  $\text{RuAl}_6$  to form  $\text{RuAl}_3$ , since this phase not only lies nearer the alloy composition (Figure 2.2), but also is the prescribed reaction according to his own phase diagram. The transformation to  $\text{RuAl}_2$  occurs at lower temperatures than that to  $\text{RuAl}_3$  (according to Obrowski), and is probably more difficult to produce, due to diffusion and energy considerations. Obrowski's proposed transformation could only occur if  $\text{RuAl}_2$  was formed at a higher temperature than  $\text{RuAl}_3$ . In addition, this transformation has not been suggested in any of his other samples containing  $\text{Ru}_2\text{Al}_3$ , and is thus inconsistent with the remainder of his work.

Obrowski's alloy containing 13.75 at% Ru looked very much like the nominal  $\text{Ru:Al}_{12}$  alloy from the current investigation. His sample contained needles, a peritectic phase surrounding the needles, and a eutectic matrix; as did the nominal  $\text{Ru:Al}_{12}$  sample from this investigation. It is proposed that Obrowski did not identify the phases correctly: the needles are actually  $\text{Ru}_4\text{Al}_{13}$  (instead of  $\text{RuAl}_6$ ), the peritectic phase is  $\text{RuAl}_6$  (instead of  $\text{RuAl}_{12}$ ), and the eutectic consists of Al-rich solid and  $\text{RuAl}_6$  (not Al-rich solid and  $\text{RuAl}_{12}$ ). This proposal is supported by the following factors. Firstly, Anlage found that  $\text{Ru}_4\text{Al}_{13}$  forms as needles due to coherent growth along ledges, and  $\text{RuAl}_6$  forms (peritectically) via continuous incoherent growth to produce more allotriomorphic structures<sup>(5)</sup>. Secondly, the

temperature such that the sample is in the solid  $\text{Ru}_2\text{Al}_3$  phase field prior to quenching, which is the heat treatment that this sample seems to imply. Slow cooling of this sample, according to Obrowski's diagram, should result in a microstructure consisting mostly of the phase  $\text{RuAl}_2$  with a small amount of  $\text{RuAl}$ . The latter phase would not be dendritic in nature, since it should have been formed from the eutectoid decomposition of  $\text{Ru}_2\text{Al}_3$ . Intermediate cooling rates should give a mixed structure (of  $\text{RuAl}$ ,  $\text{Ru}_2\text{Al}_3$ ,  $\text{RuAl}_2$ , and possibly a small amount of  $\text{Ru}_4\text{Al}_{13}$ ) because it is appreciated (from the current work) that homogenisation by diffusion is a slow process in this system.

His sample containing 25 at% Ru did obviously not reach equilibrium conditions, since it contains more than two phases. This sample actually contains three phases, as do a number of his samples. According to the phase diagram, the sample should consist only of  $\text{RuAl}_2$  if cooled under equilibrium conditions. Obrowski stated that there was a eutectic between  $\text{RuAl}_6$  and  $\text{Ru}_2\text{Al}_3$ , and that this eutectic had transformed, in places, to  $\text{RuAl}_2$ . The intimate mixture in his corresponding figure is different in morphology from the eutectic between  $\text{RuAl}_6$  and  $\text{Al}$ , and is thus unlikely to be the same eutectic misidentified. This "eutectic" had a similar appearance to the intimate mixture found in the current examination between  $\text{Ru}_2\text{Al}_3$  and  $\text{Ru}_4\text{Al}_{13}$  (Figure 4.21). The possibility exists that Obrowski identified the phases incorrectly, and that his reported eutectic of  $\text{RuAl}_6$  and  $\text{Ru}_2\text{Al}_3$  was, in fact, the intimate mixture of  $\text{Ru}_2\text{Al}_3$  and  $\text{Ru}_4\text{Al}_{13}$  found in the current investigation.

According to Obrowski's phase diagram, his sample containing 19.3 at% Ru should consist of  $\text{RuAl}_6$  and  $\text{RuAl}_2$ , if it was cooled under equilibrium conditions. He reported the presence of primary  $\text{Ru}_2\text{Al}_3$  and a eutectic between  $\text{RuAl}_6$  and  $\text{Ru}_2\text{Al}_3$ . This is only possible,

The phases identified in Obrowski's samples containing 83.5 at% Ru and 67 at% Ru are consistent with his phase diagram (Figure 2.2) if these samples were cooled slowly to room temperature. In fact, since RuAl has been found in this study to be a very stable phase, the same microstructures would have been detected in these samples even under more rapid cooling conditions.

Obrowski's sample containing 50 at% Ru was reported to have cored dendrites of RuAl. His corresponding figure shows this phenomenon well, but there appears to be an additional phase at the grain boundaries which was not reported, and was etched white. It is likely that this phase would be the RuAl and Ru-rich solid solution eutectic. The latter is possible, since the current investigation found that the eutectic mixture did occur at the grain boundaries, and the discrete RuAl in the eutectic was very fine and difficult to discern. If the composition given for this sample is the nominal value, then the possible presence of the eutectic does not detract from the validity of this region of Obrowski's phase diagram, since any small loss of Al from this sample would result in the formation of the eutectic.

Obrowski reported that he found  $\text{Ru}_2\text{Al}_3$  and primary RuAl in the sample containing 33 at% Ru. He also stated that this sample was solidified slowly. With this heat treatment, these results are not consistent with his phase diagram. According to his phase diagram, at the given composition, this microstructure is only possible if he quenched the sample from about 1300°C. This would enable the formation of primary RuAl, and allow for the peritectic reaction to produce  $\text{Ru}_2\text{Al}_3$ . However, to avoid the appearance of Obrowski's eutectic reaction ( $\text{L} \rightarrow \text{Ru}_2\text{Al}_3 + \text{RuAl}$ ), or reactions at lower temperatures, the sample should have been solid at the quenching temperature. It would be difficult to hold the



there is more chance of misinterpretation, because the energetically unfavourable phase has to be correctly identified.

From careful examination of Obrowski's report, it was obvious that there were crucial details omitted from his description (such as heat treatments), and there are inconsistencies in his results, especially the etching colours of the phases (Table 2.1). Usually an etch will attack the most reactive material preferentially. Thus one would expect the phases to have consistent relationships, that is, two particular phases should be etched (with the same etchant) such that the same phase is always more attacked than the other. This criterion is not obeyed in the 96.3 and 83.5 at% Ru samples for the Ru-rich and RuAl phases, which casts doubt on at least some of the interpretation. However, ignoring this and allowing Ru to be less reactive than RuAl, the following "nobility scale" can be deduced from Obrowski's samples by taking the lightest colour phase to be the least attacked, and thus the most noble:



The last four species cannot be differentiated any further, because they are not found together in the samples, and so cannot be compared.

Obrowski<sup>(4)</sup> reported that his sample containing 96.3 at% Ru consisted entirely of the Ru-rich solid solution. This sample had been annealed at 1800°C for 2 hours, and presumably quenched from this temperature. These findings are consistent with his subsequent phase diagram (Figure 2.2), if the sample was in fact quenched, and not cooled slowly.

## 6 DISCUSSION AND PROPOSALS

### 6.1 Critical Appraisal of Literature Survey

It is obvious from the literature survey that there are conflicting interpretations of the Ru-Al phase diagram provided in the published work. Any proposed phase diagram should explain the findings of the current work, and should also be able to explain previous workers' results. The results described in the literature survey are reviewed here, to ascertain how well they fit the various phase diagrams, and to explain the disagreements, where possible, by relating this work to the samples from the current investigation.

One possible reason for the discrepancies could originate from the difficulty that all workers had in achieving equilibrated structures. For a binary alloy to be in an equilibrated state, the maximum number of phases cannot exceed two, except at the invariant points. These are the reaction points (e.g. eutectic, peritectic, eutectoid, and peritectoid points). Since these are at a specific composition and temperature, it is unlikely that the alloy will be of that exact composition, and perfectly quenched from that temperature, and it can be assumed that the presence of more than two phases simultaneously in these studies is an indication of a non-equilibrated structure.

All of the authors either reported more than two phases simultaneously (Obrowski<sup>[4]</sup>, Edsahammar<sup>[5]</sup>, and Anlage<sup>[5]</sup>), or admitted difficulty in manufacture (Schwomma<sup>[7]</sup> with silica and oxygen contamination). As soon as these sort of anomalies are present, the interpretation of the phase diagram from the microstructure becomes more difficult, and

The average semi-quantitative analyses are reported in Appendix XIX, and the quantitative results are given in Table 5.16.

Table 5.16: Quantitative chemical analyses for nominal  $\text{Ru}_{50}\text{Al}_{50}$  (1200°C for 2 hours).

PHASE	PHASE DESCRIPTION	ATOMIC % Ru
Ru-rich solid	Eutectic with RuAl	$77.5 \pm 0.8$
RuAl	Two-phase region	$54.0 \pm 0.5$
	Single-phase centre	$53.6 \pm 0.6$

Chemical analyses of the outer two-phase region of this sample indicated that aluminium had been lost from the surface by vaporisation. Subsequent image analysis (Appendix XIX) indicated that approximately 4 at% aluminium was lost from the outer region of the sample.

Debye-Scherrer results confirmed the presence of RuAl and the Ru-rich solid in this sample. Again, accurate plane spacings could not be reported due to a lack of high angle lines. X-ray analysis of the bulk sample confirmed the existence of the eutectic by the presence of peaks of the Ru-rich phase in the results. The spectrum also contained the RuAl peaks.

#### Assessment of the Samples

Some of the above samples were contaminated with various elements, originating from either the production route, or the heat treatment in quartz ampoules.

Figure 5.35: Optical micrograph of nominal  $\text{Ru}_{50}\text{Al}_{50}$  annealed at  $1200^{\circ}\text{C}$  for 2 hours.

$\text{RuAl}$  (grey),  $\text{Ru}$ -rich solid (white).

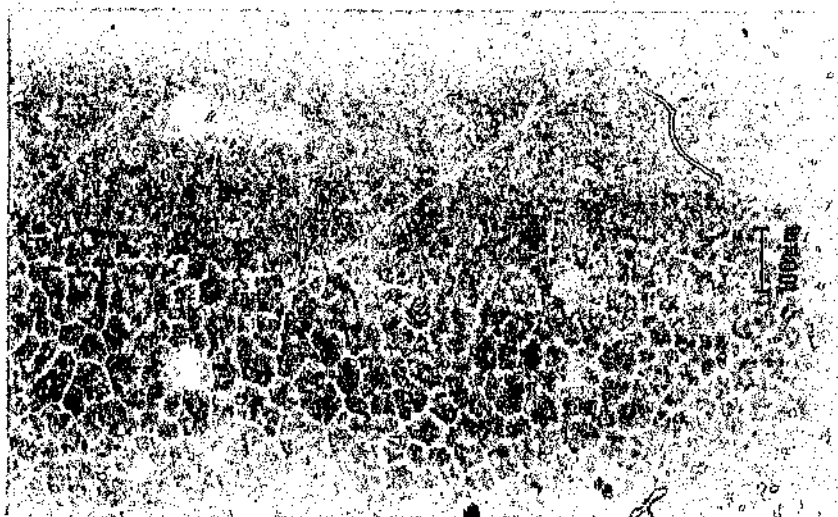
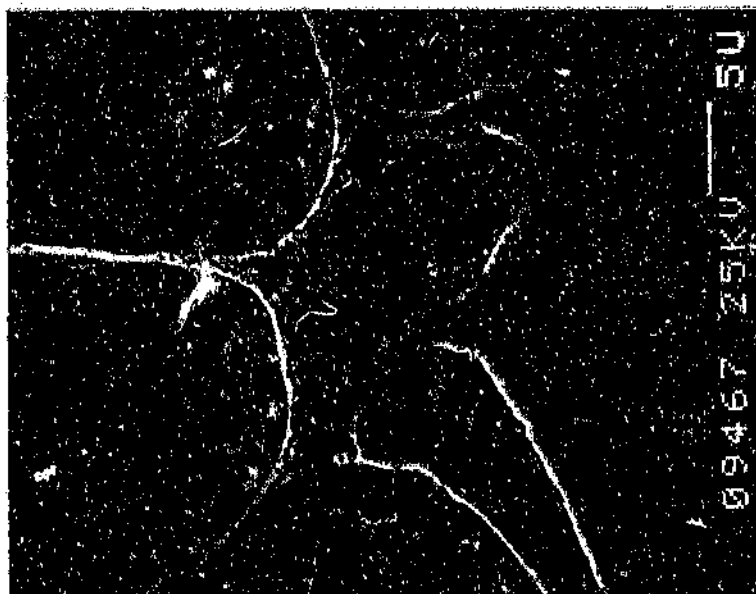


Figure 5.36: SEM micrograph of nominal  $\text{Ru}_{50}\text{Al}_{50}$  annealed at  $1200^{\circ}\text{C}$  for 2 hours

(backscattered electron mode), Eutectic of  $\text{RuAl}$  (black) and  $\text{Ru}$ -rich solid (grey).



inhomogeneities having a high ruthenium content. These appear too irregular to be eutectic or eutectoid in origin.

#### Nominal Ru<sub>35</sub>:Al<sub>65</sub>-am

Obrowski<sup>(4)</sup> predicted that there are two reactions which have higher formation temperatures than RuAl<sub>2</sub>. Hence, under rapid cooling conditions one would expect to observe Ru<sub>4</sub>Al<sub>13</sub> (or RuAl<sub>3</sub>), Ru<sub>2</sub>Al<sub>3</sub> and only traces of RuAl<sub>2</sub> and RuAl<sub>6</sub> in this sample. The abundance of RuAl<sub>2</sub> as a matrix in this alloy (Table 5.9) suggests that this phase can be formed directly from the melt. The presence of the "eutectic" mixture at the RuAl<sub>2</sub> phase boundaries, before annealing, is of little consequence to the current investigation because it was a highly contaminated region.

#### Nominal Ru<sub>35</sub>:Al<sub>65</sub>-b

Although this sample was only heated externally to about 950°C, it would have attained a much higher temperature during the exothermic reaction, allowing for the dendritic formation of Ru<sub>2</sub>Al<sub>3</sub> on solidification. The rate of cooling from this elevated temperature to 950°C would have been high. According to Obrowski's phase diagram (Figure 2.2), the eutectic should consist of Ru<sub>2</sub>Al<sub>3</sub> and RuAl<sub>6</sub>, and Ru<sub>4</sub>Al<sub>13</sub> (his RuAl<sub>3</sub>) should be a transformation product of these two phases. This sample, although contaminated, contradicts both of these suggestions (Table 5.11). Since Ru<sub>4</sub>Al<sub>13</sub> had readily formed a continuous matrix, it is possible that it solidified directly from the liquid (as proposed by Anlage<sup>(5)</sup>). The cooling history of the fine mixtures in the interdendritic regions appears to

Under equilibrium conditions, this sample was expected to consist of  $\text{RuAl}_2$  (Figure 2.2). However, it is doubtful that these conditions were obtained during the heat treatment ( $1200^\circ\text{C}$  for 168 hours and  $1050^\circ\text{C}$  for 24 hours), and one would expect to find some traces of  $\text{Ru}_4\text{Al}_{13}$  in the sample, if Obrowski's phase diagram is correct. Instead,  $\text{Ru}_2\text{Al}_3$  and  $\text{RuAl}_2$  were observed (Table 5.6). Despite the presence of impurity elements, this sample appears to indicate that  $\text{RuAl}_2$  is not as difficult to form as Obrowski depicts, and thus the sequence of reactions above this phase require modification.

#### Nominal $\text{Ru}_{28}\text{Al}_{72}$

The fact that dendrites were formed in this sample implies that at least part of the alloy must have reached a liquid state during production. It is possible that melting occurred due to the high temperatures attained during the exothermic reaction. Since the sample contained approximately 28 at% Ru and was heated to  $1300^\circ\text{C}$ , one would expect to find at least some traces of  $\text{RuAl}_2$  in this sample if Obrowski's phase diagram (Figure 2.2) is correct. Since the phase  $\text{Ru}_4\text{Al}_{13}$  was present instead (Table 5.7), this may imply that Anlage's proposals (Figure 2.3) are more accurate. According to Obrowski's phase diagram, the phase  $\text{RuAl}_2$  should not have formed as dendrites under any conditions, since he depicts this phase as only being formed by solid-state reactions. It is proposed, from this work, that  $\text{RuAl}_2$  can form directly from the liquid state, and is stable to much higher temperatures than attested by Obrowski. This microstructure suggests a higher melting point than that of  $\text{Ru}_4\text{Al}_{13}$ . The larger particles of  $\text{RuAl}_2$  observed between the dendrites (Figure 5.18) may be the result of extensive independent nucleation due to undercooling, and the smaller particles (Figure 5.19) may have resulted from solid-state decomposition of local

to be  $27.3 \pm 0.5$  at% Ru and  $72.7 \pm 0.5$  at% Al (Table 5.4). According to Obrowski's phase diagram (Figure 2.2), after quenching this sample from  $1200^\circ\text{C}$ , one would expect to find  $\text{RuAl}_4$  and  $\text{Ru}_2\text{Al}_3$  in this sample. Neither of these phases were observed. Instead the phases  $\text{RuAl}_2$ ,  $\text{Ru}_4\text{Al}_{13}$ , and the aluminium-rich solid solution were identified. The anneal had little effect on the microstructure because it still had a dendritic appearance.

The centre of this sample contained dendrites of  $\text{RuAl}_2$ , and  $\text{Ru}_4\text{Al}_{13}$  had formed in the interdendritic spaces. This suggests that  $\text{RuAl}_2$  has a higher melting point than  $\text{Ru}_4\text{Al}_{13}$ , and can form directly from the melt. It is possible that both these phases are stable to temperatures above  $1200^\circ\text{C}$  (or they are difficult to decompose).

The edges of the sample had a single-phase matrix of  $\text{RuAl}_2$ , with the aluminium-rich solid solution scattered in it, and lining the pores. The difference in the microstructures may lie in the difference in the cooling rates between the surface and centre of the sample during production. The centre of the sample cools slower than the surface, and is therefore likely to have a microstructure that is closer to that obtained under equilibrium conditions.

The presence of the aluminium-rich solid solution near the surface of the sample can again be accounted for by the rapid cooling conditions encountered during arc-melting, or by the high partial pressure of gaseous aluminium during production. The Al-rich phase appears to be unaffected by the subsequent heat treatment and thus was possibly protected by an oxide film (which is readily formed by other aluminium alloys). The phase  $\text{RuAl}_4$  did not form in this sample; this observation lends support to Anlage's proposal that  $\text{Ru}_4\text{Al}_{13}$  forms at a higher temperature than  $\text{RuAl}_4$  (Figure 2.3).

explained by the cooling conditions experienced by the arc-melted sample and the shape of the phase diagram. Once an alloy has cooled sufficiently to reach the liquidus, a Ru-rich solid forms (the more Ru-rich solids have the higher melting points). As more of the solid forms, especially if the solubility changes with temperature (which is normal for most non-linear compounds), the liquid becomes increasingly Al-rich. The liquid composition follows the liquidus line, while the solid composition follows the solidus line. The anomalies arise when a lower peritectic reaction temperature is reached while the sample is still partly liquid. This encourages another phase to be formed, or, in some cases, the reaction is missed, and the liquid composition progresses further down the liquidus. Under conditions of rapid cooling, peritectic reactions have been known to be "overshot" in other binary systems e.g. the Zn-Mg system<sup>[15]</sup> the peritectic reaction forming  $Mg_2Zn_{11}$  can be missed under these conditions. In the Ru-Al system, up to 50 at% Ru, the phase diagram slopes very steeply down to the aluminium end, and contains many peritectic reactions (Section 6.3).

Another suggested explanation is that the aluminium was liberated at high temperatures, during production of the sample, due to its high partial pressure. It was trapped in the sample, and solidified in the pores: it was only found in the outer pores, and was absent in the centre. The aluminium was not affected by the subsequent heat treatment, possibly because it was protected by a stable oxide film.

#### Nominal $Ru_{32.1}Al_{68}$

After annealing at 1200°C for 312 hours, the overall composition of this sample was found



last to solidify, implying that  $\text{RuAl}_2$  and  $\text{Ru}_2\text{Al}_3$  form at higher temperatures than this phase. It is not obvious which of the two discrete phases formed first in this sample.

The heat treatment, at  $1300^\circ\text{C}$  for 6.5 hours, had little effect on the structure of this sample, and local inhomogeneities in the composition during production, resulted in a wide range of phases in the alloy (Table 5.2). The most Ru-rich areas solidified as a eutectic between  $\text{RuAl}$  and the Ru-rich solid solution, as predicted by Obrowski's phase diagram (Figure 2.2). A layer of  $\text{Ru}_2\text{Al}_3$  formed adjacent to the  $\text{RuAl}$  via a peritectic reaction. The next region contained a  $\text{RuAl}_2$  matrix, and a bordering single-phase layer of  $\text{RuAl}_2$ . This suggests that the  $\text{RuAl}_2$  also formed via a peritectic reaction, and not a peritectoid reaction as Obrowski<sup>[4]</sup> predicted. The next region had a  $\text{Ru}_4\text{Al}_{13}$  matrix. The order of formation of these phases implies that  $\text{RuAl}_2$  has a higher melting point than  $\text{Ru}_4\text{Al}_{13}$ , but lower than that of  $\text{Ru}_2\text{Al}_3$ .

#### Nominal $\text{Ru}_{0.85}\text{Al}_{1.7}$

According to the published phase diagram<sup>[6]</sup>, if the sample was uncontaminated it would consist of the phases  $\text{RuAl}_2$ ,  $\text{Ru}_2\text{Al}_3$  and possibly some  $\text{RuAl}_3$  if cooled rapidly from  $1200^\circ\text{C}$  (after holding at temperature for 312 hours). None of these phases were observed (Table 5.3). The matrix of this sample was analysed to be  $\text{RuAl}_2$ , showing that, either  $\text{RuAl}_2$  is stable at temperatures above  $1200^\circ\text{C}$  (the annealing temperature), or it is difficult to decompose.

The presence of the aluminium-rich solid solution in some regions of the sample can be

investigators - Chapter 2). The cooling rate in the furnace following the isothermal heat treatment was not determined.

Since  $\text{RuAl}_{12}$  was not observed in this sample it is possible that this phase does not exist, or the cooling rate was too high to allow its formation. The sample, although not in an equilibrated state, lends support to Anlage's phase diagram (Figure 2.3).

#### Nominal $\text{Ru}_{20}\text{Al}_{80}$

The needle morphology of the  $\text{Ru}_4\text{Al}_{13}$  (Table 4.18) shows that this phase formed directly from the melt (in agreement with Anlage<sup>[9]</sup>). According to his diagram, however,  $\text{RuAl}_6$  should have formed peritectically between the needles. The lack of  $\text{RuAl}_6$  can be explained by Anlage's observation that this reaction can be bypassed at higher cooling rates. The solubility of Ru in the aluminium matrix is higher than that depicted in the static system (Figure 2.4), but Varich<sup>[11]</sup> reports that it can be as high as 3.2 at% Ru, depending on the cooling rate.

#### Nominal $\text{Ru}_{20}\text{Al}_{80}$

According to Obrowski's phase diagram this sample should consist of  $\text{Ru}_4\text{Al}_{13}$  (or  $\text{RuAl}_3$ ) and  $\text{RuAl}_2$  in the equilibrated state; and under non-equilibrium conditions one would expect to observe  $\text{Ru}_2\text{Al}_3$  partially transformed to  $\text{Ru}_4\text{Al}_{13}$ , and possibly some  $\text{RuAl}_2$  (formed from the  $\text{Ru}_4\text{Al}_{13}$  and  $\text{Ru}_2\text{Al}_3$ ) and  $\text{RuAl}_6$  (as part of a eutectic with  $\text{Ru}_2\text{Al}_3$ ). In the as-melted sample, the presence of  $\text{Ru}_4\text{Al}_{13}$  as the matrix phase (Table 5.1) indicates that it was the

The dendritic appearance of  $\text{Ru}_2\text{Al}_3$  and  $\text{RuAl}$  suggests that they can form directly from the melt. The microstructure of this sample appears to support Anlage's proposals<sup>[3]</sup>, and raises the possibility of modifications to Obrowski's diagram above 26 at% Ru.

#### Nominal $\text{Ru}_{13}\text{Al}_{27}$ -b

According to Obrowski's phase diagram (Figure 2.2), holding this sample at  $1100^\circ\text{C}$  should have resulted in a microstructure consisting of  $\text{RuAl}_6$  and  $\text{RuAl}_3$ . The phases observed in this sample were  $\text{Ru}_4\text{Al}_{13}$ ,  $\text{RuAl}_6$ , the aluminium-rich solid solution, and another phase containing 18 at% Ru (" $\text{RuAl}_5$ ") (Table 4.17).

It appears that  $\text{Ru}_4\text{Al}_{13}$  was the first phase to form, and the Al-rich solid solution was the last to solidify. The solidification order of  $\text{RuAl}_6$  and  $\text{RuAl}_3$  is not apparent from the microstructure, but they must have solidified after  $\text{Ru}_4\text{Al}_{13}$ . In some areas the Al-rich phase contained needles of  $\text{RuAl}_6$ , suggesting that this phase formed directly from the melt at some stage during solidification.

It is proposed that the  $\text{RuAl}_5$  is a metastable phase which formed before the  $\text{RuAl}_6$ , and partially transformed into the latter phase, during the furnace-cooling of the sample, by expelling ruthenium to the adjacent material. If the  $\text{RuAl}_5$  formed after  $\text{RuAl}_6$ , then (assuming Anlage's<sup>[3]</sup> diagram to be correct) it would have to be formed via a peritectoid reaction between  $\text{Ru}_4\text{Al}_{13}$  and  $\text{RuAl}_6$ . However, this option cannot adequately explain the microstructure observed in Figure 4.30. The proposal that  $\text{RuAl}_5$  is metastable, is borne out by the fact that it has not been observed in any other sample (including those of other

### Nominal Ru<sub>10</sub>:Al<sub>90</sub>

It is certain that the rapid cooling rates encountered during production was the cause of such a diverse microstructure. The irregular appearance of the surfaces of the phase layers seem to imply that they were formed by peritectic reactions, and the layer sequence gives an indication of the order of formation: RuAl, Ru<sub>2</sub>Al<sub>3</sub>, Ru<sub>4</sub>Al<sub>13</sub>, and then RuAl<sub>6</sub>. Some Ru<sub>4</sub>Al<sub>13</sub> formed directly from the melt as needles, as did some of the RuAl<sub>6</sub>. The remaining liquid solidified as a eutectic between RuAl<sub>6</sub> and the Al-rich solid solution. A very small amount of RuAl<sub>2</sub> was detected in the arc-melted sample, in a Ru<sub>4</sub>Al<sub>13</sub> matrix. This may imply that the latter phase solidified after the RuAl<sub>2</sub>. If RuAl<sub>2</sub> forms via a peritectoid reaction, as Obrowski predicted<sup>[14]</sup>, then it is unlikely to be found in an arc-melted button.

The fine mixture of Ru<sub>2</sub>Al<sub>3</sub> and Ru<sub>4</sub>Al<sub>13</sub> (Figures 4.21 & 4.26) could either be the result of a eutectic reaction between these two phases, or could be due to decomposition of high ruthenium local compositions (i.e. expelling of Ru in the solid state to form Ru<sub>2</sub>Al<sub>3</sub> and Ru<sub>4</sub>Al<sub>13</sub>). The mixture is unlikely to be the result of a eutectic reaction, because eutectic structures are usually uneven, or degenerate in appearance when the cooling rate is high. The solid state decomposition theory explains the fineness of this mixture, because the diffusion distances are likely to be very small, since it occurs in the solid state. It also explains the irregular appearance of these areas. This phenomenon is named cellular precipitation<sup>[14]</sup>, and a similar phenomenon occurs in spinodal decomposition, where a solid solution decomposes over short ranges, below a critical temperature, to form a fine mixture of two solid solutions.

forcing a peritectic reaction.

The fine dispersion of second phase particles in the top region of the sample suggests that the remaining liquid in the sample solidified as a eutectic between the aluminum-rich solid solution and  $\text{RuAl}_6$ .

The phase  $\text{RuAl}_{12}$  was not observed in this sample and has not been found to date. It is possibly one of the less stable phases of the system (if it exists), which requires slower cooling conditions for its formation.

#### Nominal $\text{Ru}_7\text{Al}_{21}$

According to Obrowski's phase diagram (Figure 2.2), a sample having this nominal composition should have a two-phase structure, consisting of  $\text{RuAl}_6$  and peritectically formed  $\text{RuAl}_{12}$ . However, since  $\text{RuAl}_{12}$  was not observed (Table 4.11), this phase either might not exist, or it may have been suppressed by the impurity elements. Another possibility, is that the furnace cooling of the sample was too fast to allow the formation of the relatively low temperature  $\text{RuAl}_{12}$  phase. However, this is unlikely since the cooling rate was  $1^\circ\text{C}$  per minute. It is suggested that the impurities in the sample may have suppressed the formation of a eutectic between  $\text{RuAl}_6$  and the Al-rich solid solution, which has been observed in samples of similar composition.

this could be due to the presence of impurities.

### Nominal Ru:Al<sub>12</sub>

In Chapter 4 it was observed that this sample was macroscopically inhomogeneous. It is proposed that the Ru<sub>4</sub>Al<sub>13</sub> precipitated first and sank to the bottom of the melt since it has a higher Ru content and is therefore denser than the remaining material. The morphology of the RuAl<sub>6</sub> on the Ru<sub>4</sub>Al<sub>13</sub> in the bottom region of this sample, suggests that the former solidified around the latter via a peritectic reaction. Thus Ru<sub>4</sub>Al<sub>13</sub> has a higher melting point than RuAl<sub>6</sub>. This theory is substantiated by the fact that the Ru<sub>4</sub>Al<sub>13</sub> has a needle-like morphology, indicating that this is the primary phase. The precipitation of this phase altered the composition of the liquid, producing a lower Ru content in the upper part of the specimen, thus allowing precipitation of RuAl<sub>6</sub> directly from the melt in this region. Since the sample was heated to 1200°C during production, this proposal implies that the formation of primary RuAl<sub>6</sub> occurs below that temperature.

The phase morphologies, in the bottom region of the sample, indicate that the RuAl<sub>6</sub> was formed via a peritectic reaction rather than a eutectic reaction (as it appears in Obrowski's phase diagram). This implies that either the RuAl<sub>6</sub> does form peritectically, or the cooling rate is too high, and a metastable (peritectic) reaction occurs which effectively masks the reported stable congruent formation and associated eutectic reaction. If Obrowski's eutectic reaction, under conditions of non-equilibrium cooling, was displaced to a lower Al composition then, especially as the eutectic point lies close to the congruent melting temperature and composition of RuAl<sub>6</sub>, the latter composition could be overshot, thus

peritectically. The presence of  $\text{Ru}_4\text{Al}_{13}$  needles indicates that this phase formed directly from the melt, in agreement with Anlage's findings<sup>[5]</sup>.

After heat treatment at 475°C for 168 hours, a different cross-section of the sample was examined. Layers of  $\text{RuAl}$ ,  $\text{Ru}_2\text{Al}_3$ ,  $\text{Ru}_4\text{Al}_{13}$ ,  $\text{RuAl}_6$ , and the Al-rich solid solution were observed in the microstructure (Table 4.6). There was no  $\text{RuAl}_2$  detected in this sample. It is possible that  $\text{RuAl}_2$  forms at low temperatures, as Obrowski predicts, or perhaps the reaction forming this phase was suppressed by the rapid cooling rates. The presence of small  $\text{Ru}_2\text{Al}_3$  particles in the  $\text{Ru}_4\text{Al}_{13}$  layer could be due to extensive independent nucleation from undercooling of the sample. The  $\text{Ru}_4\text{Al}_{13}$  needles must have formed directly from the melt (which is not possible with Obrowski's diagram). The  $\text{RuAl}_6$  layer adjacent to the  $\text{Ru}_4\text{Al}_{13}$  needles again suggests a peritectic reaction; this agrees with Anlage's diagram (Figure 2.3). The latter also allows for the primary formation of  $\text{RuAl}_6$  and a eutectic with the Al-rich solid solution, as was observed.  $\text{RuAl}_{12}$  was not observed in this arc-melted sample, in contradiction to Obrowski's proposals. The presence of a eutectic between  $\text{RuAl}$  and the Ru-rich solid solution conforms to Obrowski's proposals.

#### Nominal $\text{Ru}_{40}\text{Al}_{60}$ -b

The fact that at 1200°C the phase which formed primarily was  $\text{Ru}_4\text{Al}_{13}$  and not  $\text{RuAl}_6$  (Table 4.8), indicates that  $\text{Ru}_4\text{Al}_{13}$  has a higher melting point than the  $\text{RuAl}_6$  which subsequently formed around it. Allowing for the presence of other elements, it appears that the Al-rich eutectic composition of 0.5 at% Ru proposed by Obrowski<sup>[4]</sup> is correct. The lack of  $\text{RuAl}_{12}$  in this sample supports Anlage's suggestion that this phase does not exist<sup>[5]</sup>, but

#### Nominal $\text{Ru}_{13}\text{Al}_{87}$ -b

Obrowski's phase diagram<sup>[6]</sup> predicts a two-phase structure consisting of Al and peritectically formed  $\text{RuAl}_{12}$ . One phase was analysed to be almost pure Al, but the other phase was approximately  $\text{RuAl}_6$  (Table 4.2). The absence of the phase  $\text{RuAl}_{12}$  from the sample agrees with the proposals made by Anlage (Figure 2.3), but may be due to the influence of the contaminating elements in the sample. Anlage<sup>[5]</sup> predicted that the phases in this sample should form a eutectic, the absence of which may also be due to the contaminants. The source of contamination may have been the Al powder which was only 95% pure.

#### Nominal $\text{Ru}_4\text{Al}_{96}$ -a

This sample should have contained  $\text{RuAl}_{12}$ , if Obrowski's proposals are correct. The fact that this phase was not present in the sample may be a result of the rapid cooling encountered during arc-melting, but it is also possible that this phase does not exist. Most of the sample consisted of  $\text{RuAl}_6$  needles and dendrites (Table 4.4), indicating that it formed directly from the melt, and it was seen to form a eutectic with the Al-rich solid solution (in contradiction to Obrowski's results<sup>[6]</sup>). Anlage predicts that there is a very small composition range in which this phase can exist as the primary phase<sup>[5]</sup> (only up to about 1 at% Ru). However, it is possible that under rapid cooling conditions, this limit is extended. The lack of  $\text{RuAl}_6$  in the region containing  $\text{Ru}_4\text{Al}_{13}$ , can be explained by Anlage's observation that the peritectic formation of  $\text{RuAl}_6$  is restricted at rapid cooling rates, and it solidifies in a eutectic with the Al-rich solid, instead of first solidifying



Theoretically it should be possible to deduce the shape of the liquidus by considering which phases were present in alloys of known compositions, especially where there is no heat treatment. (Heat treatment should form the phases in the solid state, given enough time for diffusion to occur.) The composition limits of a peritectic reaction line can be deduced by studying the phases present in as-cast samples. The "liquid limit", here the Al-rich end, can be approximately determined by finding the lowest Ru-content sample containing the solid phase that is formed immediately above the reaction line (e.g. RuAl for the  $\text{Ru}_2\text{Al}_3$  reaction). Under equilibrium conditions this phase would be consumed, but most of these alloys have cooled at far quicker rates. The "solid limit", here the Ru-rich end, is more difficult to determine, since the small amount of peritectically-formed solid might be missed. However, in as-cast alloys, the highest Ru-content alloy containing the phase, is likely to be near the higher limit of the peritectic reaction line in a peritectic cascade.

The peritectic reaction point itself can also be approximately found. In this phase diagram (Figure 6.1), the most Ru-rich alloy to have the product of the next lowest peritectic reaction must lie on the Al-rich side of the peritectic point, but there is no way of deducing how near or far. Attempts were made to determine the peritectic reaction limits, using Edshammar's samples<sup>[8,9,10]</sup> (Table 6.6), and using the samples from this work (Table 6.7). In Table 6.6, the reaction limits for RuAl<sub>3</sub> could not be determined, since the details of the samples containing this compound were not provided.

It is proposed that the peritectic reactions forming  $\text{Ru}_2\text{Al}_3$  and  $\text{RuAl}_2$  are separated by a small temperature difference, because  $\text{Pu}_2\text{Al}_3$  did not form in any of Edshammar's arc-melted samples (see Table 2.2 and Section 6.1). Similarly, the temperature difference between the reactions forming  $\text{RuAl}_2$  and  $\text{Ru}_4\text{Al}_{13}$  must be minimal, because the peritectic formation of  $\text{RuAl}_2$  did not occur in many of the arc-melted samples from this investigation. If this is the case then, during non-equilibrium cooling, the formation of  $\text{RuAl}_2$  can be missed due to the large amount of undercooling required for nucleation under these conditions. It is known that peritectic reactions can be overshoot during rapid cooling, for example: the Mg-Zn system, in which the formation of  $\text{Mg}_2\text{Zn}_{11}$  can be missed<sup>(15)</sup>.

It is also proposed that the observed intimate mixture of  $\text{Ru}_2\text{Al}_3$  and  $\text{Ru}_4\text{Al}_{13}$  is the result of decomposition of Ru-rich inhomogeneities, by cellular precipitation, which itself was brought about by the rapid cooling conditions, rather than a eutectic reaction between these phases. It is thought to be a metastable condition for the following reasons. Firstly, it was observed in specific samples only:  $\text{Ru}_{10}\text{:Al}_{90}$  (before and after heat treatment), and  $\text{Ru}_{35}\text{:Al}_{65}$ -b.  $\text{Ru}_{10}\text{:Al}_{90}$  was arc-melted and was not in an equilibrated state, and the annealing temperature ( $475^\circ\text{C}$ ) was too low to have an effect on the high-temperature phases.  $\text{Ru}_{35}\text{:Al}_{65}$ -b had cooled rapidly from the reaction temperature, and was contaminated with zirconium, which may have had a stabilising effect on this mixture. Secondly, if the eutectic was a stable phenomenon then the phase  $\text{RuAl}_2$  would have to be metastable, but this cannot be true since it was initially present, and in some cases, formed in Edshammar's<sup>(9)</sup> samples during the anneal (Table 2.2).  $\text{RuAl}_2$  was also present in the heat treated samples from the current investigation.

Al-rich side, and formed directly from the melt at 2060°C. He depicted this phase as existing between 42 and 51 at% Ru and found that it formed a eutectic with the Ru-rich solid solution at 70 at% Ru and  $1920 \pm 20^\circ\text{C}$ . The only modification which could be suggested from the current samples (Table 6.5) was a shift of the phase boundaries, especially to allow for the formation of  $\text{RuAl}_2$  at higher temperatures.

Table 6.5: Proposals for the phase  $\text{RuAl}$ .

PROPOSAL	SUBSTANTIATING SAMPLE
The lower composition limit is $50.2 \pm 0.6$ at% Ru	$\text{Ru}_{37}\text{Al}_{63}$
The upper composition limit is $54.3 \pm 0.4$ at% Ru	$\text{Ru}_{47}\text{Al}_{53}$
$\text{RuAl}$ can form as a primary phase i.e. directly from the melt	$\text{Ru}_4\text{Al}_{96}\text{-a(ht)}$ , $\text{Ru}_{10}\text{Al}_{90}$ , $\text{Ru}_{10}\text{Al}_{90}\text{(ht)}$
$\text{RuAl}$ has a higher melting point than $\text{Ru}_2\text{Al}_3$	$\text{Ru}_4\text{Al}_{96}\text{-a(ht)}$ , $\text{Ru}_{10}\text{Al}_{90}$ , $\text{Ru}_{10}\text{Al}_{90}\text{(ht)}$ , $\text{Ru}_{28}\text{Al}_{72}\text{(ht)}$ , $\text{Ru}_{37}\text{Al}_{63}$
$\text{RuAl}$ forms a eutectic with the Ru-rich solid solution	$\text{Ru}_4\text{Al}_{96}\text{-a(ht)}$ , $\text{Ru}_{10}\text{Al}_{90}$ , $\text{Ru}_{10}\text{Al}_{90}\text{(ht)}$ , $\text{Ru}_{28}\text{Al}_{72}\text{(ht)}$ , $\text{Ru}_{37}\text{Al}_{63}$ , $\text{Ru}_{47}\text{Al}_{53}$ , $\text{Ru}_{50}\text{Al}_{50}$

The equilibrium solubility of aluminum in ruthenium could not be determined from the samples examined, since the Ru-rich solid solution was only present in the eutectic, which was too fine to obtain an accurate analysis. Thus, Obrowski's prediction of approximately 96 at% Ru<sup>(4)</sup> was accepted as being an estimate of the phase composition.

With regard to the phase  $\text{Ru}_2\text{Al}_3$ , Obrowski proposed a triangular phase boundary with a stability range over  $-1000^\circ\text{C}$  to  $-1600^\circ\text{C}$  at about 40 at% Ru, and a lower composition limit of 32.5 at% Ru. He depicted the phase to melt perfectly and to decompose eutectoidally below  $1000^\circ\text{C}$  into  $\text{RuAl}$  and  $\text{RuAl}_2$ . Suggestions regarding the modification of the phase boundaries are summarised in Table 6.4.

Table 6.4: Proposals for the phase  $\text{Ru}_2\text{Al}_3$ .

PROPOSAL	SUBSTANTIATING SAMPLE
The lower composition limit is $35.7 \pm 0.8$ at% Ru	$\text{Ru}_{28}\text{Al}_{72}$
The upper composition limit is $41.6 \pm 0.5$ at% Ru	$\text{Ru}_{37}\text{Al}_{63}$
$\text{Ru}_2\text{Al}_3$ can form as a primary phase i.e. directly from the melt	$\text{Ru}_{10}\text{Al}_{90}$ , $\text{Ru}_{10}\text{Al}_{90}(\text{ht})$ , $\text{Ru}_4\text{Al}_{96}\text{-a}(\text{ht})$
$\text{Ru}_2\text{Al}_3$ has a higher melting point than $\text{Ru}_4\text{Al}_{12}$	$\text{Ru}_4\text{Al}_{96}\text{-a}(\text{ht})$ , $\text{Ru}_{10}\text{Al}_{90}$ , $\text{Ru}_{10}\text{Al}_{90}(\text{ht})$ , $\text{Ru}_{28}\text{Al}_{72}$ , $\text{Ru}_{28}\text{Al}_{72}(\text{ht})$
$\text{Ru}_2\text{Al}_3$ has a higher melting point than $\text{RuAl}_2$	$\text{Ru}_{28}\text{Al}_{72}(\text{ht})$ , $\text{Ru}_{37}\text{Al}_{63}$
$\text{Ru}_2\text{Al}_3$ forms via a peritectic reaction	$\text{Ru}_4\text{Al}_{96}\text{-a}(\text{ht})$ , $\text{Ru}_{10}\text{Al}_{90}$ , $\text{Ru}_{10}\text{Al}_{90}(\text{ht})$ , $\text{Ru}_{28}\text{Al}_{72}(\text{ht})$ , $\text{Ru}_{37}\text{Al}_{63}$

Edshammar's heat treated samples<sup>[9]</sup> suggest that  $\text{Ru}_2\text{Al}_3$  is stable at  $950^\circ\text{C}$ , since it was formed at this temperature. The melting point of this phase cannot be predicted from the samples.

Obrowski's<sup>[4]</sup>  $\text{RuAl}$  has a sloping phase boundary with the liquid two-phase region on the

proposals regarding this phase, except for the phase composition, which he had assumed as the stoichiometric value. Again the samples providing the boundaries are on the wrong sides of the phase, due to the narrow phase width and unavoidable errors. The melting point of  $\text{Ru}_4\text{Al}_{13}$ , as predicted by Anlage, could not be confirmed from these samples, but is assumed accurate since his investigation was thorough.

Obrowski<sup>[4]</sup> depicted  $\text{RuAl}_2$  as being formed via a peritectoid reaction between  $\text{RuAl}_3$  and  $\text{Ru}_4\text{Al}_3$  at about  $1100^\circ\text{C}$ . He also depicted the composition as lying between about 31 and 33.5 at% Ru. The current investigation has shown that his proposals are incorrect, and the observations are summarised in Table 6.3.

Table 6.3: Proposals for the phase  $\text{RuAl}_2$ .

PROPOSAL	SUBSTANTIATING SAMPLE
The lower composition limit is $30.35 \pm 0.08$ at% Ru	$\text{Ru}_{22}\text{Al}_{72}$
The upper composition limit is $35.8 \pm 0.2$ at% Ru	$\text{Ru}_{32}\text{Al}_{64}$
$\text{RuAl}_2$ can form as a primary phase i.e. directly from the melt	$\text{Ru}_{32}\text{Al}_{64}$ , $\text{Ru}_{33}\text{Al}_{65}\text{-a}$
$\text{RuAl}_2$ has a higher melting point than $\text{Ru}_4\text{Al}_{13}$	$\text{Ru}_{22}\text{Al}_{72}$ , $\text{Ru}_{23}\text{Al}_{72}(\text{ht})$ , $\text{Ru}_{32}\text{Al}_{64}$ , $\text{Ru}_{33}\text{Al}_{65}\text{-a}$
$\text{RuAl}_2$ forms via a peritectic reaction	$\text{Ru}_{23}\text{Al}_{72}(\text{ht})$

Assuming that  $\text{Ru}_4\text{Al}_{13}$  melts at  $1403^\circ\text{C}$ , as Anlage reported, the melting point of  $\text{RuAl}_2$  would be above this temperature.

phase boundary, and vice versa. Although this seems incorrect, the phase is narrow, and there are errors to be considered, especially considering the difficulty in homogenising the alloys. Anlage's reaction temperatures cannot be disputed since they could not be determined from these samples. However, they are assumed accurate since the experimental techniques employed to obtain these values are rigorous.

With regard to the phase  $\text{Ru}_4\text{Al}_{13}$ , Anlage<sup>[5]</sup> depicted a line compound at 23.6 at% Ru, and stated that it melted peritectically at 1403°C. The observations made from the current investigation are summarised in Table 6.2.

Table 6.2: Proposals for the phase  $\text{Ru}_4\text{Al}_{13}$ .

PROPOSAL	SUBSTANTIATING SAMPLE
The phase is Edshammer's $\text{Ru}_4\text{Al}_{13}$ <sup>[7]</sup> , than Obrowski's $\text{RuAl}_3$ <sup>[11]</sup>	$\text{Ru}_4\text{Al}_{96}\text{-a}$ , $\text{RuAl}_{12}$ , $\text{Ru}_{13}\text{Al}_{82}\text{-b}$ , $\text{Ru}_{20}\text{Al}_{80}$ , $\text{Ru}_{28}\text{Al}_{72}$ , $\text{Ru}_{32}\text{Al}_{68}$
The lower composition limit is $25.00 \pm 0.05$ at% Ru	$\text{Ru}_{35}\text{Al}_{55}\text{-a}$
The upper composition limit is at most $26.6 \pm 0.1$ at% Ru	$\text{Ru}_{20}\text{Al}_{80}$
$\text{Ru}_4\text{Al}_{13}$ can form as a primary phase i.e. directly from the melt	$\text{Ru}_4\text{Al}_{96}\text{-a}$ , $\text{Ru}_4\text{Al}_{96}\text{-a(ht)}$ , $\text{Ru}_{10}\text{Al}_{90}$ , $\text{Ru}_{16}\text{Al}_{80}\text{(ht)}$ , $\text{RuAl}_{12}$ , $\text{Ru}_{20}\text{Al}_{80}$
$\text{Ru}_4\text{Al}_{13}$ has a higher melting point than $\text{RuAl}_6$	$\text{Ru}_4\text{Al}_{96}\text{-a(ht)}$ , $\text{Ru}_{10}\text{Al}_{90}$ , $\text{Ru}_{10}\text{Al}_{90}\text{(ht)}$ , $\text{RuAl}_{12}$ , $\text{Ru}_{13}\text{Al}_{82}\text{-b}$
$\text{Ru}_4\text{Al}_{13}$ melts peritectically	$\text{Ru}_4\text{Al}_{96}\text{-a(ht)}$ , $\text{Ru}_{10}\text{Al}_{90}$ , $\text{Ru}_{10}\text{Al}_{90}\text{(ht)}$

The observations in Table 6.2 regarding the phase  $\text{Ru}_4\text{Al}_{13}$  appear to confirm Anlage's

Anlage depicted the  $\text{RuAl}_6$  phase as a line compound at 14.3 at% Ru. He suggested a eutectic reaction with the Al-rich solid solution at about 0.3 at% Ru and 652°C, and stated that  $\text{RuAl}_6$  formed peritectically at 723°C. The deductions made from the current work regarding this phase are summarised in Table 6.1, together with a list of the samples which substantiate each point.

Table 6.1: Proposals for the phase  $\text{RuAl}_6$ .

PROPOSAL	SUBSTANTIATING SAMPLE
The lower composition limit is $15.10 \pm 0.01$ at% Ru	$\text{Ru:Al}_{12}$
The upper composition limit is at most $15.7 \pm 0.1$ at% Ru	$\text{Ru}_4\text{:Al}_{90}\text{-a}$
$\text{RuAl}_6$ melts peritectically	$\text{Ru}_4\text{:Al}_{90}\text{-a(ht)}, \text{Ru}_{10}\text{:Al}_{90}, \text{Ru}_{10}\text{:Al}_{90}\text{(ht)}, \text{Ru:Al}_{12}$
$\text{RuAl}_6$ can form as a primary phase i.e. directly from the melt	$\text{Ru}_4\text{:Al}_{90}\text{-a}, \text{Ru}_4\text{:Al}_{90}\text{-a(ht)}, \text{Ru}_{10}\text{:Al}_{90}, \text{Ru}_{10}\text{:Al}_{90}\text{(ht)}, \text{Ru:Al}_{12}$
Primary formation of $\text{RuAl}_6$ occurs below 1200°C	$\text{Ru:Al}_{12}$
$\text{RuAl}_6$ forms a eutectic with the Al-rich solid solution	$\text{Ru}_4\text{:Al}_{90}\text{-a}, \text{Ru}_4\text{:Al}_{90}\text{-a(ht)}, \text{Ru}_{10}\text{:Al}_{90}, \text{Ru}_{10}\text{:Al}_{90}\text{(ht)}, \text{Ru:Al}_{12}$

It can be seen from Table 6.1 that the observations regarding  $\text{RuAl}_6$  agree with most of those proposed by Anlage, except where the phase composition is concerned. His values, however, had been assumed, because his analyses were obtained without standards. The sample providing the upper boundary had less ruthenium than that providing the lower

\*This abbreviation refers to the sample in the annealed state

occurred on the Ru-side of  $\text{Ru}_4\text{Al}_{12}$ . Thus it is proposed that this reaction temperature corresponds to the melting of oxides present in the alloy. This possibility is promoted by the fact that the reaction peak became larger in the third scan, for which the sample was heated in air.

#### 6.4 Modifications to the Phase Diagram

Although the samples investigated here were not in a state of equilibrium, much information could be gleaned from those which were not contaminated with other elements. In the previous section the samples were discussed individually, as were those of other workers. In this chapter these discussions will be used to formulate proposals for modifications to Obrowski's phase diagram, so that the modified diagram complies with the various microstructures which were examined. These proposals are summarised below, starting from the Al-rich end of the phase diagram.

Varich<sup>[11]</sup> found the equilibrium solubility of Ru in Al to be less than 0.03 at%. This value cannot be disputed since a state of equilibrium was not achieved in the samples from this investigation.

Anlage<sup>[5]</sup> stated that the phase  $\text{RuAl}_{12}$  does not exist. It was not observed in Edshammar's<sup>[9]</sup> or Varich's<sup>[11]</sup> samples either. If this phase existed it should have been present in the annealed sections of the nominal  $\text{Ru}_4\text{Al}_{24-a}$  and  $\text{Ru}_{10}\text{Al}_{90}$  samples, if not in the  $\text{RuAl}_{12}$  sample. Hence this investigation confirmed Anlage's findings with regard to this phase.



by the second and third scans being similar. The low temperature reactions of the first scan were not present in the others, implying that no low-temperature phases (Al-rich phases) were present in the sample after the first run. Thus it is proposed that the first heating cycle had the effect of homogenising the sample. Homogenisation of the alloy under the testing conditions is possible because the sample was very small, and the diffusion distances minimal. The reaction at 656°C, in the first scan, was attributed to the melting of the Al-rich solid solution. The second endothermic reaction at 730°C was ascribed to the melting of  $\text{RuAl}_4$ , and is similar to the reaction temperature reported by Anlage<sup>[5]</sup>.

Unfortunately, it is not known what phases were present in the sample after the first cycle. However, considering the above-mentioned homogenisation, the alloy composition, and the temperature attained during the scan, it is probable that the phases present were  $\text{RuAl}_2$  and  $\text{Ru}_4\text{Al}_{13}$ . The interpretation of the results of the next two scans was based on this assumption and evidence from Anlage's DTA work<sup>[5]</sup>. The second endothermic peak at about 1417°C is close to Anlage's temperature of 1403°C for the peritectic melting of  $\text{Ru}_4\text{Al}_{13}$ , and was thus assumed to be this reaction. It is proposed that the small endothermic reaction at about 1460°C corresponds to the melting of  $\text{RuAl}_2$ . Discussions in the previous section have shown the probability of  $\text{RuAl}_2$  having a melting point just above that of  $\text{Ru}_4\text{Al}_{13}$ .

It is proposed that the first endothermic reaction at about 1348°C does not belong in the Ru-Al phase diagram. Anlage, who reported an extensive thermal analysis investigation<sup>[5]</sup>, did not detect any reaction at this temperature on the Al-rich side of  $\text{Ru}_4\text{Al}_{13}$ . Considering the results from the current investigations, it is not feasible for this reaction to have

solidification, whereas the  $\text{RuAl}_2$  should originate from a solid state transformation. The interdendritic region was analysed to contain 75.8 at% Ru ( $\pm 0.8\%$  error), which encompasses the eutectic composition on the Ru-rich side of the  $\text{RuAl}$  phase.

### Nominal $\text{Ru}_{50}\text{Al}_{50}$

According to Obrowski's phase diagram (Figure 2.2) the microstructure should be entirely  $\text{RuAl}$ . Considering the variation of the microstructure across this sample, one can conclude that the homogenisation was unsuccessful. The extreme inhomogeneity was brought about by the loss of aluminium during manufacture. The dendrites of the two-phase region consisted of  $\text{RuAl}$  (Table 5.16). The composition of the interdendritic region was given as approximately 77% Ru. This result is very close to the reported composition of the  $\text{RuAl}$  + Ru-rich eutectic<sup>[4]</sup>. The morphology of the eutectic in this sample (Figure 5.36) appears to differ from that observed in the previous one (Figure 5.34). This may be due to the samples experiencing different cooling rates during arc-melting, or merely a result of viewing the eutectic at a different orientation.

### 6.3 Discussion of the Thermal Analysis

The DTA scans for  $\text{Ru}_{23}\text{Al}_{77}$  were reported in Chapter 5. It is proposed that the first heating cycle, showing different reactions to the next two, had the effect of altering the phases in the sample, and thus stabilising the alloy. This is substantiated by the presence of the exothermic reaction in the first run, which would usually occur only for a transition from a metastable system to a stable one. The stability of the resulting alloy was indicated

balance of the sample consisted of  $\text{RuAl}_2$ . This suggests that  $\text{RuAl}_2$  is stable at temperatures above  $1200^\circ\text{C}$  (the annealing temperature), or it is difficult to anneal out of the sample due to slow diffusion. The fact that  $\text{RuAl}_2$  comprised the continuous matrix of the sample, suggests that this phase also formed directly from the melt, and not from a peritectoid reaction (Figure 2.2), which would not have had time to occur.

#### Nominal $\text{Ru}_{47}\text{Al}_{53}$

Since the edges were two-phase and a eutectic was observed (Table 5.15), it appears, according to Obrowski's phase diagram, that Al was lost from this region. This loss was by vaporisation occurring during the repeated inverting and remelting of the sample during production, which had been employed to ensure complete alloying of the elements. The button arc furnace has a water-cooled copper hearth, and preparing the sample on this hearth led to the heat being concentrated at the top surface of the sample. Hence vaporisation of aluminium from the surface took place, before the entire sample could reach a molten state. The argon pressure in the arc furnace during the manufacture of this alloy was just below 1 atmosphere. The boiling point of aluminium at this pressure is about  $2400^\circ\text{C}$ . The temperature of the arc would have been higher than  $2060^\circ\text{C}$ , the melting point of the intermetallic. Thus it is conceivable that the temperature may have risen above the boiling point of aluminium, and since Al has a high vapour pressure, it indeed vaporised from the surface of the sample.

The published phase diagram<sup>[6]</sup> shows that this sample (in the equilibrated state) should be two-phase, containing  $\text{RuAl}$  and  $\text{RuAl}_2$ .  $\text{RuAl}$  would have been formed by direct

be complex, but is not discussed here, since it involves large quantities of impurity elements, and thus has no bearing on the Ru-Al binary system.

#### Nominal $\text{Ru}_{37}\text{Al}_{63}$

The vast range of phases present in this sample resulted from local inhomogeneity in composition during cooling (Table 5.12), and the subsequent heat treatment ( $1200^\circ\text{C}$  for 168 hours) was obviously too inadequate to rectify this problem. According to Obrowski's phase diagram (Figure 2.2) the entire sample should have consisted of  $\text{Ru}_2\text{Al}_3$ .

The chemical analysis of the area depicted in Figure 5.29 and the individual phase analyses fit the existing phase diagram quite well (Figure 2.2). The chemical analysis of the Ru-rich phase in the sample is of little consequence, since the phase is very fine and the error is likely to be larger than that quoted, due to collecting the signal from the underlying matrix material. However, the morphology of this phase does confirm that it was formed via a eutectic reaction.

The variation in the composition of the RuAl phase is consistent with the sloping phase boundary depicted on the phase diagram above  $1600^\circ\text{C}$  (Figure 2.2). This inhomogeneity was not rectified during heat treatment since diffusion in these samples is very slow, and the compound (RuAl) itself is apparently very stable once formed<sup>[3]</sup>. It appears that  $\text{Ru}_2\text{Al}_3$  was the next phase to form upon cooling (via a peritectic reaction), and the fine precipitates of the latter in the RuAl phase are consistent with the reported decrease in solubility of aluminium in the RuAl phase<sup>[4]</sup> (i.e. the sloping RuAl phase boundary below  $1600^\circ\text{C}$ ). The

EXPERIMENTAL DATA FOR  $\text{Ru}_3\text{Al}_{17}\text{-b}$ CHEMICAL ANALYSES (EDAX)SAMPLE:  $\text{Ru}_3\text{Al}_{17}\text{-b}$  (No heat treatment)

SPECTRUM: Overall composition (semi-quantitative)

ELEMENT	RELATIVE K	WT %	ATOMIC %
Al	0.8199	91.81	97.67
Ru	0.0492	8.19	2.33
Total		100.00	100.00

SPECTRUM: Overall composition (semi-quantitative)

ELEMENT	RELATIVE K	WT %	ATOMIC %
Al	0.8382	92.70	97.94
Ru	0.0436	7.30	2.06
Total		100.00	100.00

SPECTRUM: Contaminated  $\text{RuAl}_3$  (semi-quantitative)

ELEMENT	RELATIVE K	WT %	ATOMIC %
Al	0.3329	56.52	78.56
Si	0.0133	4.38	5.85
Fe	0.0323	3.61	2.43
Ru	0.2441	35.48	13.16
Total		100.00	100.00

SPECTRUM: Contaminated  $\text{RuAl}_3$  (semi-quantitative)

ELEMENT	RELATIVE K	WT %	ATOMIC %
Al	0.3265	56.20	77.91
Si	0.0137	4.51	6.01
Fe	0.0459	5.13	3.44
Ru	0.2344	34.16	12.64
Total		100.00	100.00

EXPERIMENTAL DATA FOR  $\text{Ru}_3\text{Al}_{17}$ -aCHEMICAL ANALYSES (EDAX)SAMPLE:  $\text{Ru}_3\text{Al}_{17}$ -a (550°C for 528 hours)SPECTRUM: Contaminated  $\text{RuAl}_6$  (semi-quantitative)

ELEMENT	RELATIVE K	WT %	ATOMIC %
Al	0.3175	54.05	77.58
Ru	0.2746	38.82	14.87
Si	0.0124	3.80	5.24
Cr	0.0003	0.04	0.03
Mn	0.0030	0.35	0.25
Fe	0.0247	2.75	1.91
Ni	0.0019	0.20	0.13
Cu	0.0000	0.00	0.00
Total		100.00	100.00

SPECTRUM: Contaminated Al-rich matrix (semi-quantitative)

ELEMENT	RELATIVE K	WT %	ATOMIC %
Al	0.9955	99.76	99.82
Ru	0.0000	0.01	0.00
Si	0.0003	0.14	0.13
Fe	0.0003	0.04	0.02
Cu	0.0005	0.05	0.02
Total		100.00	100.00

## EMSSA CONFERENCE PAPER

## MODIFICATIONS TO THE Ru-Al PHASE DIAGRAM

T.D. Boniface and L.A. Cornish

Department of Metallurgy and Materials Engineering, University of the Witwatersrand

The first phase diagram of the ruthenium - aluminium system (Fig. 1) was published in 1963 by Obrowski<sup>1</sup>. His publication was developed from limited experimental findings and he was unsure of the accuracy of the results. In 1985 Anlage<sup>2</sup> stated that the aluminium-rich region of this phase diagram was incorrect, and proposed a new phase diagram for the region 0 - 26 at% Ru (Fig. 2) where the major modification is the formation of  $Ru_4Al_{13}$  (Obrowski's  $RuAl_3$ ) peritectically. This paper presents part of an investigation of some ruthenium-aluminium alloys, and discusses the feasibility of the proposed phase diagrams.

Samples were selected at intervals across the phase diagram, and a number of techniques were attempted in their manufacture. Most of the samples were produced in a button arc-furnace in an argon atmosphere, and then subjected to a solid state homogenisation treatment, for extensive periods, in an attempt to reduce the effects of segregation. The samples were then water-quenched. They were observed using optical and Scanning Electron Microscopes. Compositions of the observed phases were determined using Energy Dispersive Analysis of X-rays.

A sample with nominal atomic composition  $RuAl_{12}$  was melted in a muffle furnace at 1200°C and furnace-cooled. In the bottom region of the sample (Fig. 3), needles of  $Ru_4Al_{13}$  were surrounded by a layer of  $RuAl_3$ . The nature of this region confirms Anlage's proposed peritectic formation<sup>2</sup> of  $RuAl_3$  and indicates that of the two phases  $Ru_4Al_{13}$  has the higher melting point. The matrix consisted of the Al-rich solid solution, which contained a fine dispersion of small  $RuAl_3$  particles. The top of the sample was different, and contained dendritic  $RuAl_3$  with a matrix of apparently eutectic Al-rich solid and  $RuAl_3$ . This difference is thought to be due to the  $Ru_4Al_{13}$  phase solidifying initially, and sinking to the bottom of the melt because of its higher density, thus altering the composition of the remaining melt. The presence of primary dendrites of  $RuAl_3$  in the top of the sample is an indication that this phase melts below 1200°C. Allowing for the changing melt composition, these observations, as well as the absence of  $RuAl_{12}$ , agree with Anlage's phase diagram<sup>2</sup>.

A sample having nominal atomic composition  $Ru_{12}Al_{68}$  was quenched from 1200°C. It was two-phase with primary dendrites of  $RuAl_3$  and interdendritic  $Ru_4Al_{13}$  (Fig. 4). The presence of  $Ru_4Al_{13}$  suggests that this compound is stable above 1200°C. The dendritic form of  $RuAl_3$  implies that its melting point is higher than that of  $Ru_4Al_{13}$ , which is in contradiction to Obrowski<sup>1</sup> (Fig. 1). For  $RuAl_3$  to form at such high temperatures, the width of the  $Ru_4Al_{13}$  phase field must be reduced, and  $RuAl_3$  can no longer be formed via a peritectoid reaction.

A further specimen (nominal  $Ru_{17}Al_{83}$ ) revealed the formation of bulk  $RuAl$ ,  $Ru_2Al$ , and  $RuAl_2$  in that order, which suggests a series of peritectic reactions.

This work has shown that Obrowski's phase diagram is adequate above 50 at% Ru, but requires modification below this region. It is suggested that the higher aluminium part comprises a cascade of peritectic reactions.

The assistance and financial support of MINTEK is gratefully acknowledged.

## References

1. Obrowski, W. (1963) Metall 17, 108.
2. Anlage, S.M. (1988) J. Less Common Met. 136, 237.
3. Massalski, T.B., ed. (1986) Binary Alloy Phase Diagrams, Vol 1, American Society for Metals, 158.

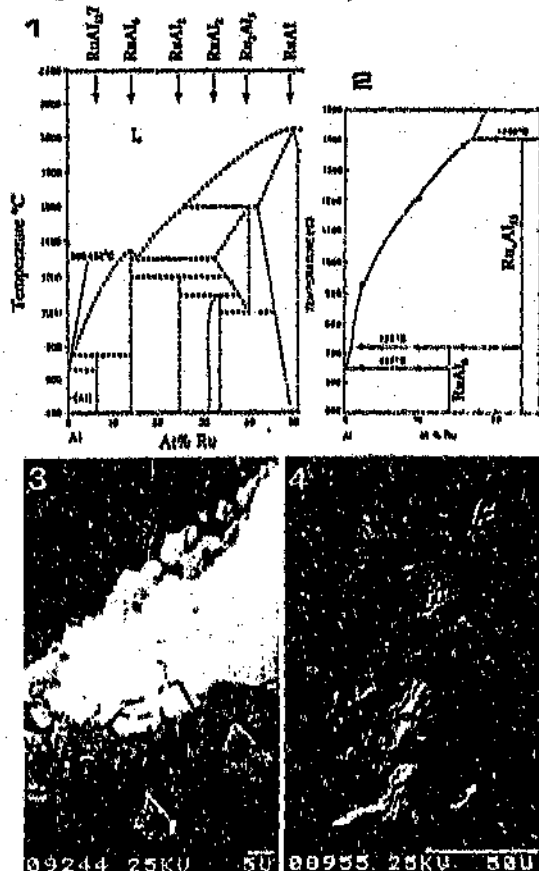


Fig. 1. Ru-Al phase diagram<sup>1</sup> proposed by Obrowski<sup>1</sup>  
 Fig. 2. Ru-Al phase diagram proposed by Anlage<sup>2</sup>  
 Fig. 3. Part of microstructure in the bottom of the nominally  $RuAl_{12}$  sample.  
 Fig. 4. Dendritic two-phase nature of nominal  $Ru_{12}Al_{68}$ .

## 7 CONCLUSIONS AND RECOMMENDATIONS

### 7.1 Summary and Conclusions

The preceding arguments have shown that the original (Obrowski's) phase diagram of the Ru-Al system requires modification below 50 at% ruthenium. The proposed modifications are that  $\text{RuAl}_2$ ,  $\text{Ru}_4\text{Al}_{13}$ , and  $\text{RuAl}_6$  form via peritectic reactions, at about 1460°C, 1403°C, and 723°C respectively. The shape and location of the phase boundaries have also been altered slightly. This work has shown that the compound  $\text{RuAl}_{12}$  does not exist, and the information provided by the former investigators, Edshammar and Anlage, appears to be adequately accurate.

### 7.2 Recommendations for Future Work

The most obvious recommendation, stemming from the entire course of this investigation, is that homogeneous samples be made for this alloy system, possibly by hot isostatic pressing. The DTA work was limited, and more thermal analyses should be undertaken, since they yield much useful information. Transmission Electron Microscopy (TEM) would enable determination of the lattice structures (and parameters) without needing to isolate the phases, and is therefore recommended. A combination of heat treatment and TEM work would also make it possible to investigate the reported "CsCl-like phases"<sup>[9]</sup> in the RuAl region of the phase diagram.



The lattice data for pure ruthenium and pure aluminium were used to identify the peaks belonging to their respective solid solutions. However, it is known that the peaks for the pure element shift as solute atoms are added. Since both of the solid solutions have a narrow composition range, it was expected that the shift of the lines from those of the pure elements would be minimal.

The Debye-Scherrer data was not used for precise lattice parameter calculations. There are a number of precautions which should be taken to reduce error sources, which were not considered in this work<sup>[17]</sup>. For example, the phases were not isolated, and this led to shifting of some compound peaks, as well as difficulty in identification due to peak overlap. The lack of high angle reflections on many films also precluded calculation of the shrinkage factors. Hence, the films are not considered accurate enough to warrant extensive analysis. Klug and Alexander<sup>[17]</sup> also state that "powder diffraction data are not suitable for the precision measurement of crystals belonging to the orthorhombic, monoclinic, and triclinic systems". A simple method for determining the lattice constants, in systems with higher symmetry, can only be employed if there are several  $hk0$  and  $00l$  reflections in the range  $2\theta = 30$  to  $90^\circ$ . Since there are insufficient reflections of this kind in the data, more complex, and timeous methods would have to be employed for the calculations.

The X-ray diffraction work in this investigation was useful both to confirm the phases identified by X-ray analysis during SEM studies, and to distinguish between phases with similar compositions. Thus  $\text{RuAl}_2$  and  $\text{Ru}_2\text{Al}_3$  were distinguished by X-ray diffraction, and the identity of  $\text{Ru}_4\text{Al}_{13}$  (rather than  $\text{RuAl}_3$ ) was confirmed.

that all the high intensity peaks lie at low diffraction angles, and the low angle lines are known to have the greatest inaccuracy. This inaccuracy is due to the large variation of  $\sin\Theta$  with  $\Theta$  at low angles.

Only those films having backscattered (high angle) lines could be used for calculation of accurate interplanar spacings, since these lines are required for calculation of the film shrinkage factor (the Straumanis factor, in this case, because the Straumanis method<sup>[16]</sup> was used for film analysis). Since the planar spacings could not be calculated for those films which did not have backscattered lines, the phases were identified by graphical methods, as described in Chapter 3.

The calculated lattice data for  $\text{RuAl}_3$  (Appendix XX) indicated the 100% peak to correspond to a d-value of 0.368 nm.  $\text{Ru}_4\text{Al}_{13}$  is reported to have two 100% peaks; one corresponding to a d-value of 0.36 nm, and the other corresponding to 0.332 nm. It is the latter peak which is the most distinguishing factor between  $\text{RuAl}_3$  and  $\text{Ru}_4\text{Al}_{13}$ . There was no film which had only the 0.36 nm peak, i.e. the phase present was definitely  $\text{Ru}_4\text{Al}_{13}$ , and not  $\text{RuAl}_3$ . In all cases the 0.36 nm peak was of lower intensity than the 0.332 nm peak, and it is suggested that the former has a relative intensity below 100%.

Of the unidentified diffraction peaks, there are some which were found in several of the samples. However, the abundance of phases in these samples prohibited the former fact being of any use. The only strong peak which remained unidentified was in nominal  $\text{Ru}_4\text{Al}_{13}$  in the heat treated condition.

## 6.5 X-Ray Diffraction

The purpose of the Debye-Scherrer diffraction experiments were two-fold. Firstly, they confirmed the presence of the phases identified from the quantitative analyses (assuming Edshammar's crystal structures to be accurate<sup>(8,9,10)</sup>). Secondly, they served as a confirmation of the reported lattice data.

In most cases, the high intensity lines in each of the Debye-Scherrer films were identified, but there were some very low intensity lines which did not match the plane spacings ( $d$ -values) reported by Edshammar. Since the phases had not been isolated, the latter lines could not be identified.

In some cases there were compounds in the samples which were not represented on the Debye-Scherrer films. This could be due to one of the following three factors. Firstly, the powder was filed from the surface of each sample. Since the samples were very inhomogeneous, it is possible that the powder was filed from an area which did not contain all of the phases present in the sample. Secondly, the powder was "screened" using acetone, and only the finer particles were collected for testing. This could further diminish the variety of phases tested. Thirdly, masking of the phases can occur. This phenomenon occurs when the distance between planes of two compounds are very similar. It causes the lines corresponding to these planes to lie in the same position on the Debye-Scherrer film, and can lead to problems in identification of the lines. In this particular system, the high intensity peaks of some of the phases are in similar positions, and phase identification was difficult when such phases were present. Another reason that identification was difficult is

Anlage's data points (depicted as dots in Figure 2.3) were used for the low ruthenium end, even though his analyses were obtained without Ru-Al standards. The solid solubility temperature dependence of RuAl has not been altered, but that of  $\text{Ru}_2\text{Al}_3$  has been re-specified. The  $\text{Ru}_2\text{Al}_3$  phase boundary was reconstructed to accommodate evidence from this work and Edshammar's. The other phases have been indicated with no temperature dependence, since this information was not available.

The layered structure which was present in many of samples, e.g.  $\text{Ru}_4\text{Al}_{13}$ ,  $\text{Ru}_{10}\text{Al}_{30}$ , etc., can be well explained by the proposed cascade of peritectic reactions and steep liquidus. With the very high cooling rates produced in arc button manufacture, the sample solidified in stages, with the higher melting point intermetallics freezing first. These are the higher ruthenium ones. The remaining liquid was then more Al-rich than the solid, and the next layer of intermetallic to solidify had a lower melting point and higher aluminium content (as described in discussion of  $\text{Ru}_{23.3}\text{Al}_{71.7}$ ). Thus, this process was repeated with RuAl solidifying initially, then  $\text{Ru}_2\text{Al}_3$ . In most cases no layer of  $\text{RuAl}_2$  was formed, probably due to severe undercooling and the formation temperature of  $\text{RuAl}_2$  lying just above that of  $\text{Ru}_4\text{Al}_{13}$ . The latter phase solidified next, but as the  $\text{RuAl}_2$  phase was missed, there was an excess of ruthenium in the matrix. In some cases, small discrete amounts of  $\text{RuAl}_2$  formed by cellular precipitation, and in others, an intimate mixture of  $\text{Ru}_4\text{Al}_{13}$  and  $\text{Ru}_2\text{Al}_3$ . It was proposed earlier (Chapter 4) that the latter was the result of a solid-state decomposition of the Ru-rich inhomogeneities.

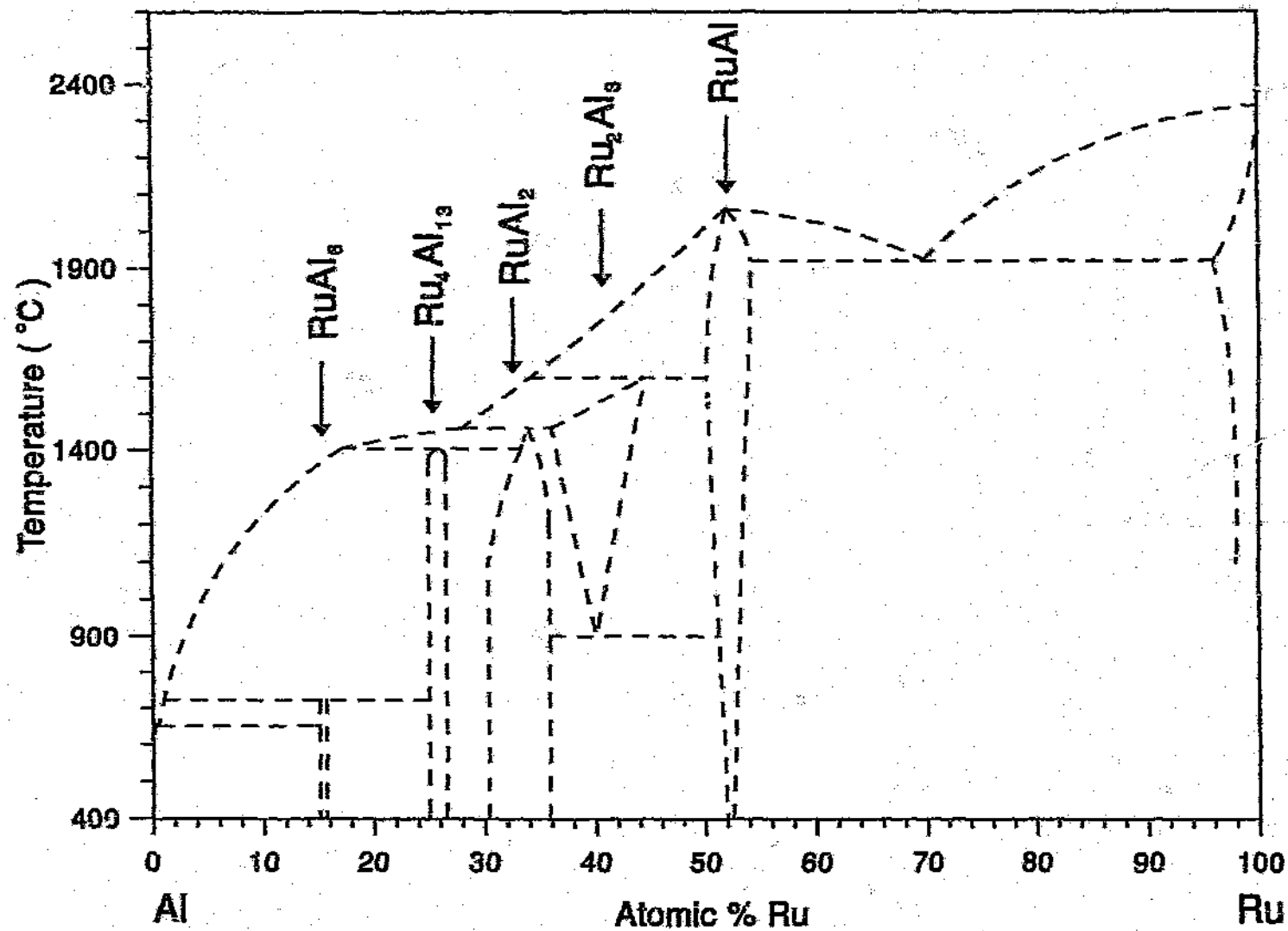


Figure 6.1: Modified Ru-Al Phase Diagram.

**Table 6.9:** Deduction of limits of peritectic reaction lines, and peritectic reaction points, using all available data.

PERITECTIC REACTION LINE	Al-RICH LIMIT (at % Ru)	PERITECTIC POINT (at % Ru)	Ru-RICH LIMIT (at % Ru)
$\text{Ru}_2\text{Al}_3$	33.33 - 36.36	> 44.44	Cannot deduce
$\text{RuAl}_2$	> 27.64	> 33.33	Cannot deduce
$\text{Ru}_4\text{Al}_{13}$	< 27.64	> 13.7	33.33 - 36.36

The deductions contained in Table 6.9 indicate that the composition range for  $\text{Ru}_2\text{Al}_3$  is slightly wider than reported in Table 6.8. It should be remembered that some of the values in Tables 6.6, 6.7 and 6.9 are highly speculative, but they do give some indication of the shape of the liquidus. Unfortunately, both the extreme slope of the liquidus across the phase diagram, and the lack of control on the arc-melting technique, means that if the liquid reaches a very high temperature (say, above the formation of  $\text{RuAl}$  at  $\sim 2060^\circ\text{C}$ ) then the formation of nearly all the phases in small amounts is possible. This makes for very inhomogeneous alloys (e.g.  $\text{Ru}_4\text{Al}_{36}\text{-a(ht)}$ ,  $\text{Ru}_{16}\text{Al}_{30}$ , etc.) and makes deduction of the liquidus more difficult. Ideally one would want to control the maximum temperature of the arc-melt to about  $100^\circ\text{C}$  above the estimated liquidus.

The above observations are summarised simply in a sketch of a new phase diagram (Fig 6.1). The lines are not solid because they are only the best estimate that could be obtained from the work covered here, and may not accurately represent the true situation. The phase diagram depicted in Figure 6.1 is based, not only on the samples made during the course of this work, but is also consistent with other workers.

standards, due to software limitations.

The data for  $\text{RuAl}_6$  does not yield any new information regarding the reaction limits (Table 6.7). Comparing the rough deductions from the current work (Table 6.7) with those from Edshammar's work (Table 6.6), it can be seen that there is some agreement, but the data from the current work is sparse. However, the most likely limits were found by considering the phase compositions and the deduced phase widths (Table 6.8). The latter were determined from those samples (discussed in chapters 4 & 5) which were deemed to be the most homogeneous. In Table 6.8 the left and right boundaries of  $\text{RuAl}_6$  and  $\text{Ru}_4\text{Al}_{13}$  have been interchanged (as in Tables 6.1 & 6.2), since they otherwise represent an impossible situation. This modification cannot increase the error in the results, which must be large for this situation to occur. The combined data for the peritectic reaction limits is given in Table 6.9.

Table 6.8: Phase Composition Boundaries.

PHASE	Al-RICH BOUNDARY (at % Ru)	Ru-RICH BOUNDARY (at % Ru)
$\text{RuAl}_6$	$15.10 \pm 0.01$	$15.7 \pm 0.1$
$\text{Ru}_4\text{Al}_{13}$	$25.00 \pm 0.05$	$26.6 \pm 0.1$
$\text{RuAl}_2$	$30.35 \pm 0.08$	$35.8 \pm 0.2$
$\text{Ru}_2\text{Al}_3$	$35.7 \pm 0.8$	$41.6 \pm 0.5$
$\text{RuAl}$	$50.2 \pm 0.6$	$54.3 \pm 0.4$

**Table 6.6:** Deduction of limits of peritectic reaction lines, and peritectic reaction points, using Edshammar's data.

PERITECTIC REACTION LINE	Al-RICH LIMIT (at % Ru)	PERITECTIC POINT (at % Ru)	Ru-RICH LIMIT (at % Ru)
$\text{Ru}_2\text{Al}_3$	33.33 - 36.36	> 44.44	Cannot deduce
$\text{RuAl}_2$	33.33 - 36.36*	> 33.33	44.44 - 50**
$\text{Ru}_4\text{Al}_{13}$	28.57 - 30.77	$\text{RuAl}_6$ not found	33.33 - 36.36

**Table 6.7:** Deduction of limits of peritectic reaction lines, and peritectic points, using the samples from this work.

PERITECTIC REACTION LINE	Al-RICH LIMIT (at % Ru)	PERITECTIC POINT (at % Ru)	Ru-RICH LIMIT (at % Ru)
$\text{Ru}_2\text{Al}_3$	> 28.2	> 28.2	> 28.2
$\text{RuAl}_2$	> 27.6	> 28.2	> 28.2
$\text{Ru}_4\text{Al}_{13}$	< 27.6	> 13.7	> 28.2
$\text{RuAl}_6$	< 3.1	< 19.84	> 13.7

It is difficult to undertake a similar analysis using the alloys from this work (Table 6.7), because many had the whole range of phases, and some were of little use due to contamination. It should also be noted that the overall analyses were obtained without

---

\*Since no  $\text{Ru}_2\text{Al}_3$  was formed,  $\text{RuAl}$  was used to determine this limit.

\*\*This limit does not fit the phase diagram, because non-equilibrium cooling caused the reaction forming  $\text{Ru}_2\text{Al}_3$  to be overshoot.



SPECTRUM: Ru<sub>4</sub>Al<sub>13</sub> centre of needle (quantitative)

ELEMENT	WEIGHT %	% ERROR	ATOMIC %
Al	47.66	0.54	76.42
Ru	55.11	0.82	23.58
Total	102.77		100.00

SPECTRUM: RuAl<sub>6</sub> on edge of needle (quantitative)

ELEMENT	WEIGHT %	% ERROR	ATOMIC %
Al	59.91	0.62	84.91
Ru	39.91	0.66	15.09
Total	99.83		100.00

SPECTRUM: RuAl<sub>6</sub> on edge of needle (quantitative)

ELEMENT	WEIGHT %	% ERROR	ATOMIC %
Al	59.90	0.62	84.89
Ru	39.95	0.66	15.11
Total	99.86		100.00

SPECTRUM: Al-rich matrix (quantitative)

ELEMENT	WEIGHT %	% ERROR	ATOMIC %
Al	95.49	0.87	99.20
Ru	2.89	0.22	0.80
Total	98.38		100.00

SPECTRUM: Al-rich matrix (quantitative)

ELEMENT	WEIGHT %	% ERROR	ATOMIC %
Al	94.72	0.87	99.17
Ru	2.98	0.21	0.83
Total	97.69		100.00

EXPERIMENTAL DATA FOR Ru:Al<sub>12</sub>

## CHEMICAL ANALYSES (EDAX)

SAMPLE: Ru:Al<sub>12</sub> (No heat treatment)

Semi-quantitative Analyses

PHASE	ATOMIC % RUTHENIUM
Al-rich matrix	0.01
RuAl <sub>6</sub> (dendrites)	13.65
RuAl <sub>6</sub> (layer)	13.2 ± 0.4
Ru <sub>4</sub> Al <sub>13</sub> (needles)	22.4 ± 0.1

SPECTRUM: Overall composition (semi-quantitative)

ELEMENT	RELATIVE K	WT %	ATOMIC %
Al	0.8656	93.68	98.23
Ru	0.0382	6.32	1.77
Total		100.00	100.00

SPECTRUM: Overall composition (semi-quantitative)

ELEMENT	RELATIVE K	WT %	ATOMIC %
Al	0.9695	98.30	99.54
Ru	0.0100	1.70	0.46
Total		100.00	100.00

SPECTRUM: Ru<sub>4</sub>Al<sub>13</sub> centre of needle (quantitative)

ELEMENT	WEIGHT %	% ERROR	ATOMIC %
Al	47.44	0.54	75.80
Ru	56.75	0.83	24.20
Total	104.19		100.00

**SPECTRUM: RuAl<sub>3</sub> at edge of needle (quantitative)**

ELEMENT	WEIGHT %	% ERROR	ATOMIC %
Al	50.82	0.60	82.83
Ru	39.48	0.74	17.17
Total	90.30		100.00

**SPECTRUM: RuAl<sub>3</sub> at edge of needle (quantitative)**

ELEMENT	WEIGHT %	% ERROR	ATOMIC %
Al	49.59	0.59	82.14
Ru	40.41	0.75	17.86
Total	90.01		100.00

**SPECTRUM: Al-rich matrix (quantitative)**

ELEMENT	WEIGHT %	% ERROR	ATOMIC %
Al	94.89	0.94	99.41
Ru	2.11	0.24	0.59
Total	96.99		100.00

SPECTRUM: Ru<sub>4</sub>Al<sub>13</sub> needle (quantitative)

ELEMENT	WEIGHT %	% ERROR	ATOMIC %
Al	49.12	0.60	75.18
Ru	60.76	1.01	24.82
Total	109.88		100.00

SPECTRUM: Ru<sub>4</sub>Al<sub>13</sub> needle (quantitative)

ELEMENT	WEIGHT %	% ERROR	ATOMIC %
Al	47.29	0.58	75.30
Ru	58.14	0.97	24.70
Total	105.43		100.00

SPECTRUM: Ru<sub>4</sub>Al<sub>13</sub> needle (quantitative)

ELEMENT	WEIGHT %	% ERROR	ATOMIC %
Al	47.28	0.58	75.34
Ru	57.98	0.97	24.66
Total	105.26		100.00

SPECTRUM: RuAl<sub>4</sub> at edge of needle (quantitative)

ELEMENT	WEIGHT %	% ERROR	ATOMIC %
Al	50.84	0.60	83.39
Ru	37.94	0.72	16.61
Total	88.78		100.00

SPECTRUM: RuAl<sub>4</sub> at edge of needle (quantitative)

ELEMENT	WEIGHT %	% ERROR	ATOMIC %
Al	48.49	0.59	80.37
Ru	44.39	0.80	19.63
Total	92.88		100.00

EXPERIMENTAL DATA FOR  $Ru_4Al_{36-b}$ CHEMICAL ANALYSES (EDAX)SAMPLE:  $Ru_4Al_{36-b}$  (No heat treatment)

Semi-quantitative Analyses

PHASE	ATOMIC % RUTHENIUM
Al-rich eutectic	$0.37 \pm 0.02$
Al particle	0.65
$RuAl_6$	$13.1 \pm 0.6$
$Ru_4Al_{13}$	$22.1 \pm 0.3$

SPECTRUM: Overall composition (semi-quantitative)

ELEMENT	RELATIVE K	WT %	ATOMIC %
Al	0.7706	89.02	96.81
Ru	0.0677	10.98	3.19
Total		100.00	100.00

SPECTRUM: Overall composition (semi-quantitative)

ELEMENT	RELATIVE K	WT %	ATOMIC %
Al	0.7704	89.02	96.81
Ru	0.0677	10.98	3.19
Total		100.00	100.00

SPECTRUM: Overall composition (semi-quantitative)

ELEMENT	RELATIVE K	WT %	ATOMIC %
Al	0.7864	89.86	97.08
Ru	0.0623	10.14	2.92
Total		100.00	100.00

**SPECTRUM: Al-rich matrix (quantitative)**

ELEMENT	WEIGHT %	% ERROR	ATOMIC %
Al	87.48	0.88	99.41
Ru	1.93	0.22	0.59
Total	89.41		100.00

**SPECTRUM: Al-rich matrix (quantitative)**

ELEMENT	WEIGHT %	% ERROR	ATOMIC %
Al	86.12	0.87	99.13
Ru	2.82	0.23	0.87
Total	88.95		100.00

SPECTRUM: Ru<sub>4</sub>Al<sub>13</sub> phase layer and centre of needles (quantitative)

ELEMENT	WEIGHT %	% ERROR	ATOMIC %
Al	46.61	0.57	74.00
Ru	61.37	1.01	26.00
Total	107.97		100.00

SPECTRUM: Ru<sub>4</sub>Al<sub>13</sub> phase layer and centre of needles (quantitative)

ELEMENT	WEIGHT %	% ERROR	ATOMIC %
Al	42.25	0.54	74.80
Ru	53.32	0.91	25.20
Total	95.57		100.00

SPECTRUM: Ru<sub>4</sub>Al<sub>13</sub> phase layer and centre of needles (quantitative)

ELEMENT	WEIGHT %	% ERROR	ATOMIC %
Al	42.54	0.54	73.55
Ru	57.31	0.95	26.45
Total	99.85		100.00

SPECTRUM: RuAl<sub>6</sub> phase layer, fine needles, and surrounding Ru<sub>4</sub>Al<sub>13</sub> (quantitative)

ELEMENT	WEIGHT %	% ERROR	ATOMIC %
Al	63.03	0.70	84.42
Ru	43.60	0.81	15.58
Total	106.63		100.00

SPECTRUM: RuAl<sub>6</sub> phase layer, fine needles, and surrounding Ru<sub>4</sub>Al<sub>13</sub> (quantitative)

ELEMENT	WEIGHT %	% ERROR	ATOMIC %
Al	54.45	0.63	83.63
Ru	39.95	0.75	16.37
Total	94.40		100.00

SAMPLE: Ru<sub>4</sub>:Al<sub>96</sub>-a (475°C for 168 hours)  
 SPECTRUM: RuAl core region (quantitative)

ELEMENT	WEIGHT %	% ERROR	ATOMIC %
Al	23.15	0.38	53.45
Ru	75.54	1.15	46.55
Total	98.69		100.00

SPECTRUM: RuAl core region (quantitative)

ELEMENT	WEIGHT %	% ERROR	ATOMIC %
Al	21.40	0.37	50.88
Ru	77.42	1.17	49.12
Total	98.82		100.00

SPECTRUM: Ru<sub>2</sub>Al<sub>3</sub> phase layer (quantitative)

ELEMENT	WEIGHT %	% ERROR	ATOMIC %
Al	31.93	0.46	64.18
Ru	66.79	1.06	35.82
Total	98.73		100.00

SPECTRUM: Ru<sub>2</sub>Al<sub>3</sub> phase layer (quantitative)

ELEMENT	WEIGHT %	% ERROR	ATOMIC %
Al	32.60	0.46	65.41
Ru	64.58	1.03	34.59
Total	97.18		100.00

SPECTRUM: Ru<sub>2</sub>Al<sub>3</sub> phase layer (quantitative)

ELEMENT	WEIGHT %	% ERROR	ATOMIC %
Al	32.80	0.46	64.03
Ru	69.04	1.09	35.97
Total	101.84		100.00



SPECTRUM: Al-rich matrix (quantitative)

ELEMENT	WEIGHT %	% ERROR	ATOMIC %
Al	89.37	0.90	99.63
Ru	1.25	0.20	0.37
Total	90.61		100.00

SPECTRUM: Overall composition (quantitative)

ELEMENT	WEIGHT %	% ERROR	ATOMIC %
Al	82.57	0.85	96.72
Ru	10.50	0.37	3.28
Total	93.08		100.00

SPECTRUM: Overall composition (quantitative)

ELEMENT	WEIGHT %	% ERROR	ATOMIC %
Al	82.95	0.85	96.67
Ru	10.71	0.37	3.33
Total	93.66		100.00

SPECTRUM: Ru<sub>4</sub>Al<sub>13</sub> needles (quantitative)

ELEMENT	WEIGHT %	% ERROR	ATOMIC %
Al	43.44	0.55	74.13
Ru	56.81	0.95	25.87
Total	100.25		100.00

SPECTRUM: Ru<sub>4</sub>Al<sub>13</sub> needles (quantitative)

ELEMENT	WEIGHT %	% ERROR	ATOMIC %
Al	42.26	0.54	74.05
Ru	55.48	0.93	25.95
Total	97.74		100.00

EXPERIMENTAL DATA FOR  $\text{Ru}_{12}\text{Al}_{85}\text{-a}$ CHEMICAL ANALYSES (EDAX)SAMPLE:  $\text{Ru}_{12}\text{Al}_{85}\text{-a}$  (No heat treatment)SPECTRUM:  $\text{RuAl}_6$  needles (quantitative)

ELEMENT	WEIGHT %	% ERROR	ATOMIC %
Al	57.80	0.66	84.39
Ru	40.08	0.76	15.61
Total	97.88		100.00

SPECTRUM:  $\text{RuAl}_6$  needles (quantitative)

ELEMENT	WEIGHT %	% ERROR	ATOMIC %
Al	57.62	0.66	84.09
Ru	40.85	0.77	15.91
Total	98.48		100.00

SPECTRUM:  $\text{RuAl}_6$  needles (quantitative)

ELEMENT	WEIGHT %	% ERROR	ATOMIC %
Al	56.13	0.64	84.46
Ru	38.69	0.74	15.54
Total	94.83		100.00

SPECTRUM: Al-rich matrix (quantitative)

ELEMENT	WEIGHT %	% ERROR	ATOMIC %
Al	90.24	0.90	99.57
Ru	1.46	0.21	0.43
Total	91.70		100.00

SPECTRUM: Al-rich matrix (quantitative)

ELEMENT	WEIGHT %	% ERROR	ATOMIC %
Al	83.99	0.86	99.39
Ru	1.94	0.20	0.61
Total	85.93		100.00

**SPECTRUM: Contaminated RuAl<sub>6</sub> (semi-quantitative)**

ELEMENT	RELATIVE K	WT %	ATOMIC %
Al	0.3048	52.63	76.81
Si	0.0122	3.70	5.18
Fe	0.0285	3.18	2.24
Ru	0.2888	40.50	15.77
Total		100.00	100.00

**SPECTRUM: Contaminated Al-rich matrix (semi-quantitative)**

ELEMENT	RELATIVE K	WT %	ATOMIC %
Al	0.9841	98.99	99.42
Si	0.0010	0.43	0.41
Fe	0.0003	0.04	0.02
Ru	0.0032	0.54	0.14
Total		100.00	100.00

**SPECTRUM: Contaminated Al-rich matrix (semi-quantitative)**

ELEMENT	RELATIVE K	WT %	ATOMIC %
Al	0.9983	99.91	99.93
Si	0.0001	0.06	0.06
Fe	0.0001	0.01	0.01
Ru	0.0001	0.02	0.00
Total		100.00	100.00

**SPECTRUM: Contaminated Al-rich matrix (semi-quantitative)**

ELEMENT	RELATIVE K	WT %	ATOMIC %
Al	0.9938	99.61	99.69
Si	0.0006	0.26	0.25
Fe	0.0011	0.12	0.06
Ru	0.0001	0.01	0.00
Total		100.00	100.00

**SPECTRUM: Contaminated Al-rich matrix (semi-quantitative)**

ELEMENT	RELATIVE K	WT %	ATOMIC %
Al	0.9915	99.47	99.64
Si	0.0006	0.28	0.27
Fe	0.0013	0.14	0.07
Ru	0.0006	0.11	0.03
Total		100.00	100.00

**SPECTRUM: Al-Si crystals in sample (semi-quantitative)**

ELEMENT	RELATIVE K	WT %	ATOMIC %
Al	0.5129	52.62	53.63
Si	0.1814	47.34	46.35
Fe	0.0001	0.01	0.01
Ru	0.0001	0.03	0.01
Total		100.00	100.00

**SAMPLE:  $Ru_3Al_{17}$ -b (550°C for 1176 hours)**

**SPECTRUM: Contaminated  $RuAl_6$  (semi-quantitative)**

ELEMENT	RELATIVE K	WT %	ATOMIC %
Al	0.3175	54.52	77.42
Si	0.0123	3.83	5.22
Fe	0.0462	5.14	3.53
Ru	0.2565	36.51	13.83
Total		100.00	100.00

**SPECTRUM: Contaminated  $RuAl_6$  (semi-quantitative)**

ELEMENT	RELATIVE K	WT %	ATOMIC %
Al	0.3362	56.64	80.05
Si	0.0080	2.52	3.43
Fe	0.0331	3.69	2.52
Ru	0.2612	37.14	14.01
Total		100.00	100.00

SPECTRUM: RuAl core region (quantitative)

ELEMENT	WEIGHT %	% ERROR	ATOMIC %
Al	20.98	0.37	49.93
Ru	78.85	1.19	50.07
Total	99.84		100.00

SPECTRUM: Ru<sub>2</sub>Al<sub>3</sub> phase layer (quantitative)

ELEMENT	WEIGHT %	% ERROR	ATOMIC %
Al	33.03	0.47	64.85
Ru	67.07	1.06	35.15
Total	100.10		100.00

SPECTRUM: Ru<sub>2</sub>Al<sub>3</sub> phase layer (quantitative)

ELEMENT	WEIGHT %	% ERROR	ATOMIC %
Al	32.35	0.46	63.43
Ru	69.89	1.09	36.57
Total	102.25		100.00

SPECTRUM: Ru<sub>2</sub>Al<sub>3</sub> phase layer (quantitative)

ELEMENT	WEIGHT %	% ERROR	ATOMIC %
Al	32.64	0.46	63.61
Ru	69.97	1.10	36.39
Total	102.60		100.00

SPECTRUM: Ru<sub>4</sub>Al<sub>13</sub> phase layer and centre of needles (quantitative)

ELEMENT	WEIGHT %	% ERROR	ATOMIC %
Al	42.23	0.54	74.23
Ru	54.94	0.93	25.77
Total	97.17		100.00

**SPECTRUM: Thin RuAl<sub>6</sub> layer and needles (quantitative)**

ELEMENT	WEIGHT %	% ERROR	ATOMIC %
Al	58.41	0.66	84.47
Ru	40.24	0.76	15.53
Total	98.65		100.00

**SPECTRUM: Thin RuAl<sub>6</sub> layer and needles (quantitative)**

ELEMENT	WEIGHT %	% ERROR	ATOMIC %
Al	62.92	0.70	84.54
Ru	43.11	0.80	15.46
Total	106.03		100.00

**SPECTRUM: Al-rich matrix of needle region (quantitative)**

ELEMENT	WEIGHT %	% ERROR	ATOMIC %
Al	87.02	0.88	99.15
Ru	2.78	0.24	0.85
Total	89.80		100.00

**SPECTRUM: Al-rich matrix of needle region (quantitative)**

ELEMENT	WEIGHT %	% ERROR	ATOMIC %
Al	89.31	0.90	99.45
Ru	1.85	0.22	0.55
Total	91.16		100.00

**SAMPLE: Ru<sub>10</sub>:Al<sub>90</sub> (475°C for 168 hours)**

**SPECTRUM: RuAl core region (quantitative)**

ELEMENT	WEIGHT %	% ERROR	ATOMIC %
Al	22.02	0.37	51.34
Ru	78.21	1.18	48.66
Total	100.23		100.00

SPECTRUM: "Eutectic"-like mixture (quantitative)

ELEMENT	WEIGHT %	% ERROR	ATOMIC %
Al	37.99	0.51	69.17
Ru	63.44	1.02	30.83
Total	101.42		100.00

SPECTRUM: Small RuAl<sub>2</sub> grains (quantitative)

ELEMENT	WEIGHT %	% ERROR	ATOMIC %
Al	39.19	0.51	70.37
Ru	61.84	1.01	29.63
Total	101.03		100.00

SPECTRUM: Small RuAl<sub>2</sub> grains (quantitative)

ELEMENT	WEIGHT %	% ERROR	ATOMIC %
Al	38.89	0.51	70.05
Ru	62.31	1.01	29.95
Total	101.20		100.00

SPECTRUM: Small RuAl<sub>2</sub> grains (quantitative)

ELEMENT	WEIGHT %	% ERROR	ATOMIC %
Al	39.14	0.51	70.20
Ru	62.27	1.01	29.80
Total	101.41		100.00

SPECTRUM: Thin RuAl<sub>2</sub> layer and needles (quantitative)

ELEMENT	WEIGHT %	% ERROR	ATOMIC %
Al	63.55	0.70	85.19
Ru	41.39	0.78	14.81
Total	104.94		100.00

SPECTRUM: Ru<sub>4</sub>Al<sub>13</sub> phase layer and needles (quantitative)

ELEMENT	WEIGHT %	% ERROR	ATOMIC %
Al	43.24	0.55	73.90
Ru	57.22	0.95	26.10
Total	100.46		100.00

SPECTRUM: Ru<sub>4</sub>Al<sub>13</sub> phase layer and needles (quantitative)

ELEMENT	WEIGHT %	% ERROR	ATOMIC %
Al	43.18	0.55	74.20
Ru	56.25	0.94	25.80
Total	99.43		100.00

SPECTRUM: Ru<sub>4</sub>Al<sub>13</sub> phase layer and needles (quantitative)

ELEMENT	WEIGHT %	% ERROR	ATOMIC %
Al	43.40	0.55	73.91
Ru	57.40	0.96	26.09
Total	100.80		100.00

SPECTRUM: "Eutectic"-like mixture (quantitative)

ELEMENT	WEIGHT %	% ERROR	ATOMIC %
Al	38.89	0.51	70.00
Ru	62.46	1.01	30.00
Total	101.35		100.00

SPECTRUM: "Eutectic"-like mixture (quantitative)

ELEMENT	WEIGHT %	% ERROR	ATOMIC %
Al	38.19	0.51	69.17
Ru	63.77	1.03	30.83
Total	101.96		100.00



SPECTRUM: RuAl core region (quantitative)

ELEMENT	WEIGHT %	% ERROR	ATOMIC %
Al	19.08	0.35	46.72
Ru	81.52	1.22	53.28
Total	100.60		100.00

SPECTRUM: RuAl core region (quantitative)

ELEMENT	WEIGHT %	% ERROR	ATOMIC %
Al	18.59	0.34	46.05
Ru	81.62	1.22	53.95
Total	100.21		100.00

SPECTRUM: Ru<sub>2</sub>Al<sub>3</sub> phase layer (quantitative)

ELEMENT	WEIGHT %	% ERROR	ATOMIC %
Al	31.97	0.46	63.47
Ru	68.94	1.08	36.53
Total	100.91		100.00

SPECTRUM: Ru<sub>2</sub>Al<sub>3</sub> phase layer (quantitative)

ELEMENT	WEIGHT %	% ERROR	ATOMIC %
Al	31.84	0.46	63.30
Ru	69.17	1.09	36.70
Total	101.01		100.00

SPECTRUM: Ru<sub>2</sub>Al<sub>3</sub> phase layer (quantitative)

ELEMENT	WEIGHT %	% ERROR	ATOMIC %
Al	32.35	0.46	63.88
Ru	68.54	1.08	36.12
Total	100.89		100.00

EXPERIMENTAL DATA FOR  $Ru_{10}:Al_{90}$ CHEMICAL ANALYSES (EDAX)SAMPLE:  $Ru_{10}:Al_{90}$  (as-cast)

SPECTRUM: Ru-rich solid in eutectic (quantitative)

ELEMENT	WEIGHT %	% ERROR	ATOMIC %
Al	7.81	0.25	24.09
Ru	92.26	1.33	75.91
Total	100.07		100.00

SPECTRUM: Ru-rich solid in eutectic (quantitative)

ELEMENT	WEIGHT %	% ERROR	ATOMIC %
Al	6.07	0.23	19.59
Ru	93.32	1.34	80.41
Total	99.39		100.00

SPECTRUM: Ru-rich solid in eutectic (quantitative)

ELEMENT	WEIGHT %	% ERROR	ATOMIC %
Al	7.79	0.25	24.20
Ru	91.42	1.32	75.80
Total	99.21		100.00

SPECTRUM: RuAl core region (quantitative)

ELEMENT	WEIGHT %	% ERROR	ATOMIC %
Al	18.27	0.34	45.45
Ru	82.16	1.23	54.55
Total	100.43		100.00

SPECTRUM: Contaminated RuAl<sub>3</sub> (semi-quantitative)

ELEMENT	RELATIVE K	WT %	ATOMIC %
Al	0.3329	55.59	80.05
Si	0.0082	2.55	3.53
Fe	0.0094	1.05	0.73
Ru	0.2902	40.81	15.69
Total		100.00	100.00

SPECTRUM: Contaminated Al-rich matrix (semi-quantitative)

ELEMENT	RELATIVE K	WT %	ATOMIC %
Al	0.9949	99.69	99.77
Si	0.0004	0.18	0.18
Fe	0.0010	0.00	0.05
Ru	0.0001	0.02	0.01
Total		100.00	100.00

SPECTRUM: Contaminated Al-rich matrix (semi-quantitative)

ELEMENT	RELATIVE K	WT %	ATOMIC %
Al	0.9869	99.18	99.51
Si	0.0008	0.36	0.35
Fe	0.0009	0.10	0.05
Ru	0.0021	0.36	0.10
Total		100.00	100.00

SPECTRUM: Contaminated Al-rich matrix (semi-quantitative)

ELEMENT	RELATIVE K	WT %	ATOMIC %
Al	0.9892	99.29	99.56
Si	0.0008	0.36	0.34
Fe	0.0000	0.00	0.00
Ru	0.0021	0.35	0.09
Total		100.00	100.00

SPECTRUM: Contaminated RuAl<sub>3</sub> (semi-quantitative)

ELEMENT	RELATIVE K	WT %	ATOMIC %
Al	0.4027	64.19	86.87
Fe	0.0060	0.67	0.44
Ru	0.2417	35.14	12.69
Total		100.00	100.00

SPECTRUM: Contaminated Al-rich matrix (semi-quantitative)

ELEMENT	RELATIVE K	WT %	ATOMIC %
Al	0.9930	99.61	99.89
Fe	0.0000	0.00	0.00
Ru	0.0023	0.39	0.10
Total		100.00	100.00

SAMPLE: Ru<sub>7</sub>:Al<sub>91</sub> (550°C for 1176 hours)

SPECTRUM: Contaminated RuAl<sub>3</sub> (semi-quantitative)

ELEMENT	RELATIVE K	WT %	ATOMIC %
Al	0.3093	52.66	77.05
Si	0.0130	3.91	5.50
Fe	0.0139	1.56	1.10
Ru	0.2991	41.87	16.35
Total		100.00	100.00

SPECTRUM: Contaminated RuAl<sub>3</sub> (semi-quantitative)

ELEMENT	RELATIVE K	WT %	ATOMIC %
Al	0.4188	64.86	86.95
Si	0.0006	0.20	0.26
Fe	0.0093	1.03	0.67
Ru	0.2343	33.91	12.13
Total		100.00	100.00

# APPENDIX VII

## EXPERIMENTAL DATA FOR $\text{Ru}_7\text{Al}_{23}$

### CHEMICAL ANALYSES (EDAX)

SAMPLE:  $\text{Ru}_7\text{Al}_{23}$  (No heat treatment)

SPECTRUM: Overall composition (semi-quantitative)

ELEMENT	RELATIVE K	WT %	ATOMIC %
Al	0.6222	81.01	93.98
Fe	0.0051	0.57	0.32
Ru	0.1164	18.42	5.70
Total		100.00	100.00

SPECTRUM: Overall composition (semi-quantitative)

ELEMENT	RELATIVE K	WT %	ATOMIC %
Al	0.6226	81.02	93.99
Fe	0.0047	0.52	0.29
Ru	0.1167	18.46	5.71
Total		100.00	100.00

SPECTRUM: Contaminated  $\text{RuAl}_3$  (semi-quantitative)

ELEMENT	RELATIVE K	WT %	ATOMIC %
Al	0.3437	58.56	83.74
Fe	0.0129	1.44	1.00
Ru	0.2830	40.00	15.27
Total		100.00	100.00

SPECTRUM: Contaminated  $\text{RuAl}_3$  (semi-quantitative)

ELEMENT	RELATIVE K	WT %	ATOMIC %
Al	0.3395	58.11	83.49
Fe	0.0129	1.44	1.00
Ru	0.2869	40.45	15.51
Total		100.00	100.00

X-RAY DIFFRACTION DATA FOR Ru:Al<sub>12</sub> CONTINUED:

NUMBER	2 THETA	d (nm)	CPS	INTENSITY(%)
21	27.694	0.14817	78.08	0.50
22	28.661	0.14327	33.68	0.21
23	31.074	0.13239	10.71	0.07
24	31.775	0.12954	9.43	0.06
25	32.680	0.12605	12.31	0.08
26	33.660	0.12248	80.64	0.51
27	35.309	0.11693	79.69	0.51
28	37.187	0.11122	33.79	0.21
29	38.135	0.10855	16.04	0.10
30	43.620	0.09545	10.32	0.07
31	44.831	0.09300	33.43	0.21
32	46.193	0.09040	15.00	0.10
33	50.819	0.08264	151.79	0.96
34	51.176	0.08211	81.21	0.52
35	53.087	0.07935	6.20	0.04
36	54.889	0.07694	29.20	0.19

# X-RAY DIFFRACTION DATA FOR Ru:Al<sub>12</sub>:

NUMBER	2 THETA	d (nm)	CPS	INTENSITY(%)
1	8.188	0.49672	60.30	0.38
2	9.048	0.44960	39.64	0.25
3	10.840	0.37543	19.72	0.13
4	12.000	0.33925	32.16	0.20
5	12.255	0.33223	67.88	0.43
6	13.182	0.30896	1.14	0.01
7	14.139	0.288.4	23.22	0.15
8	15.540	0.26250	8.82	0.06
9	15.941	0.25574	4.05	0.03
10	17.387	0.23461	15747.22	100.00
11	18.040	0.22619	393.49	2.50
12	18.847	0.21658	202.61	1.29
13	19.725	0.20704	157.28	1.00
14	21.458	0.19048	24.82	0.16
15	22.098	0.18503	12.81	0.08
16	22.930	0.17841	7.80	0.05
17	23.786	0.17207	12.56	0.08
18	24.611	0.16639	13.01	0.08
19	25.330	0.16174	24.51	0.16
20	26.759	0.15325	17.24	0.11

SPECTRUM: Discrete  $\text{RuAl}_6$  in top of sample (semi-quantitative)

ELEMENT	WEIGHT %	% ERROR	ATOMIC %
Al	62.30	0.64	84.79
Ru	41.89	0.69	15.21
Total	104.19		100.00

SPECTRUM: Discrete  $\text{RuAl}_6$  in top of sample (semi-quantitative)

ELEMENT	WEIGHT %	% ERROR	ATOMIC %
Al	61.57	0.64	84.82
Ru	41.28	0.68	15.18
Total	102.85		100.00



SPECTRUM: Overall composition (quantitative)

ELEMENT	WEIGHT %	% ERROR	ATOMIC %
Al	42.14	0.54	72.31
Ru	60.48	0.99	27.69
Total	102.62		100.00

SAMPLE: Ru<sub>23</sub>Al<sub>72</sub> (1300°C for 6.5 hours)

SPECTRUM: Ru-rich solid in eutectic (quantitative)

ELEMENT	WEIGHT %	% ERROR	ATOMIC %
Al	3.43	0.20	11.99
Ru	94.29	1.35	88.01
Total	97.72		100.00

SPECTRUM: Ru-rich solid in eutectic (quantitative)

ELEMENT	WEIGHT %	% ERROR	ATOMIC %
Al	3.42	0.20	12.00
Ru	94.02	1.35	88.00
Total	97.44		100.00

SPECTRUM: RuAl core region (quantitative)

ELEMENT	WEIGHT %	% ERROR	ATOMIC %
Al	19.67	0.35	47.48
Ru	81.54	1.22	52.52
Total	101.21		100.00

SPECTRUM: RuAl core region (quantitative)

ELEMENT	WEIGHT %	% ERROR	ATOMIC %
Al	17.78	0.34	44.94
Ru	81.62	1.22	55.06
Total	99.40		100.00

SPECTRUM: Discrete RuAl<sub>2</sub> grains (quantitative)

ELEMENT	WEIGHT %	% ERROR	ATOMIC %
Al	38.83	0.51	69.62
Ru	63.50	1.02	30.38
Total	102.33		100.00

SPECTRUM: Discrete RuAl<sub>2</sub> grains (quantitative)

ELEMENT	WEIGHT %	% ERROR	ATOMIC %
Al	38.65	0.51	69.54
Ru	63.43	1.02	30.46
Total	102.08		100.00

SPECTRUM: Discrete Ru<sub>2</sub>Al<sub>3</sub> (quantitative)

ELEMENT	WEIGHT %	% ERROR	ATOMIC %
Al	32.82	0.46	63.48
Ru	70.75	1.10	36.52
Total	103.57		100.00

SPECTRUM: Discrete Ru<sub>2</sub>Al<sub>3</sub> (quantitative)

ELEMENT	WEIGHT %	% ERROR	ATOMIC %
Al	34.07	0.47	65.07
Ru	68.53	1.08	34.93
Total	102.59		100.00

SPECTRUM: Overall composition (quantitative)

ELEMENT	WEIGHT %	% ERROR	ATOMIC %
Al	42.18	0.54	72.42
Ru	60.20	0.99	27.58
Total	102.38		100.00

# APPENDIX XI

## EXPERIMENTAL DATA FOR $Ru_{23}Al_{73}$

### CHEMICAL ANALYSES (EDAX)

SAMPLE:  $Ru_{23}Al_{73}$  (as-cast)

SPECTRUM:  $Ru_4Al_{13}$  matrix (quantitative)

ELEMENT	WEIGHT %	% ERROR	ATOMIC %
Al	43.59	0.55	73.71
Ru	58.26	0.97	26.29
Total	101.85		100.00

SPECTRUM:  $Ru_4Al_{13}$  matrix (quantitative)

ELEMENT	WEIGHT %	% ERROR	ATOMIC %
Al	43.96	0.55	73.46
Ru	59.53	0.98	26.54
Total	103.50		100.00

SPECTRUM:  $Ru_4Al_{13}$  matrix (quantitative)

ELEMENT	WEIGHT %	% ERROR	ATOMIC %
Al	44.12	0.55	73.53
Ru	59.50	0.98	26.47
Total	103.61		100.00

SPECTRUM: Discrete  $RuAl_2$  grains (quantitative)

ELEMENT	WEIGHT %	% ERROR	ATOMIC %
Al	38.62	0.51	69.80
Ru	62.61	1.02	30.20
Total	101.23		100.00

**SPECTRUM: Overall composition (quantitative)**

ELEMENT	WEIGHT %	% ERROR	ATOMIC %
Al	52.09	0.61	80.16
Ru	48.31	0.85	19.84
Total	100.40		100.00

EXPERIMENTAL DATA FOR Ru<sub>20</sub>:Al<sub>80</sub>

## CHEMICAL ANALYSES (EDAX)

SAMPLE: Ru<sub>20</sub>:Al<sub>80</sub> (as-cast)SPECTRUM: Ru<sub>4</sub>Al<sub>13</sub> needles (quantitative)

ELEMENT	WEIGHT %	% ERROR	ATOMIC %
Al	43.76	0.55	73.29
Ru	59.75	0.98	26.71
Total	103.52		100.00

SPECTRUM: Ru<sub>4</sub>Al<sub>13</sub> needles (quantitative)

ELEMENT	WEIGHT %	% ERROR	ATOMIC %
Al	43.89	0.55	73.54
Ru	59.18	0.98	26.46
Total	103.07		100.00

SPECTRUM: Al-rich matrix (quantitative)

ELEMENT	WEIGHT %	% ERROR	ATOMIC %
Al	86.14	0.87	99.24
Ru	2.47	0.22	0.76
Total	88.60		100.00

SPECTRUM: Al-rich matrix (quantitative)

ELEMENT	WEIGHT %	% ERROR	ATOMIC %
Al	90.29	0.90	99.48
Ru	1.77	0.22	0.52
Total	92.06		100.00

X-RAY DIFFRACTION DATA FOR Ru<sub>10</sub>Al<sub>2</sub>-b CONTINUED:

NUMBER	2 THETA	d (nm)	CPS	INTENSITY(%)
30	31.323	0.13136	14.45	1.59
31	32.089	0.12830	42.05	4.63
32	33.874	0.12173	107.29	11.82
33	35.004	0.11791	37.77	4.16
34	36.100	0.11445	26.10	2.87
35	37.582	0.11009	85.13	9.38
36	38.174	0.10844	26.19	2.88
37	39.126	0.10591	5.91	0.65
38	41.091	0.10104	40.95	4.51
39	42.366	0.09814	29.81	3.28
40	44.321	0.09401	32.15	3.54
41	44.640	0.09337	44.29	4.88
42	45.361	0.09197	91.14	10.04
43	45.700	0.09132	37.49	4.13
44	46.129	0.09052	32.64	3.59
45	47.925	0.08731	29.58	3.26
46	48.260	0.08674	21.20	2.33
47	48.745	0.08593	25.38	2.9
48	49.083	0.08538	16.61	1.83
49	49.723	0.08435	24.63	2.71
50	50.288	0.08346	27.91	3.07
51	51.741	0.08127	70.07	7.72
52	52.104	0.08074	32.38	3.57
53	54.231	0.07780	21.94	2.42
54	55.431	0.07625	14.16	1.56
55	56.380	0.07507	20.6	2.29
56	56.880	0.07446	17.51	1.93
57	57.300	0.07396	16.97	1.87

**X-RAY DIFFRACTION DATA FOR Ru<sub>18</sub>Al<sub>12</sub>-b:**

NUMBER	2 THETA	d (nm)	CPS	INTENSITY(%)
1	8.260	0.49239	104.81	11.54
2	8.599	0.47303	97.13	10.70
3	9.003	0.45181	52.15	5.74
4	9.500	0.42824	38.21	4.21
5	10.124	0.40191	57.77	6.36
6	10.560	0.38535	33.90	3.73
7	11.368	0.35806	48.30	5.32
8	12.325	0.33034	353.35	38.92
9	12.806	0.31797	15.08	1.66
10	14.243	0.28604	26.39	2.91
11	14.787	0.27557	28.69	3.16
12	16.005	0.25472	16.14	1.78
13	16.400	0.24863	3.74	0.4
14	16.920	0.24104	17.19	1.89
15	17.830	0.22884	269.68	29.70
16	18.759	0.21759	124.23	13.68
17	19.224	0.21238	908.00	100.00
18	19.762	0.20665	205.67	22.65
19	20.278	0.20145	210.55	23.19
20	22.342	0.18304	57.90	6.38
21	23.560	0.17370	14.85	1.64
22	23.860	0.17155	28.58	3.15
23	24.580	0.16660	16.24	1.79
24	25.285	0.16202	33.78	3.72
25	26.904	0.15244	28.20	3.11
26	27.700	0.14814	81.39	8.96
27	28.004	0.14656	110.89	12.21
28	29.045	0.14142	304.36	33.52
29	30.092	0.13660	23.85	2.63

SPECTRUM: Majority phase -  $\text{Ru}_4\text{Al}_{13}$  (quantitative)

ELEMENT	WEIGHT %	% ERROR	ATOMIC %
Al	46.06	0.53	74.93
Ru	57.74	0.84	25.07
Total	103.80		100.00

SPECTRUM: " $\text{RuAl}_5$ " minor phase (quantitative)

ELEMENT	WEIGHT %	% ERROR	ATOMIC %
Al	53.32	0.58	81.48
Ru	45.41	0.72	18.52
Total	98.73		100.00

SPECTRUM: " $\text{RuAl}_5$ " minor phase (quantitative)

ELEMENT	WEIGHT %	% ERROR	ATOMIC %
Al	54.22	0.58	81.44
Ru	46.30	0.73	18.56
Total	100.52		100.00

SPECTRUM:  $\text{RuAl}_6$  minor phase (quantitative)

ELEMENT	WEIGHT %	% ERROR	ATOMIC %
Al	60.30	0.63	85.00
Ru	39.89	0.66	15.00
Total	100.19		100.00

SPECTRUM:  $\text{RuAl}_6$  minor phase (quantitative)

ELEMENT	WEIGHT %	% ERROR	ATOMIC %
Al	60.38	0.63	84.78
Ru	40.61	0.67	15.22
Total	100.99		100.00



SPECTRUM: Overall composition (semi-quantitative)

ELEMENT	RELATIVE K	WT %	ATOMIC %
Al	0.3992	62.81	86.35
Ru	0.2606	37.19	13.65
Total		100.00	100.00

SPECTRUM: Al-rich solid solutic : (quantitative)

ELEMENT	WEIGHT %	% ERROR	ATOMIC %
Al	95.28	0.87	99.15
Ru	3.05	0.22	0.85
Total	98.34		100.00

SPECTRUM: Al-rich solid solution (quantitative)

ELEMENT	WEIGHT %	% ERROR	ATOMIC %
Al	96.00	0.88	99.12
Ru	3.18	0.23	0.88
Total	99.19		100.00

SPECTRUM: Majority phase - Ru<sub>4</sub>Al<sub>13</sub> (quantitative)

ELEMENT	WEIGHT %	% ERROR	ATOMIC %
Al	45.69	0.52	74.83
Ru	57.59	0.84	25.17
Total	103.28		100.00

SPECTRUM: Majority phase - Ru<sub>4</sub>Al<sub>13</sub> (quantitative)

ELEMENT	WEIGHT %	% ERROR	ATOMIC %
Al	44.12	0.51	75.34
Ru	54.11	0.80	24.66
Total	98.23		100.00

EXPERIMENTAL DATA FOR  $\text{Ru}_{18}\text{Al}_{22}\text{-b}$ CHEMICAL ANALYSES (EDAX)SAMPLE:  $\text{Ru}_{18}\text{Al}_{22}\text{-b}$  (No heat treatment)

Semi-quantitative Analyses

PHASE	ATOMIC % RUTHENIUM
Al-rich solid	$0.06 \pm 0.02$
$\text{RuAl}_6$	$13.1 \pm 0.1$
" $\text{RuAl}_3$ "	$16.4 \pm 0.2$
$\text{Ru}_4\text{Al}_{13}$	$22.0 \pm 0.1$

SPECTRUM: Overall composition (semi-quantitative)

ELEMENT	RELATIVE K	WT %	ATOMIC %
Al	0.4081	63.65	86.77
Ru	0.2536	36.35	13.23
Total		100.00	100.00

SPECTRUM: Overall composition (semi-quantitative)

ELEMENT	RELATIVE K	WT %	ATOMIC %
Al	0.4189	64.64	87.26
Ru	0.2454	35.36	12.74
Total		100.00	100.00

SPECTRUM: Overall composition (semi-quantitative)

ELEMENT	RELATIVE K	WT %	ATOMIC %
Al	0.3660	59.55	84.65
Ru	0.2882	40.45	15.35
Total		100.00	100.00

**SPECTRUM: Al-rich matrix in needle region (quantitative)**

ELEMENT	WEIGHT %	% ERROR	ATOMIC %
Al	85.90	0.87	99.57
Ru	1.40	0.20	0.43
Total	87.30		100.00

SPECTRUM: Ru<sub>4</sub>Al<sub>13</sub> phase layer and centre of needles (quantitative)

ELEMENT	WEIGHT %	% ERROR	ATOMIC %
Al	42.04	0.54	74.00
Ru	55.36	0.93	26.00
Total	97.40		100.00

SPECTRUM: Ru<sub>4</sub>Al<sub>13</sub> phase layer and centre of needles (quantitative)

ELEMENT	WEIGHT %	% ERROR	ATOMIC %
Al	43.58	0.55	73.90
Ru	57.69	0.96	26.10
Total	101.27		100.00

SPECTRUM: RuAl<sub>6</sub> phase layer, surrounding Ru<sub>4</sub>Al<sub>13</sub>, and finer needles (quantitative)

ELEMENT	WEIGHT %	% ERROR	ATOMIC %
Al	56.22	0.65	84.22
Ru	39.49	0.75	15.78
Total	95.71		100.00

SPECTRUM: RuAl<sub>6</sub> phase layer, surrounding Ru<sub>4</sub>Al<sub>13</sub>, and finer needles (quantitative)

ELEMENT	WEIGHT %	% ERROR	ATOMIC %
Al	56.94	0.65	84.19
Ru	40.08	0.76	15.81
Total	97.02		100.00

SPECTRUM: Al-rich matrix in needle region (quantitative)

ELEMENT	WEIGHT %	% ERROR	ATOMIC %
Al	85.05	0.86	99.45
Ru	1.77	0.20	0.55
Total	86.82		100.00

SPECTRUM: RuAl<sub>2</sub> matrix in most regions (quantitative)

ELEMENT	WEIGHT %	% ERROR	ATOMIC %
Al	33.61	0.47	63.41
Ru	72.65	1.13	36.59
Total	106.26		100.00

SPECTRUM: RuAl<sub>2</sub> matrix in most regions (quantitative)

ELEMENT	WEIGHT %	% ERROR	ATOMIC %
Al	33.69	0.47	63.40
Ru	72.90	1.13	36.60
Total	106.59		100.00

SPECTRUM: RuAl<sub>2</sub> matrix in most regions (quantitative)

ELEMENT	WEIGHT %	% ERROR	ATOMIC %
Al	33.03	0.47	63.35
Ru	71.60	1.11	36.65
Total	104.63		100.00

SPECTRUM: Small inclusions (quantitative)

ELEMENT	WEIGHT %	% ERROR	ATOMIC %
Al	19.41	0.35	48.64
Ru	76.78	1.17	51.36
Total	96.19		100.00

SPECTRUM: Small inclusions (quantitative)

ELEMENT	WEIGHT %	% ERROR	ATOMIC %
Al	21.76	0.38	51.73
Ru	76.10	1.16	48.27
Total	97.86		100.00

SPECTRUM: RuAl<sub>2</sub> in two-phase region (quantitative)

ELEMENT	WEIGHT %	% ERROR	ATOMIC %
Al	34.25	0.48	62.95
Ru	75.55	1.16	37.05
Total	109.80		100.00

SPECTRUM: Al-rich solid lining cavities (quantitative)

ELEMENT	WEIGHT %	% ERROR	ATOMIC %
Al	60.41	0.68	99.71
Ru	0.65	0.17	0.29
Total	61.06		100.00

SPECTRUM: Al-rich solid lining cavities (quantitative)

ELEMENT	WEIGHT %	% ERROR	ATOMIC %
Al	61.42	0.68	99.65
Ru	0.81	0.17	0.35
Total	62.23		100.00

SPECTRUM: Al-rich solid lining cavities (quantitative)

ELEMENT	WEIGHT %	% ERROR	ATOMIC %
Al	52.05	0.61	99.85
Ru	0.30	0.15	0.15
Total	52.35		100.00

SPECTRUM: Al-rich solid - oxide analysis (quantitative)

ELEMENT	WEIGHT %	% ERROR	ATOMIC %
Al	54.07	0.60	40.00
O	48.10		60.00
Total	102.17		100.00

## CHEMICAL ANALYSES (EDAX)

SAMPLE:  $\text{Ru}_{32}\text{Al}_{68}$  (After additional heat treatment)

SPECTRUM: Discrete  $\text{Ru}_2\text{Al}_3$  in two-phase region (quantitative)

ELEMENT	WEIGHT %	% ERROR	ATOMIC %
Al	26.95	0.42	55.99
Ru	79.38	1.20	44.01
Total	106.33		100.00

SPECTRUM: Discrete  $\text{Ru}_2\text{Al}_3$  in two-phase region (quantitative)

ELEMENT	WEIGHT %	% ERROR	ATOMIC %
Al	26.83	0.42	55.72
Ru	79.89	1.20	44.28
Total	106.72		100.00

SPECTRUM: Discrete  $\text{Ru}_2\text{Al}_3$  in two-phase region (quantitative)

ELEMENT	WEIGHT %	% ERROR	ATOMIC %
Al	26.96	0.42	55.89
Ru	79.73	1.20	44.11
Total	106.69		100.00

SPECTRUM:  $\text{RuAl}_2$  in two-phase region (quantitative)

ELEMENT	WEIGHT %	% ERROR	ATOMIC %
Al	33.90	0.47	62.90
Ru	74.93	1.15	37.10
Total	108.83		100.00

SPECTRUM:  $\text{RuAl}_2$  in two-phase region (quantitative)

ELEMENT	WEIGHT %	% ERROR	ATOMIC %
Al	34.06	0.48	62.96
Ru	75.11	1.16	37.04
Total	109.17		100.00

X-RAY DIFFRACTION DATA FOR  $Ru_{32}Al_{68}$  (1200°C for 312 hours) CONTINUED:

NUMBER	2 THETA	d (nm)	CPS	INTENSITY(%)
30	35.638	0.11588	39.67	8.24
31	36.703	0.11263	10.21	2.12
32	37.583	0.11009	141.34	29.36
33	37.820	0.10942	99.92	20.75
34	38.670	0.10711	59.02	12.26
35	39.364	0.10529	18.84	3.91
36	39.890	0.10396	47.04	9.77
37	40.503	0.10245	39.96	8.30
38	42.215	0.09847	55.24	11.47
39	43.212	0.09630	7.34	1.52
40	44.818	0.09302	26.90	5.59
41	45.360	0.09197	28.37	5.89
42	46.374	0.09007	30.71	6.38
43	46.825	0.08925	33.83	7.03
44	48.040	0.08712	30.82	6.40
45	48.400	0.08651	79.51	16.51
46	48.740	0.08594	37.80	7.85
47	49.323	0.08499	16.93	3.52
48	50.212	0.08358	23.53	5.93
49	51.006	0.08236	18.55	3.85
50	53.137	0.07928	35.80	7.44
51	53.507	0.07878	22.43	4.66
52	53.944	0.07819	35.73	7.42
53	54.641	0.07726	22.39	4.65
54	55.823	0.07575	186.72	38.78
55	56.168	0.07533	81.18	16.86
56	57.761	0.07342	12.66	2.63



**X-RAY DIFFRACTION DATA FOR  $\text{Ru}_{52}\text{Al}_{48}$  (1200°C for 312 hours):**

NUMBER	2 THETA	d (nm)	CPS	INTENSITY(%)
1	8.365	0.48623	44.60	9.26
2	8.749	0.46491	32.42	6.73
3	9.272	0.43872	30.22	6.28
4	9.992	0.40721	43.16	8.97
5	11.099	0.36670	277.09	57.55
6	12.077	0.33710	12.36	2.57
7	12.380	0.32888	23.63	4.91
8	13.830	0.29454	185.39	38.51
9	14.685	0.27748	10.71	2.22
10	15.957	0.25549	17.94	3.73
11	17.199	0.23715	146.79	30.49
12	18.243	0.22370	481.45	100.00
13	18.700	0.21827	131.29	27.27
14	19.221	0.21241	136.94	28.44
15	19.706	0.20723	376.10	78.12
16	20.476	0.19951	88.21	18.32
17	22.562	0.18127	263.27	54.68
18	23.608	0.17335	16.87	3.50
19	25.499	0.16069	55.85	11.60
20	27.079	0.15147	45.61	9.47
21	27.842	0.14740	113.64	23.60
22	28.611	0.14352	79.76	16.57
23	29.403	0.13973	137.05	28.47
24	30.141	0.13639	46.91	9.74
25	30.754	0.13373	114.78	23.84
26	32.235	0.12774	144.26	29.96
27	33.224	0.12404	84.99	17.65
28	33.580	0.12276	50.07	10.40
29	34.464	0.11971	57.39	11.92

SPECTRUM: RuAl<sub>2</sub> in central region (Microprobe)

WT% Al	WT% Ru	TOTAL	AT% Al	AT% Ru	TOTAL
32.52	67.63	100.15	64.31	35.69	100.00
32.58	67.31	99.89	64.46	35.54	100.00
32.27	67.30	99.57	64.24	35.76	100.00
32.82	67.89	100.71	64.43	35.57	100.00
32.63	67.26	99.89	64.51	35.49	100.00
33.51	67.34	100.85	65.09	34.91	100.00
32.26	67.54	99.81	64.16	35.84	100.00
31.45	66.88	98.33	63.80	36.20	100.00
31.37	66.90	98.27	63.73	36.27	100.00
31.22	67.33	98.55	63.47	36.53	100.00

SPECTRUM: Ru<sub>4</sub>Al<sub>3</sub> in central region (Microprobe)

WT% Al	WT% Ru	TOTAL	AT% Al	AT% Ru	TOTAL
44.25	55.45	99.70	74.94	25.06	100.00
43.74	55.01	98.75	74.87	25.06	100.00
43.49	55.32	98.81	74.66	25.34	100.00
43.49	55.03	98.54	74.76	25.24	100.00
44.10	55.17	99.27	74.97	25.03	100.00
44.02	55.70	99.72	74.76	25.24	100.00
44.42	55.53	99.95	74.98	25.02	100.00
43.87	54.55	98.42	75.08	24.92	100.00
44.96	55.60	100.56	75.19	24.81	100.00
44.59	55.69	100.28	75.00	25.00	100.00

EXPERIMENTAL DATA FOR  $\text{Ru}_{32}\text{Al}_{68}$ CHEMICAL ANALYSES (EDAX)SAMPLE:  $\text{Ru}_{32}\text{Al}_{68}$  (1200°C for 312 hours)

SPECTRUM: Overall composition (semi-quantitative)

ELEMENT	RELATIVE K	WT %	ATOMIC %
Al	0.2215	42.44	73.43
Ru	0.4484	57.56	26.57
Total		100.00	100.00

SPECTRUM: Overall composition (semi-quantitative)

ELEMENT	RELATIVE K	WT %	ATOMIC %
Al	0.2243	42.84	73.74
Ru	0.4443	57.16	26.25
Total		100.00	100.00

SPECTRUM: Overall composition (semi-quantitative)

ELEMENT	RELATIVE K	WT %	ATOMIC %
Al	0.2077	40.48	71.82
Ru	0.4688	59.52	28.18
Total		100.00	100.00

SPECTRUM: Overall composition (semi-quantitative)

ELEMENT	RELATIVE K	WT %	ATOMIC %
Al	0.2084	40.58	71.91
Ru	0.4678	59.42	28.09
Total		100.00	100.00

## APPENDIX XII

EXPERIMENTAL DATA FOR  $\text{Ru}_{28.3}\text{Al}_{71.7}$ CHEMICAL ANALYSES (EDAX)SAMPLE:  $\text{Ru}_{28.3}\text{Al}_{71.7}$  (1200°C for 312 hours)SPECTRUM:  $\text{RuAl}_2$  matrix (semi-quantitative)

ELEMENT	RELATIVE K	WT %	ATOMIC %
Al	0.1859	37.26	68.94
Ru	0.5020	62.56	30.90
Mn	0.0006	0.07	0.07
Fe	0.0010	0.11	0.10
Total		100.00	100.00

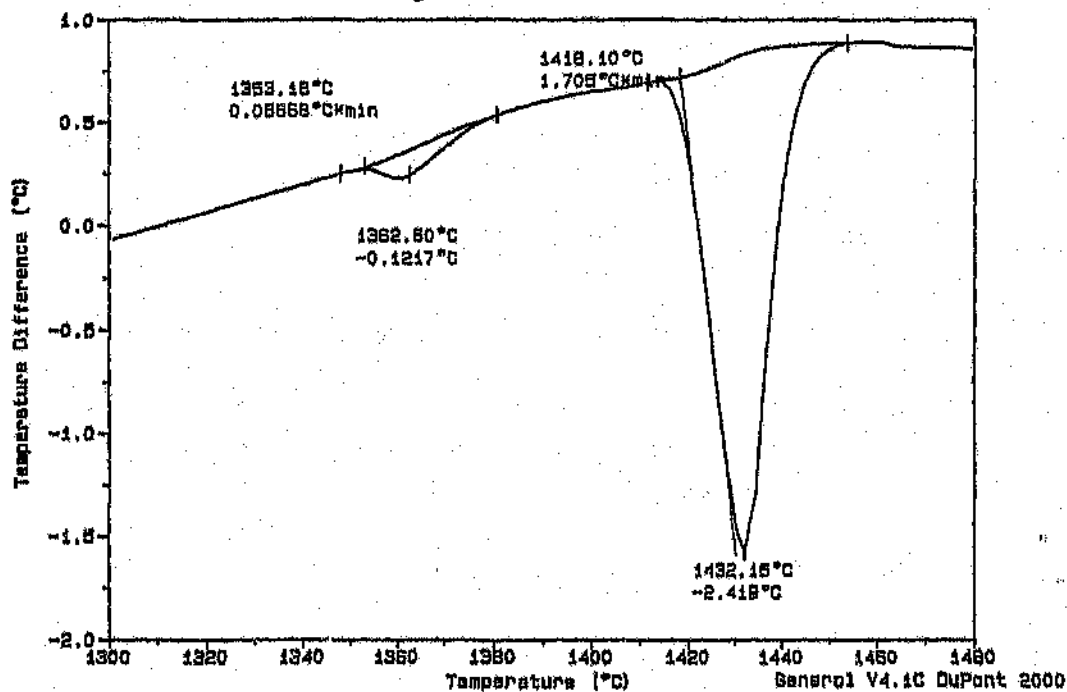
SPECTRUM: Al-rich solid lining cavities (semi-quantitative)

ELEMENT	RELATIVE K	WT %	ATOMIC %
Al	0.9691	98.27	99.51
Ru	0.0097	1.64	0.44
Mn	0.0002	0.02	0.01
Fe	0.0007	0.08	0.04
Total		100.00	100.00

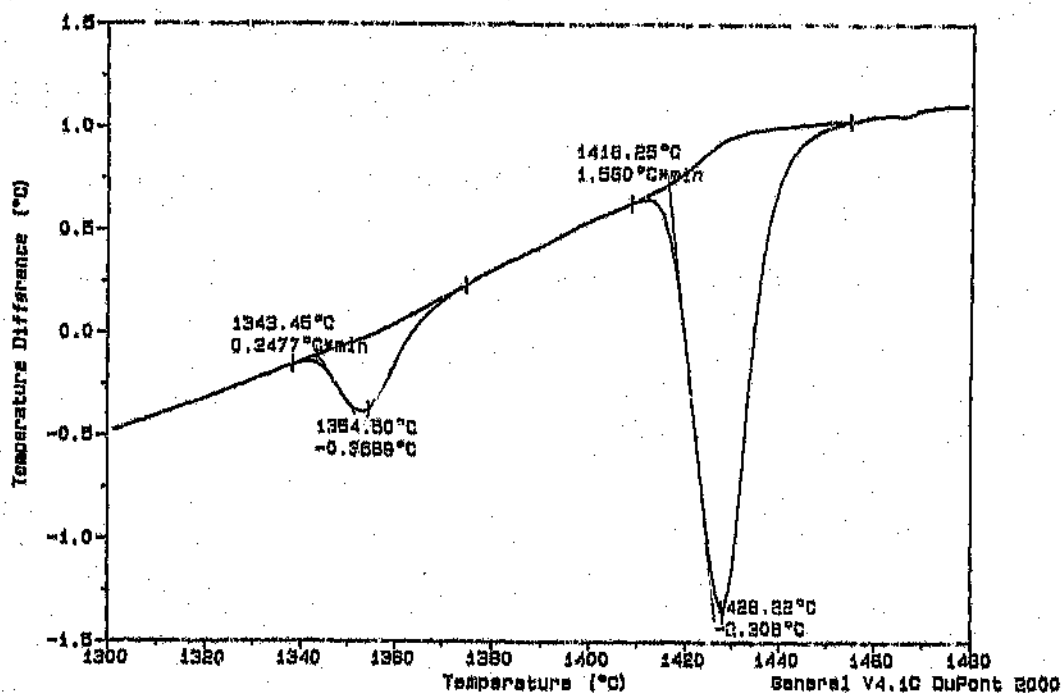
SPECTRUM: Small inclusion (semi-quantitative)

ELEMENT	RELATIVE K	WT %	ATOMIC %
Al	0.1083	24.81	53.84
Ru	0.5926	69.65	40.34
Mn	0.0078	0.91	0.97
Fe	0.0421	4.62	4.85
Total		100.00	100.00

SCAN 2: 1300°C to 1480°C - Nitrogen flow 100ml/minute.

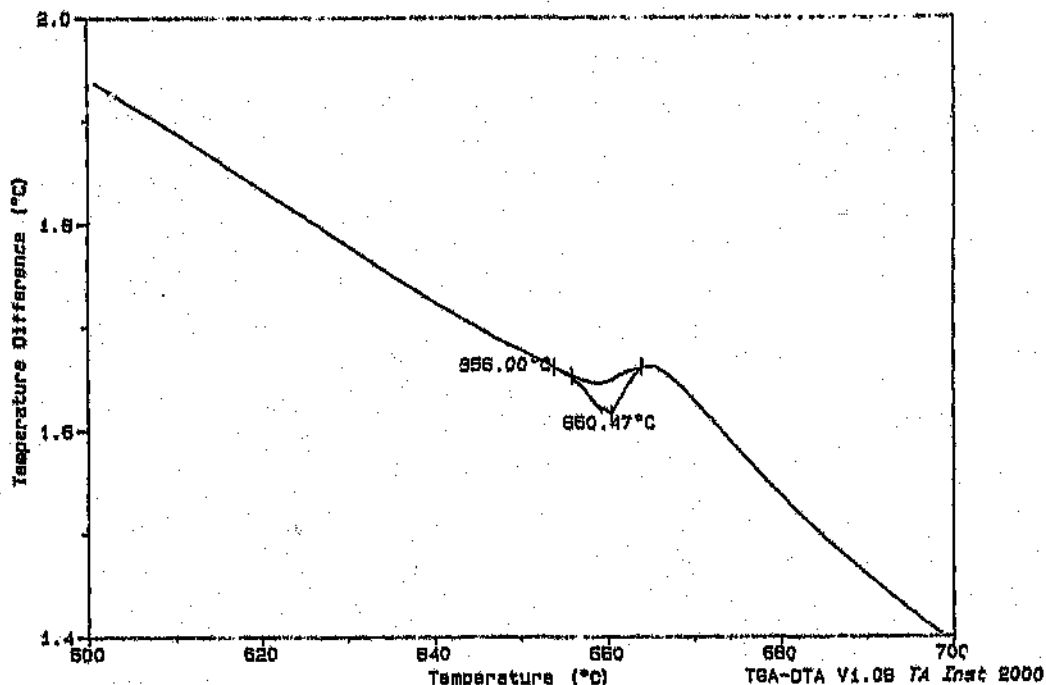


SCAN 3: 1300°C to 1480°C - Static air atmosphere.

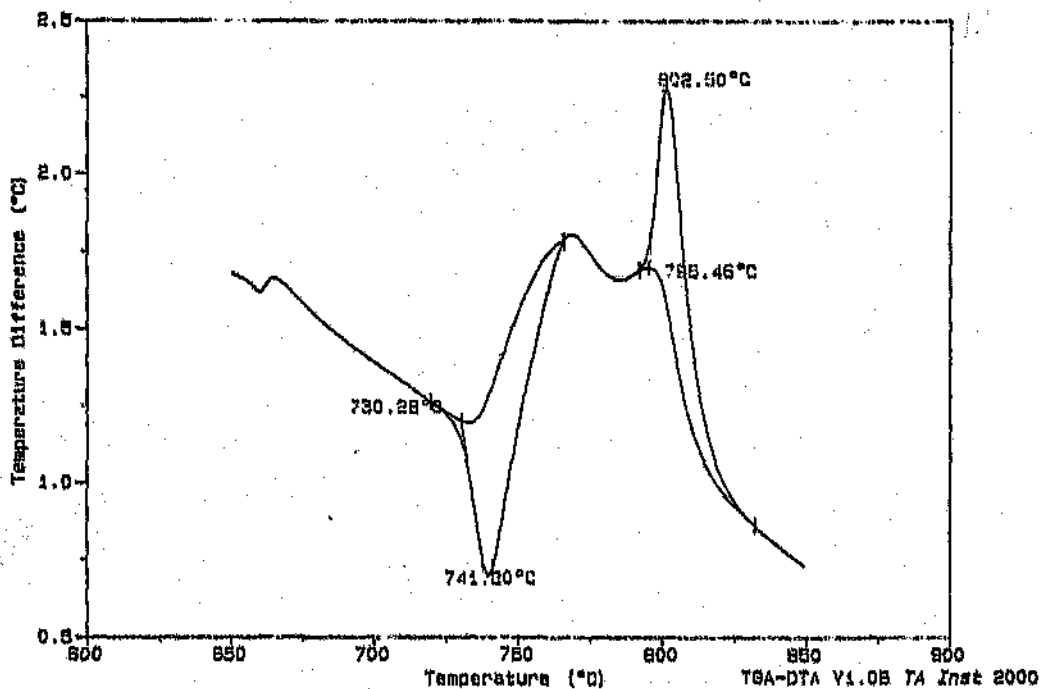


DIFFERENTIAL THERMAL ANALYSIS OF NOMINAL Ru<sub>75</sub>Al<sub>25</sub>

SCAN 1: 600°C to 700°C - Nitrogen flow 100ml/minute.



SCAN 1: 600°C to 900°C - Nitrogen flow 100ml/minute.



SPECTRUM: RuAl<sub>2</sub> layer (quantitative)

ELEMENT	WEIGHT %	% ERROR	ATOMIC %
Al	32.65	0.46	63.98
Ru	68.89	1.08	36.02
Total	101.54		100.00

SPECTRUM: RuAl<sub>2</sub> layer (quantitative)

ELEMENT	WEIGHT %	% ERROR	ATOMIC %
Al	32.91	0.47	63.90
Ru	69.68	1.09	36.10
Total	102.59		100.00

SPECTRUM: Ru<sub>4</sub>Al<sub>13</sub> matrix of third layer (quantitative)

ELEMENT	WEIGHT %	% ERROR	ATOMIC %
Al	43.35	0.55	74.05
Ru	56.92	0.95	25.95
Total	100.27		100.00

SPECTRUM: Ru<sub>4</sub>Al<sub>13</sub> matrix of third layer (quantitative)

ELEMENT	WEIGHT %	% ERROR	ATOMIC %
Al	43.99	0.55	73.80
Ru	58.54	0.97	26.20
Total	102.53		100.00

SPECTRUM: Ru<sub>4</sub>Al<sub>13</sub> matrix of third layer (quantitative)

ELEMENT	WEIGHT %	% ERROR	ATOMIC %
Al	44.10	0.55	73.86
Ru	58.48	0.97	26.14
Total	102.58		100.00

SPECTRUM: RuAl core region (quantitative)

ELEMENT	WEIGHT %	% ERROR	ATOMIC %
Al	18.39	0.34	45.30
Ru	83.20	1.24	54.70
Total	101.59		100.00

SPECTRUM: Ru<sub>2</sub>Al<sub>3</sub> layer (quantitative)

ELEMENT	WEIGHT %	% ERROR	ATOMIC %
Al	25.97	0.41	55.11
Ru	79.29	1.20	44.89
Total	105.26		100.00

SPECTRUM: Ru<sub>2</sub>Al<sub>3</sub> layer (quantitative)

ELEMENT	WEIGHT %	% ERROR	ATOMIC %
Al	27.74	0.42	57.57
Ru	76.63	1.17	42.43
Total	104.37		100.00

SPECTRUM: Ru<sub>2</sub>Al<sub>3</sub> layer (quantitative)

ELEMENT	WEIGHT %	% ERROR	ATOMIC %
Al	27.84	0.42	57.54
Ru	76.98	1.17	42.46
Total	104.83		100.00

SPECTRUM: RuAl<sub>2</sub> layer (quantitative)

ELEMENT	WEIGHT %	% ERROR	ATOMIC %
Al	32.70	0.46	63.98
Ru	68.97	1.09	36.02
Total	101.67		100.00



EXPERIMENTAL DATA FOR  $\text{Ru}_{37}\text{Al}_{63}$ CHEMICAL ANALYSES (EDAX)SAMPLE:  $\text{Ru}_{37}\text{Al}_{63}$  (1200°C for 168 hours)

Semi-quantitative Analyses

PHASE	ATOMIC % RUTHENIUM
Ru-rich solid	$88 \pm 3$
$\text{RuAl}$	$47 \pm 2$
$\text{Ru}_2\text{Al}_3$	$37.2 \pm 0.4$
$\text{RuAl}_2$	$31.0 \pm 0.4$
Area in Figure 5.29	42

SPECTRUM:  $\text{RuAl}$  in un-cracked region (quantitative)

ELEMENT	WEIGHT %	% ERROR	ATOMIC %
Al	19.74	0.33	48.27
Ru	79.25	1.04	51.73
Total	98.99		100.00

SPECTRUM:  $\text{RuAl}$  in un-cracked region (quantitative)

ELEMENT	WEIGHT %	% ERROR	ATOMIC %
Al	20.79	0.34	50.11
Ru	77.58	1.02	49.89
Total	98.37		100.00

SPECTRUM:  $\text{RuAl}$  in un-cracked region (quantitative)

ELEMENT	WEIGHT %	% ERROR	ATOMIC %
Al	21.48	0.34	51.56
Ru	75.62	1.01	48.44
Total	97.10		100.00

**SPECTRUM: Larger discrete phase in interdendritic regions (quantitative)**

ELEMENT	WEIGHT %	% ERROR	ATOMIC %
Al	40.00	0.52	71.20
Ru	60.62	1.00	28.80
Total	100.62		100.00

**SPECTRUM: Overall composition (semi-quantitative)**

ELEMENT	RELATIVE K	WEIGHT %	ATOMIC %
Al	0.1951	38.49	70.04
Zr	0.0101	1.54	0.83
Ru	0.4666	59.97	29.13
Total		100.00	100.00

SPECTRUM: Ru<sub>4</sub>Al<sub>13</sub> matrix phase (quantitative)

ELEMENT	WEIGHT %	% ERROR	ATOMIC %
Al	44.26	0.55	73.06
Ru	61.17	1.00	26.94
Total	105.43		100.00

SPECTRUM: Ru<sub>4</sub>Al<sub>13</sub> matrix phase (quantitative)

ELEMENT	WEIGHT %	% ERROR	ATOMIC %
Al	44.81	0.56	73.46
Ru	60.66	1.00	26.54
Total	105.47		100.00

SPECTRUM: Fine "eutectic"-like mixture (quantitative)

ELEMENT	WEIGHT %	% ERROR	ATOMIC %
Al	40.79	0.53	69.85
Ru	65.98	1.06	30.15
Total	106.77		100.00

SPECTRUM: Fine "eutectic"-like mixture (quantitative)

ELEMENT	WEIGHT %	% ERROR	ATOMIC %
Al	40.64	0.53	69.96
Ru	65.38	1.05	30.04
Total	106.03		100.00

SPECTRUM: Fine "eutectic"-like mixture (quantitative)

ELEMENT	WEIGHT %	% ERROR	ATOMIC %
Al	40.78	0.53	69.97
Ru	65.60	1.05	30.03
Total	106.39		100.00

EXPERIMENTAL DATA FOR  $Ru_{35}Al_{65}$ -bCHEMICAL ANALYSES (EDAX)SAMPLE:  $Ru_{35}Al_{65}$ -b (No heat treatment)SPECTRUM:  $Ru_2Al_3$  dendrites (quantitative)

ELEMENT	WEIGHT %	% ERROR	ATOMIC %
Al	35.09	0.48	63.44
Ru	75.78	1.16	36.56
Total	110.87		100.00

SPECTRUM:  $Ru_2Al_3$  dendrites (quantitative)

ELEMENT	WEIGHT %	% ERROR	ATOMIC %
Al	34.03	0.48	63.50
Ru	73.31	1.14	36.50
Total	107.34		100.00

SPECTRUM:  $Ru_2Al_3$  dendrites (quantitative)

ELEMENT	WEIGHT %	% ERROR	ATOMIC %
Al	33.46	0.47	63.48
Ru	72.12	1.12	36.52
Total	105.58		100.00

SPECTRUM:  $Ru_4Al_{12}$  matrix phase (quantitative)

ELEMENT	WEIGHT %	% ERROR	ATOMIC %
Al	44.91	0.56	73.37
Ru	61.08	1.00	26.63
Total	105.99		100.00

SPECTRUM: RuAl<sub>2</sub> matrix in two-phase region (quantitative)

ELEMENT	WEIGHT %	% ERROR	ATOMIC %
Al	32.08	0.46	64.17
Ru	67.11	1.06	35.83
Total	99.19		100.00

SPECTRUM: RuAl<sub>2</sub> matrix in two-phase region (quantitative)

ELEMENT	WEIGHT %	% ERROR	ATOMIC %
Al	31.95	0.46	64.02
Ru	67.29	1.07	35.98
Total	99.25		100.00

SPECTRUM: Analysis of RuAl showing impurities in alloy (semi-quantitative)

ELEMENT	RELATIVE K	WEIGHT %	ATOMIC %
Al	0.0936	21.19	49.77
Ru	0.6676	77.27	48.42
Si	0.0019	0.44	0.98
Fe	0.0013	0.14	0.16
Zr	0.0072	0.96	0.67
Total			100.00

SPECTRUM: Small RuAl region (quantitative)

ELEMENT	WEIGHT %	% ERROR	ATOMIC %
Al	17.34	0.33	44.94
Ru	79.62	1.20	55.06
Total	96.96		100.00

SPECTRUM: Small RuAl region (quantitative)

ELEMENT	WEIGHT %	% ERROR	ATOMIC %
Al	18.10	0.34	46.85
Ru	76.92	1.17	53.15
Total	95.01		100.00

SPECTRUM: Discrete Ru<sub>2</sub>Al<sub>3</sub> phase in two-phase region (quantitative)

ELEMENT	WEIGHT %	% ERROR	ATOMIC %
Al	25.84	0.41	56.77
Ru	73.74	1.13	43.23
Total	99.57		100.00

SPECTRUM: Discrete Ru<sub>2</sub>Al<sub>3</sub> phase in two-phase region (quantitative)

ELEMENT	WEIGHT %	% ERROR	ATOMIC %
Al	25.62	0.40	57.22
Ru	71.78	1.11	42.78
Total	97.41		100.00

SPECTRUM: Discrete Ru<sub>2</sub>Al<sub>3</sub> phase in two-phase region (quantitative)

ELEMENT	WEIGHT %	% ERROR	ATOMIC %
Al	25.87	0.41	57.72
Ru	71.03	1.10	42.28
Total	96.91		100.00

SPECTRUM: RuAl<sub>2</sub> matrix phase (quantitative)

ELEMENT	WEIGHT %	% ERROR	ATOMIC %
Al	31.95	0.46	63.10
Ru	70.01	1.10	36.90
Total	101.97		100.00

SPECTRUM: RuAl<sub>2</sub> matrix phase (quantitative)

ELEMENT	WEIGHT %	% ERROR	ATOMIC %
Al	32.14	0.46	63.21
Ru	70.09	1.10	36.79
Total	102.23		100.00

SPECTRUM: Thin network (semi-quantitative)

ELEMENT	RELATIVE K	WEIGHT %	ATOMIC %
Al	0.1374	27.48	57.72
Zr	0.1956	26.90	16.71
Ru	0.2635	45.61	25.57
Total		100.00	100.00

SPECTRUM: Overall composition (quantitative)

ELEMENT	WEIGHT %	% ERROR	ATOMIC %
Al	29.94	0.44	61.34
Ru	70.69	1.10	38.66
Total	100.63		100.00

SAMPLE: Ru<sub>35</sub>Al<sub>65</sub>-am (1300°C for 6.5 hours, 1100°C for 65.5 hours)

SPECTRUM: Small RuAl region (quantitative)

ELEMENT	WEIGHT %	% ERROR	ATOMIC %
Al	19.10	0.35	47.95
Ru	77.68	1.18	52.05
Total	96.77		100.00

EXPERIMENTAL DATA FOR  $Ru_{1.5}Al_{0.5}$ -am

## CHEMICAL ANALYSES (EDAX)

SAMPLE:  $Ru_{1.5}Al_{0.5}$ -am (Arc-melted)SPECTRUM:  $Ru_2Al_3$  dendritic phase (quantitative)

ELEMENT	WEIGHT %	% ERROR	ATOMIC %
Al	24.10	0.39	53.72
Ru	77.79	1.18	46.28
Total	101.90		100.00

SPECTRUM:  $Ru_2Al_3$  dendritic phase (quantitative)

ELEMENT	WEIGHT %	% ERROR	ATOMIC %
Al	23.93	0.39	53.42
Ru	78.19	1.18	46.58
Total	102.12		100.00

SPECTRUM:  $Ru_2Al_3$  dendritic phase (quantitative)

ELEMENT	WEIGHT %	% ERROR	ATOMIC %
Al	23.62	0.39	53.10
Ru	78.17	1.18	46.90
Total	101.79		100.00

SPECTRUM:  $RuAl_2$  matrix phase (quantitative)

ELEMENT	WEIGHT %	% ERROR	ATOMIC %
Al	31.84	0.46	63.67
Ru	68.08	1.07	36.33
Total	99.92		100.00



**SPECTRUM: Ru<sub>4</sub>Al<sub>13</sub> matrix phase (quantitative)**

ELEMENT	WEIGHT %	% ERROR	ATOMIC %
Al	45.62	0.52	75.05
Ru	56.84	0.83	24.95
Total	102.46		100.00

**SPECTRUM: Small RuAl area (quantitative)**

ELEMENT	WEIGHT %	% ERROR	ATOMIC %
Al	18.96	0.35	46.62
Ru	81.35	1.22	53.38
Total	100.31		100.00

**SPECTRUM: Small RuAl area (quantitative)**

ELEMENT	WEIGHT %	% ERROR	ATOMIC %
Al	18.83	0.35	46.17
Ru	82.24	1.23	53.83
Total	101.06		100.00

SPECTRUM: RuAl<sub>2</sub> dendritic phase (quantitative)

ELEMENT	WEIGHT %	% ERROR	ATOMIC %
Al	33.06	0.43	64.17
Ru	69.17	0.95	35.83
Total	102.23		100.00

SPECTRUM: RuAl<sub>2</sub> dendritic phase (quantitative)

ELEMENT	WEIGHT %	% ERROR	ATOMIC %
Al	33.36	0.43	64.13
Ru	69.93	0.96	35.87
Total	103.29		100.00

SPECTRUM: RuAl<sub>2</sub> dendritic phase (quantitative)

ELEMENT	WEIGHT %	% ERROR	ATOMIC %
Al	33.34	0.43	64.27
Ru	69.45	0.95	35.73
Total	102.79		100.00

SPECTRUM: Ru<sub>4</sub>Al<sub>13</sub> matrix phase (quantitative)

ELEMENT	WEIGHT %	% ERROR	ATOMIC %
Al	45.67	0.52	75.01
Ru	57.04	0.83	24.99
Total	102.71		100.00

SPECTRUM: Ru<sub>4</sub>Al<sub>13</sub> matrix phase (quantitative)

ELEMENT	WEIGHT %	% ERROR	ATOMIC %
Al	45.65	0.52	74.95
Ru	57.17	0.84	25.05
Total	102.83		100.00

EXPERIMENTAL DATA FOR  $\text{Ru}_{33}\text{Al}_{67}\text{-a}$ CHEMICAL ANALYSES (EDAX)SAMPLE:  $\text{Ru}_{33}\text{Al}_{67}\text{-a}$  (No heat treatment)

Semi-quantitative Analyses

PHASE	ATOMIC % RUTHENIUM
$\text{Ru}_4\text{Al}_{13}$	$21.19 \pm 0.09$
$\text{RuAl}_2$	$30.55 \pm 0.03$

SPECTRUM: Overall composition (semi-quantitative)

ELEMENT	RELATIVE K	WT %	ATOMIC %
Al	0.2054	40.14	71.53
Ru	0.4724	59.86	28.47
Total		100.00	100.00

SPECTRUM: Overall composition (semi-quantitative)

ELEMENT	RELATIVE K	WT %	ATOMIC %
Al	0.2069	40.36	71.71
Ru	0.4702	59.64	28.29
Total		100.00	100.00

SPECTRUM: Overall composition (semi-quantitative)

ELEMENT	RELATIVE K	WT %	ATOMIC %
Al	0.2102	40.83	72.11
Ru	0.4652	59.17	27.89
Total		100.00	100.00

**SPECTRUM: Small inclusions (quantitative)**

ELEMENT	WEIGHT %	% ERROR	ATOMIC %
Al	19.22	0.35	48.81
Ru	75.55	1.15	51.19
Total	94.77		100.00

**X-RAY DIFFRACTION DATA FOR  $\text{Ru}_{47}\text{Al}_{53}$  (1200°C for 2 hours):**

NUMBER	POSITION (deg)	d (nm)	PEAK HEIGHT	% H.F.
1	13.649	0.29844	3091	100.0
2	14.338	0.28417	266	8.6
3	16.250	0.25092	104	3.4
4	19.247	0.21213	701	22.7
5	23.699	0.17270	139	4.5
6	27.459	0.14942	3012	97.4
7	30.788	0.13359	1409	45.6
8	31.595	0.13026	78	2.5
9	33.817	0.12193	777	25.1
10	38.210	0.10835	42	1.4
11	41.697	0.09964	448	14.5
12	41.897	0.09919	247	8.0
13	44.020	0.09463	2412	78.0
14	44.266	0.09413	1285	41.6
15	46.331	0.09015	976	31.6
16	46.610	0.08964	517	16.7
17	48.553	0.08625	91	2.9
18	52.762	0.07981	97	3.1
19	56.637	0.07476	514	16.6
20	57.009	0.07431	260	8.4
21	58.560	0.07251	409	13.2
22	58.960	0.07206	225	7.3
23	60.455	0.07044	178	5.8
24	60.822	0.07006	115	3.7
25	64.059	0.06687	1261	40.8
26	64.483	0.06647	645	20.9

# IMAGE ANALYSIS:

Sample	$\text{Ru}_{47}\text{Al}_{53}$
Magnification	435X
# Fields	6
Area fraction of secondary phase	1.803%
Max.	
Min.	2.062%
Std. deviation	1.345%
	0.2767%

Therefore, according to the phase diagram<sup>[6]</sup>, the overall composition of the two-phase outer region is  $\text{Ru}_{52}\text{Al}_{48}$ .

**SPECTRUM: Eutectic area of two-phase region (quantitative)**

ELEMENT	WEIGHT %	% ERROR	ATOMIC %
Al	6.97	0.23	22.62
Ru	89.30	1.31	77.38
Total	96.26		100.00

**SPECTRUM: Eutectic area of two-phase region (quantitative)**

ELEMENT	WEIGHT %	% ERROR	ATOMIC %
Al	7.96	0.24	24.94
Ru	89.75	1.32	75.06
Total	97.71		100.00

**SPECTRUM: Eutectic area of two-phase region (quantitative)**

ELEMENT	WEIGHT %	% ERROR	ATOMIC %
Al	7.99	0.24	25.06
Ru	89.48	1.31	74.94
Total	97.47		100.00

**SPECTRUM: RuAl in central region (quantitative)**

ELEMENT	WEIGHT %	% ERROR	ATOMIC %
Al	19.52	0.35	48.29
Ru	78.32	1.19	51.71
Total	97.84		100.00

**SPECTRUM: RuAl in central region (quantitative)**

ELEMENT	WEIGHT %	% ERROR	ATOMIC %
Al	19.50	0.35	48.17
Ru	78.61	1.20	51.83
Total	98.11		100.00

EXPERIMENTAL DATA FOR  $\text{Ru}_{47}\text{Al}_{53}$ CHEMICAL ANALYSES (EDAX)SAMPLE:  $\text{Ru}_{47}\text{Al}_{53}$  (1200°C for 2 hours)

Semi-quantitative Analyses

PHASE	ATOMIC % RUTHENIUM
Ru-rich solid	$75 \pm 6$
RuAl (2-phase region)	$47.0 \pm 0.3$
RuAl (single-phase)	$46.5 \pm 0.4$

SPECTRUM: RuAl grains in two-phase region (quantitative)

ELEMENT	WEIGHT %	% ERROR	ATOMIC %
Al	18.42	0.34	46.14
Ru	80.57	1.22	53.86
Total	98.99		100.00

SPECTRUM: RuAl grains in two-phase region (quantitative)

ELEMENT	WEIGHT %	% ERROR	ATOMIC %
Al	18.24	0.34	46.08
Ru	79.99	1.21	53.92
Total	98.23		100.00

SPECTRUM: RuAl grains in two-phase region (quantitative)

ELEMENT	WEIGHT %	% ERROR	ATOMIC %
Al	17.23	0.33	44.99
Ru	78.94	1.20	55.01
Total	96.17		100.00



**SPECTRUM: Discrete RuAl phase (semi-quantitative)**

ELEMENT	RELATIVE K	WT %	ATOMIC %
Al	0.1082	24.06	53.67
Si	0.0024	0.56	1.20
Fe	0.0049	0.54	0.58
Ru	0.6452	74.85	44.56
Total		100.00	100.00

SPECTRUM: Ru<sub>2</sub>Al<sub>3</sub> matrix (semi-quantitative)

ELEMENT	RELATIVE K	WT %	ATOMIC %
Al	0.1415	29.96	61.15
Si	0.0019	0.48	0.94
Fe	0.0005	0.05	0.05
Ru	0.5798	69.51	37.86
Total		100.00	100.00

SPECTRUM: Ru<sub>2</sub>Al<sub>3</sub> matrix (semi-quantitative)

ELEMENT	RELATIVE K	WT %	ATOMIC %
Al	0.1390	29.51	60.51
Si	0.0025	0.61	1.20
Fe	0.0011	0.12	0.12
Ru	0.5827	69.76	38.17
Total		100.00	100.00

SPECTRUM: Discrete RuAl phase (semi-quantitative)

ELEMENT	RELATIVE K	WT %	ATOMIC %
Al	0.1082	24.10	53.79
Si	0.0018	0.42	0.91
Fe	0.0064	0.71	0.77
Ru	0.6446	74.77	44.53
Total		100.00	100.00

SPECTRUM: Discrete RuAl phase (semi-quantitative)

ELEMENT	RELATIVE K	WT %	ATOMIC %
Al	0.1080	24.01	53.58
Si	0.0025	0.58	1.25
Fe	0.0049	0.55	0.59
Ru	0.6454	74.87	44.59
Total		100.00	100.00

SPECTRUM: Ru-rich solid in eutectic (semi-quantitative)

ELEMENT	RELATIVE K	WT %	ATOMIC %
Al	0.0066	1.72	6.10
Si	0.0019	0.35	1.21
Fe	0.0011	0.12	0.20
Ru	0.9690	97.81	92.50
Total		100.00	100.00

SPECTRUM: Ru-rich solid in eutectic (semi-quantitative)

ELEMENT	RELATIVE K	WT %	ATOMIC %
Al	0.0115	2.97	10.20
Si	0.0020	0.38	1.25
Fe	0.0009	0.10	0.17
Ru	0.9504	96.55	88.38
Total		100.00	100.00

SPECTRUM: Ru-rich solid in eutectic (semi-quantitative)

ELEMENT	RELATIVE K	WT %	ATOMIC %
Al	0.0087	2.26	7.93
Si	0.0009	0.17	0.58
Fe	0.0001	0.01	0.02
Ru	0.9654	97.56	91.46
Total		100.00	100.00

SPECTRUM: Ru<sub>2</sub>Al<sub>3</sub> matrix (semi-quantitative)

ELEMENT	RELATIVE K	WT %	ATOMIC %
Al	0.1417	30.01	61.25
Si	0.0017	0.42	0.83
Fe	0.0006	0.07	0.07
Ru	0.5796	69.49	37.85
Total		100.00	100.00

# CHEMICAL ANALYSES (EDAX)

SAMPLE: Ru<sub>27</sub>:Al<sub>63</sub> (1200°C for 840 hours)

SPECTRUM: Uncracked RuAl bands (semi-quantitative)

ELEMENT	RELATIVE K	WT %	ATOMIC %
Al	0.0906	20.63	48.94
Si	0.0020	0.45	1.02
Fe	0.0012	0.14	0.15
Ru	0.6946	78.79	49.89
Total		100.00	100.00

SPECTRUM: Uncracked RuAl bands (semi-quantitative)

ELEMENT	RELATIVE K	WT %	ATOMIC %
Al	0.0946	21.39	50.02
Si	0.0024	0.54	1.21
Fe	0.0010	0.11	0.12
Ru	0.6837	77.96	48.65
Total		100.00	100.00

SPECTRUM: Uncracked RuAl bands (semi-quantitative)

ELEMENT	RELATIVE K	WT %	ATOMIC %
Al	0.0970	21.90	50.91
Si	0.0015	0.35	0.79
Fe	0.0011	0.12	0.13
Ru	0.6798	77.63	48.17
Total		100.00	100.00

SPECTRUM: Uncracked RuAl bands (semi-quantitative)

ELEMENT	RELATIVE K	WT %	ATOMIC %
Al	0.0945	21.37	49.85
Si	0.0031	0.69	1.55
Fe	0.0012	0.14	0.15
Ru	0.6816	77.81	48.44
Total		100.00	100.00

X-RAY DIFFRACTION PATTERN OF  $\text{Ru}_{27}\text{Al}_{63}$  (1200°C for 168 hours) CONTINUED

NUMBER	2 THETA	d (nm)	CPS	INTENSITY(%)
30	35.583	0.11606	243.70	23.16
31	37.516	0.11027	129.48	12.30
32	38.681	0.10708	71.01	6.75
33	39.328	0.10538	27.90	2.65
34	40.461	0.10255	165.72	15.75
35	42.266	0.09836	44.20	4.20
36	43.180	0.09637	18.20	1.73
37	44.123	0.09441	31.17	2.96
38	45.299	0.09209	46.49	4.42
39	46.508	0.08982	55.01	5.23
40	47.457	0.08812	12.52	1.19
41	48.379	0.08654	28.44	2.70
42	49.304	0.08502	11.40	1.08
43	50.305	0.08343	3.55	0.34
44	51.138	0.08216	16.74	1.59
45	52.700	0.07989	34.73	3.30
46	53.163	0.07925	63.31	6.02
47	53.950	0.07818	25.18	2.39
48	55.896	0.07566	13.86	1.32
49	56.836	0.07451	24.06	2.29
50	58.892	0.07213	39.43	3.75
51	60.100	0.07082	25.31	2.41
52	60.550	0.07034	12.49	1.19

**X-RAY DIFFRACTION PATTERN OF Ru<sub>37</sub>:Al<sub>63</sub> (1200°C for 168 hours):**

NUMBER	2 THETA	d (nm)	CPS	INTENSITY(%)
1	5.750	0.70701	365.57	34.74
2	6.330	0.64534	628.91	59.76
3	7.200	0.56476	971.82	92.35
4	7.634	0.53269	1052.33	100.00
5	8.072	0.50384	1020.63	96.99
6	8.750	0.46486	871.93	82.86
7	9.250	0.43978	675.96	64.23
8	10.864	0.37461	396.40	37.67
9	13.806	0.29505	147.56	14.02
10	15.444	0.26392	3.20	0.30
11	17.197	0.23718	63.19	6.00
12	18.148	0.22485	81.58	7.75
13	18.800	0.21712	29.46	2.80
14	19.300	0.21155	109.19	10.38
15	19.704	0.20725	180.48	17.15
16	20.250	0.20172	53.95	5.13
17	22.501	0.18176	287.03	27.28
18	23.729	0.17248	13.44	1.28
19	25.451	0.16098	25.55	2.43
20	27.000	0.15190	25.95	2.47
21	27.619	0.14856	145.00	13.78
22	28.564	0.14375	88.05	8.37
23	29.383	0.13982	142.08	13.50
24	30.200	0.13613	22.74	2.16
25	30.818	0.13346	143.82	13.67
26	31.650	0.13004	2.85	0.27
27	32.302	0.12748	101.02	9.60
28	33.572	0.12279	114.25	10.86
29	35.000	0.11793	11.22	1.07

SPECTRUM: Ru<sub>2</sub>Al<sub>3</sub> layer (quantitative)

ELEMENT	WEIGHT %	% ERROR	ATOMIC %
Al	26.92	0.39	58.88
Ru	70.47	0.96	41.12
Total	97.39		100.00

SPECTRUM: Ru<sub>2</sub>Al<sub>3</sub> layer (quantitative)

ELEMENT	WEIGHT %	% ERROR	ATOMIC %
Al	26.84	0.39	58.24
Ru	72.12	0.98	41.76
Total	98.96		100.00

SPECTRUM: Ru<sub>2</sub>Al<sub>3</sub> layer (quantitative)

ELEMENT	WEIGHT %	% ERROR	ATOMIC %
Al	26.93	0.39	58.02
Ru	73.00	0.98	41.98
Total	99.94		100.00

SPECTRUM: RuAl in un-cracked region (quantitative)

ELEMENT	WEIGHT %	% ERROR	ATOMIC %
Al	20.56	0.34	50.38
Ru	75.87	1.01	49.62
Total	96.43		100.00

SPECTRUM: RuAl in un-cracked region (quantitative)

ELEMENT	WEIGHT %	% ERROR	ATOMIC %
Al	19.98	0.33	48.76
Ru	73.70	1.04	51.24
Total	98.69		100.00

SPECTRUM: RuAl<sub>2</sub> matrix in cracked region (quantitative)

ELEMENT	WEIGHT %	% ERROR	ATOMIC %
Al	33.25	0.43	65.84
Ru	64.64	0.90	34.16
Total	97.90		100.00

SPECTRUM: RuAl<sub>2</sub> matrix in cracked region (quantitative)

ELEMENT	WEIGHT %	% ERROR	ATOMIC %
Al	33.13	0.43	65.31
Ru	65.95	0.92	34.69
Total	99.08		100.00

SPECTRUM: RuAl<sub>2</sub> matrix in cracked region (quantitative)

ELEMENT	WEIGHT %	% ERROR	ATOMIC %
Al	33.12	0.43	64.84
Ru	67.30	0.93	35.16
Total	100.42		100.00



DATA CARD: RuAl<sub>3</sub> Calculated Card

CRYSTAL STRUCTURE: Hexagonal

LATTICE PARAMETERS:  $a = 0.481$  nm,  $c = 0.784$

d (nm)	Intensity	h k l
0.41716	5	1 0 0
0.39252	14	0 0 2
0.36816	100	1 0 1
0.28584	40 6	1 0 2
0.24076	33.9	2 1 0
0.22166	24.7	1 0 3
0.20525	13.9	2 1 2
0.20155	35.2	2 0 1
0.19621	15.6	0 0 4
0.18412	33.4	2 0 2
0.17759	0.9	1 0 4
0.16309	17.7	2 0 3
0.15762	0.6	3 1 0
0.15452	15.4	3 1 1
0.15212	51.7	2 1 4
0.14628	10	3 1 2

d (nm)	Intensity	h k l
0.16259	3	4 2 0
0.16159	8	3 1 4
0.15726	2	0 2 5
0.15434	5	3 3 2
0.15309	6	1 3 4
0.15281	11	4 2 2
0.14934	3	0 0 6
0.14810	9	2 4 1
0.14601	3	5 1 0
0.14364	1	4 0 4
0.14278	5	4 2 3
0.14239	7	2 4 2
0.14212	5	3 1 5
0.13872	5	2 0 6
0.13627	3	1 3 5
0.13416	4	2 4 3
0.13229	5	0 4 4
0.13159	4	4 2 4
0.13124	3	5 1 3
0.12776	8	2 2 6
0.12579	6	3 1 6
0.12481	4	6 0 0

DATA CARD: RuAl<sub>3</sub> JCPDS Card 30-35

CRYSTAL STRUCTURE: Orthorhombic

LATTICE PARAMETERS: a = 0.74886 nm, b = 0.65563 nm, c = 0.89610

d (nm)	Intensity	h k l
0.49295	100	1 1 0
0.44803	42	0 0 2
0.43206	16	1 1 1
0.37418	26	2 0 0
0.33166	66	1 1 2
0.32783	22	0 2 0
0.30786	8	0 2 1
0.28734	24	2 0 2
0.25546	5	1 1 3
0.24663	12	2 2 0
0.23329	2	3 1 0
0.22576	27	3 1 1
0.22404	22	0 0 4
0.22078	21	0 2 3
0.21603	63	2 2 2
0.20980	30	1 3 0
0.20688	66	3 1 2
0.20396	55	1 1 4
0.19013	13	2 2 3
0.18719	7	4 0 0
0.18497	9	0 2 4
0.18385	2	3 1 3
0.17276	5	4 0 2
0.17168	4	1 3 3
0.16582	9	2 2 4
0.16440	1	3 3 0
0.16392	2	0 4 0

DATA CARD:  $\text{Ru}_4\text{Al}_{13}$  JCPDS Card 18-56

CRYSTAL STRUCTURE: Monoclinic

LATTICE PARAMETERS:  $a = 1.5862 \text{ nm}$ ,  $b = 0.8188 \text{ nm}$ ,  $c = 1.2736 \text{ nm}$ ,  $\beta = 107.8^\circ$

d (nm)	Intensity	h k l
0.72	10	1 1 0
0.663	20	1 1 1
0.582	20	1 1 1
0.568	5	2 0 1
0.565	10	2 0 2
0.415	80	2 0 2
0.413	80	2 0 3
0.410	50	0 2 0
0.404	80	0 0 3
0.397	50	4 0 1
0.388	10	0 2 1
0.378	80	4 0 0
0.376	80	4 0 2
0.360	100	2 2 0
0.339	80	0 2 2
0.332	100	2 2 1
0.318	10	2 0 3
0.317	10	2 0 4
0.303	10	0 0 4
0.2915	10	2 2 2
0.2906	10	2 2 3
0.2875	10	0 2 3

DATA CARD:  $\text{RuAl}_2$  JCPDS Card 19-45

CRYSTAL STRUCTURE: Orthorhombic

LATTICE PARAMETERS:  $a = 0.8012 \text{ nm}$ ,  $b = 0.4717 \text{ nm}$ ,  $c = 0.8785 \text{ nm}$

d (nm)	Intensity	h k l
0.369	100	1 1 1
0.296	60	2 0 2
0.2376	50	1 1 3
0.2247	100	3 1 1
0.2197	60	0 0 4
0.2078	100	2 2 2
0.2033	50	2 2 0
0.2003	20	4 0 0
0.18206	50	3 1 3
0.16130	10	1 1 5
0.15198	10	1 3 1
0.14951	10	5 1 1
0.14917	50	2 2 4
0.14801	20	4 0 4
0.14421	50	4 2 2
0.14017	50	3 1 5
0.13753	10	2 0 6
0.13651	10	1 3 3
0.13470	10	5 1 3
0.13392	50	3 3 1

DATA CARD: RuAl JCPDS Card 29-1404

CRYSTAL STRUCTURE: Cubic

LATTICE PARAMETERS:  $a = 0.295$  nm

d (nm)	Intensity	h k l
0.295	55	1 0 0
0.2086	100	1 1 0
0.1703	10	1 1 1
0.1475	15	2 0 0
0.1319	10	2 1 0
0.1204	25	2 1 1
0.1043	10	2 2 0
0.09833	5	3 0 0
0.09330	10	3 1 0
0.08895	5	3 1 1
0.08516	5	2 2 2
0.08182	5	3 2 0
0.07884	25	3 2 1

DATA CARD: Ru<sub>2</sub>Al<sub>3</sub> JCPDS Card 19-46

CRYSTAL STRUCTURE: Tetragonal

LATTICE PARAMETERS:  $a = 0.3079$  nm,  $c = 1.433$  nm

d (nm)	Intensity	h k l
0.715	20	0 0 2
0.358	50	0 0 4
0.301	30	1 0 1
0.2588	50	1 0 3
0.2177	90	1 1 0
0.2098	100	1 0 5
0.1861	50	1 1 4

DATA CARD: Ru JCPDS Card 6-663

CRYSTAL STRUCTURE: Hexagonal

LATTICE PARAMETERS:  $a = 0.27058$  nm,  $c = 0.42819$  nm

d (nm)	Intensity	h k l
0.2343	40	1 0 0
0.2142	35	0 0 2
0.2056	100	1 0 1
0.15808	25	1 0 2
0.13530	25	1 1 0
0.12189	25	1 0 3
0.11715	6	2 0 0
0.11434	25	1 1 2
0.11299	20	2 0 1
0.10705	4	0 0 4
0.10278	8	2 0 2
0.09738	6	1 0 4
0.09056	16	2 0 3
0.08857	6	2 1 0
0.08673	25	2 1 1
0.08395	18	1 1 4
0.08185	10	2 1 2
0.08043	16	1 0 5

## JCPDS LATTICE DATA CARDS

DATA CARD: Al JCPDS Card 4-787

CRYSTAL STRUCTURE: Cubic

LATTICE PARAMETERS:  $a = 0.40494$  nm

d (nm)	Intensity	h k l
0.2338	100	1 1 1
0.2024	47	2 0 0
0.1431	22	2 2 0
0.1221	24	3 1 1
0.1169	7	2 2 2
0.10124	2	4 0 0
0.09289	8	3 3 1
0.09055	8	4 2 0
0.08266	8	4 2 2



**X-RAY DIFFRACTION DATA FOR  $\text{Ru}_{50}\text{Al}_{50}$  (1200°C for 2 hours):**

NUMBER	POSITION (deg)	d (nm)	PEAK HEIGHT	% H.P.
1	12.394	0.32853	624	18.5
2	13.654	0.29833	1310	38.8
3	17.448	0.23381	252	7.5
4	19.337	0.21116	2271	67.3
5	19.911	0.20513	314	9.3
6	23.714	0.17259	325	9.6
7	25.061	0.16345	58	1.7
8	27.410	0.14968	860	25.5
9	28.377	0.14468	59	1.7
10	29.053	0.14138	51	1.5
11	30.669	0.13410	734	21.7
12	30.825	0.13344	576	17.1
13	33.828	0.12189	2814	83.4
14	34.730	0.11882	108	3.2
15	39.254	0.10558	211	6.3
16	40.514	0.10242	96	2.8
17	41.740	0.09955	3375	100.0
18	44.157	0.09435	219	6.5
19	44.325	0.09401	146	4.3
20	48.575	0.08622	183	5.4
21	48.825	0.08580	135	4.0
22	50.663	0.08289	174	5.2
23	51.008	0.08236	138	4.1
24	52.714	0.07988	3184	94.3
25	53.057	0.07940	1502	44.5
26	55.664	0.07596	62	1.8
27	58.557	0.07251	115	3.4
28	58.937	0.07209	75	2.2
29	60.053	0.07087	53	1.6
30	63.176	0.06770	47	1.4

### IMAGE ANALYSIS:

Sample	$\text{Ru}_{50}\text{:Al}_{50}$
Magnification	230X
# Fields	30
Area fraction of secondary phase	6.686%
Max.	
Min.	8.150%
Std. deviation	5.424%
	0.5553%

Therefore, according to the phase diagram<sup>[6]</sup>, the overall composition of the two-phase outer region is  $\text{Ru}_{54}\text{:Al}_{46}$ .

SPECTRUM: Eutectic area of two-phase region (quantitative)

ELEMENT	WEIGHT %	% ERROR	ATOMIC %
Al	6.98	0.22	23.05
Ru	87.32	1.11	76.95
Total	94.30		100.00

SPECTRUM: Eutectic area of two-phase region (quantitative)

ELEMENT	WEIGHT %	% ERROR	ATOMIC %
Al	6.87	0.22	21.96
Ru	91.53	1.16	78.04
Total	98.42		100.00

SPECTRUM: RuAl in central region (quantitative)

ELEMENT	WEIGHT %	% ERROR	ATOMIC %
Al	18.26	0.32	45.98
Ru	80.38	1.05	54.02
Total	98.64		100.00

SPECTRUM: RuAl in central region (quantitative)

ELEMENT	WEIGHT %	% ERROR	ATOMIC %
Al	18.66	0.32	46.81
Ru	79.45	1.04	53.19
Total	98.11		100.00

EXPERIMENTAL DATA FOR  $\text{Ru}_{50}\text{Al}_{50}$ CHEMICAL ANALYSES (EDAX)SAMPLE:  $\text{Ru}_{50}\text{Al}_{50}$  (1200°C for 2 hours)

Semi-quantitative Analyses

PHASE	ATOMIC % RUTHENIUM
Ru-rich solid	$73 \pm 2$
RuAl (2-phase region)	$48.1 \pm 0.7$
RuAl (single-phase)	$46.6 \pm 0.3$

SPECTRUM: RuAl grains in two-phase region (quantitative)

ELEMENT	WEIGHT %	% ERROR	ATOMIC %
Al	18.58	0.32	46.45
Ru	80.28	1.05	53.55
Total	98.86		100.00

SPECTRUM: RuAl grains in two-phase region (quantitative)

ELEMENT	WEIGHT %	% ERROR	ATOMIC %
Al	17.83	0.31	45.50
Ru	80.02	1.05	54.50
Total	97.85		100.00

SPECTRUM: RuAl grains in two-phase region (quantitative)

ELEMENT	WEIGHT %	% ERROR	ATOMIC %
Al	18.28	0.32	46.16
Ru	79.88	1.05	53.84
Total	98.16		100.00



## REFERENCES

- [1] Fleischer, R.L. J. Mat. Sci. 22, (1987), p2281-2288
- [2] Wopersnow, W.; Raub, J. Metall 33, (1979), 7, p736-740
- [3] Dr I. Wolff, Council for Mineral Technology, Randburg, South Africa, Private Communication
- [4] Obrowski, W. Metall, 17, (1963), p108-112
- [5] Anlage, S.M.; Nash, P.; Ramachandran, R.; Schwarz, R.B. J. Less Common Met. 136, (1988), p237-247
- [6] Massalski, T.B., ed. "Binary Alloy Phase Diagrams, Vol 1", American Society for Metals (1986), p158
- [7] Schwomma, O.; Nowotny, H.; Wittmann, A. M. Chem. 94, (1963), p924-926
- [8] Edshammar, L. Acta Chem. Scand. 19, (1965), p2124-2130
- [9] Edshammar, L. Acta Chem. Scand. 20, (1966), p427-431
- [10] Edshammar, L. Acta Chem. Scand. 22, (1968), p2374-2375
- [11] Varich, A.N.; Lyukevich, R.B. Russian Metallurgy 1, (1973), p73-75
- [12] Joint Committee on Powder Diffraction Standards (1989)
- [13] Villars, P.; Calvert, L.D. "Pearson's Handbook of Crystallographic Data for Intermetallic Phases", Vol 2, American Society for Metals (1985)
- [14] Jena, A.K.; Chaturvedi, M.C. "Phase Transformations in Materials", Prentice Hall Inc. (1992)
- [15] Chadwick, G.A. "Metallography of Phase Transformations", Butterworth & Co. (1972)
- [16] Straumanis, M.E. J. Applied Physics 20, (1949), p726-734
- [17] Klug, H.P.; Alexander, L.E. "X-Ray Diffraction Procedures For Polycrystalline and

**Author: Boniface Tracy Diane.**

**Name of thesis: The ruthenium-aluminium phase diagram.**

***PUBLISHER:***

**University of the Witwatersrand, Johannesburg**

**©2015**

***LEGALNOTICES:***

**Copyright Notice:** All materials on the University of the Witwatersrand, Johannesburg Library website are protected by South African copyright law and may not be distributed, transmitted, displayed or otherwise published in any format, without the prior written permission of the copyright owner.

**Disclaimer and Terms of Use:** Provided that you maintain all copyright and other notices contained therein, you may download material (one machine readable copy and one print copy per page) for your personal and/or educational non-commercial use only.

The University of the Witwatersrand, Johannesburg, is not responsible for any errors or omissions and excludes any and all liability for any errors in or omissions from the information on the Library website.